

**AN INVESTIGATION INTO THE HYDROLYTIC PRECIPITATION
OF IRON(III) FROM SULPHATE-BEARING EFFLUENTS**


Janice M. Zinck

Department of Mining and Metallurgical Engineering
McGill University
Montreal, Canada

November, 1993

A Thesis submitted to the Faculty of
Graduate Studies and Research
in partial fulfillment of the requirements
of the degree of Master of Engineering

© J.M. Zinck, 1993



Hydrolytic precipitation of Fe(III) from sulphate-bearing effluents

To Glen,

in appreciation for his refreshing
perspective on life.

*The most important thing is not
to stop questioning*

Albert Einstein

ABSTRACT

The neutralization of industrial acidic mineral effluents generates sludge of large volume, low solids content (1-2%) and slow settling rates. The hydrolysis of iron(III) from sulphate bearing aqueous solutions was investigated to significantly improve the neutralization of acidic mineral effluents. Both theoretical and experimental studies were undertaken. A literature review and a thermodynamic analysis of the Fe(III)-SO₄-H₂O system were performed. The literature review revealed that despite the numerous investigations reported to date, none has examined iron(III) hydrolysis, using a crystallization approach, as it pertains to effluent treatment. This observation prompted a critical review of the principles of crystallization and colloid stability, followed by an application of these principles to the design and interpretation of the precipitation tests.

The thermodynamic analysis determined that Fe(III)-sulphato complexes dominate in the acidic pH range (pH < 4) while at neutral to mild alkaline pH range Fe(OH)₃^o_(aq) is the dominant species. It was found that a relationship exists between the precipitation pH and the sulphate content of the precipitate (17% at pH 3, 7-9% at pH 6 and 1-2% at pH 9) and it was attributed in part to the existence of the precursor Fe(III)-sulphato complexes and in part to SO₄²⁻ adsorption on the Fe(III) oxyhydroxide solid phase.

Several variables were examined for their influence on the properties of the iron(III) hydrolysis products, such as: pH, neutralization rate, temperature, agitation rate, sulphate concentration and ionic strength. Tests were performed in a batch reactor and NaOH was selected as the most effective neutralizing reagent. Treatment sludges were characterized physically (e.g., solids content, settling rate, etc.), chemically and morphologically, while the treated effluent was examined for residual iron(III) content. These tests proved only partially successful as the precipitates produced were highly amorphous with low solids content (< 8%) and poor settling (< 3 m/hr). However, exceptionally good precipitates were produced when the hydrolysis tests were performed under supersaturation control. This work

led to the development of a novel approach to neutralization of effluents involving sludge recycling and staged neutralization in order to maintain a low and controlled supersaturation level. Via this novel method partially crystallized precipitates of excellent properties (55% solids, average particle size 20 micrometres, settling rate 12 m/hr) were produced at 50°C after eight recycles.

RÉSUMÉ

La neutralisation des effluents minéraux industriels acides génère un important volume de boue à faible teneur en solides (1-2%) et avec une faible vitesse de sédimentation. On a étudié l'hydrolyse du fer(III) provenant de solutions aqueuses à teneur de sulfates dans le but d'améliorer substantiellement la méthode de neutralisation des effluents acides. L'étude comportait un volet théorique et un volet expérimental. On a effectué un examen exhaustif de la documentation et une analyse thermodynamique de l'équilibre de la solution de $\text{Fe(III)-SO}_4\text{-H}_2\text{O}$. D'après la documentation, il était manifeste qu'aucune des études antérieures n'avait envisagé l'hydrolyse du fer(III) dans le traitement des effluents du point de vue de cristallisation. On a d'abord procédé à un examen critique des principes de cristallisation et de la stabilité colloïdale, pour ensuite les appliquer à la conception et à l'interprétation des épreuves de précipitation.

L'analyse thermodynamique a permis de constater que les complexes de sulfate de Fe(III) prédominent dans les solutions acides ($\text{pH} < 4$), tandis que le $\text{Fe(OH)}_3^0_{(\text{aq})}$ est l'espèce principale dans les solutions neutres et légèrement alcalines. On a observé qu'il existe un lien entre le pH de précipitation et la teneur en sulfate du précipité (de 17% à pH 3, de 7 à 9% à pH de 6 et de 1 à 2% à pH 9). On a attribué ce phénomène à la présence des complexes de sulfate de Fe(III) précurseurs et à l'adsorption du SO_4^{2-} par la phase solide de l'oxyhydroxyde de Fe(III).

On a examiné l'incidence de nombreux facteurs à variable unique sur les propriétés des produits d'hydrolyse du fer(III), dont : le pH, le taux de neutralisation, la température, le degré d'agitation, la concentration de sulfate et la force ionique. Des essais en discontinu ont été réalisés et le NaOH a été choisi comme étant le réactif de neutralisation de plus effectif. On a caractérisé les propriétés physiques (teneur en solides, vitesse de sédimentation, etc.), chimiques et morphologiques des boues de traitement et on a déterminé la teneur en fer(III) résiduel des effluents traités. Ces essais n'ont donné que des résultats partiels car les précipités produits

étaient grandement amorphes, à faible teneur en solides ($< 8\%$) et présentaient une faible vitesse de sédimentation (< 3 m/hr). Cependant, lorsque les essais d'hydrolyse étaient effectués en solution sursaturée, les précipités étaient d'une qualité exceptionnelle. Ces travaux ont mené à la conception d'une approche, tout à fait nouvelle pour la neutralisation des effluents, qui s'appuie sur le recyclage des boues et sur une neutralisation par étapes permettant de maintenir un niveau de sursaturation faible et stable. En suivant cette nouvelle méthode, on a obtenu, à 50°C et après huit recyclages, des précipités partiellement cristallisés présentant d'excellentes propriétés : 55% de solides d'une granulométrie moyenne de 20 micromètres et avec une vitesse de sédimentation de 12 m/hr.

ACKNOWLEDGEMENTS

I would like to thank Professor G.P. Demopoulos for the opportunity to study under him. His creative brilliance and dedication to research will serve as a source of inspiration throughout my career.

I wish to thank all of the members of the Hydrometallurgy research group of McGill University for their assistance and support during my stay in Montreal.

At CANMET, I am indebted to Ray Macdonald and Mike Campbell for encouraging and supporting my educational leave proposal, without which this Master's degree would not have been possible.

As well a sincere appreciation to the director of the Mineral Sciences Laboratories (MSL), Dr. I.J. Itzkovitch for giving me this extraordinary opportunity and to the Manager of the Environmental Laboratory, Dr. A.J. Oliver for continual sponsorship and support.

Thanks to my CANMET colleagues who assisted me this in endeavour; Wesley Griffith, technical guidance and comic relief; David Hardy, surface area analysis; Daniel Laforest, particle size analysis; Dr. John Hopkins, statistical design consultation, Paul Carriere and DeAlton Owens, XRD analysis, Irene Lafferty, word processing assistance; chemical laboratory staff, CANMET library, and to everyone in MSL.

Thanks to Errol van Huyssteen for his dedication to the mineralogical and morphological analysis of the, at times less than stimulating sludges, insightful discussions and his inspiring approach to science.

A special thanks to Dr. Peter Kondos for supporting and encouraging me to be the best I can be, showing me the ropes, making time when there was not any, and being a mentor.

I would also like to thank and congratulate all the strong women who have gone before me for taking paths less travelled and exploring new horizons for they have created opportunities for me and others like me to come that were not always possible.

Especially, I wish to thank those closest to me; my parents for encouragement and continual support and most of all to my husband, friend, and soul-mate, Glen Meade, for more than he will ever know.

TABLE OF CONTENTS

ABSTRACT	iv
RÉSUMÉ	vi
ACKNOWLEDGEMENTS	viii
LIST OF FIGURES AND PLATES	xv
LIST OF TABLES	xxi
CHAPTER 1: INTRODUCTION	1
1.1 The Issue	1
1.2 The Method of Treatment	1
1.3 The Present Research	2
CHAPTER 2: LITERATURE SURVEY	6
2.1 Neutralization	6
2.2 Fe(III) Hydrolysis	13
2.2.1 <u>Speciation</u>	13
2.2.1.1 <i>Polymer formation</i>	16
2.2.2 <u>Precipitation Pathways</u>	18
2.2.2.1 <i>Olation</i>	19
2.2.2.2 <i>Oxolation</i>	22
2.2.3 <u>Solids Formation and Phase Transformations</u>	23
2.2.3.1 <i>Oxides and hydroxides of iron(III)</i>	27
2.2.3.2 <i>Sulphate containing iron(III)</i>	

<i>compounds</i>	29
2.2.4 <u>Factors Affecting Solids Formation</u>	30
2.2.4.1 <i>Rate of neutralization</i>	30
2.2.4.2 <i>Temperature</i>	31
2.2.4.3 <i>Aging</i>	32
2.2.4.4 <i>Adsorption</i>	32
2.2.4.5 <i>Effect of anions and cations</i>	34
2.2.4.6 <i>Solubility</i>	36
2.3 Summary	36
 CHAPTER 3: THEORETICAL BACKGROUND	39
3.1 Fundamentals of Crystallization	39
3.1.1 <u>Nucleation</u>	41
3.1.1.1 <i>Primary nucleation</i>	41
3.1.1.2 <i>Secondary nucleation</i>	44
3.1.2 <u>Growth Kinetics</u>	46
3.1.2.1 <i>Growth by aggregation</i>	48
3.1.3 <u>Effect of Impurities on Crystallization</u>	51
3.1.4 <u>Batch versus Continuous Precipitation</u>	52
3.2 Destabilization of Colloidal Dispersions	53
3.2.1 <u>Electrical Double Layer</u>	53
3.2.2 <u>Destabilization Mechanisms</u>	57
3.2.2.1 <i>Double layer compression</i>	59
3.2.2.2 <i>Adsorption and charge neutralization</i>	63
3.2.2.3 <i>Enmeshment</i>	63
3.2.2.4 <i>Interparticle bridging</i>	63
3.2.3 <u>Flocculation of Hydroxides</u>	68
3.3 Summary	68

CHAPTER 4: THERMODYNAMIC PREDICTION OF THE

Fe(III)-SO₄-H₂O AQUEOUS EQUILIBRIA	70
4.1 Thermodynamic Calculations	70
4.1.1 <u>Thermodynamic Data</u>	70
4.1.2 <u>Assumptions</u>	70
4.2 Predominance Area Diagrams	73
4.2.1 <u>Effect of Fe(OH)₃ Precipitation</u>	73
4.2.2 <u>Speciation</u>	73
4.2.3 <u>Effect of Temperature</u>	75
4.3 Speciation Diagrams	75
4.4 Solubility Diagrams	77
4.5 Summary	84

CHAPTER 5: EXPERIMENTAL

5.1 Synthetic Effluents	86
5.2 Apparatus	88
5.3 Procedure	88

CHAPTER 6: RESULTS

6.1 Precipitation Profiles	91
6.2 Single Variable Effects	98
6.2.1 <u>Effect of Final pH</u>	98
6.2.2 <u>Rate of Neutralization</u>	107
6.2.3 <u>Effect of Agitation Speed</u>	110
6.2.4 <u>Effect of Retention Time</u>	118
6.2.5 <u>Effect of Temperature</u>	119
6.2.6 <u>Effect of Sulphate Concentration</u>	120
6.3 Statistical Design	127
6.3.1 <u>Settling Rate</u>	131
6.3.2 <u>Sludge Volume</u>	132

6.3.3 <u>Final Iron Concentration</u>	135
6.3.3.1 <i>Solubility diagrams</i>	135
6.4 Recycling	141
6.4.1 <u>Series A</u>	141
6.4.2 <u>Series B</u>	144
CHAPTER 7: DISCUSSION	164
7.1 Solids Composition	164
7.2 Reaction Pathways	166
7.3 Crystallization Mechanism	167
7.3.1 <u>Absence of seed</u>	167
7.3.2 <u>Recycling</u>	169
7.4 Colloid Stability	171
7.5 Implications of Current Research on the Existing Practise of Neutralization	174
CHAPTER 8: CONCLUSIONS AND FUTURE WORK	177
8.1 Conclusions	177
8.2 Future Work	179
REFERENCES	180
APPENDIX A: THERMODYNAMIC CALCULATIONS	194
A-1 Predominance Area Diagrams	195
A-2 Speciation Diagrams	196
A-3 Solubility Diagrams	196
APPENDIX B: EXPERIMENTAL PROCEDURES	197
B-1: Sulphate Determination by Barium Sulphate Precipitation	198
B-2: Settling Rate Determination Procedure	199

B-3: Percent Solids Determination Procedure	200
B-4: Sludge Volume Determination Procedure	201
APPENDIX C: THE INPUT OF HSO_4^- -DISSOCIATION IN Fe(III)	
PRECIPITATION CALCULATIONS	202
APPENDIX D: STATISTICAL DESIGN DERIVED SOLUBILITY DATA ..	204
APPENDIX E: RECYCLING	207
E-1: Dissolution Tests	208

LIST OF FIGURES AND PLATES

Description	Page #
Figure 2-1: Precipitation of heavy metals as hydroxides.	8
Figure 2-2: Lime neutralization process alternatives.	9
Figure 2-3: Formation of iron(III) oxide phase from acidic solution.	17
Figure 2-4: Chains of $\text{Fe}(\text{O},\text{OH},\text{H}_2\text{O})_6$ octahedra.	20
Figure 2-5: Schematic crystal structures.	21
Figure 2-6: The development of a hydrous iron oxyhydroxide.	24
Figure 2-7: Olation reaction matrix.	25
Figure 2-8: Generation of goethite in iron(III) nitrate solutions at room temperature.	28
Figure 2-9: Hydrolysis processes in Fe(III) solutions.	33
Figure 3-1: Solubility - supersolubility diagram for explanation of stable, metastable and labile.	40
Figure 3-2: Variation in supersaturation with time in a batch reactor.	42
Figure 3-3: Classification of nucleation mechanisms.	42
Figure 3-4: Generalized nucleation rate diagram describing the characteristic difference between homogeneous, heterogeneous and surface nucleation for these specific values.	45
Figure 3-5: The energies of crystal growth from solution.	47
Figure 3-6: Two-dimensional growth of surface nuclei by (a) mononuclear growth and (b) polynuclear growth models.	49
Figure 3-7: Stern model for electrical double layer.	56

Figure 3-8:	Repulsive and attractive energies as a function of particle separation.	58
Figure 3-9:	Charge distribution in the diffuse double layer of a negative particle surface at two electrolyte concentrations for a constant surface charge.	60
Figure 3-10:	Effect of electrolyte concentration on double layer compression.	62
Figure 3-11:	Schematic of reactions between colloidal particles and polymers.	65
Figure 3-12:	(a) Low ionic strength - bridging prevented by electrical repulsion. (b) High ionic strength - bridging across the effective repulsion distance.	67
Figure 4-1:	Predominance area diagrams for the $\text{Fe(III)-SO}_4\text{-H}_2\text{O}$ system for varying Fe(III) concentrations showing the region of Fe(OH)_3 precipitation.	74
Figure 4-2:	Predominance area diagrams for the $\text{Fe(III)-SO}_4\text{-H}_2\text{O}$ system for varying Fe(III) concentrations when Fe(OH)_3 precipitation is suppressed to illustrate the speciation.	76
Figure 4-3a:	The effect of temperature on the precipitation of ferric hydroxide.	78
Figure 4-3b:	The effect of temperature on the speciation of Fe(III) .	79
Figure 4-4:	Speciation diagram for the $\text{Fe(III)-SO}_4\text{-H}_2\text{O}$ system calculated by using $\text{F}^*\text{A}^*\text{C}^*\text{T}$.	80
Figure 4-5a:	Speciation diagram for the $\text{Fe(III)-SO}_4\text{-H}_2\text{O}$ system calculated by using $\text{F}^*\text{A}^*\text{C}^*\text{T}$ for low sulphate concentrations.	81
Figure 4-5b:	Speciation diagram for the $\text{Fe(III)-SO}_4\text{-H}_2\text{O}$ system calculated by using $\text{F}^*\text{A}^*\text{C}^*\text{T}$ for 80°C .	82
Figure 4-6:	Solubility diagram for Fe(III) calculated by using $\text{F}^*\text{A}^*\text{C}^*\text{T}$.	83
Figure 5-1:	Schematic representation of hydrolysis apparatus.	90
Figure 6-1:	Change in pH with time during hydrolysis of Fe(III) to pH 6.	92

Figure 6-2:	Precipitation profile of Fe(III) hydrolysis - change in Fe(III) concentration with pH.	94
Figure 6-3:	Change in saturation ratio in a batch reactor with time.	97
Figure 6-4:	Change in pH during neutralization.	99
Figure 6-5:	Effect of final solution pH on settling rate.	100
Figure 6-6a:	XRD pattern of the hydrolysis precipitate generated from simple (with no seed) neutralization to pH 3.	102
Figure 6-6b:	XRD pattern of the hydrolysis precipitate generated from simple (with no seed) neutralization to pH 6.	103
Figure 6-6c:	XRD pattern of the hydrolysis precipitate generated from simple (with no seed) neutralization to pH 9.	104
Figure 6-7:	The relationship between sulphate reported in the solids and final solution pH in both $\text{NO}_3\text{-SO}_4$ and SO_4 media.	108
Figure 6-8:	Effect of neutralization rate on settling rate.	109
Figure 6-9:	Effect of neutralization rate on sludge volume.	111
Figure 6-10:	Effect of neutralization rate on the percent of solids in the treatment sludge.	112
Figure 6-11:	Effect of neutralization rate on the nucleation mechanisms.	113
Figure 6-12:	Effect of agitation rate on settling rate.	115
Figure 6-13:	Effect of agitation rate on sludge volume.	116
Figure 6-14:	Effect of agitation rate on the percent of solids in the treatment sludge.	117
Figure 6-15:	Effect of temperature on Fe(III) removal.	121
Figure 6-16:	Effect of sulphate concentration on settling rate.	125
Figure 6-17:	Effect of sulphate concentration on sludge volume.	126

Figure 6-18: Effect of sulphate concentration on the percent of solids in the treatment sludge.	126
Figure 6-19: Predicted settling rate (m/s) response surface (pH = 6.0, neutralization rate = 1.9×10^{-3} moles OH^- / min.	131
Figure 6-20: Predicted settling rate (m/s) response surface ($[\text{SO}_4] = 5600$ mg/L, neutralization rate = 1.9×10^{-3} moles OH^- / min.	133
Figure 6-21: Predicted sludge volume (mL) response surface (pH = 6.0, neutralization rate = 1.9×10^{-3} moles OH^- / min.	134
Figure 6-22: Predicted final iron concentration (mg/L) response surface (Temp = 50°C , neutralization rate = 6.4×10^{-4} moles OH^- / min.	136
Figure 6-23: Fe(III) solubility for various sulphate concentrations at 50°C .	137
Figure 6-24: Effect of temperature on Fe(III) solubility.	139
Figure 6-25: Comparison of Fe(III) solubility lines.	140
Figure 6-26: Effect of recycling on sludge densification (Series A).	143
Figure 6-27: Particle size distribution for conventionally recycled (20x) solids (Series A).	145
Figure 6-28: Schematic representation and derivation of the staged-neutralization process.	150
Figure 6-29: Comparison of staged-neutralization recycling with simple conventional recycling in terms of sludge densification.	152
Figure 6-30: Effect of staged-neutralization recycling on sludge settleability.	154
Figure 6-31: XRD pattern of the hydrolysis precipitate (goethite) generated from staged-neutralization recycling (series B - 20x).	155
Figure 6-32: Particle size distribution for solids produced from staged-neutralization recycling (20x).	156

Figure 7-1:	Possible precipitation pathways for Fe(III) hydrolysis from sulphate-bearing solutions.	168
Figure 7-2:	Summary of proposed crystallization mechanisms.	170
Figure 7-3:	Sedimentation in a peptized and in an aggregated suspension (a) suspension; dense close-packed sludge (b) aggregated suspension; loose, voluminous sediment.	173
Figure 7-4:	Set-up for continuous staged-neutralization recycling process for S=5.	176
Figure D-1:	Fe(III) solubility for various sulphate concentrations at 25°C.	205
Figure D-2:	Fe(III) solubility for various sulphate concentrations at 75°C.	206
Plate 6-1:	Effect of pH on sludge produced - pH 3 (magnification: 5000 x).	105
Plate 6-2:	Effect of pH on sludge produced - pH 9 (magnification: 5500 x).	106
Plate 6-3:	Effect of conventional recycling on sludge produced - 20x (magnification: 1000x).	146
Plate 6-4:	Effect of conventional recycling on sludge produced - 20x (magnification: 2000x).	147
Plate 6-5:	Effect of conventional recycling on sludge produced - 20x (magnification: 5000x).	148
Plate 6-6:	Effect of conventional recycling on sludge produced - 20x (magnification: 5000x).	148
Plate 6-7:	Effect of staged-neutralization recycling on sludge produced - 10x (magnification: 1000 x).	157
Plate 6-8:	Effect of staged-neutralization recycling on sludge produced - 10x (magnification: 5000 x).	158
Plate 6-9:	Effect of staged-neutralization recycling on sludge produced - 20x (magnification: 1000 x).	160

Plate 6-10:	Effect of staged-neutralization recycling on sludge produced - 20x (magnification: 5000 x).	161
Plate 6-11:	Effect of staged-neutralization recycling on sludge produced - 20x (magnification: 1000 x).	162
Plate 6-12:	Effect of staged-neutralization recycling on sludge produced - 20x (magnification: 3300 x).	162

LIST OF TABLES

Description	Page #
Table 1-1: Federal metal mine effluent standards.	2
Table 1-2: Provincial effluent quality limits.	3
Table 2-1: Comparison of low density and high density sludge ponds.	10
Table 2-2: Comparison of neutralizing reagents.	11
Table 2-3: Some reported sludge characteristics.	12
Table 2-4: State of Fe(III) ions in solution, possible content of crystal forming compounds and phase content of the precipitate.	15
Table 2-5: Comparison of industrial iron precipitation processes.	30
Table 2-6: Solubility products of several ferric oxides reported in the literature	37
Table 3-1: Zero point charges of iron(III) oxides and hydroxides.	54
Table 3-2: The effect of polymer addition on effluent metal concentration and slurry settling rate.	66
Table 4-1: Iron species and thermodynamic data used for the construction of predominance area diagrams.	71
Table 5-1: Summary of tests and relationships examined.	87
Table 6-1: Precipitation profile data for Fe(III) hydrolysis to pH 6.	95
Table 6-2: Hydroxyl ions requirement to maintain final pH for 60 minutes.	101
Table 6-3: The effect of agitation on sludge characteristics.	114
Table 6-4: Experimental conditions for time variable tests.	118
Table 6-5: Effect of retention time: Summary of experimental results.	119

Table 6-6:	Summary of solutions treated to evaluate the ionic strength/complexation effect.	120
Table 6-7:	Summary of results from nitrate and sulphate media tests.	123
Table 6-8:	Process variables investigated.	128
Table 6-9:	Fe(III) hydrolysis: Response surface four-variable data.	129
Table 6-10:	Best conditions and results derived from the statistical design.	132
Table 6-11:	Summary of neutralization stages for Series B recycling.	151
Table F-1:	Dissolution test results.	208
Table F-2:	Typical data from a series B stage-neutralization recycling test.	208

CHAPTER 1: INTRODUCTION

1.1 The Issue

Acidic drainage and mine/mill effluent treatment using lime is a common practice in the Canadian mineral industry, where lime is utilized to neutralize acidity and precipitate heavy metals. This methodology is simple and economically advantageous, however it tends to produce large volumes of potentially hazardous sludge, has high maintenance requirements and often fails to meet new, more stringent environmental standards.

Mine/mill effluents and particularly acid mine drainage (AMD) may contain relatively high (from an environmental point of view) concentrations of sulphate and ferric ions. High concentrations of base metals such as copper, nickel, zinc, aluminum, or cadmium, are also encountered at pH values significantly below 7. If acidic drainage is left uncollected and untreated, the drainage could contaminate groundwater and local watercourses, damaging the health of plants, wildlife and fish (Filon et al., 1991).

Acidic mineral effluents are treated to meet federal and provincial threshold values by removing suspended solids, neutralizing free acidity and removing iron and other metals, particularly arsenic, copper, lead, nickel, cadmium and zinc. The federal and provincial regulations are outlined in Tables 1-1 and 1-2 (Wildman, 1993; Scott, 1992). Provincial requirements are stricter in most cases, while public pressures continue to demand further reductions of acceptable metal concentrations and inclusion of new substances in the regulations list.

1.2 The Method of Treatment

The Canadian industry is attempting to meet these regulations by using lime neutralization technology, which is considered the "Best Available Technology Economically Achievable" (Dinardo et al., 1992). This technology involves:

- neutralization of the effluent with hydrated lime (Ca(OH)_2)
- oxidation of ferrous iron under mildly alkaline conditions by aeration

- precipitation of ferric iron and base metals at pH of 9 to 10, and
- clarification following coagulant/flocculant addition.

Table 1-1: Federal metal mine effluent standards (Scott, 1992).

Parameter	Monthly Average	Daily Average	Grab Sample
Arsenic (mg/L)	0.5	0.75	1.0
Copper (mg/L)	0.3	0.45	0.6
Lead (mg/L)	0.2	0.3	0.4
Nickel (mg/L)	0.5	0.75	1.0
Zinc (mg/L)	0.5	0.75	1.0
Suspended Solids (mg/L)	25	37.5	50
Ra 226 (Bq/L)	0.37	0.75	1.11
pH (minimum)	6.0	5.5	5.0

1.3 The Present Research

In view of the increasingly more stringent environmental standards applied to the discharge of acidic mineral effluents and the disposal of the treatment sludges, it was the author's objective to revisit neutralization from a fundamental chemical point of view and to elucidate the principal factors which determine the properties of the generated sludges. By establishing these underlying fundamental relationships it was hoped to generate ideas, on the basis of which means could be devised or process modifications could be suggested, to overcome the limitations of the conventional neutralization technology.

The task of reviewing the literature on neutralization as it pertains to effluent treatment was arduous, as neutralization is a well-established process and has been in use for decades. A careful examination of the lime neutralization process as applied to predominately $\text{Fe}_2(\text{SO}_4)_3/\text{H}_2\text{SO}_4$ effluents shows it to be dominated by the following two principal reaction;

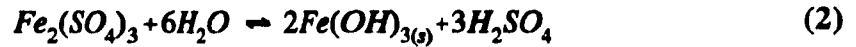
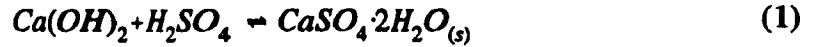


Table 1-2: Provincial effluent quality limits (Wildman, 1993; Scott, 1992).

Parameter (mg/L) ¹	Newfoundland	Quebec	Ontario	Saskatchewan ²	British Columbia ^{3,4}	New Brunswick Nova Scotia Manitoba ⁵
As (total)	0.5	0.5	0.5	0.5	0.10-1.0	0.5
As (trivalent)					0.05-0.25	
Cu	0.3	0.3	0.3	0.3	0.05-0.3	0.3
Cd	0.05	0.001	0.001		0.01-0.1	
CN		1.5	1.0	1.0	0.1-0.5	
Fe		3.0	1.0		0.3-1.0	
Pb	0.2	0.2	0.2	0.2	0.05-0.2	0.2
Hg	0.005	0.001			NIL-0.005	
Ni	0.5	0.5	0.5	0.5	0.2-1.0	0.5
Zn		0.5	0.5	0.5	0.2-1.0	0.5
Ra 226 (Diss) Bq/L						0.37
Ra 226 (Total) Bq/L				0.37		
Suspended Solids	30.0	25.0	15.0		25-75	25
pH	5.5-9.0	6.5-9.5	6.0-9.5	6.0-9.5	6.5-8.5, 6.5-10	>6.0

1 - Concentrations are given in mg/L, except for Ra 226.

2 - Additional standards for Saskatchewan (total values): Pb 210 - 0.92 Bq/L; Th 230 - 1.85 Bq/L and U - 2.5 mg/L.

3 - Concentrations are total values, except for British Columbia and the federal limit for Ra 226, where dissolved values specified. However, the limit for Hg in British Columbia is total Hg.

4 - The lower values are for new mines and the higher values are for old mines.

5 - New Brunswick, Nova Scotia, and Manitoba use federal limits

To elucidate the fundamental chemistry of the system reactions [1] and [2] had to be isolated. The choice was made to focus the research on the iron(III) hydrolysis reaction [2] as the product of this reaction was taken to be primarily responsible for the undesirable physical sludge properties. The hydrolysis reaction was isolated from

the gypsum producing reaction by choosing a neutralization reagent (other than lime) that did not precipitate a secondary product (such as gypsum). After preliminary tests, caustic soda (NaOH) was chosen as the neutralizing reagent since it was found not to cause any (undesirable) jarosite precipitation under the conditions applied in the present investigation.

Due to the fundamental approach taken in this research an extensive literature survey was required. The first cycle of the literature review centred on the industrial practice of neutralization. This part is covered in section 2.1. It was then necessary to shift the focus to iron(III) hydrolysis. Iron(III) hydrolysis literature was reviewed in four topics; speciation, precipitation pathways, solids formation, and factors affecting solids formation. This literature review that is covered in Section 2.2 revealed that the literature was dominated by colloid chemistry studies, absent was an analysis of the hydrolysis of Fe(III) from a crystallization point of view.

In light of the fact that crystallization theory had not been used in the past for the analysis of hydrometallurgical precipitation systems, it was decided that a review of crystallization theory comprising aspects of nucleation, growth and aggregation of particles in solution was necessary. This review of the background theory is presented in Chapter 3.

After reviewed the available literature and acquiring the knowledge specific to the system, a thermodynamic evaluation of the solution complexes and solubility diagrams of the Fe(III)-SO₄-H₂O system was completed with aid of the F*A*C*T program (Bale et al., 1991). Documentation is contained in Chapter 4.

The experimental work was conducted (Chapters 5, 6) in three stages. The first stage involved an evaluation of single variable effects such as pH, neutralization rate, and temperature. The second stage examined the interactive effects of these variables via statistical design. Finally, neutralization tests were performed involving the recycling of solids both in the absence of, and under controlled supersaturation. It was at this point that the fruits of the extensive literature survey became apparent. This was the first time in a hydrometallurgical system that supersaturation control had been applied and the results were truly superior to results obtained in similar

systems without supersaturation control.

The results and the practical implications of the present investigation are discussed in Chapter 7, while Chapter 8 concludes the thesis.

CHAPTER 2: LITERATURE SURVEY

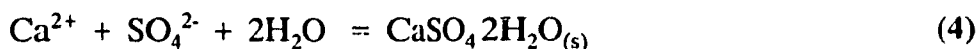
2.1 Neutralization

The neutralization of free acid and the concurrent removal of metals by precipitation as hydroxides under alkaline conditions is the most common method of chemical treatment for wastewaters at both active and non-active mines in Canada (Environment Canada, 1987). Many of the mining operations that discharge acidic waters from the mine or mill use a lime neutralization process to treat the acidity as well as to co-precipitate the heavy metals. A range of pH 9.5 - 11 is adequate for treating most mine and metallurgical waste streams with lime. Sludge handling and dewatering can, however, be a problem with the thixotropic sludge which contains only 1-2% solids (Bell, 1975) and therefore requires large storage areas. Several extensive reviews on the treatment of acidic mineral effluents can be found in the literature (Skelley and Loy, 1973; Environment Canada, 1987; Vachon et al., 1987; Ritcey, 1989).

The reactions commonly given for neutralization and precipitation (Okoro and Taylor, 1974) are as follows:



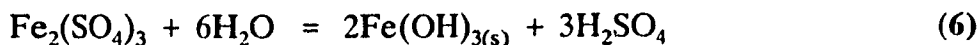
When the product of the calcium and sulphate ion activities exceeds the solubility product, gypsum precipitates:



Dissolved ferrous sulphate is oxidized to ferric sulphate with air:



and ferric sulphate undergoes hydrolysis producing an amorphous hydroxide phase:



The iron hydroxide sludge will dehydrate and form a stable hematite precipitate with time as hematite is more thermodynamically stable than ferric hydroxide.



In addition to ferric iron, which readily precipitates as hydroxide, most of the other common base metals ions (including ferrous iron) precipitate with the progressive

neutralization of the solution as well. The order of heavy metal hydroxide precipitation as a function of pH is given in Figure 2-1. Because of this sequential order of hydroxide precipitation investigators on the past have proposed the recovery of metals from wastewaters by selective titration (Jenke and Diebold, 1983).

The solid/liquid separation of neutralization sludges is arguably the most difficult aspect of the treatment process. Metal hydroxide precipitates tend to be colloidal and amorphous, retaining a lot of water in the precipitate structure. Over the years, different neutralization approaches have been practised by the industry with the aim of improving the quality of the treatment sludges. At present, three alternative neutralization routes, as shown in Figure 2-2 (Kuit, 1980) exist. The first scheme simply involves the addition of lime to the effluent and subsequent disposal in the tailings pond. This is obviously the least expensive of the routes. The direct mechanical agitation process (Type 2) requires an independent plant incorporating a vessel for lime reaction and iron oxidation and precipitation followed by a clarifier or settling pond. The major drawback of this process variant is sludge handling. Due to the low density the sludge tends to remain uncompacted for considerable time and requires large retention volume. The high density sludge route (Type 3), by contrast, results in a minimum of sludge volume to handle.

The Bethlehem High Density Sludge (HDS) process (Temmel, 1972) was developed to treat acid-metal sulphate solutions and produce a coarse, relatively compact and easily settleable sludge. The developers of this process found that at least five factors were important in successful implementation of the process. First, a high ferrous to ferric ratio is advocated (>70% ferrous produced high density sludge). Second, the process requires at least 25 times recycle of sludge. Third, the process requires the dilution of the lime by the recycled sludge ahead of the neutralization step. Direct dosing of lime to the wastewater results in voluminous, hard to settle precipitates. Fourth, the optimal neutralization pH was 7.2 to 7.7. At this pH air oxidation of ferrous iron was satisfactory. Higher pHs were detrimental to solids quality. Fifth, the optimal retention times were determined to be one minute in the sludge reaction tank and 10 minutes in the neutralization and oxidation

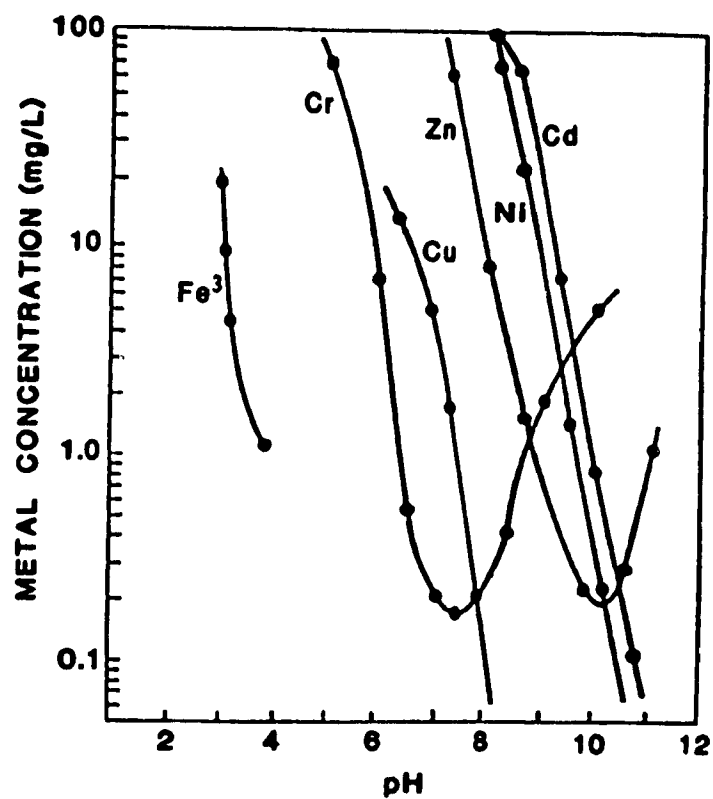
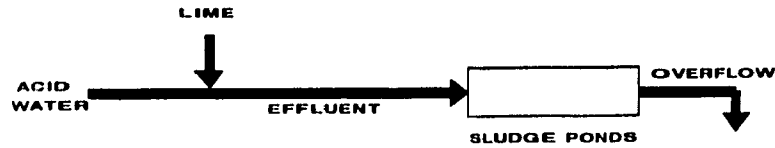
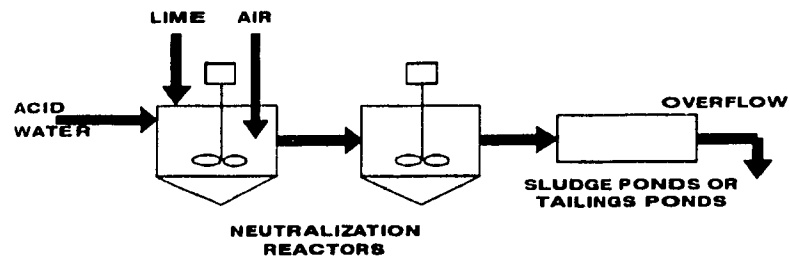


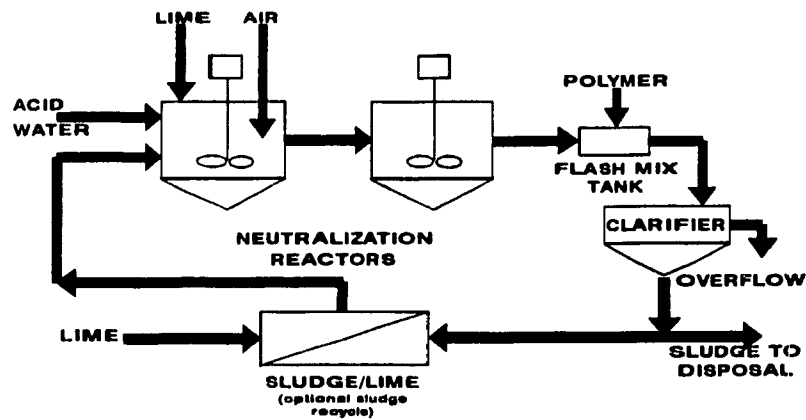
Figure 2-1: Precipitation of heavy metals as hydroxides (Skelley and Loy, 1973).



TYPE 1: Lime addition to effluent or tailings lines.



TYPE 2: Lime addition to neutralization reactors.
Solid/liquid separation in ponds



TYPE 3: Lime addition to neutralization reactors.
Solid/liquid separation in clarifiers.

Figure 2-2: Lime neutralization process alternatives (Kuit, 1980)

tank. The reactors were not prone to scale formation in the Bethlehem study.

The main advantages and disadvantages of low density and high density sludge ponds are shown in Table 2-1.

Table 2-1: Comparison of low density (Type 2) and high density (Type 3) sludge process (Bell, 1975; Vachon, 1987).

LOW DENSITY SLUDGE

Advantages

- low maintenance costs
- low operating costs
- low capital costs
- sludge storage facility (lagoons)

Disadvantages

- wind or thermal disturbance
- will re-suspend settled flocs
- requires large area
- large reclamation costs
- poor control over discharge
- short circuiting can occur
- not acceptable for final discharge

HIGH DENSITY SLUDGE

Advantages

- minimal area requirements
- reduced volume for disposal
- may be suited for long term storage
- generation of high sludge densities, so settling is rapid
- more efficient utilization of lime
- non-amphoteric precipitate
- increased clarifier overflow solution

Disadvantages

- higher capital, operating and maintenance costs
 - requires closer control
-

Lime is the common neutralizing agent used in effluent treatment, however several other neutralizing agents are available. A comparison of the neutralizing effectiveness of various alkalis that can be used for neutralization is given in Table 2-2 (Skelley and Loy, 1973; Ritcey, 1989). The basicity factor or available alkalinity is the grams of CaCO_3 equivalent per gram of alkaline agent.

Reagent utilization is a measure of how much of the added reagent was consumed in the precipitation reaction versus how much was unreacted or consumed by side reactions. In the case of soluble reagents such as NaOH , reagent utilization

is almost complete. Solid reagents on the other hand, tend to become encapsulated by metal hydroxides or other precipitates and thus their utilization is reduced. Maximum reagent utilization for solid reactants is achieved by minimizing initial particle size (fine grinding of lime, limestone, etc.), slaking in the case of lime or magnesite to solubilize the maximum amount of reagent before precipitation (this is not effective for limestone) or abrading the encapsulated precipitate layer away from the surface of the unreacted particles.

Table 2-2: Comparison of neutralizing reagents (Skelley and Loy, 1973; Ritcey, 1989).

Reagent	Basicity Factor
Quick Lime (calcium oxide)	1.786
Ammonium hydroxide	1.429
Hydrated lime (calcium hydroxide)	1.351
Caustic Soda (sodium hydroxide, 50%)	1.250
Magnesite (magnesium carbonate)	1.186
Limestone (calcium carbonate)	1.000
Soda Ash (sodium carbonate, 50%)	0.943
Dolomite (calcium-magnesium carbonate)	0.543

The existing practice of treating acidic mineral effluents with excess lime addition is clearly not satisfactory because of the ferric hydroxide gel formation that has poor filtering and settling properties. Some typical values for percent solids and settling rates are given in Table 2-3. These data represent sludges generated via lime neutralization. Industry data suggest that the use of vacuum filters for dewatering lime sludges will achieve a 45% to 50% filter cake, while sodium hydroxide sludges generally dewater to 20% in vacuum or press filters making them more difficult to handle but contain no gypsum (Gionet et al., 1987; MacDonald et al., 1989).

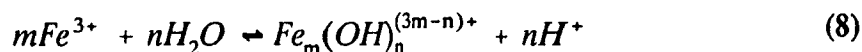
Table 2-3: Some reported sludge characteristics.

#	Solids (wt %)	Settle Rate (m/hr)	SO ₄ (wt %)	Fe (wt %)	Comments	References
1	2.08		0.86	3.7	sp/cc	MacDonald et al., 1989
2	3.63		0.05	1.2	sp/cc	"
3	7.74		2.84		sp/cc	"
4	20.55		0.45	0.3	HDS	"
5	3.93		0.11	0.7	sp/cc	"
6	1.87		0.43	29.4	sp/cc	"
7	0.59		0.12	10.1	sp/cc	"
8	0.35		0.12	6.6	sp/cc	"
9	20.60		1.87	25.3	HDS, f	"
9	79.00		9.72	25.0	HDS, a	"
10	15.40		1.17	19.3	HDS, f	"
10	25.90		2.83	20.5	HDS, a	"
11	48.7		3.60	7.0	sp/cc	"
12		1.14			p, r(e)	Huck et al., 1974
13		2.03			p	"
14		2.23			p	"
15		1.73			p	"
16		1.78				"
17		7.31			p	"
18		1.01			r(2:1)	"
19		1.47			r(5:1)	"
20		1.72			r(8:1)	"
21		6.70			p, r(14:1)	"
22		4.27			p, r(21:1)	"
23		1.40			p, r(19:1)	"
24		1.12			p, r(11:1)	"
25		3.25			p, r(35:1)	"
26		0.45				"
27		2.36			p	"
28	14.2	2.21			p, r(14:1)	"
29	2				cc	Kuit, 1980
30	20-30				HDS	"
31	1-2				cc	Bell, 1975
32	13				p	"
33	25.2				p, r(3:1)	"
34	18				p, r(2.5:1)	"
35	3.4					"
36	7.2				p	"
37	1.4					"
38	3.1				p	"
39	6.8				r(5.3:1)	"
40	14.0				r(14.3:1)	"
41	14.7				p, r(40:1)	"
42	22.8				p, r(18:1)	"
43	2					Kuyucak et al., 1991
44	2.4				p	"
45	2.4				r	"
46	6.8				HDS	"
47	22.0				HDS	Bosman, 1974

NOTE: sp = settling pond; cc = conventional clarifier; HDS = high density sludge clarifier; f = fresh precipitate; a = aged precipitate; p = polymer added; r() = recycled precipitate ratio (kg solid recycled/kg solid precipitated), (e) = erratic recycle ratio.

2.2 Fe(III) Hydrolysis

The hydrolysis of Fe(III) can be represented by the equation (Yakovlev et al., 1977)



where $Fe_m(OH)_n^{(3m-n)+}$ is the partially hydrolyzed Fe(III) species:

$$* \beta_{mn} = \frac{[Fe_m(OH)_n^{(3m-n)+}][H^+]^n}{[Fe^{3+}]^m} \quad (9)$$

When the concentration of Fe^{3+} is high or the concentration of H^+ is low Fe(III) hydroxide ($Fe(OH)_3$), oxyhydroxide ($FeOOH$), or oxide (Fe_2O_3) phases form depending on the temperature of precipitation. Further complications with the precipitation reaction and the type of solids produced are caused by the method and rate of neutralization, and the presence of complexing anions. In subsequent sections the aqueous speciation of Fe(III), the mechanism of Fe(III) hydrolysis and the properties of the precipitated solids are reviewed.

2.2.1 Speciation

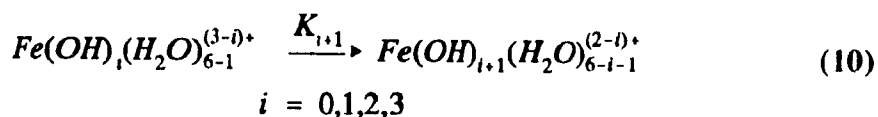
Ferric ion forms octahedral hydrates ($Fe(H_2O)_6^{3+}$) or complexes in solution. The literature shows that ferric ions readily hydrolyze at room temperature to give $FeOH^{2+}$, $Fe(OH)_2^+$, $Fe_2(OH)_2^{4+}$, and $Fe_3(OH)_4^{5+}$ (Lamb and Jacques, 1938, Biedermann and Schindler, 1957). Assessments of magnetic, infrared, and kinetic data on aqueous Fe(III) solutions have confirmed the existence of the dimeric species $Fe_2(OH)_2^{4+}$ (Flynn, 1984). It was also reported that ferric hydroxide has a strong tendency to form supersaturated solutions (Biedermann and Schindler, 1957; Feitknecht and Michaelis, 1962; Sylva, 1972) containing significant amounts of neutral molecular $Fe(OH)_3^o_{(aq)}$ species.

Much less is known about hydrolysis products of ferric ions at elevated temperatures. However, it is well known that heating salt solutions accelerates metal hydrolysis and promotes polynuclear compound formation (Matijevic et al., 1975).

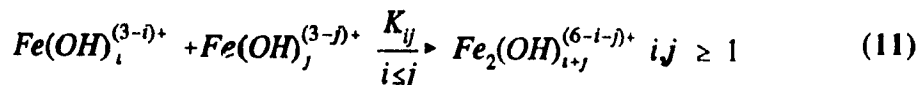
Thus it is expected that at higher temperatures species of the kind $\text{Fe}_2(\text{OH})_2^{4+}$ and $\text{Fe}(\text{OH})_3^0$ will be more abundant.

The presence of sulphate is reported to accelerate the condensation of hydrolyzed ferric ions (Wendt, 1962) and to cause the formation of other complex solutes. In acidic solutions the FeSO_4^+ ion dominates (Sillén and Martell, 1964). In somewhat less acidic solutions, or with heating, more complex basic ferric sulphates are reported to form, such as $\text{Fe}_2(\text{OH})_3(\text{SO}_4)_{3/2}$, $\text{Fe}_3(\text{OH})_2(\text{SO}_4)_{1/2}$ (Kiyama and Takada, 1973) or $(\text{FeOH})(\text{HSO}_4)_2$ (Arden, 1951). Although the unequivocal characterization of those species has not been presented.

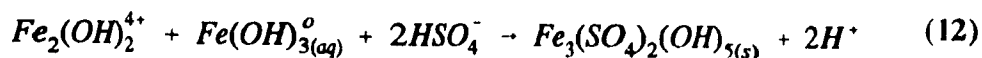
The mononuclear species $\text{Fe}(\text{OH})_i^{(3-i)+}$ (abbreviation of $\text{Fe}(\text{OH})_i(\text{H}_2\text{O})_{6-i}^{(3-i)+}$) react with each other to form dinuclear and, subsequently, polynuclear complexes



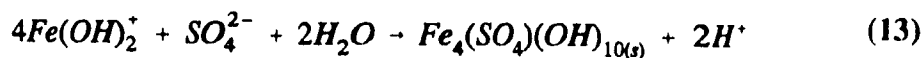
(Schneider and Schwyn, 1987)



Hsu and Ragone (1972) suggested that the species $\text{Fe}(\text{OH})_{3(\text{aq})}$ is involved in ferric hydroxide precipitation processes. The proposed reaction [12] does not preclude the formation of basic ferric sulphate compounds as intermediates.



For the formation of the compound $\text{Fe}_4(\text{SO}_4)(\text{OH})_{10}$, which is found to coprecipitate on aging ferric sulphate solutions, Arden (1951) suggested a reaction of the type,



with initial formation of $\text{Fe}(\text{OH})\text{SO}_4$ and $[\text{Fe}(\text{OH})_2]_2\text{SO}_4$. All suggested mechanisms involve simple complexes which have been found in hydrolyzed ferric salt solutions.

The proposed reactions [12] and [13] remain, however, speculative.

Sylva (1972) stated that despite innumerable studies of precipitation in hydrolyzed iron(III) solutions very little is known about the relationship between hydrolysis products in solution and the mechanism by which a solid product is produced. It is obvious from the data reported in Table 2-4, that the pH of the medium has a dominating influence on the chemical composition of the precipitate formed.

Table 2-4: State of Fe(III) ions in solution and phase content of the precipitate (modified from Paspopov et al., 1991).

pH	Predominant Complex(es) Present	Content of the precipitate
pH < 2	$\text{Fe}(\text{OH})_2^+ (\text{aq})$ $\text{FeSO}_4^+ (\text{aq})$	$(\text{H}_3\text{O})\text{Fe}_3(\text{SO}_4)_2(\text{OH})_6$ $\text{Fe}_4\text{SO}_4(\text{OH})_{10}$
$2 < \text{pH} < 4.5$	$\text{Fe}(\text{OH})_3^\circ (\text{aq})$	$\alpha\text{-FeOOH}$ $\alpha\text{-Fe}_2\text{O}_3$
$4.5 < \text{pH} < 6$	$\text{Fe}(\text{OH})_3^\circ (\text{aq})$	$\alpha\text{-FeOOH}$
$6 < \text{pH} < 9$	$\text{Fe}(\text{OH})_3^\circ (\text{aq})$	$\alpha\text{-FeOOH}$
$9 < \text{pH} < 12$	$\text{Fe}(\text{OH})_3^\circ (\text{aq})$	$\gamma, \alpha\text{-FeOOH}$
pH > 12	$\text{Fe}(\text{OH})_4^- (\text{aq})$	$\alpha\text{-FeOOH}$

Yakovlev et al. (1977) showed the hydrolysis behaviour of Fe(III) in sulphate solutions to be approximately the same as in uncomplexed Fe(III) solutions, while they concluded that the sulphate-hydroxyl dimer, $\text{Fe}_2(\text{OH})_2(\text{SO}_4)_2$ was the prevalent species. This or similar species would appear necessary to explain the precipitation of iron hydroxo-sulphates in acidic media, the incorporation of anions in FeOOH precipitates and the effect of the anion on the compound precipitated (eg., α , β or $\gamma\text{-FeOOH}$). Later, Yakovlev et al. (1978) confirmed the presence of mixed species and noted that the extent of hydrolysis was slightly less in sulphate than in perchlorate or nitrate media.

Equilibrium data on hydrolysis up to 1974 are presented in an excellent

monograph (Baes and Mesmer, 1976), where selected equilibrium constants are compiled and discussed.

2.2.1.1 Polymer formation

The formation of Fe(III) oxyhydroxide or oxide phases from acidic solution, as shown in Figure 2-3, goes through the formation of polymers (Dousma et al., 1979). These polymers consist of spheres 1.5-3.0 nm in diameter (Davis and Leckie, 1978), containing $\sim 10^2$ Fe(III) ions, most likely in octahedral $\text{Fe}(\text{O},\text{OH},\text{H}_2\text{O})_6$ coordination. These $\text{Fe}(\text{O},\text{OH},\text{H}_2\text{O})_6$ octahedra are condensed most probably by sharing edges or vertices; as suggested by Spiro et al. (1966) for their tetrahedral interpretation, they may form long chains or ribbons which are coiled and to some extent cross linked (Flynn, 1984) via oxobridges or SO_4 or OH bridges (Dutrizac, 1980). The structural studies of Brady et al. (1968) suggest that initially, the polymer is formed as a narrow ribbon approximately 100 times longer than is wide.

The isolated hydrolytic polymer generated in the presence of sulphate ions is cationic. The OH/Fe mole ratios in the polymer range between 2.74 - 2.90. The OH/Fe ratio in the polymer increases with age, this observation being consistent with the pH decrease observed on aging of solution containing the polymer (Murphy et al., 1976; Davis and Leckie, 1978; Flynn, 1984).

Dissociation of the polymer is a very slow reaction (Spiro et al., 1966), although the reaction is accelerated with temperature (Dousma and de Bruyn, 1976). Dissociation of the polymer is first order in $[\text{H}^+]$ and [polymer] and the rate is slow ($k_{\text{diss}} \sim 5 \times 10^{-4} \text{ Msec}^{-1}$). The polymer composition is almost independent of the degree of hydrolysis, although there is a small increase in OH/Fe ratios with increasing degree of hydrolysis (Spiro et al., 1966).

Polymer aging and precipitation are apparently not consecutive processes. It may well be that precipitation proceeds not from the polymer, but from low molecular weight components of hydrolyzed solutions. A weight-average molecular weight of 1.4×10^5 was assigned to the iron polymer $([\text{Fe}(\text{OH})_x^{(3-x)+}]_n, 2.3 < x < 2.5)$ in the solution analyzed (Spiro et al., 1966).

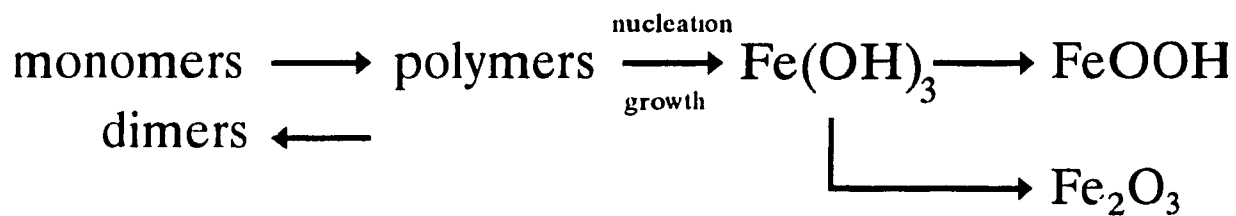


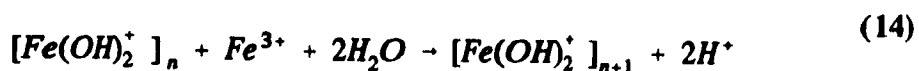
Figure 2-3: Formation of iron(III) oxide phase from acidic solution (Dousma et al., 1979).

The growth of the large polymers into crystallites and eventual agglomeration of the crystallites into coarse precipitates has also been studied, at least for FeOOH precipitation. The individual rods mat together to form relatively coarse particles which settle rapidly, but the conditions affecting the agglomeration are ill defined (Dutrizac, 1980).

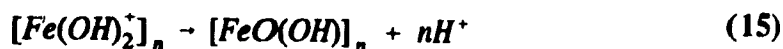
The amount of iron present as polymer increases linearly with base addition. The formation of polymer is indicated by changes in solution from the yellow characteristic of FeOH^{2+} and $\text{Fe}_2(\text{OH})_2^{4+}$ which have strong adsorption bands in the 300-360 nm wavelength region, to the deep red-brown of the polymers which adsorb strongly in the visible region (Knight and Sylva, 1974).

2.2.2 Precipitation Pathways

Mechanisms suggested for formation and aging of the hydrolytic polymer involve condensation of monomeric species $[\text{Fe}(\text{H}_2\text{O})_6-n(\text{OH})_n]^{(3-n)+}$ to form polymers in which Fe(III) ions are bridged by OH^- groups (olation, reaction 14) or O^{2-} ions (oxolation, reaction 15) (Dousma and de Bruyn, 1976, 1978, 1979; Dousma et al., 1979; Flynn, 1984).

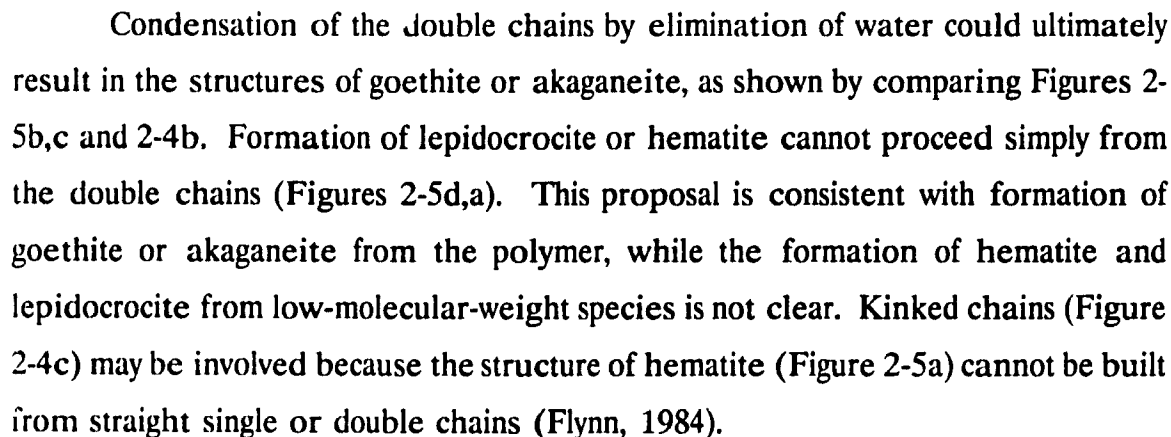


(I)



(II)

The structures of polymers I and II are given below in equation 16. The oxolation reaction 15 is considered to be much slower than the ololation reaction 14 (Dousma and de Bruyn, 1976, 1978, 1979; Dousma et al., 1979; Flynn, 1984). The representation of oxolation by reaction 15 suggests straightforward deprotonation, which should be fast and reversible. A more plausible representation of oxolation is reaction 17 (Flynn, 1984), which represents it as a condensation-deprotonation of



2.2.2.1 Olation



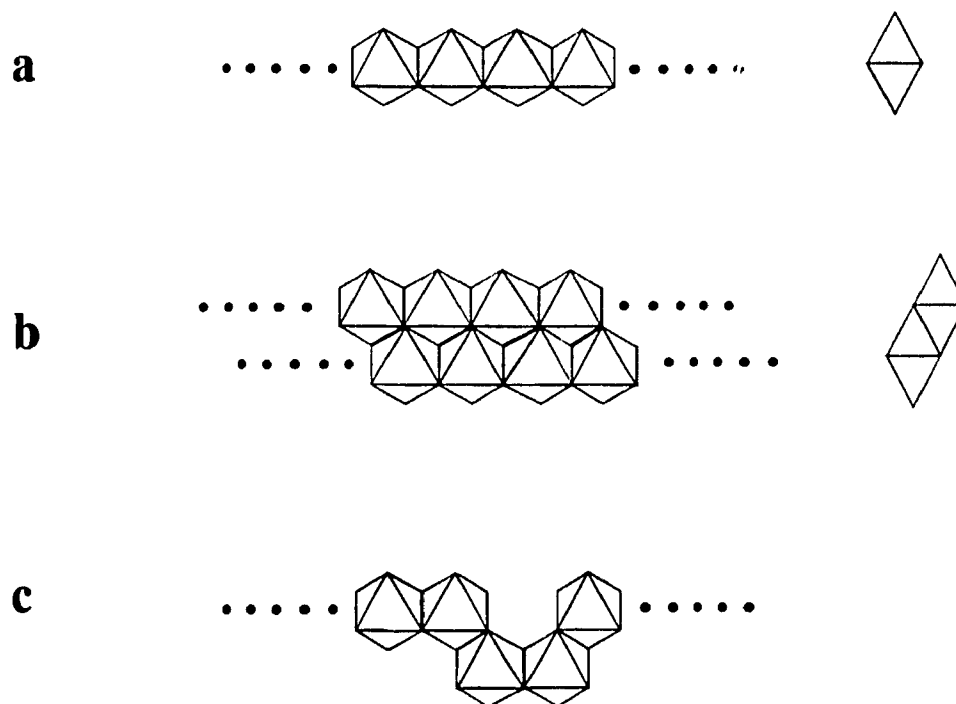


Figure 2-4: Chains of $\text{Fe}(\text{O}, \text{OH}, \text{H}_2\text{O})_6$ octahedra: (a) Single straight chain, *trans*- $\text{FeX}_2\text{-X}_{4/2}$; side and end views. (b) Double straight chain, *cis-fac*- $\text{FeXX}_{2/2}\text{X}_{3/3}$; side and end views. (c) Single kinked chain, *trans*- and *cis*- $\text{FeX}_2\text{X}_{4/2}$ (Flynn, 1984).

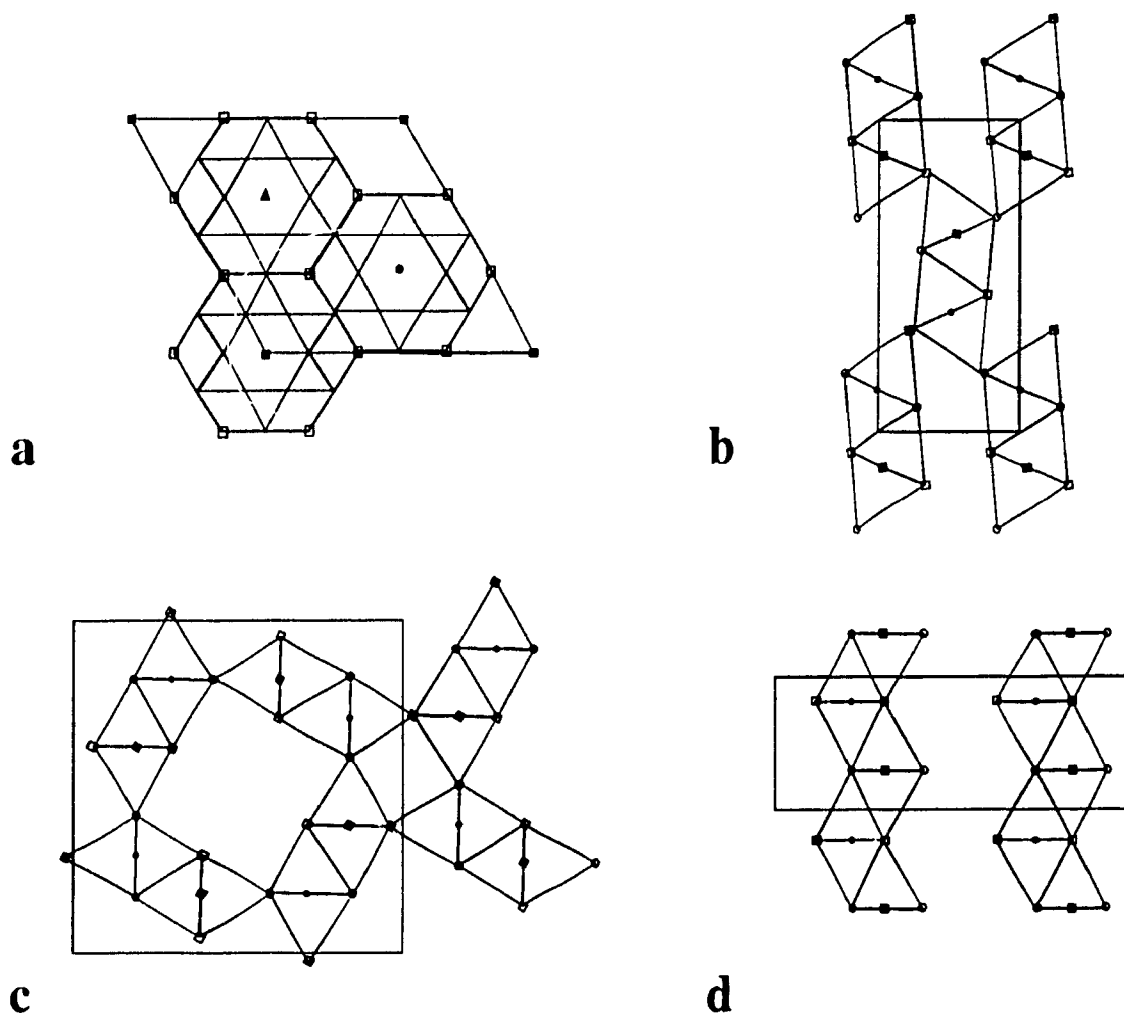
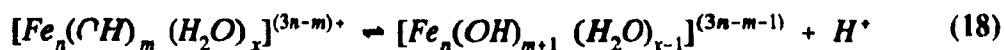


Figure 2-5: Schematic crystal structures: (a) Hematite (α -Fe₂O₃) (R3c, Z=6; a=503, c=1375 pm); projection along [001], (●) Fe at z=0, 1/2, 2/3; (Δ) Fe at z=0, 1/3, 1/2, 5/6; (■) Fe at z=1/6, 1/3, 2/3 5/6; (□) O at z=1/4, 7/12, 11/12. (b) Goethite (α -FeOOH) (Pbnm, Z=4; a=464, b=998, c=303 pm); projection along [001], (●) Fe at z=1/4; (■) Fe at z=3/4; (○) O at z=1/4; (□) O at 3/4. (c) Akaganeite (β -FeOOH) (I4/m, Z=8; a=1048, c=302 pm); projection along [001], (●) Fe at z=0; (■) Fe at z=1/2; (○) O at z=0; (□) O at z=1/2. (d) Lepidocrocite (γ -FeOOH) (Bbmm, Z=4, A=1253, b=388, c=307 pm); projection along [001], (●) Fe at z=0; (■) Fe at z=1/2; (○) O at z=0; (□) O at z=1/2 (Flynn, 1984).

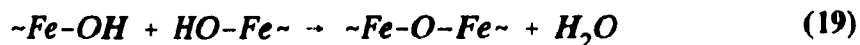


Reactions involving water displacement become faster as the charge per iron atom decreases; consequently, the polymerization rate increases as one proceeds in the reaction in Figure 2-7 from left to right. The rates also increase when the reaction is transversed vertically, because the acidity of polymers is noticeably higher than the acidity of the corresponding monomer, due to the charge effect on the protolytic equilibrium.

The complex manifold of Figure 2-7 represents just one type of the polymerization process, i.e., through the formation of hydroxide bridges, $Fe-O_{II}-Fe$. This process is known as olation, and seems to be predominant in the first stages of polymerization. Experimental data from Dousma and de Bruyn (1976, 1978, 1979, 1979) support the notion that olation processes are reversible; depolymerization may be easily achieved by acidifying the solution. Gel formation (olation) is promoted by the presence of excess base, rapid addition of base, poor agitation, and low temperatures (Dutrizac, 1980).

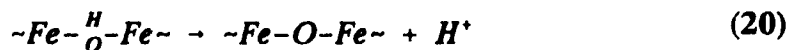
2.2.2.2 Oxolation

The second type of polymerization also involved in the formation of hydrous $Fe_2O_3 \cdot xH_2O$ is oxolation; here oxobridges are formed (Blesa and Matijević, 1989):



In the above equation [19], the reactants must be understood as polymers of variable size. An oxobridge results from two hydroxide ligands through dehydration. Dousma and de Bruyn (1976, 1978) consider oxolation to be essentially irreversible.

Although the process does not involve protons, formation of oxobridges is very sensitive to pH, because hydrolyzed species are involved as reactants. Other authors (Dousma and de Bruyn, 1976, 1978; Dutrizac, 1980; Flynn, 1984) have chosen to write oxolation as deprotonation of olated complexes:

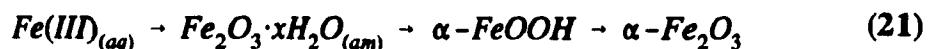


Flynn (1984) pointed out that such a process could not explain the slowness and the irreversibility of oxolation. It is probable that chain folding and cross-linking is involved in oxolation, giving rise to oxygen atoms with high coordination numbers. Such oxide ions are known to be less reactive (Lewis and Farmer, 1986). Furthermore, cross-linking should provide sterically protected groups of much decreased reactivity. A similar interpretation, assigning to oxolated complexes structures in which up to five ligands may be shared, was proposed by Flynn (1984).

Particles result both from the operation of the polymerization processes depicted in Figure 2-7 and from interactions of the type shown in Equations [19, 20]. Although it is possible, in principle, to generate solids through olation only (i.e., resulting in $\text{Fe}(\text{OH})_3 \cdot x\text{H}_2\text{O}$), experimental studies seem to indicate that reactions represented in equations [19,20] always begin to take place before the solid is generated through neutralization of the originally acidic solutions (Dousma and de Bruyn, 1976). It is thus only gels prepared at high pH that may contain little or no oxobridges, but no evidence is available on the structure of these gels.

2.2.3 Solids Formation and Phase Transformations

The formation of the stable solid phase proceeds through the following stages:



reflecting the relative ease of homogeneous nucleation in each phase. This is an example of Stranski's rule (Kern, 1985) which states that the least stable phase nucleates first, because the interfacial energy requirements are less stringent. The validity of the rule (also called the "Ostwald Step Rule") is quite general, provided that homogeneous nucleation determines the rate.

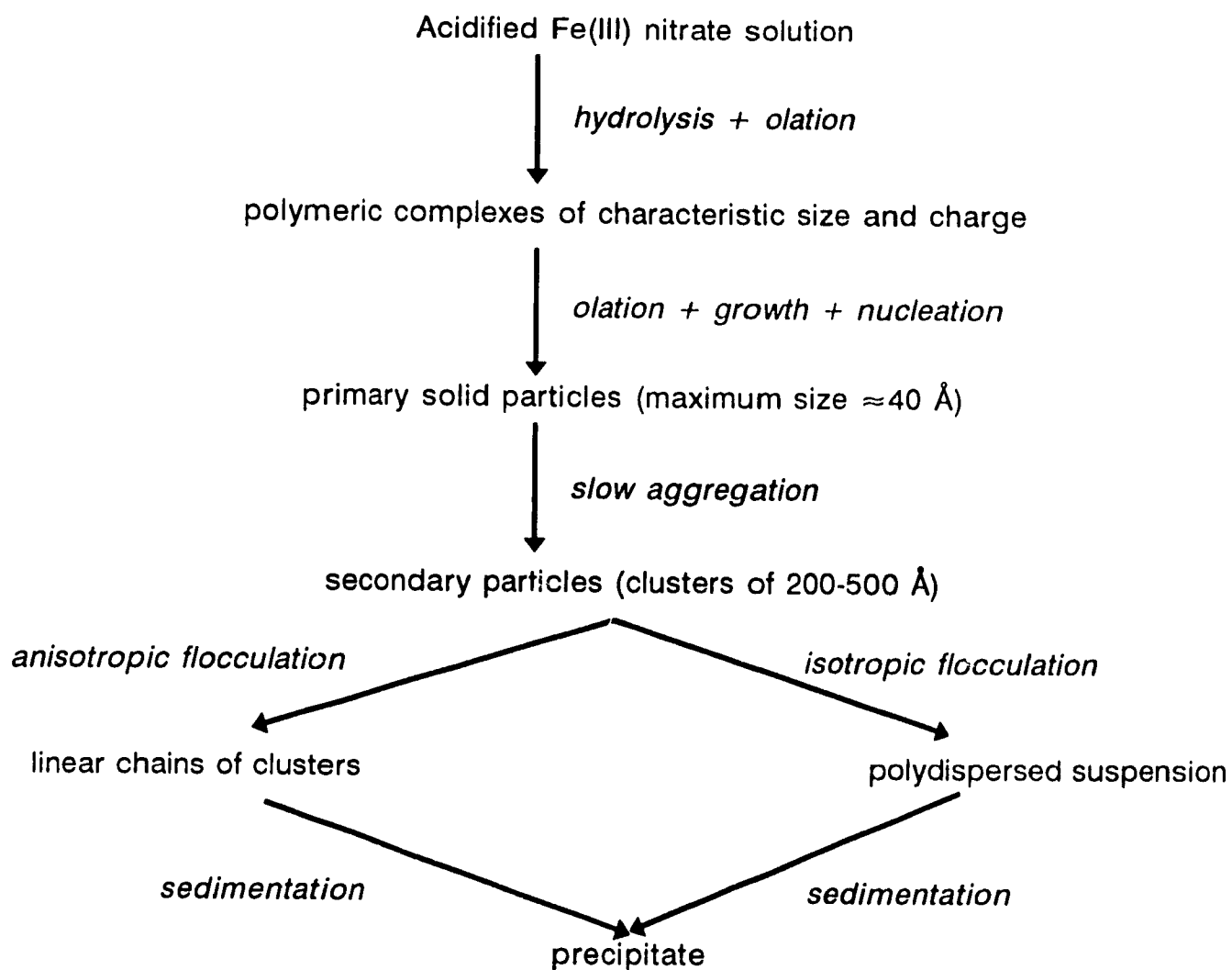


Figure 2-6: The development of a hydrous iron oxyhydroxide (Dousma and de Bruyn, 1978).

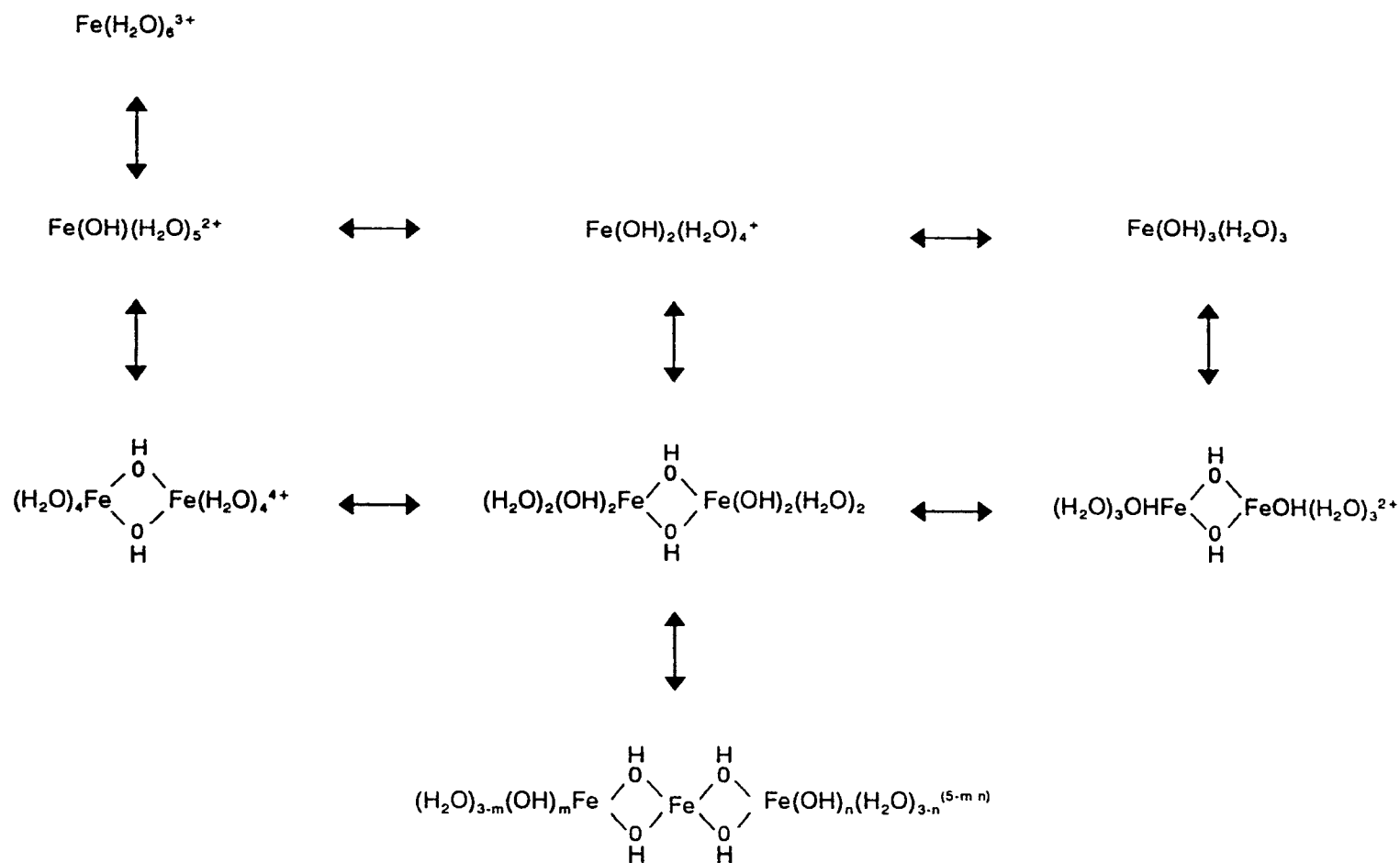


Figure 2-7: Olation reaction matrix (Blesa and Matijević, 1989).

The fundamental features of solid formation as a result of hydrolysis involve the following stages (Blesa and Matijević, 1989).

- (1) Slow release of ionic species (precursor) susceptible to further transformation. These precursors build up while undergoing dynamic transformations without solid phase formation, until a certain supersaturation is reached.
- (2) At this stage, a burst of nuclei takes place relieving, to a large extent, the supersaturation of the solution. It has been suggested that nuclei of several phases may form simultaneously, the ratio of which is determined by solubility considerations (Sugimoto and Matijević, 1980; Ozaki and Matijević, 1985).
- (3) Continued slow release of the precursor species into solution is compensated by the growth of the nuclei. The final size of the particles formed depends on the number of nuclei formed and the anion incorporated during the particle growth.

Goethite is generated through dissolution-recrystallization of the intermediate amorphous compounds [21] (Knight and Sylva, 1974). Hematite on the other hand is reported to form through transformations within the amorphous phase (Blesa and Matijević, 1989). Different anions and cations will affect the overall rate of crystallization as well as the relative yield of both solids. The reaction may also be directed by adequate seeding.

Van der Woude (1983a,b, 1984a,b) studied processes whereby amorphous iron oxides (formed by hydrolysis of Fe(III) salts) evolve into goethite, in a process involving water release and densification. Two stages are proposed: the formation of needle-like units and a further change of these units to the final goethite crystals. Van der Woude proposes that both the incorporation of low molecular weight soluble Fe(III) species (i.e., usual crystal growth) and the stacking and cementing of aged primary particles on needle-like crystals, although other alternatives are considered. The complexity of the involved phenomena is depicted in Figure 2-8 (Blesa and Matijević, 1989). The kinetics of iron oxide transformation are determined by the pH of the solution, time and temperature of aging (Christensen et al., 1983).

2.2.3.1 Oxides and hydroxides of iron(III)

Goethite (α -FeOOH) is the most common product of Fe(III) hydrolysis carried out at temperatures near the atmospheric boiling point of the solution, pH 1.5-3.5 and total sulphate content less than 3 M and it is the polymorph to which most other FeOOH phases eventually revert to upon aging (McAndrew et al., 1975; Davey and Scott, 1976, Dutrizac, 1980). The goethite structure consists of alternating double chains of linked [Fe(O,OH)] octahedra (Murray, 1979; Flynn, 1984). Goethite contains 62.9% Fe (Chen and Cabri, 1986). Available kinetic evidence suggests that equilibrium is approached very slowly (McAndrew et al., 1975; Umetsu et al., 1977) and that intermediate products such as amorphous Fe(OH)₃ may be formed (Feitknecht and Schindler, 1963). Davey and Scott (1976) showed that goethite precipitates incorporated significant concentrations of both SO₄²⁻ and Cl⁻; furthermore prolonged washings reduced but never removed the impurities (Davey and Scott, 1976; Dutrizac, 1980, 1987). Similar behaviour has been noted in commercial precipitates where 5-15% SO₄ contents have been observed (Patrizi et al., 1985). Some of the sulphate is likely present as amorphous basic iron sulphate although some may be structurally incorporated in the goethite itself (Dutrizac, 1980). Recent studies by Ardizzone and Formaro (1985) showed that sulphate plays a key role in forming α -FeOOH (goethite).

Dehydration of goethite to form hematite is thermodynamically feasible. The reaction direction can be retarded and reversed by the incorporation of foreign ions in the goethite and due to variations in surface area (Dutrizac, 1980). Hematite's (α -Fe₂O₃) basic structure is one of a hexagonal close-packed array of oxygen anions in which 2/3 of the octahedral in every layer are occupied by Fe³⁺. The stoichiometric number of iron atoms occupy octahedral interstices between the oxygen monolayers. Hematite contains 69.9% Fe (Chen and Cabri, 1986).

Amorphous hydrous iron(III) oxides (or otherwise called ferric hydroxides, ferrihydrites, and amorphous ferric oxyhydroxides) are the first to form during the

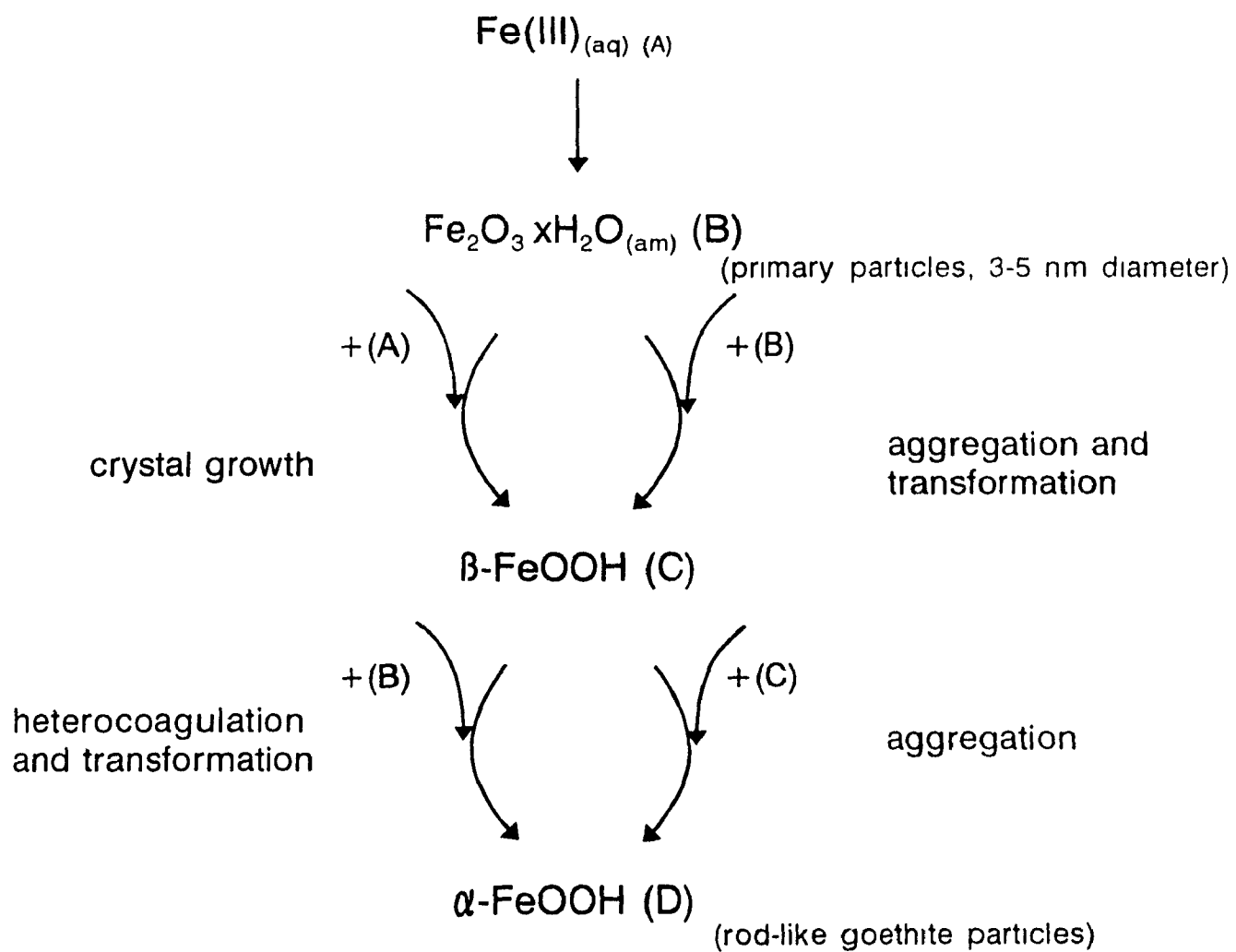


Figure 2-8: Generation of goethite in iron(III) nitrate solutions at room temperature (Blesa and Matijević, 1989).

hydrolysis and precipitation of iron from solution. These gel-like particles are proposed to have a cubic structure and a density dependent on the degree of hydration ($2.44\text{--}3.60\text{ g cm}^{-3}$). The structure of ferrihydrite is based on the hexagonal close packing of oxygens (Murray, 1979). The ferric hydroxide precipitate has a large surface area as well as unsatisfied Fe and OH bonds. Such a precipitate has the ability to collect various impurity elements by chemisorption.

In contrast to hematite, the position of the iron is partly vacant and the period is not six but four layers of hexagonal anionic packing. Thus, the structure proposed by Towe and Bradley (1967) is related to hematite but differs by containing some H_2O and OH instead of O and less Fe in the octahedral portions. This leads to a much lower Fe/O ratio.

2.2.3.2 Sulphate containing iron(III) compounds

Two principle sulphate containing iron(III) compounds are formed during hydrolysis; jarosite ($\text{RFe}_3(\text{SO}_4)_2(\text{OH})_6$, where $\text{R} = \text{H}_3\text{O}^+, \text{Na}^+, \text{K}^+, \text{Rb}^+, \text{Ag}^+, \text{NH}_4^+, \text{Ti}^+, \frac{1}{2}\text{Pb}^{2+}, \frac{1}{2}\text{Hg}^{2+}$) and basic iron sulphate ($\text{Fe}_4(\text{SO}_4)(\text{OH})_{10}$).

The jarosite structure consists of sheets of hydroxyl and sulphate-bridged Fe^{3+} distorted octahedra wherein each Fe^{3+} is bonded to 4OH^- groups and 2SO_4^{2-} groups. The major control parameters in the jarosite process are the acid concentration, temperature and molar ratio of cation to iron. Seeding is also an important factor in jarosite precipitation (Dutrillac, 1987).

Basic ferric sulphate is formed at relatively low iron concentrations and could be produced during the terminal stages of jarosite formation when the iron concentration is $1\text{ to }5\text{ g.L}^{-1}$. These two compounds seem to be characteristic of the products of hydrolysis at elevated temperatures of solutions containing ferric and sulphate ions.

The amorphous basic sulphate can be converted not only to jarosite but also to goethite. This process becomes significant at $[\text{Fe}] \leq 1.8\text{ g.L}^{-1}$ and $\text{pH} \geq 1.10$. At sufficiently high pH and low $[\text{Fe}]$, the amorphous sulphate is converted into goethite, as the most stable crystalline product (Margulis et al., 1977).

Several key features of the major industrial iron removal processes are outlined in Table 2-5.

Table 2-5: Comparison of industrial iron precipitation processes (Davey and Scott, 1976; Dutrizac and Kaiman, 1976; Dutrizac, 1980; Langmuir and Whittemore, 1971).

	Fe(III) Hydrolysis Process			
	Goethite	Jarosite	Hematite	Ferric Hydroxide
Operating conditions				
pH	2-3.5	< 1.5	< 2	1.5-3.5
Temperature	70-90°C	90-100°C	~200°C	Any
Anion	Any	SO ₄ ²⁻ only	Any	Any
Added cations required	Nil	R ⁺	Nil	Nil
Precipitant	Calcine, CaO, NaOH	Calcine, CaO, NaOH	Nil	Calcine, CaO, NaOH
Product				
Compound formed	α - and β -FeOOH (α -Fe ₂ O ₃)	RFe ₃ (SO ₄) ₂ (OH) ₆	α -Fe ₂ O ₃	Fe(OH) ₃
Cationic impurities	Medium	Low (apart from "R")	Low	Medium
Anionic impurities	Medium	High	Medium	High
Filterability	Good	Good	Fair	Poor
Fe in filtrate	< 1 g/L	1-5 g/L	~3 g/L	5-10 mg/L
Specific Gravity (g/cm ₃)	4.28	2.66-3.54	5.26	2.44-3.60 ¹

* R = H₃O⁺, Na⁺, K⁺, Rb⁺, Ag⁺, NH₄⁺, Tl⁺, 1/2Pb²⁺, 1/2Hg²⁺

1 - density decreases as the degree of hydration increases (Dénès, 1988).

2.2.4 Factors Affecting Solids Formation

2.2.4.1 Rate of neutralization

The behaviour of hydrolyzed Fe(III) solutions depends on the nature and mode of addition of basic reagent (Murphy et al., 1975; Spiro et al., 1966; Knight and Sylva, 1974, Dutrizac, 1980). If the OH/Fe ratio in solution is less than 2.5, the

precipitate dissolves.

At low base additions precipitate formation occurs, while the rate of the process increases with base addition. Increasing the base addition rate results in polycation formation which can inhibit precipitation (Knight and Sylva, 1974).

2.2.4.1(a) Titration curves

When Fe(III) solutions are titrated with NaOH the resulting titration curve consists of three regions. In the first region, OH/Fe 0 to ~ 1 , the pH increases. In the second region, OH/Fe mole ratio ~ 1 to 2.5, the pH curve is flattened to a plateau. In the third region, OH/Fe mole ratio ≥ 2.5 , the pH increases steeply and precipitation occurs (Flynn, 1984).

The forced hydrolysis of Fe(III) by titration with NaOH is characterized by an increase in the optical density followed by visible formation of a precipitate. A striking feature of the titration curves is a more pronounced plateau with increasing initial Fe(III) concentration. The location of the plateau of the titration curve is determined by the pH. With increasing ionic strength the plateau is seen to shift to progressively lower pH values at a given Fe(III) concentration. The ionic strength also affects the shape of the titration curve. As well, the shape of the titration curve varies with the rate of NaOH addition. Temperature also influences the shape and location of the plateau on the titration curve. The plateau suggests that chemical changes take place here which consume practically all the added base (Dousma and de Bruyn, 1976).

2.2.4.2 Temperature

At higher temperatures, in acidic media, crystalline phases are formed much faster. One of the most noticeable effects of temperature increase is the trend to enhance crystallinity.

Temperature also determines the compound precipitated, as can be seen in the following data obtained from oxidation of 0.33M FeBr₂ solution at various temperatures (Kiyama and Takada, 1972).

<u>Temperature (°C)</u>	<u>Compound</u>
10	β -FeOOH
20	β -FeOOH > α -FeOOH
40	γ -FeOOH \sim α -FeOOH
65	α -FeOOH > γ -FeOOH > α -Fe ₂ O ₃
80	α -Fe ₂ O ₃ \sim α -FeOOH > γ -FeOOH

2.2.4.3 Aging

Spiro et al. (1966) inferred a two-step aging process of the polymer spheres from their data, which include kinetics of dehydration by acid. The first stage consists of "hardening" of the polymer spheres, and the second of agglomeration of the spheres. Dousma and de Bruyn (1978, 1979) expanded on this theory proposing a three-step hydrolysis process consisting of formation of the polymer spheres from low molecular weight species, aggregation of the spheres, and subsequent precipitation. While Flynn's (1984) data justifies discerning a four-step hydrolysis process (Figure 2-9).

Aging of the amorphous gels formed during Fe(III) hydrolysis often requires years at room temperature, and hours to days at 100°C (Flynn, 1984). The products formed are goethite or hematite and depend on solution compositions, temperature, time, and the presence of water (Atkinson, et al., 1967; Flynn, 1984). FeOOH particles suspended in water undergo transformations to α -Fe₂O₃ at elevated temperatures much more readily than when kept in air (Matijević and Scheiner, 1978; Flynn, 1990).

2.2.4.4 Adsorption

Hydrolyzed compounds have a high capacity to adsorb other ions. Polymerization and olation increase dramatically the capacity to which ions are adsorbed (Erikson et al., 1973). Sulphate adsorption on α -FeOOH was observed when precipitation occurred under neutral conditions, regardless of solution composition (Inouye et al., 1986). According to Bryson and Te Riele (1986) sulphate adsorption is a temperature dependent process. Sulphate in the growth process of β -FeOOH adsorbs on the colloid surface, impedes the cohesion process or recrystallization and makes the crystallite minute (Inouye et al., 1986).

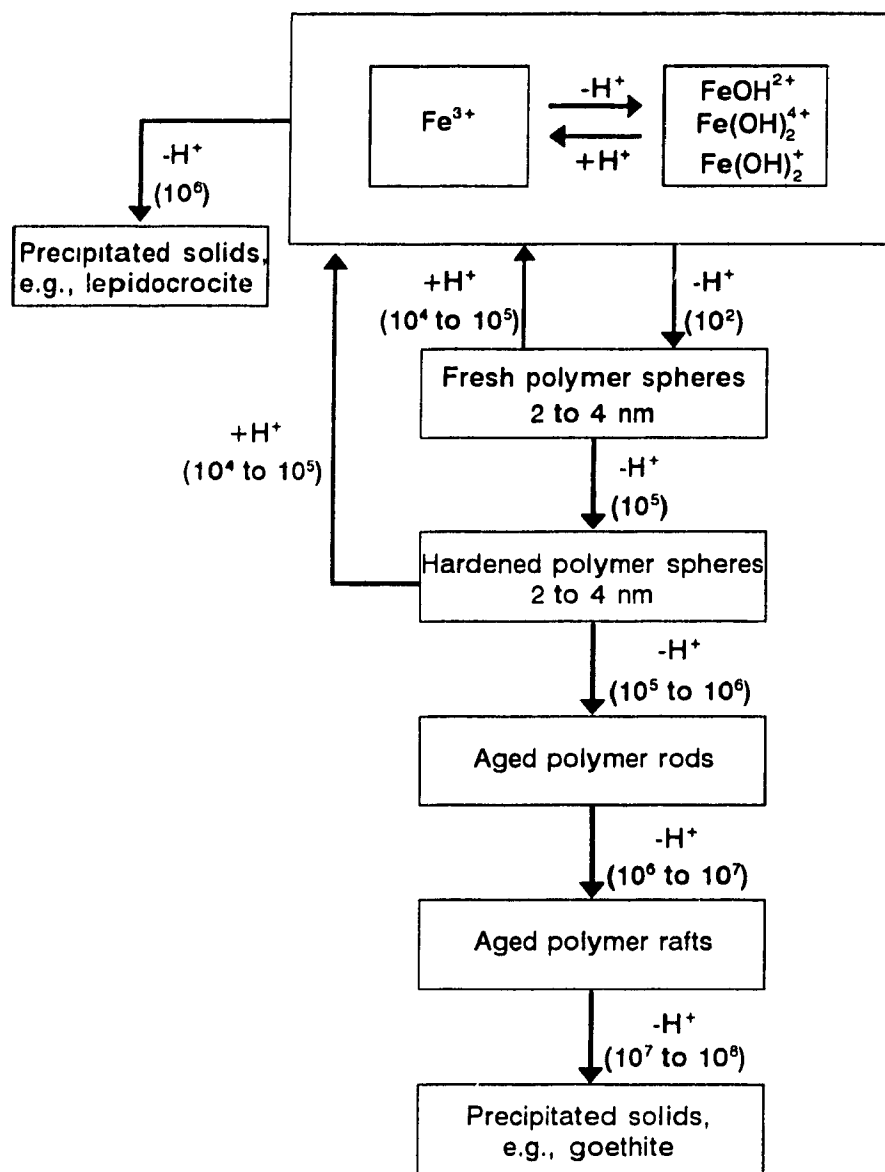
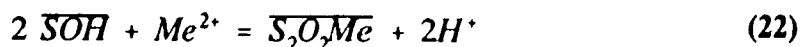


Figure 2-9: Hydrolysis processes in Fe(III) solutions. Numbers in parentheses give reaction time(s) at 25°C (Flynn, 1984).

Similarly, the degree to which a solid is capable of adsorption depends on its surface area. The surface area of amorphous iron oxyhydroxide has been estimated in the range of 270-335 m².g⁻¹ at pH 4 and ~700 m².g⁻¹ at pH 5 (Davis and Leckie, 1978). Specific surface areas as large as 700 m².g⁻¹ have been observed for other gelatinous oxide precipitates (Iler, 1973).

Adsorption of Cd²⁺, Zn²⁺, Cu²⁺ and Pb²⁺ occurs within a narrow pH band where fractional adsorption increases from nil to nearly 100% (Benjamin and Leckie, 1981). Kinetic experiments indicated that adsorption of all four metals is rapid initially (1 hr.), followed by a much slower second step, possibly related to solid state diffusion.

If all surface sites are equivalent, surface proton would be released per site occupied when a trace metal ion adsorbs. In a few studies in which adsorption stoichiometry has been characterized, generally more than one proton is released to solution per metal adsorbed (Hohl and Stumm, 1976; Loganathan and Burau, 1973). This phenomenon has been explained by postulating bidentate bonding [22] (Hohl and Stumm, 1976) or simultaneous adsorption and hydrolysis [23] (Davis et al., 1978):



\overline{SOH} represents a protonated surface site and $\overline{S_2O_2Me}$ and \overline{SOMeOH} represent surface sites occupied by metal ions.

2.2.4.5 Effect of anions and cations

The influence of anions in the precipitation processes may appear in three distinct ways (Blesa and Matijevic, 1989):

- (1) The anions may be incorporated in the solid phase generating basic salts, or just hydrated salts, rather than hydrous oxides.
- (2) The structure of the particles may be determined by the nature of an anion, even if this is not present, in significant amounts, in the resulting solid.

(3) The morphology and the size of the particles may be highly dependent on the nature and concentration of the anions in solution due to anion adsorption. These variations of the final crystalline phases are due to the effect of anions in the very early stages of polymerization.

The presence of anions (such as SO_4^{2-} and Cl^-) in solution are expected to affect not only the composition of the precipitate but also its tendency to flocculate, the degree to which it can be washed free of metal ions and its nucleation and growth mechanisms. These effects result from changes in the surface chemistry invoked by the presence of these anions. The simplest possible effect a complexing anion might have is the blocking of one or more coordination sites on Fe(III) solute species. Very strong metal-anion bonds are required and in the extreme case, the complexing anion is incorporated into the solid phase. The bridging action is at least partially responsible for the incorporation of the sulphate ion into the solid. Pathways leading to the formation of species such as:



compete effectively with ololation and oxolation, because a less stringent activation barrier has to be overcome. Eventually, oxolation of small SO_4^{2-} -containing polymers make sulphate incorporation irreversible (Blesa and Matijević, 1989).

The presence of sodium results in variations in the observed lattice parameters, while some other cations (Li^+ , Cs^+ , Mg^{2+} , Ni^{2+} , Cu^{2+}) completely inhibited particle formation and consequently growth (Matijević et al., 1975). Laboratory studies have shown that the transformation of noncrystalline iron(III) hydroxide into products having greater crystallinity is retarded by the presence of inorganic cations, such as Al^{3+} , Mn^{2+} , or Cu^{2+} and enhanced by organic ligands such as L-Cysteine (Lewis and Schwertmann, 1979; Cornell, 1987, 1988; Cornell and Giovanoli, 1988). Similarly, phosphate and silicate ions block goethite formation by adsorbing on noncrystalline iron(III) hydroxide in preference to cysteine (Cornell and Schneider, 1989).

2.2.4.6 Solubility

The solubility of ferric hydroxide has been studied extensively. Reported solubility products (Table 2-6) vary over several orders of magnitude. The wide range of values is a result of several factors. Foremost of these are size (Langmuir, 1969) and composition of suspended ferric hydroxide solids (Langmuir and Whittemore, 1971), failure to consider relevant ferric complexes (Langmuir, 1969), and variations in the chemical composition of solutions from which solubility data were gathered. Several trends however, were apparent. For example, active hydroxides were orders of magnitude more soluble than the similar inactive hydroxides. As well, the oxygen containing hydrolysis compounds are several orders of magnitude less soluble than the simple hydroxides.

Ferric hydroxide solubility is a function of particle size and degree of hydration (Murray, 1979); the smaller the particles, the less stable (i.e., the more soluble) the phase (Dove and Rimstidt, 1987). As ferric hydroxides with decreasing solubilities are formed, the $\text{Fe}(\text{OH})_3$ solubility curve moves to lower and lower pH (Dove and Rimstidt, 1987). As well, ferric hydroxide becomes less soluble with increasing temperature, while it is more soluble at elevated sulphate concentrations.

2.3 Summary

Neutralization of acidic mineral effluents in practice leads to voluminous, hard to settle, sludges. Several lime addition facilities exist, each with its own set of advantages and disadvantages. The most successful treatment processes advocate recycling the sludge and controlling the addition of the neutralizing agent. In many cases as well, organic polymers are added to enhance agglomeration and aid settling.

It is the hydrolysis reaction which is responsible for metal removal during effluent treatment. Hydrolysis is essentially a four step process which involves: (a) hydrolysis of $\text{Fe}(\text{III})$ into monomers and dimers (e.g., $\text{Fe}(\text{OH})^{2+}$, $\text{Fe}(\text{OH})_2^+$, $\text{Fe}_2(\text{OH})_2^{4+}$, $\text{Fe}_3(\text{OH})_4^{5+}$, $\text{Fe}(\text{OH})_3^0_{(\text{aq})}$); (b) reversible, rapid growth to small polymers; (c) formation of slowly reacting large polymers; and (d) precipitation of the solid phase. Precipitation can occur through a combination of olation and oxolation.

Table 2-6: Solubility products of several amorphous and crystalline ferric hydroxides and oxides reported in the literature

Probable Solid phase	Log Solubility Product (pK _{sp})	Method	Reference
Fe(OH) ₃ (amorphous)	-39.02 ± 0.35	Chelation	Vlek et al., 1974
α-FeOOH	-42.48 ± 0.23	Chelation	Vlek et al., 1974
Fe(OH) ₃	-38.6	Thermodynamics	Monhemius, 1977
Fe(OH) ₃ (amorphous)	-38.4 ± 0.2	1.0M KNO ₃	Christensen & Borggaard, 1977
Fe(OH) ₃ (amorphous)	-37.0	—	Gayer & Wootner, 1956
Fe(OH) ₃ (most active)	-38.0	3M NaClO ₄	Biedermann & Schindler, 1957
Fe(OH) ₃ (active)	-38.7/39.7 ± 0.2*	3M NaClO ₄	Biedermann & Schindler, 1957
Fe(OH) ₃ (inactive)	-39.1	3M NaClO ₄	Schindler et al., 1963
α-Fe ₂ O ₃	-42.7	Thermodynamics	Feitknecht & Schindler, 1963
Fe(OH) ₃ (amorphous)	-37.9/-39.4 ± 0.5*	0.5M Cl ⁻ (14°C)	Jellinek & Gordan, 1924 ¹
Fe(OH) ₃ (amorphous)	-37.7/-39.0 ± 0.1*	0.5M Cl ⁻ (18°C)	Britton, 1925 ¹
Fe(OH) ₃ (amorphous)	-35.6 ± 1.4/-38.7*	0.05M (SO ₄ ²⁻) (18°C)	Kriukov & Awsejewitch, 1933 ¹
Fe(OH) ₃ (amorphous)	-35.5/-37.5*	0.1M FeNH ₄ (SO ₄) ₂ (20°C)	Evan & Pryor, 1949 ¹
Fe(OH) ₃ (amorphous)	-38.8/-39.6 ± 0.3*	3M NaClO ₄	Biedermann & Chow, 1966 ¹
Fe(OH) ₃ (amorphous)	-38.5/-39.5*	0.1M SO ₄ ²⁻	Langmuir and Whittemore, 1971
Fe(OH) ₃ (amorphous)	-36.6 TO -39.2	0.05M NO ₃ ⁻	Fox, 1988
Fe(OH) ₃ (amorphous)	-39.2*	—	Copper, 1938 ¹
Fe(OH) ₃ (amorphous)	-36.5 ± 1.1*	0.05M Cl ⁻	Elder, 1930 ¹
Fe(OH) ₃ (amorphous)	-38.3 ± 0.6*	—	Elder, 1930 ²
Fe(OH) ₃ (amorphous)	-37.2	—	Schinder, 1962 ²
Fe(OH) ₃ (amorphous)	-38.4	—	Platford, 1964 ²
Fe(OH) ₃ (amorphous)	-38.6	—	Bohn, 1967 ²
Fe(OH) ₃ (amorphous)	-39.0	—	Norvell, 1970 ²
α-FeOOH	-39.4	—	Elder, 1930 ²
Fe ₂ O ₃	-42.2	—	Elder, 1930 ²
Fe ₂ O ₃	-42.2	—	Garrels & Christ, 1965 ²
α-FeOOH	-42.7	—	Schindler, 1962 ²
α-FeOOH	-40.6	—	Schuylenborgh, 1969 ²
α-FeOOH	-44.0	—	Elder, 1930 ²

* Ion activity solubility based on original data, calculations by Fox, 1988.

1 Data and references cited by Fox, 1988.

2 Data and references cited by Vlek et al., 1974.

Olation, the simplest pathway, involves deprotonation of the polymer, in turn forming hydroxyl bridges. This mechanism tends to produce a gelatinous precipitate with poor handling properties. Conversely, oxolation forms oxobridges through dehydration and subsequently produces a denser precipitate.

Several factors influence both the chemical (i.e. solid composition) and physical properties of the hydrolysis product. These factors include, both the concentration of iron(III) and the concentration of sulphate, pH, temperature, rate of neutralization, degree of aging, and cation/anion adsorption.

From this survey several parameters apparently require further investigation,

these include; (1) solution speciation, (2) solubility, (3) hydrolysis control (i.e. pH, temperature, etc.), (4) hydrolysis pathways (oxolation versus ololation or sulphate bridging), and (5) ion adsorption. While this chapter presented an exhaustive review of Fe(III) hydrolysis, the picture is not complete without a review of the relevant background theory in crystallization and colloid chemistry, which is presented in the next chapter.

CHAPTER 3: THEORETICAL BACKGROUND

While considerable literature is available on the chemistry of iron(III) hydrolysis no studies are available on the crystallization phenomena governing the solid formation process and which eventually determine the physical properties of the precipitates. Since it was one of the principal objectives of the present research to study the hydrolysis of Fe(III) from a crystallization point of view it is considered to be fully appropriate to delve into the theory of crystallization theory and colloid chemistry, which are less common to hydrometallurgy and effluent treatment.

3.1 Fundamentals of Crystallization

The crystallization of a new solid phase out of solution consists of nucleation, growth of the nuclei with molecular solute diffusing to the crystal surface, and agglomeration (in most of the cases) of the tiny particles (Toyokura, 1981). The driving force for crystallization is supersaturation.

Supersaturation is the concentration in excess of saturated concentration and is expressed by the difference from the saturation concentration or the ratio to the saturation concentration. The supersaturated solution is composed of two zones, the metastable and the unstable zone, as shown in Figure 3-1 (Toyokura, 1981).

These two zones are defined in such a way that the metastable region is where crystals grow without nucleating, but in the unstable region numerous crystals appear as a result of homogeneous nucleation. Supersolubility is defined as the boundary concentration between these two zones.

The level of saturation is defined by the saturation ratio, S , where:

$$S = \frac{C}{C_{eq}} \quad (25)$$

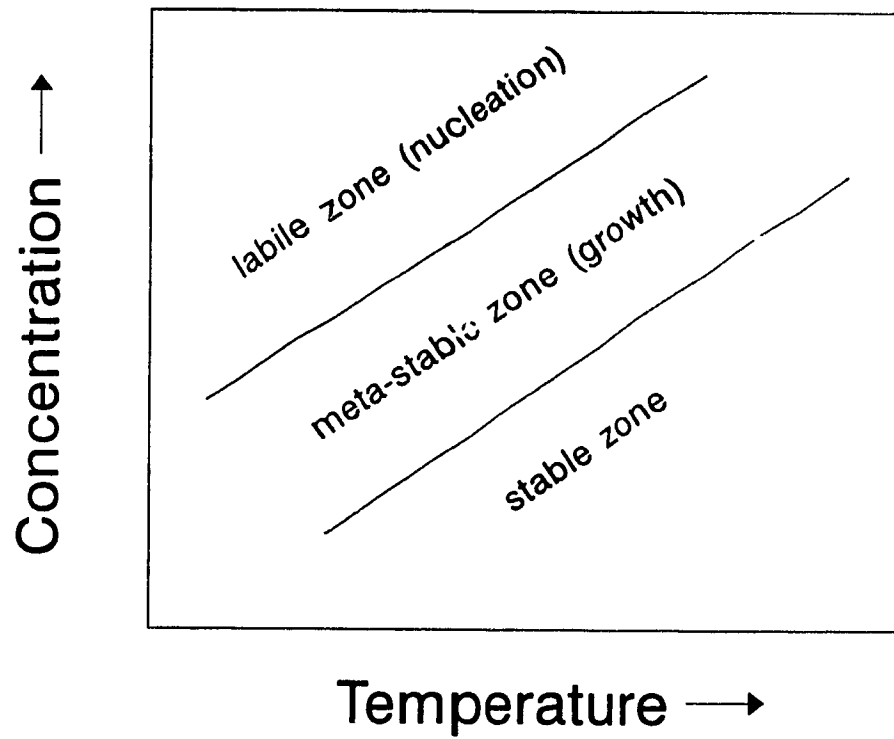
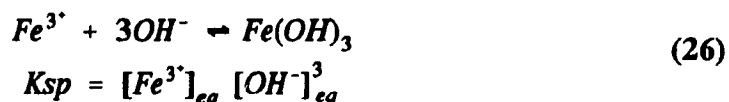


Figure 3-1: Solubility - supersolubility diagram for explanation of stable, metastable and labile (unstable) zones (Toyokura, 1981).

C being the solute (e.g. $[\text{Fe}^{3+}][\text{OH}^-]^3$) concentration in the bulk solution and C_{eq} , the equilibrium solubility of the solute (K_{sp}) (Dirksen and Ring, 1991). From Equation 25 the supersaturation ratio can be defined as $(C-C_{eq})/C_{eq} = S-1$. In the case of $\text{Fe}(\text{OH})_3$ precipitation, the solubility is represented as follows:



The saturation ratio can be written as:

$$S = \frac{[\text{Fe}^{3+}] [\text{OH}^-]^3}{K_{sp}} \quad (27)$$

and is a function of pH for this system.

3.1.1 Nucleation

The rate of nucleation in batch processes is maximum at time=0 and decreases very rapidly until supersaturation reaches the metastable zone (S_{crit} in Figure 3-2) (Dunning, 1973). Beyond this point homogeneous nucleation is negligible and the continued decline in S is solely the result of growth.

The mechanism of nucleation plays an important role in controlling the final particle size distribution. The nucleation process can be distinguished into three main mechanisms: (1) primary homogeneous (2) primary heterogeneous and (3) secondary nucleation (Dirksen and Ring, 1991; Garside, 1985). Homogeneous nucleation occurs in the absence of a solid interface; heterogeneous nucleation occurs in the presence of a solid interface of a foreign seed and secondary nucleation occurs in the presence of a solute-particle interface (Figure 3-3).

3.1.1.1 *Primary nucleation*

Classical theories of primary, or spontaneous homogeneous nucleation assume that in supersaturated solutions, solute atoms or molecules are combined in a series of bimolecular reactions to produce ordered aggregates or "embryos" (Garside, 1985). The overall free energy of these embryos goes through a maximum at some critical

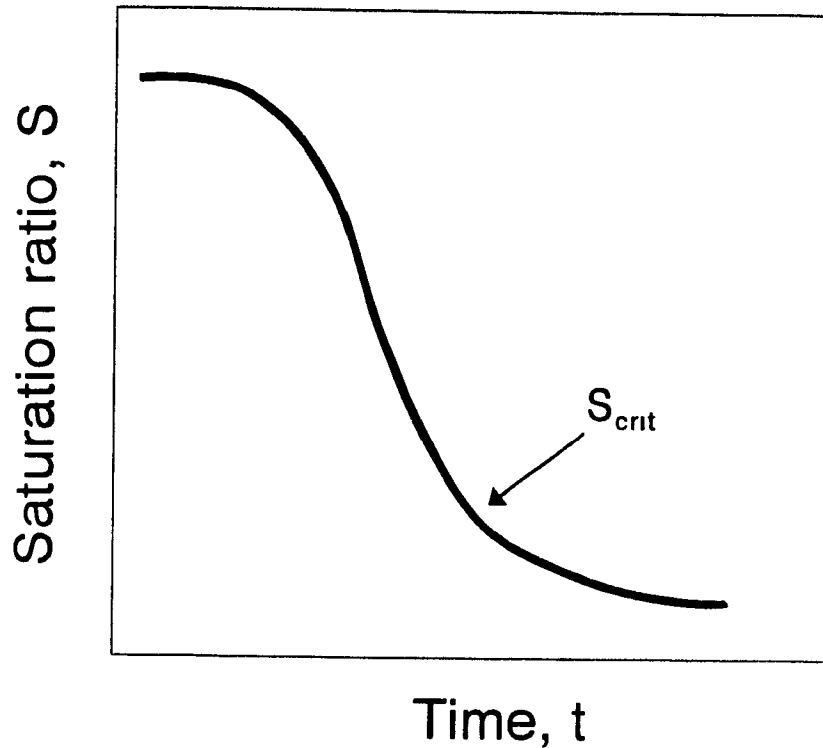


Figure 3-2: Variation in supersaturation with time in a batch reactor (Dunning, 1973).

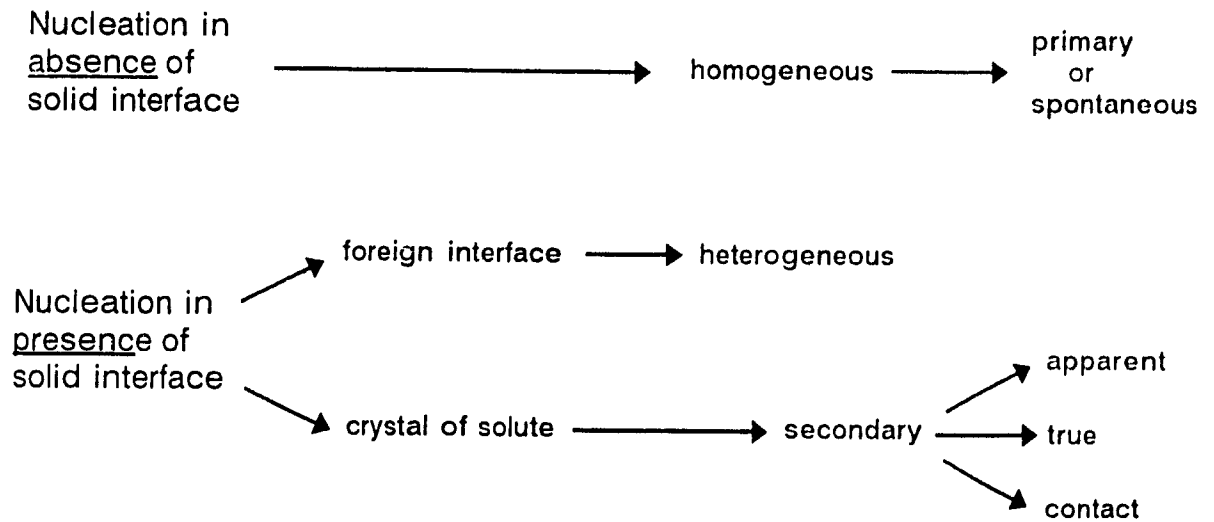


Figure 3-3: Classification of nucleation mechanisms (Garside, 1985).

size (r^*) which is inversely proportional to the logarithm of the solution saturation (Walton, 1967). Embryos larger than this critical size will decrease their free energy by further growth; they are "stable nuclei" and grow to form macroscopic crystals. The primary nucleation rate is highly nonlinear in solution supersaturation, being near-zero for low values of S (the metastable region) but increasing extremely rapidly once some critical supersaturation is reached (the labile region) (Garside, 1985). Nucleation on a foreign surface requires a lower activation energy than that necessary to induce nucleation in the bulk solution and although the exact mechanism by which this occurs is unclear, it is thought to be the result of a local ordering process brought about by interactions across the interface (Walton, 1967).

3.1.1.1(a) Homogeneous Nucleation

As mentioned above, when a critical saturation (S_{crit}) is exceeded spontaneous homogeneous nucleation occurs producing nuclei with ratios $r > r^*$. For a given value of S all particles with $r > r^*$ will grow and all particles with $r < r^*$ will dissolve. The latter phenomenon is referred to as Ostwald ripening. Ostwald (Dunning, 1973) propounded his law of stages to describe the case when an unstable compound crystallizes first. According to this, a supersaturated state does not spontaneously transform directly into that phase which is the most stable of the possible states but into the phase which is next more stable than itself (this is otherwise called Stranski's rule as mentioned in the previous chapter).

The rate of nucleation increases sharply from a critical value of supersaturation then asymptotically reaches a maximum value (Nielsen, 1964). Thus, increasing the supersaturation increases the number and decreases the size of the nuclei formed by homogeneous nucleation. When the precipitant is added, the resulting chemical reaction usually proceeds rapidly and very high levels of supersaturation are created, making homogeneous nucleation the dominant mode of nucleation.

3.1.1.1(b) Heterogeneous Nucleation

Nucleation on a foreign surface, which has a lower surface energy than that of a new solute particle, takes place at a lower critical supersaturation ($S_{\text{crit,hetero}}$).

Heterogeneous nucleation is similar to homogeneous nucleation, the difference being that the surface energy of the solid/liquid interface is replaced by the surface energy of the precipitated solid/foreign interface (Dirksen and Ring, 1991). The physical difference between homogeneous and heterogeneous nucleation is that once the heteronuclei are used up, heterogeneous nucleation stops, thus limiting maximum possible heterogeneous nucleation rate. Homogeneous and heterogeneous nucleations are not likely to occur simultaneously since $S_{crit,homo} > S_{crit,hetero}$.

The characteristic shape of the generalized nucleation rate diagram (Figure 3-4) shows that at high supersaturation ratios primary nucleation dominates (either by homogeneous or heterogeneous means). At lower levels of supersaturation, secondary nucleation can take place; it is induced by the presence of other particles of the solute (surface nucleation).

3.1.1.2 Secondary nucleation

The occurrence of secondary nucleation depends on the presence of existing solute crystals (seed) in the solution (Botsaris, 1976). Certain reviews (Botsaris, 1976; Estrin, 1976) have emphasized that secondary nuclei can originate from a number of different sources and the division of the phenomenon into three separate categories, apparent, true and contact secondary nucleation is a reflection of these origins.

Apparent secondary nucleation is a somewhat trivial case and refers, for example, to the small fragments washed from the surface of a dry crystal when it is introduced into solution (Garside, 1985). In true secondary nucleation the presence of solute crystals facilitates the surface nucleation of the newly deposited material due to lower activation energy barriers (Viola and Botsaris, 1979).

In contact secondary nucleation, contacts between a growing particle and walls of the container or the agitation impeller results in the formation of contact nuclei (Bennett et al., 1973; Garside and Davey, 1980). The rate of contact nucleation depends on the stirrer rotation, particle mass density, saturation ratio and the reactor size and geometry (Garside and Davey, 1980). Changes in nucleation mechanism can result from excessively long residence times (Keight, 1979) or at very high magma

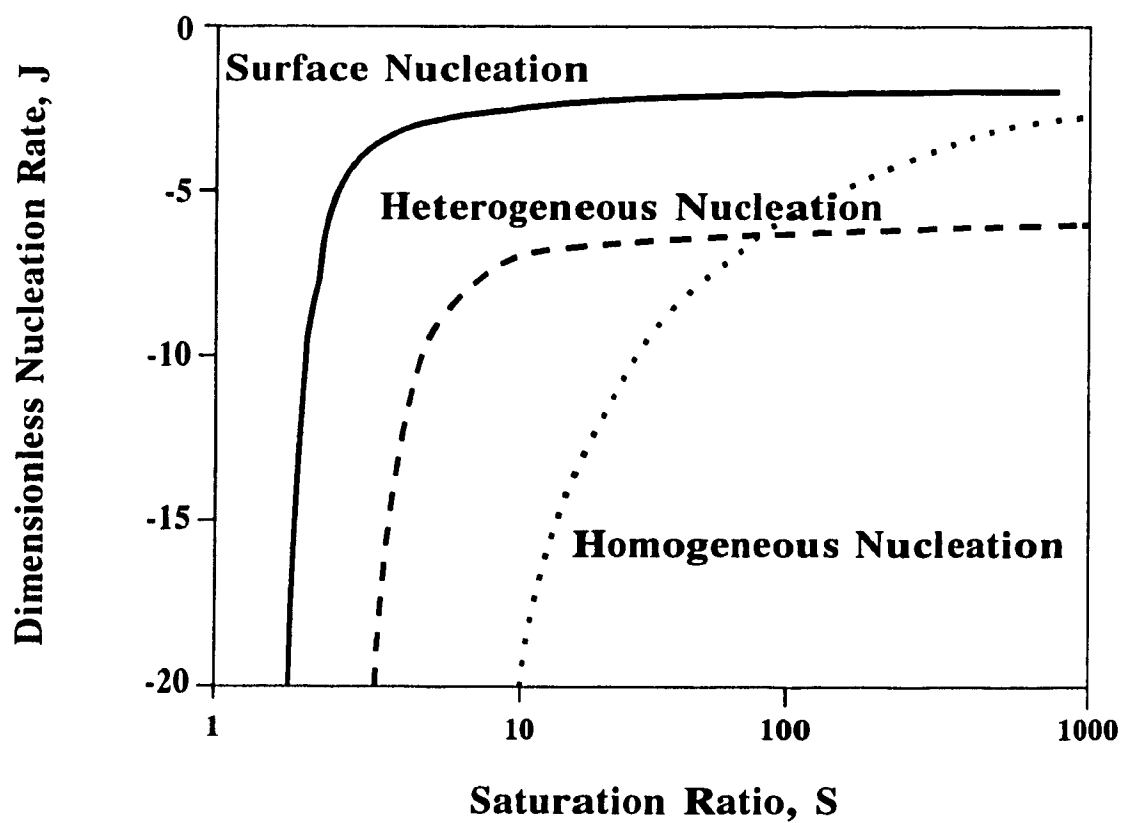


Figure 3-4: Generalized nucleation rate diagram describing the characteristic difference between homogeneous, heterogeneous and surface nucleation for these specific values (Dirksen and Ring, 1991).

(slurry) densities (Nienow and Conti, 1978).

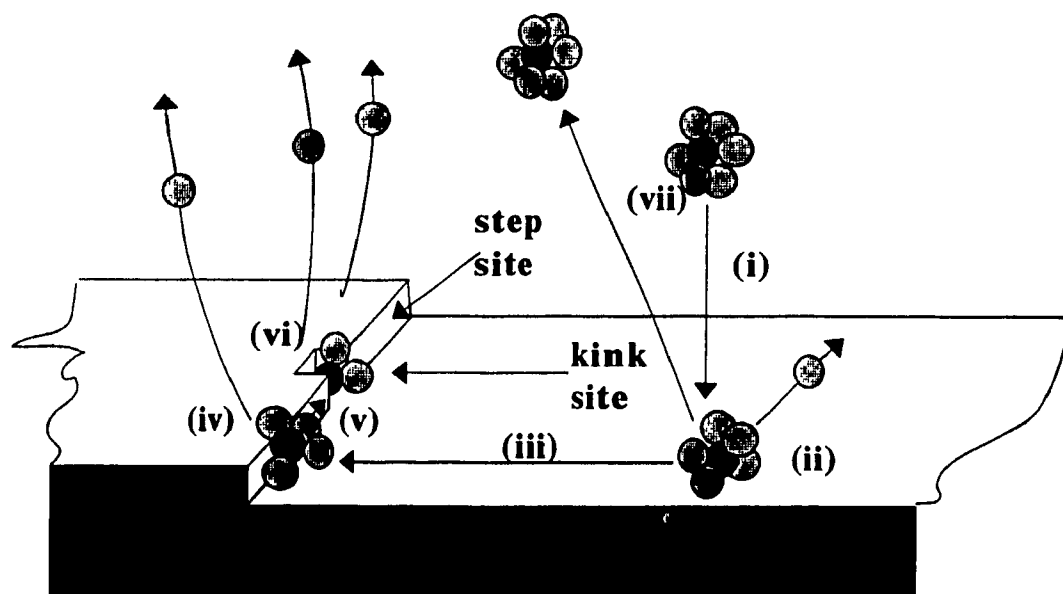
3.1.2 Growth Kinetics

The process of crystal growth can be described at three different levels: molecular, microscopic and macroscopic and occurs in the following stages (Elwell and Scheel, 1975) (Figure 3-5):

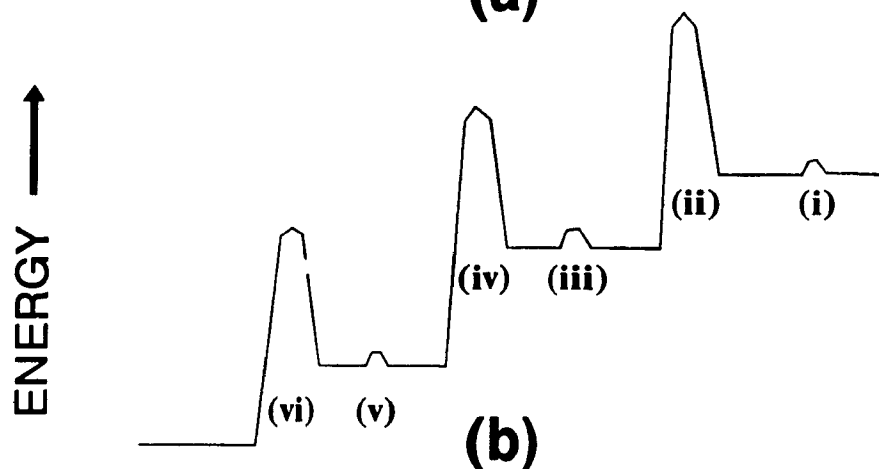
- (i) Transport of solute from the bulk to the crystal surface.
- (ii) Adsorption on the crystal surface.
- (iii) Diffusion over the surface.
- (iv) Attachment to a step.
- (v) Diffusion along a step.
- (vi) Integration into the crystal at a kink site.
- (vii) Diffusion of coordination shell of solvent molecules away from crystal surface.
- (viii) Liberation of heat of crystallization and its transport away from crystal.

The growth of surface nuclei is achieved by either the surface or bulk diffusion of a growth unit to the step and kink site at the edge of the growing nucleus. The meaning of the terms "step" and "kink" is illustrated in Figure 3-5. To gain further insight into the rate determining step of crystal growth, the two-dimensional growth rates must be compared to the surface nucleation rate. If the rate of surface nucleation is less than the rate of growth, then mononuclear growth is observed (Figure 3-6(a)). When the rate at which surface nuclei are formed exceeds the growth rate, then polynuclear growth happens (Figure 3-6(b)).

At the molecular level growth units are envisaged to attach themselves to the crystal surface, diffuse over this surface and eventually either integrate into the lattice at a kink site or return to the fluid phase. The chance of reaching such a site depends on the concentration of kinks in the surface and so the mechanism and rate of growth depends on the nature of the crystal surface at this molecular level. In a rough interface there are many potential kink sites and neither surface diffusion nor fine details of the surface topography are important. Under such conditions continuous or polynuclear growth models apply. On the other hand when the interface is smooth, growth is more difficult and is governed by layer growth or



(a)



(b)

Figure 3-5: The energies of crystal growth from solution: (a) Movement of the solvated solute molecule and (b) corresponding energy changes for each transformation (Elwell and Scheel, 1975).

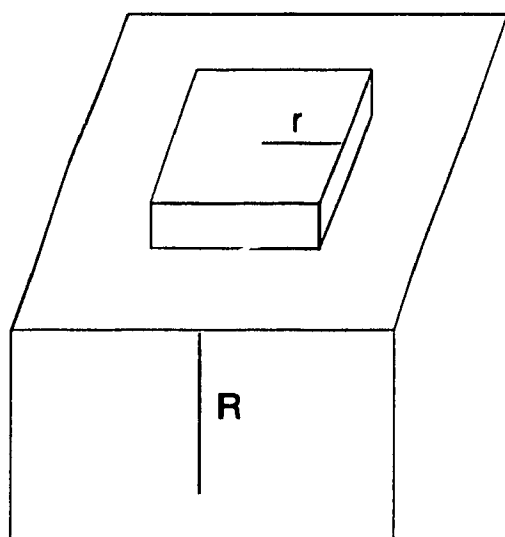
mononuclear models. At the microscopic scale surface layers or step bunches are often observed. At still larger size scales the effect of mass transfer limitations on growth rate can be seen. Supersaturation gradients in the solution phase can influence the surface profiles and cause discontinuities.

For a crystal moving in a supersaturated solution, solute diffusion is enhanced by increased mass transfer. The effect of mixing on particulate growth becomes very important when the average energy transferred to a fluid is less than what is needed for elimination of concentration gradients in the precipitator. When pockets of local supersaturation develop within the reactor, a broad particle size distribution results. These pockets of local supersaturation ensue in systems where particles are smaller than the mean size. For crystals smaller than $\sim 1 \mu\text{m}$, the slip velocity is very small and the growth rate is typically controlled by Brownian diffusion (Dirksen and Ring, 1991). When the density of these small particles is high, the interparticle distances are comparable to the boundary layer thickness, and consequently higher growth rates are observed.

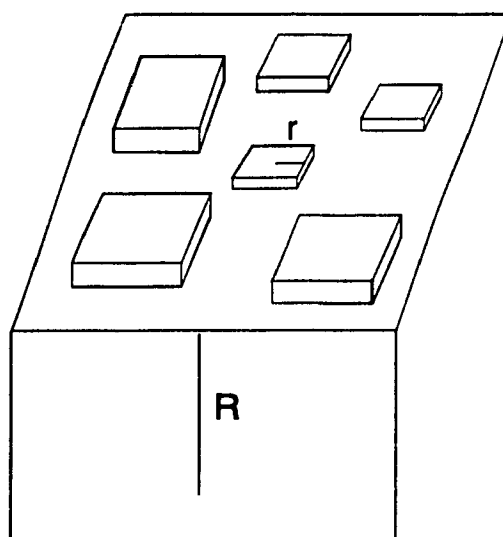
If a chemical reaction is used to produce the insoluble species (e.g., hydrolysis), the rate of reaction can be another rate limiting step. The growth rate is diffusion-controlled if growth is limited by diffusion of the growth units to the particle surface. This often occurs in non-agitated systems, in gel systems, or in systems where the precipitant is released slowly by hydrolysis or after decomposition reaction of a substance in solution. In an agitated system where the precipitant is added directly, the growth rate will usually reach a maximum value as the level of agitation increases. At this point it is sometimes considered that the surface reaction becomes the rate-limiting step (Burkhart and Voigt, 1986).

3.1.2.1 *Growth by aggregation*

An extension of diffusion-controlled growth theory is the process of particle aggregation. The size of the growth units in the aggregation case (i.e., $0.01\text{-}0.1 \mu\text{m}$) is typically much larger than that of an atom or a molecule. For particles which have low surface potentials, the colloid stability factor (Verwey and Overbeek, 1948) is essentially unity, which means that the small growth units will minimize their surface



a) Mononuclear



b) Polynuclear

Figure 3-6: Two-dimensional growth of surface nuclei by (a) mononuclear growth and (b) polynuclear growth models (Dirksen and Ring, 1991).

area (i.e., minimize the Gibbs free energy) by forming a larger aggregate. The colloid stability factor, W , is defined by Verwey and Overbeek (1948) (for two spheres with radii a and b , separated by distance R) as follows:

$$W = (a+b) \int_{a+b}^{\infty} \exp \left(\frac{V(R)}{K_B T} \right) \frac{dR}{R^2} \quad (28)$$

The interaction potential of the two double layers (these colloid concepts are discussed in detail in the next section of this chapter) is determined by the potential energy function [i.e., $V(R)$] (K_B = Boltzmann constant; T = temperature).

The extent to which aggregation takes place is not only a function of the colloid stability factor but as well as of the population density of the growth units in suspension. By controlling the homogeneous nucleation event one can control the population density of nuclei formed, which controls the atomistic growth of nuclei to clusters and consequently controls the further aggregation, of clusters into agglomerates.

In stirred batch reactors the shear forces will tend to compact the aggregates (Mates and Ring, 1987). If particles grow by cluster-cluster aggregation in the presence of shear aggregation, the final particle structure will be composed of nuclei and first-generation aggregates.

The primary particles, frequently called "crystallites" (even though they are often amorphous), agglomerate into dense "aggregates" which have low porosity and are a few micrometers in size. Firth and Hunter (1976) found that the aggregates are of rather uniform size and that their size is a function of the maximum shear level which exists in the precipitator. The aggregates in turn agglomerate into larger particles which may be called "flocs". The aggregates in the flocs are less strongly bonded to each other than the crystallites in the aggregates. The flocs are also much more porous than the aggregates and can be easily broken apart.

An often overlooked aspect of floc particles in a precipitator is that their characteristics may change markedly when the precipitate is filtered and dried. During filtration the flocs become closely packed and may increase in size as a result

of the greater particle-particle contact. The size distribution of the flocs after filtration and drying is usually skewed toward larger sizes than the distribution measured when the flocs are still suspended in the precipitator. The strength and porosity of the flocs also may be modified during the filtration and drying steps. If the precipitate is not thoroughly washed, dissolved salts from the mother liquor will remain. As the liquid evaporates from the floc pores during the drying process, the dissolved salts become concentrated in the remaining liquid. Because of surface tension effects, the last liquid to leave is that of the points of contact among the aggregates in the flocs. When this remaining liquid is gone, salt bridges are formed at these contact points and the strength of the floc is increased (Burkhart and Voigt, 1986).

3.1.3 Effect of Impurities on Crystallization

Impurities commonly exist in acidic mineral effluents, and some of them may influence the crystallization kinetics. In many cases the impurities affect the surface reaction and/or the crystal habit, thus causing a change in the crystal shape. In addition, some impurities change the phase diagram and affect not only the solubility, but also the nucleation and growth rate (Dirksen and Ring, 1991).

Since crystal growth is a surface phenomenon, it is not surprising that impurities that concentrate at the crystal face will affect the growth rate of those faces and hence the crystal shape. These impurities can (Mullin et al., 1970; Burrill, 1972; Dirksen and Ring, 1991):

- (1) Reduce the supply of material to the crystal face.
- (2) Reduce the specific surface energy.
- (3) Block surface sites and inhibit the steps of the growing crystal.
- (4) Hinder the aggregation of growth units.

Impurities which modify crystal habit fall into four categories.

- (1) Ions, either anions or cations.
- (2) Ionic surfactants, either anionic or cationic.
- (3) Non ionic surfactants like polymers.
- (4) Chemical binding complexes like organic dye compounds.

The adsorption of a particular type of ion (positively or negatively charged) usually predominates at a certain pH (and concentration of any other potential-determining ions). The isoelectric point¹ is a measure of this equilibrium propensity to adsorb these ions. An additional measure of specific adsorbance of ions is the zero point charge, which describes the pH value when the crystal surface has a zero charge. The preferential and strong adsorption of ionic surfactants is frequently used industrially to control crystal morphology during precipitation.

When a crystal grows from an impure solution or from one containing an additive, it will generally reject the impurity if this is less soluble in the crystal than the solution. The impurity concentration in the solid will be determined by the impurity concentration in the enriched diffusion layer and not by the mean concentration of the solution. Whether or not the impurity is incorporated into the crystal depends upon two opposing processes. The rate at which it can escape into the solution either directly or through surface migration and the rate at which growth layers submerge it, i.e., upon the rate of vertical growth of that face (Dunning, 1973).

3.1.4 Batch versus Continuous Precipitation

Overall, precipitation is a result of competing kinetic rate phenomena involving nucleation, crystal growth, and agglomeration. In batch precipitation, which is a nonsteady-state process, each rate will vary with time and a different phenomenon will dominate at different times. One may vary the reactant ratio, the rate of addition of the reactants, and other variables, but the degree of control that can be applied is limited. If the precipitant is added to the solution containing the cation to be precipitated (called direct strike), lower saturations are encountered in the precipitator. If the cation to be precipitated is added to a solution of the precipitant (called reverse strike), very high levels of supersaturation are created. Nucleation rates are very different in the two cases and the precipitate is likely to

¹ **Isoelectric point (IEP)** is the pH or salt concentration at which a colloidal particle acquires zero charge, i.e. when the zeta potential equals zero, and it will no longer move in an electric field.

have different physical characteristics (Burkhart and Voigt, 1986).

Continuous precipitation on the other hand, is a steady state process. Once the initial transient start-up period has passed, the conditions in the reactor remain constant. This permits much better control over the supersaturation level by adjusting the flow rates, residence time, and agitation rate.

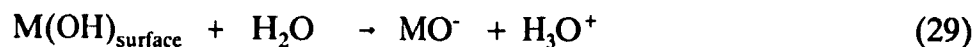
The crystal size distribution produced influences the supersaturation at which the crystallizer operates and so effects the crystal nucleation and growth rates, crystal habit and purity, fouling of solid surfaces and the stability of the operation. The size distribution is determined by the mean residence time and by the rates of the two kinetic processes, nucleation and growth (Garside, 1985). In batch crystallization the largest crystals are those which were nucleated first at the highest supersaturation and subjected to rates of growth varying from highest to lowest (Dunning, 1973).

Staging, (Tavare and Chivate, 1977) whereby, the product from one crystallizer is passed to a second and perhaps subsequent crystallizer, can in principle achieve significant narrowing of size distribution. Such narrowing depends on preventing any appreciable homogeneous nucleation in the second and subsequent stages.

3.2 Destabilization of Colloidal Dispersions

3.2.1 Electrical Double Layer

Insoluble oxides and hydroxides in aqueous suspensions develop surface electrical charges by surface hydration followed by dissociation of surface hydroxyls (Parks, 1965). The negative charge originates from acidic dissociation of the surface hydroxyls (equation 29), and the positive charge is best explained based on proton addition to the neutral surface (equation 30).



Here, H^+ and OH^- are the potential-determining ions for oxides and hydroxides, and the surface potential depends on the pH of solution. Table 3-1 lists zero point charges for Fe(III) oxides and hydroxides. Suspensions in solution at pH above the

Table 3-1: Zero point charges of iron(III) oxides and hydroxides (modified from Parks, 1965).

ZPC	Mineral	Reference
5.7	Natural α -Fe ₂ O ₃ (Hematite)	Joy et al., 1964*
5.4	"	"
4.5-5.0	"	Chwastiak, 1963*
6.6±0.2	"	Parks, 1965
6.7±0.1	"	Iwasaki et al., 1960*
6.9±0.2	"	Korpi, 1960*
4.2	"	Johansen and Buchanan, 1957a*
6.7	"	Johansen and Buchanan, 1957b*
4.8	"	Fuerstenau, 1971*
8.7±0.1	Synthetic α -Fe ₂ O ₃ (Hematite)	Albrethson, 1963*
8.85±0.2	"	"
9.04±0.05	"	Korpi, 1960*
9.03±0.05	"	Parks and de Bruyn, 1962
8.77	"	"
8.7±0.2	"	"
8.4±0.1	"	Parks, 1960*
8.0±0.2	"	Miaw, 1957*
8.0	"	Johansen and Buchanan, 1957b*
6.5	"	"
8.3	"	Troelstra and Kruij, 1942*
8.6	"	Fuerstenau, 1971*
8.5	"	Breccusma and Iykema, 1971*
6.7±0.2	γ -Fe ₂ O ₃	Iwasaki et al., 1962*
6.1±0.1	α -FeOOH (Goethite)	Haningham, 1960*
6.7±0.2	"	Iwasaki et al., 1960*
6.7	"	Lengweiler et al., 1961*
5.7-7.2	"	Schuylenborgh et al., 1950a,b*
6.0-6.8	"	"
7.4±0.2	γ -FeOOH (Lepidocrocite)	Iwasaki et al., 1962*
5.4-7.3	"	Schuylenborgh et al., 1950a,b*
6.6	"	"
5.3-5.7	"	"
7	"Amorphous Hydroxides"	Zhabrova and Igorov, 1961*
8.5	"	Schuylenborgh et al., 1950a,b*
6.0	"	"
8.6	"	Hazel and Ayres, 1931*
7.2	"	Mattson, 1934*
7.0	"	Michaelis, 1926*
8.8±0.5	"	"
7.9	"	Davis and Leckie, 1978
8.0	"	Yates, 1975
7.5	"	Atkinson et al., 1975
7.5	"	Yates and Healy, 1975

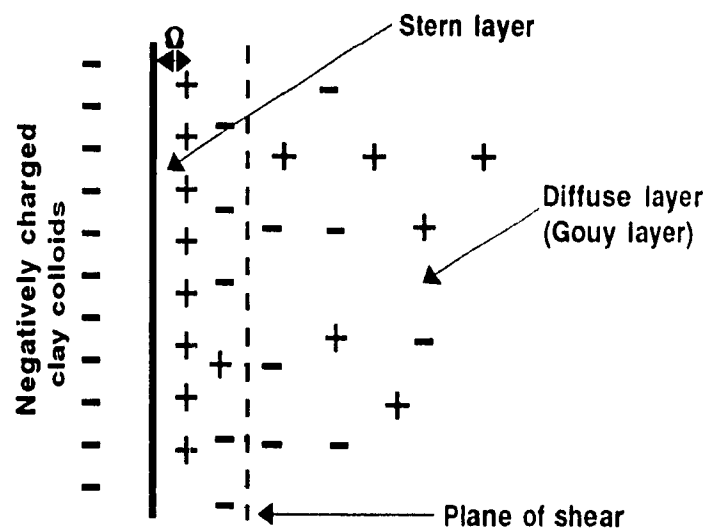
* ZPC values are taken from Parks (1965). Consult Parks (1965) for complete reference

ZPC are negatively charged, and at pH lower than the ZPC they are positively charged (Stumm and O'Melia, 1968; Tewari and Campbell, 1978). Natural hematite has a zero point charge comparable to goethite (5.5-7), while synthetically produced hematite has a higher ZPC between 7.5 and 9, similar to that for amorphous ferric hydroxide. Discrepancies between reported values of ZPC data stem from variations in formation conditions (e.g. media) also slight differences in lattice structures and the effect of impurities. Since the solution is neutral, there exists a layer of ions of opposite charge (counter-ions) at the interface of the suspended particles and the liquid phase. The ions involved in this electroneutrality are arranged in a way that constitutes what is called the electrical double layer (Benefield, 1982).

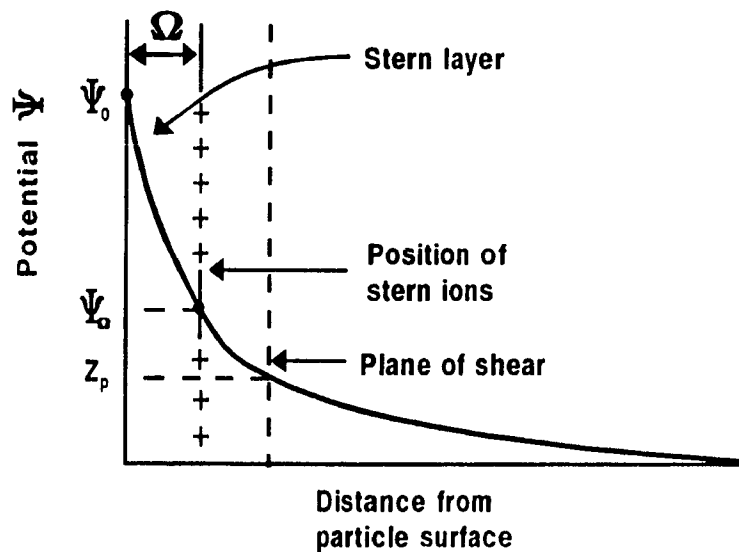
The complete model proposed by Stern is shown in Figure 3-7. According to this model the centre of the closest counter-ion is separated from the surface charge by a layer of thickness Ω (a distance approximately equal to the hydrated radius of the ion) in which there is no charge. This layer is referred to as the Stern layer. The electrical potential drops linearly across the Stern layer from a value of ψ_0 (Nernst potential) at the particle surface to a value of ψ_Ω , which is called the Stern potential. Beyond this point, in what is called the diffuse (Gouy) layer, the electrical potential decreases exponentially with increasing distance from the particle.

Since like charges repel, similarly charged colloids are held apart because of their electrical charge. The magnitude of this charge on a colloidal particle cannot be measured directly; however, a value of the potential at some distance from the particle can be calculated from a measurement of the electrophoretic mobility of the particle. This potential is called the zeta potential (Z_p). The magnitude of the zeta potential is a rough measure of the stability of a colloidal particle. At maximum or minimum zeta potentials one can expect slower settling rates, slower filtration and denser sludges (Wakeman et al., 1989). Coagulation is more successful at or near zero zeta potential.

As two similarly charged particles approach each other, their diffuse counter-ion atmospheres begin to interfere and cause the particles to be repelled. The amount of work required to overcome this repulsion and bring the particles from



a) Distribution of charges in the vicinity of a colloidal particle



b) Distribution of potential in the electrical double layer

Figure 3-7: Stern model for electrical double layer (van Olphen, 1977).

finite separation to a given distance apart is called the repulsive energy or repulsive potential, V_R , at that distance. Consequently, the repulsive energy between two particles decreases roughly exponentially with increasing particle separation as shown in Figure 3-8. The van der Waal's forces of attraction, which oppose the repulsive forces are largely due to universal attractive forces (also called dispersion forces). The London-van der Waal's attractive energy of interaction V_A , between two particles is inversely proportional to the second power of the distance separating the particles and thus decreases very rapidly with increasing intermolecular distance (O'Melia, 1969). The variation in particle attractive energy with particle separation distance is shown in Figure 3-8.

The repulsion and attraction curves can be combined to form a curve representing the resultant energy of interaction. To come together, the particles must possess enough kinetic energy to overcome the energy barrier on the total energy curve.

3.2.2 Destabilization Mechanisms

The effective removal of the colloidal and suspended particulates from water depends on a reduction in particulate stability. To induce colloidal particles to aggregate, two distinct steps must occur: (1) the repulsion forces must be reduced (i.e. the particle must be destabilized), and (2) particle transport must be achieved to provide contacts between the destabilized particles (Stumm and O'Melia, 1968). Colloidal particle destabilization can be achieved by four mechanisms; (1) double layer compression, (2) adsorption and charge neutralization, (3) enmeshment in a precipitate, and (4) adsorption and interparticle bridging.

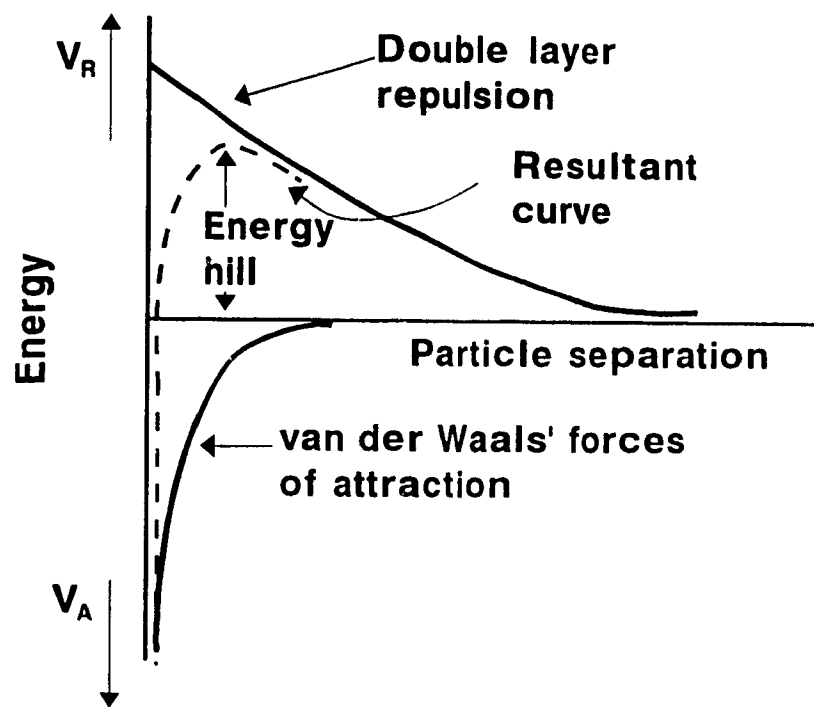


Figure 3-8: Repulsive and attractive energies as a function of particle separation (van Olphen, 1977).

3.2.2.1 Double layer compression

It has long been known that colloidal systems could be destabilized by the addition of ions having a charge opposite to that of the colloid. The Schulze-Hardy rule documents this phenomenon:

The coagulating power of a salt is determined by the valency of one of its ions. The prepotent ion is either the negative or positive ion, according to whether the colloidal particles move down or up the potential gradient. The coagulating ion is always of the opposite electrical sign to the particle.

The Schulze-Hardy rule is valid for indifferent electrolytes that do not engage in any sort of reaction with the sol.

The phenomenon observed by Schulze and Hardy is attributed to compression of the electrical double layer surrounding the colloidal particle and can be explained by the theory developed by Verwey and Overbeek (1948). The diffuse layer contains a quantity of counter ions sufficient to balance the electrical charge on the particle. The charge distribution in the diffuse layer of a negatively charged colloid can be represented by curve ABCD in Figure 3-9. The line BD represents the concentration of both cations and anions at a large distance. The average local concentration of ions of opposite charge, to the charge of the particle, is given by curve DA, and the concentration of ions with the same charge as that of the particle, is given by curve DC. The surface area CAD represents the total, net, diffuse layer charge, which is equivalent to the surface charge (van Olphen, 1977).

If an electrolyte is added to the colloidal dispersion, the surface charge on the particles will remain unchanged if that charge originates from crystal imperfections. However, the added electrolyte will increase the charge density of the diffuse layer required to neutralize the surface charge, thus the diffuse layer is compressed towards the particle surface as shown by curve A'B'C'D' in Figure 3-9. The total net charge in the diffuse layer has not changed (area CAD = area C'A'D'), but the thickness of the layer has been reduced. The effect of this compression is to change the distribution of double layer repulsion forces about the colloid and cause reduction in surface potential with increasing electrolyte concentration, which allows

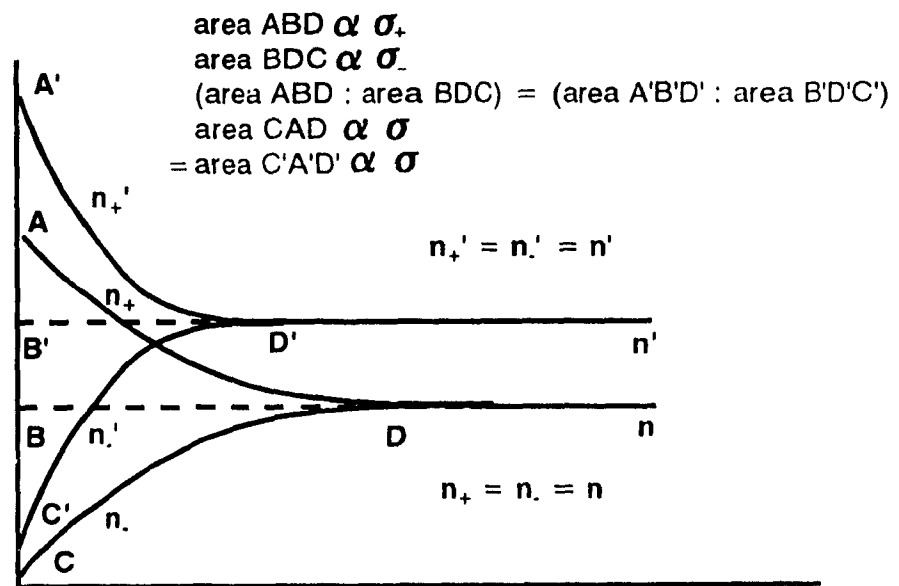


Figure 3-9: Charge distribution in the diffuse double layer of a negative particle surface at two electrolyte concentrations for a constant surface charge (after van Olphen, 1977). (n = total ion concentration, n_+ and n_- are local concentrations of positive and negative ions, respectively; σ = surface charge, σ_+ and σ_- are the positive and negative surface charges respectively).

the van der Waal's attractive forces to be more dominant, thus enhancing particle aggregation (Benefield, 1982).

The effect on particle stability through increasing the electrolyte concentration is shown in Figure 3-10. At low electrolyte concentrations, the resultant of repulsion and attractive forces shows a high energy barrier that must be overcome if agglomeration is to occur. At a high electrolyte concentration, the double layer has been compressed, and the resultant curve shows no repulsion at any distance. Particle agglomeration occurs very rapidly.

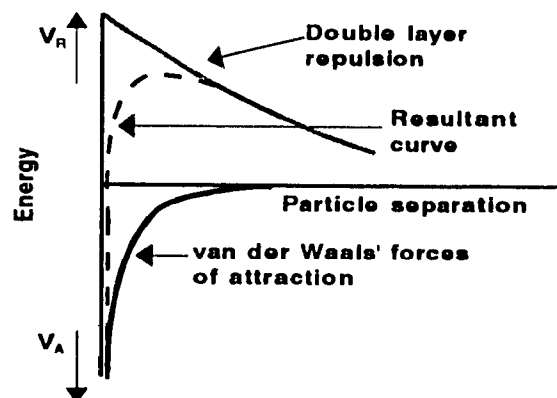
A mathematical model developed by Derjaguin and Landau (1941) and Verwey and Overbeek (1948) make it possible to calculate the concentration of an indifferent electrolyte required to cause coagulation. This model predicts that the coagulation concentration for counter-ions with charge number 1, 2, and 3 should be in the ratio of

$$\frac{1}{1^6} : \frac{1}{2^6} : \frac{1}{3^6} \quad \text{or equivalent ratios } 1000: 16: 1.3 \text{ (Shaw, 1970)}$$

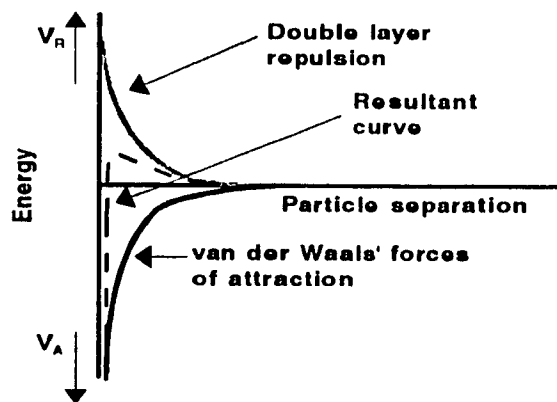
Thus, the theoretical model is in good agreement with the empirical Schulze-Hardy Rule.

Two interesting aspects of double layer compression are (1) the concentration of indifferent electrolyte necessary to destabilize the colloid depends on the valence of the ions, and conforms to the Schulze-Hardy rule. The critical coagulation concentration (CCC), the minimum concentration above which coagulation or more precisely destabilization is produced, is practically independent of the concentration of the dispersed phase. (2) Concentration of electrolyte in excess of CCC cannot restabilize the colloidal dispersion (Stumm and O'Melia, 1968). Therefore, it is not possible to cause charge reversal on a colloid by double-layer compression, regardless of how much electrolyte is added.

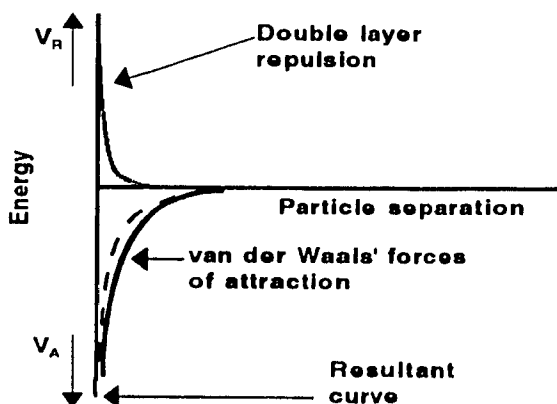
The double-layer model, although of great theoretical importance, is restricted in its application to lyophobic colloids and simple electrolytes. This arises primarily from the fact that this model neglects the dominating role that chemical forces may



(a) Low electrolyte concentration with normal double layer thickness. System is stable and agglomeration is imperceptible.



(b) Intermediate electrolyte concentration causes some double layer compression. Slow agglomeration can occur.



(c) High electrolyte concentration causes severe double layer compression. Rapid agglomeration can occur.

Figure 3-10: Effect of electrolyte concentration on Double Layer Compression (after van Olphen, 1977).

play in causing adsorption. Apparently the electrostatic repulsive forces between similar colloidal particles can be overcome by adsorbable ions.

3.2.2.2 *Adsorption and charge neutralization*

Some chemical species can be adsorbed at the surface of colloidal particles. If the adsorbed species carries a charge opposite to that of the colloid, such adsorption causes a reduction of surface potential and a resulting destabilization of the colloidal particle (Gregory, 1978). Destabilization by adsorption differs from destabilization by double layer compression in three important ways. First, adsorbable species can destabilize colloids at much lower dosages than non-sorbable, "double layer compressing" ions (Tamamushi and Tamaki, 1959). Second, destabilization by adsorption is stoichiometric. In other words the dosage of the coagulant required increases as the concentration of colloid (more specifically, the total surface area of the colloid) increases. Contrastingly, the amount of electrolyte required to achieve coagulation by double-layer compression is not stoichiometric and is practically independent of colloid concentration.

Third, it is possible to overdose a system with an adsorbable species and cause restabilization as a result of charge reversal on the colloid particle. The fact that ions can be adsorbed beyond neutralization to a point of charge reversal suggests specific chemical interactions can outweigh electrostatic repulsion effects occasionally (Stumm and O'Melia, 1968).

3.2.2.3 *Enmeshment*

Enmeshment is the mechanism of destabilization (Packham, 1965; Stumm and O'Melia, 1968), in which finely divided particulates are entrapped in the amorphous precipitate formed. This mechanism is otherwise called sweep floc. Packham explained enmeshment or sweep coagulation as a nonstoichiometric behaviour of colloids and coagulants.

3.2.2.4 *Interparticle bridging*

Natural polyelectrolytes as starch, cellulose, polysaccharide gums, and proteinous materials, as well as a variety of synthetic polymeric compounds are effective coagulating agents. These materials are characterized by a large molecular

size and most have multiple electrical charges along a chain of carbon atoms (Benefield et al., 1982).

Research has revealed that both cationic and anionic polymers can destabilize negatively charged colloidal particles. Neither the double layer compression model nor the charge neutralization model can be used to explain these results. Ruehrwein and Ward (1952) and La Mer and Healy (1963) have developed a chemical bridging theory that is consistent in explaining the observed behaviour of polymeric compounds.

The chemical bridging theory proposes that a polymer molecule will become attached to a colloidal particle at one or more sites as shown in reaction 1, Figure 3-11. Attachment may result from coulombic attraction if the polymer and particle are of opposite charge, or from ion-exchange, hydrogen bonding, van der Waals forces if they are of similar charge (O'Melia, 1969). The "tail" of the adsorbed polymer will extend out into the bulk of the solution and can become attached to vacant sites on the surface of another particle to form a chemical bridge as shown in reaction 2 (Figure 3-11). This bridging action results in the formation of a floc particle having favourable settling characteristics. If the extended segment fails to contact another particle, it may fold back and attach to other sites on the original surface, thus destabilizing the particle as shown in reaction 3.

Inefficient coagulation may result from an overdose of polymer to the system or from intense prolonged agitation (Huck et al., 1977). If excessive polymer is added, the segments may saturate the surface of the colloidal particles so no sites are available for the formation of polymer bridges (reaction 4). This can restabilize the particles (Gregory, 1978) and may or may not be accompanied by charge reversal. This is contrary to electrolyte addition in which overdosing the system does not lead to restabilization or charge reversal. Intense or prolonged mixing may destroy previously formed bridges and lead to restabilization as shown in reactions 5 and 6 (Figure 3-11).

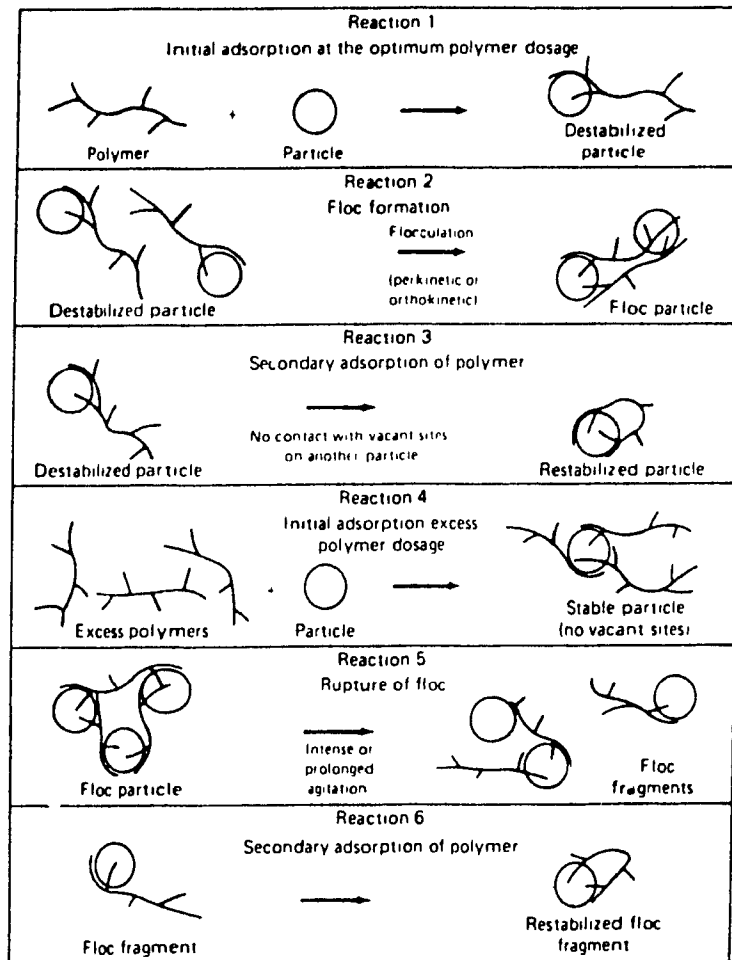


Figure 3-11: Schematic of reactions between colloidal particles and polymers (Black, Birkner, and Morgan, 1965).

In the case of flocculation by polyelectrolytes of the same charge as the particle, the effect of added salts is difficult to interpret since ionic strength significantly influences interparticle bridging as shown in Figure 3-12. As well, the size, shape, degree of hydration, character of ligands in complexes, and other parameters also play an important role on colloidal stability (Matijević, 1973).

Synthetic organic polymers can be used in the place of natural polyelectrolytes. Although polymers are beneficial in water treatment (Table 3-2), their use is limited due to high cost and uncertainties regarding chemical impurities associated with polymer synthesis (Montgomery, 1985). Such uncertainties have restricted the maximum concentration recommended by regulatory agencies.

Table 3-2: The effect of polymer addition on effluent metal concentration and slurry settling rate (Huck and LeClair, 1976).

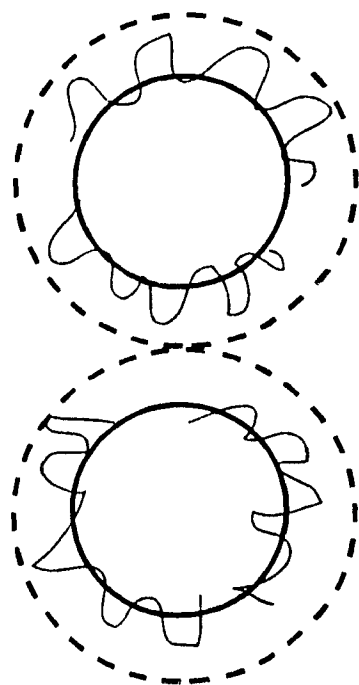
Condition	Metal Concentration (mg/L)			Settling Rate (m/s)
	Fe	Zn	Cu	
No Polymer	2.24	3.22	0.58	1.78
Polymer	0.20	0.11	0.06	7.31

Dosages of only 0.5 to 1.5 g/L are often effective for coagulation, whereas as much as 10 to 20 times that amount of alum would be required to achieve the same results. Without precise dosage control, polymers will not yield satisfactory performance (Huck et al., 1977).

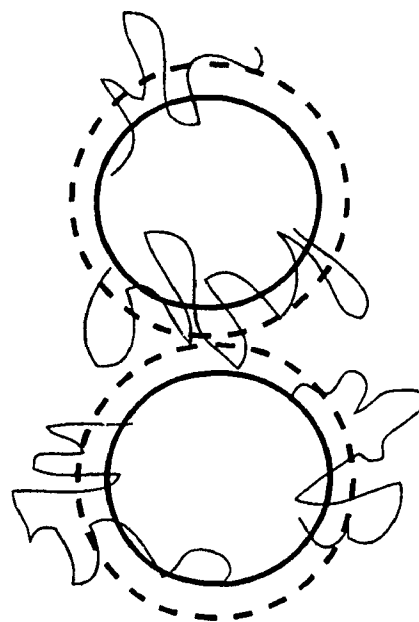
Data for the adsorption of polymer in various systems have been found to fit the Langmuir adsorption isotherm (AWWA, 1971).

$$\frac{\theta}{(1-\theta)} = bP \quad (\text{Huck et al., 1977})$$

Where: θ is the fraction of adsorbent surface covered by adsorbed segments,
 b is the equilibrium constant for the adsorption-desorption reaction,
and, P is the activity of the polymer in solution.



(a)



(b)

Figure 3-12: (a) Low ionic strength-bridging prevented by electrical repulsion. (b) High ionic strength-bridging across the effective repulsion distance (Gregory, 1978).

Although the mathematical theory developed by La Mer and Smellie (1956) predicts maximum flocculation when the particle surface is half covered by polymer molecules ($\theta = 1/2$), other factors such as particle concentration, interparticle repulsive forces, solution ionic strength, polymer configuration in the adsorbed state and intensity and duration of agitation are probably more important in determining the extent of destabilization (AWWA, 1971). The overall flocculation reaction is rapid and to a great degree is irreversible (Huck et al., 1977).

3.2.3 Flocculation of Hydroxides

The few reported studies on polymer flocculation of metal hydroxides are cursory. Schwoyer and Luttinger (1973), in discussing polymer conditioning for the dewatering of metal hydroxide sludges, mentioned only the need for high molecular weight and (usually) for a polymer with charge opposite to that of the sludge particles. Graczyk and Hornof (1984) tested cellulose and its graft co-polymers as lime additives on flocculation experiments in simulated mine water containing iron, zinc, and copper salts. The results showed that all the cellulosic products had a beneficial effect on the removal of ferric iron. As well, the U.S. Environmental Protection Agency (EPA, 1970) investigated the addition of various substances, including anionic polymers to achieve the isoelectric point for ferrous and ferric hydroxide sludges. Dosages were obtained for various polymers and brief tests were carried out on the improvement in settling rate caused by their addition. The choice of sodium or calcium hydroxide as the neutralizing agent may affect flocculation, because of the difference in valence of the two cations (Huck et al., 1977).

3.3 Summary

There are two principal crystallization mechanisms, 1) nucleation and 2) growth. Both mechanisms are controlled by the saturation ratio of the precipitating solution. High levels of supersaturation promote homogeneous nucleation and the production of colloids. As well, the higher is S the faster the rate of nucleation and the greater the number of nuclei forms. Heterogeneous and secondary (surface) types of nucleation predominate at lower supersaturation levels and involve the

formation of nuclei on the surface of an existing solid. The growth of the surface nuclei is enhanced by increased mass transfer of the solute (accelerated agitation), low supersaturation levels, and particle roughness. Certain ions (commonly found in acidic mineral effluents) can retard this growth process by altering the surface chemistry of the hydroxide.

Colloidal particles produced through homogeneous nucleation can be destabilized by four mechanisms; (1) double layer compression, (2) adsorption and charge neutralization, (3) enmeshment in the precipitate, and (4) adsorption and interparticle bridging using polymer additives. These additives significantly improve the physical properties of the sludge, most notably the settling rate.

The material presented in this chapter is of great significance with respect to effluent treatment. By neutralizing in such a way so to maintain and control the level of supersaturation in the solution, hydroxide particles in solution will grow and crystallization will be promoted. In most existing treatment operations the hydrolysis reaction is forced to completion very quickly through a rapid adjustment of pH, in turn, leading to homogeneous nucleation and the formation of the infamous ferric hydroxide gels that plague treatment operations.

Besides encouraging chemical growth of the precipitate, physical growth, or aggregation can also be achieved by varying the hydrolysis conditions (e.g., pH, rate of agitation, etc.) or by introducing a chemical additive to the system that will enhance aggregation.

Therefore, several changes to the simple neutralization process can be examined so to improve the properties of the treatment sludge. Many of these possible modifications will be experimentally investigated in the upcoming chapters.

CHAPTER 4: THERMODYNAMIC PREDICTION OF THE Fe(III)-SO₄-H₂O AQUEOUS EQUILIBRIA

Prior to the commencement of the experimental investigation a thorough thermodynamic analysis was undertaken with the aim to establish quantitatively the solution (speciation) and the solid-solution equilibria of the Fe(III)-SO₄-H₂O system under a variety of possible operating conditions (i.e. pH, temperature, sulphate ion concentration).

The establishment of the respective equilibria was accomplished with the aid of the Facility for the Analysis of Chemical Thermodynamics system or F*A*C*T (Bale et al., 1991) which is available at McGill University. Three types of thermodynamically defined diagrams were calculated for the Fe(III)-SO₄-H₂O system: predominance area diagrams, speciation diagrams, and solubility diagrams.

4.1 Thermodynamic Calculations

4.1.1 Thermodynamic Data

Prior to performing the calculations it was necessary to identify all possible complexes that may exist in the solution and obtain consistent thermodynamic data to enter into F*A*C*T. Table 4-1 outlines the Fe(III) complexes considered and the thermodynamic data collected. Ternary ferric hydroxyl-sulphato complexes probably exist. There are no published data for these species; however a comparison of pK values for other metal species suggests that the pK² for Fe(OH)SO₄ and Fe(OH)₂SO₄⁻ at 25°C would be in the order of 2.3 and 0.8 respectively (Stipp, 1990).

4.1.2 Assumptions

Several assumptions were made in order to make the calculations possible, as outlined below:

$$^2 K = \exp (-\Delta G_{\text{rxn}}^{\circ} / RT)$$

Table 4-1: Iron species and thermodynamic data used for the construction of predominance area diagrams. (Data from Bale et al.; Barin et al., 1977; Barners and Scheurman, 1978; Papangelakis and Demopoulos, 1990; Wagman et al, 1968, 1971).

Compound	ΔG_f kJ/mol	ΔH_f kJ/mol	S°_{298} J/mol K	Cp [A,B,C] J/K/mol
FeSO_4^+	-772.8	-931.78	-129.704	37.70,316.77,-1.00
FeHSO_4^{2+}	-768.38	-894.29	-18.68	0
$\text{Fe}_2(\text{SO}_4)_3$	-2243	-2825.04	-571.534	0
$\text{Fe}(\text{SO}_4)_2^-$	-1524	-1828.39	-43.069	0
$\text{FeSO}_4\text{HSO}_4$	-1514	-	+ 159.863	0
HSO_4^-	-756.01	-887.008	+ 131.796	-547.3,1342.1,266.8
H_2SO_4	-744.63	-909.267	+ 20.083	-292.88
OH^-	-157.293	-230.878	-10.878	506.4,-1181.3,-246
FeOH^{2+}	-229.41	-290.80	-142.256	19.39,-21.21,29.13
$\text{Fe}(\text{OH})_2^+$	-446.4	-543.80	-29.288	0
$\text{Fe}(\text{OH})_3^0_{(\text{aq})}$	-647.6	-795.73	+ 75.4	0
$\text{Fe}(\text{OH})_4^-$	-830.1	-1050.40	+ 24.5	0
$\text{Fe}_2(\text{OH})_2^4$	-467.3	-611.38	-355.64	124.7,-619.2,13.8
H_2O	-237.178	-285.851	+ 69.959	75.438
Fe_2O_3	-742.2	-825.503	+ 87.446	98.3,77.8,-14.85
Fe^{3+}	-4.6	-48.50	-315.892	-79.09,-219.4,15.4
SO_4^{2-}	-744.63	-909.183	+ 20.083	874.6,-1759.7,-520
H^+	0	0	0	0
$\text{Fe}(\text{OH})_3(\text{s})$	-696.63	-832.61	+ 104.6	85.51,123.24,-15.12
FeOOH	-489.00	-558.98	+ 234.83	74.4

- (1) The F*A*C*T system assumes zero ionic strength, therefore activity is equivalent to concentration. This assumption is generally valid at low concentrations where the solution approaches ideality, but at higher ionic

strengths ($I > 2$) the assumption becomes invalid. For this reason trends observed at a high sulphate concentration may significantly deviate from reality. In this chapter, the thermodynamic calculations are reported in molar concentration units as given by $F^*A^*C^*T$, but rigorously speaking they should be activities.

- (2) $F^*A^*C^*T$ assumes the most predominant species always has a concentration equal to that defined by the Fe(III) concentration (line 102 in the PREDOM program). Therefore, the assumption that the total Fe(III) concentration remains constant over the entire pH range was taken to be valid when the less dominant species constituted less than 10% of the total Fe(III) in solution. Deviation from reality is then more probable when two or more species have concentrations close to that of the predominant species.
- (3) Another source of error introduced in the calculations is the extrapolation of the heat capacity (C_p) data to higher temperatures. Since the temperature difference was moderate (55°C) this extrapolation should not cause significant errors.
- (4) Thermodynamic predictions calculated at low temperatures often do not accurately represent what is observed experimentally. This is due to slower kinetics. At low temperatures, kinetics generally determine what species will be present and which compounds will precipitate. Thermodynamically, Fe_2O_3 is more stable but at low temperatures precipitation is kinetically controlled and ferric hydroxide has been observed to form instead. For that reason the formation of all iron hydrolysis precipitates except ferric hydroxide were suppressed.
- (5) In order to simplify the system all the sulphate in solution was assumed to be free (SO_4^{2-}). Bisulphate species were assumed negligible since they only dominate below pH 2 (Burkin, 1966) while most acidic mineral effluents possess a pH greater than 2.

4.2 Predominance Area Diagrams

The methodology and conditions used in the calculation of the predominance area diagrams are outlined in Appendix A.

4.2.1 Effect of $\text{Fe}(\text{OH})_3$ Precipitation

Predominance area diagrams were calculated at 25°C for the case when $\text{Fe}(\text{OH})_3$ is allowed to precipitate. The diagram calculated for several iron concentrations is shown in Figure 4-1 (0.1 M $\text{Fe}(\text{III})_T$ (5.585 mg/L) and lower). For all iron(III) concentrations, except for very dilute $[\text{Fe}(\text{III})]$ (10^{-5} M), only three species appear. At low sulphate concentrations (generally less than 10^{-4} M SO_4^{2-}) the precipitation precursor is the free ferric ion. Exceeding this sulphate concentration results in the predominance of sulphate complexes, first with FeSO_4^+ and then $\text{Fe}(\text{SO}_4)_2^-$ when the concentration of free sulphate exceeds approximately 3.5 g/L. At extremely low $\text{Fe}(\text{III})$ concentrations (10^{-5} M) the formation of FeOH^{2+} is thermodynamically stable and forms over a narrow pH range. The pH at which ferric hydroxide precipitates is dependent on the aqueous precursor. Precipitation occurs at a lower pH (pH = 1) if the dominant iron(III) species is Fe^{3+} . However, at intermediate sulphate concentrations hydrolysis occurs at a higher pH, suggesting sulphate complexation depresses hydrolysis. The pH of precipitation appears to be directly related to the amount of free sulphate in solution. As the concentration of $\text{Fe}(\text{III})$ in solution is decreased the pH at which precipitation occurs increases. As less iron(III) is available for $\text{Fe}(\text{OH})_3$ precipitation, a higher pH is required to yield a greater concentration of hydroxyl ions required to exceed the solubility product for $\text{Fe}(\text{OH})_3$.

4.2.2 Speciation

Ferric hydroxide is the predominant compound/species present in the hydrolyzing system above pH 3 (once more all other solid phases were suppressed in this thermodynamic analysis). For this reason, these predominance area diagrams provide limited information at higher pH values (pH > 3). However, by suppressing the formation of all solids, including $\text{Fe}(\text{OH})_3$, predominance area diagrams were calculated in order to observe the $\text{Fe}(\text{III})$ - SO_4 - H_2O speciation and in turn suggest

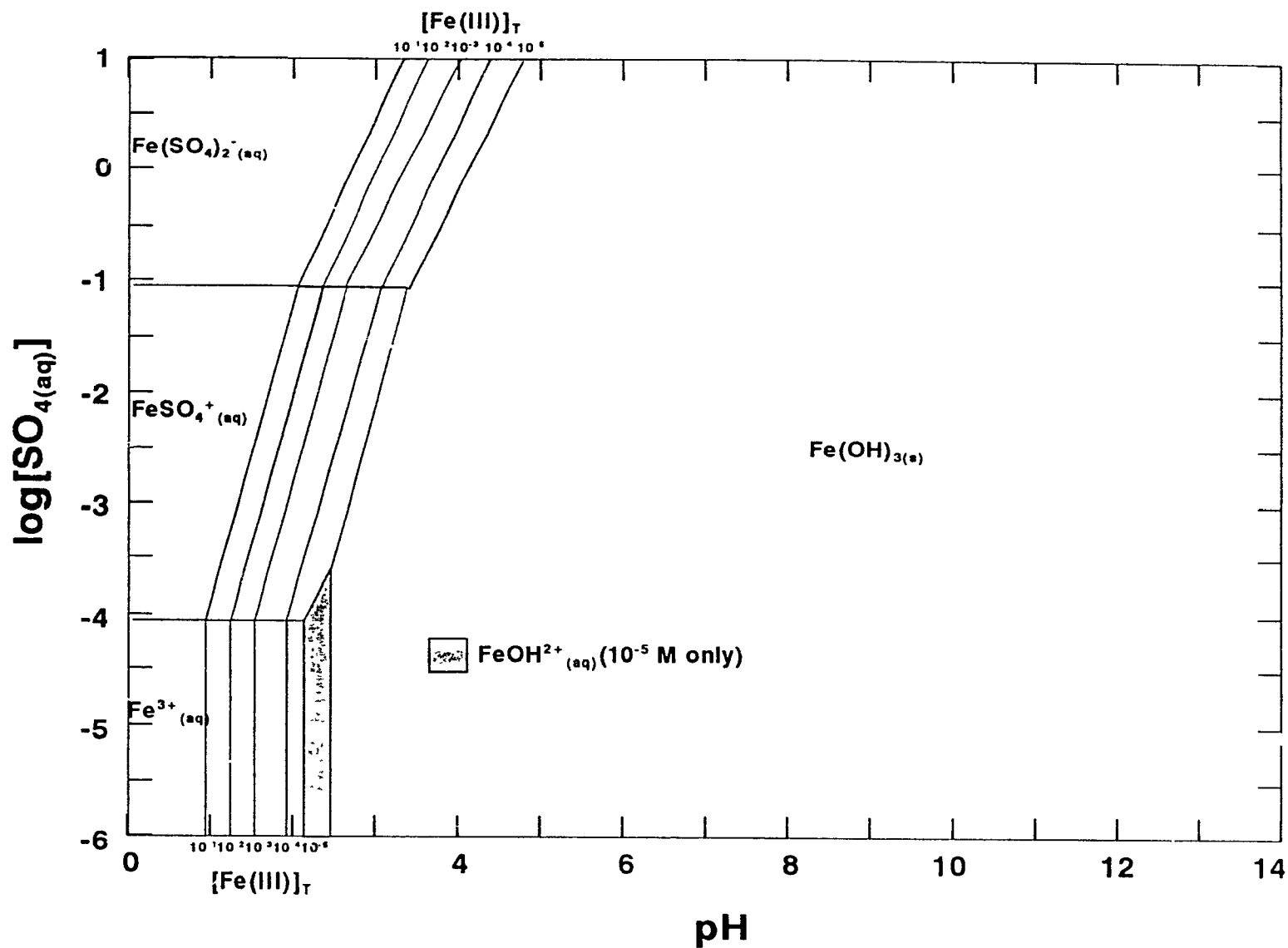


Figure 4-1: Predominance area diagram for the Fe(III)-SO₄-H₂O system for varying Fe(III) concentrations showing the region of Fe(OH)₃ precipitation.

possible precipitation precursors. A predominance area diagram was calculated for varying Fe(III) concentrations and is given in Figure 4-2.

Seven iron(III) species are defined by the diagram. Iron(III) sulphate complexes are more abundant when the sulphate concentration is high and the pH is less than 2. Under these conditions the formation of $\text{Fe}(\text{SO}_4)_2^-$ and FeSO_4^+ depends on a direct relationship between free sulphate concentration and pH. As the pH increases the concentration of hydroxyl ions also increases. Hydroxyl and sulphate ions compete for ferric ion. At low sulphate concentrations ferric hydroxide pair formation is favoured at a lower pH than in sulphate abundant solutions due to the surplus of hydroxyl ions present. The variation in Fe(III) concentration on the speciation observed is negligible except at high Fe(III) concentration (0.1 M). In this case the formation of FeOH^{2+} is inhibited by the generation of the polynuclear complex $\text{Fe}_2(\text{OH})_2^{4+}$.

4.2.3 The Effect of Temperature

With increasing temperature the equilibrium pH decreases and hydrolysis is favoured (Figure 4-3a). The effect is less significant at higher sulphate concentrations. The decrease in hydrolysis pH at 80°C when $\text{Fe}(\text{SO}_4)_2^-$ is the precursor is approximately five times less than when ferric ion is the predominant species, suggesting sulphato complexes to be more resistant to hydrolysis.

$\text{Fe}(\text{OH})_3^{\circ}_{(\text{aq})}$ continues to dominate the diagram at higher temperatures (Figure 4-3b). At elevated temperatures the predominant monomer is FeOH^{2+} , however, at 25°C, the dimer, $\text{Fe}_2(\text{OH})_2^{4+}$, is also common. The dimer is a more ordered species as indicated by its entropy (Table 4-1). Raising the temperature favours disorder so the monomer species prevails.

4.3 Speciation Diagrams

The predominance area diagrams only display the predominant compound or species present in a defined (pH, $[\text{SO}_4]$) region. In order to reveal all species present in the system speciation diagrams need to be constructed. Several speciation diagrams for Fe(III) in the absence of sulphate ion have been published (Baes and

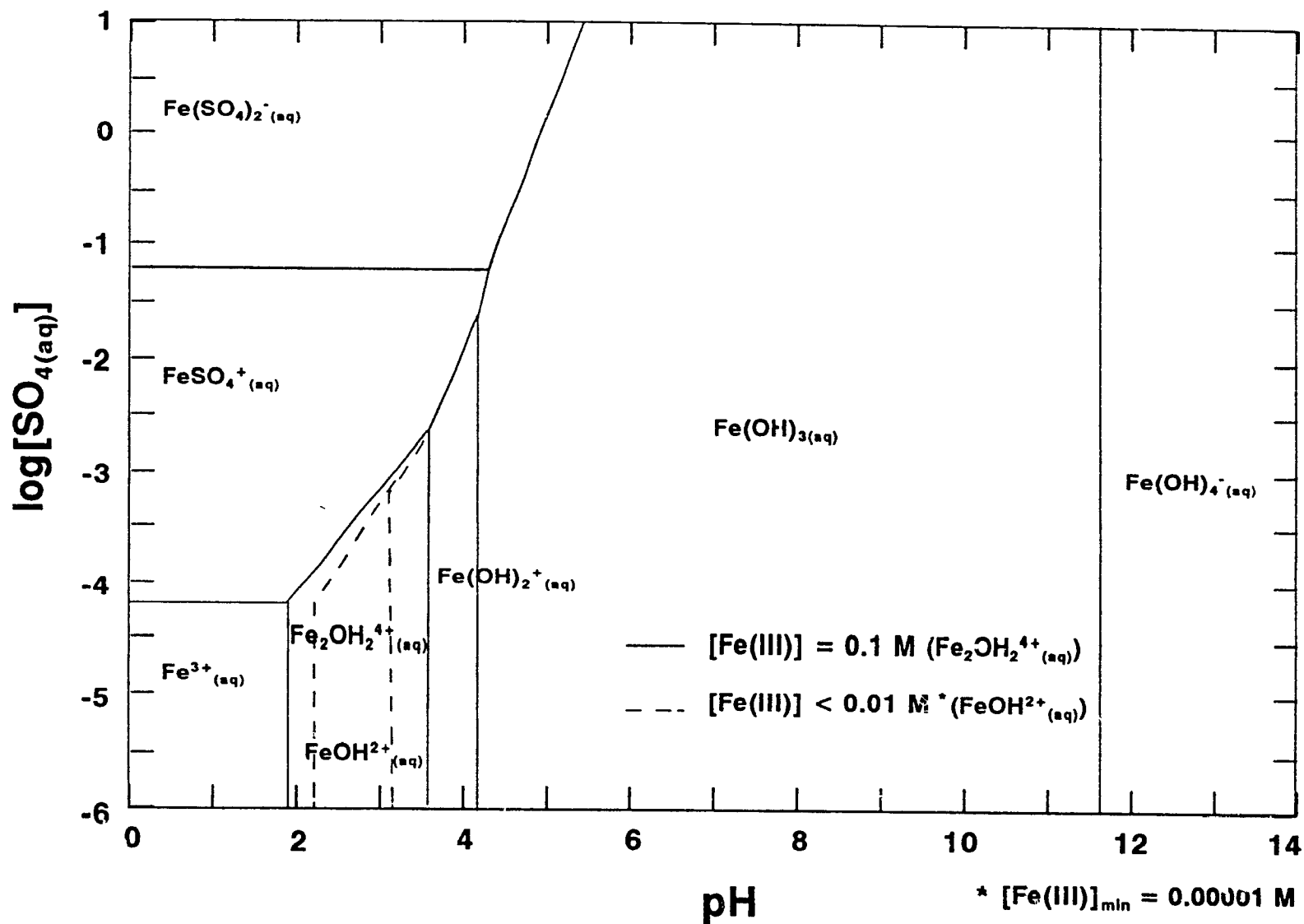


Figure 4-2: Predominance area diagram for the Fe(III)-SO₄-H₂O system for varying Fe(III) concentrations when Fe(OH)₃ precipitation is suppressed to illustrate the speciation.

Mesmer, 1976; Sapieszko et al., 1977) however, the literature on distribution of species in the Fe(III)-SO₄-H₂O system is limited. Sapieszko et al. (1977) calculated diagrams for a narrow pH range (0.7 - 2.2). Comprehensive speciation diagrams in the same pH range (< 2.5) were recently published by Filippou et al. (1993) at various temperatures for the same system as well. In the present study speciation diagrams were calculated for varying sulphate concentrations. The methodology and conditions used in the calculation of the speciation diagrams are outlined in Appendix A.

Under intermediate conditions ([SO₄²⁻] = 0.1 M, [Fe(III)]_T ~ 0.1 M, 298 K) five species appear to be present in a significant amount. The speciation diagrams calculated (Figures 4-4 and 4-5) indicate an absence of free Fe³⁺ in solution with the exception of very low [SO₄²⁻] (10⁻⁵ M). All the iron(III) in solution is either complexed with sulphate or with hydroxyl ions. At pH < 3 the iron exists in sulphate complexes, the most common of which is Fe(SO₄)₂⁻, which is almost twice as abundant as FeSO₄⁺. Above pH 3, ferric hydroxide complexes become more abundant due to the increased OH⁻ concentration. The formation of Fe(OH)₂⁺ is over-shadowed by the predominant Fe(OH)_{3(aq)}⁰ neutral species which represents most of the iron(III) in solution in the pH region between pH 5 and 11. Above pH 12, Fe(OH)₄⁻ is the most common hydroxyl complex and by pH 13 all the Fe(III) in solution exists as Fe(OH)₄⁻.

Decreasing the sulphate ion concentration (Figure 4-5a) effectively causes the Fe(III)-SO₄²⁻ complexes to disappear and instead of Fe(III)-OH⁻ complexes to dominate in a wider pH range. By increasing the temperature (Figure 4-5b), the abundance of sulphato complexes is increased at a lower pH, especially Fe(SO₄)₂⁻. As well, Fe(OH)_{3(aq)}⁰ becomes less stable while Fe(OH)₄⁺ is more abundant.

4.4 Solubility Diagrams

The solubility of Fe(III) has been widely investigated as discussed in Chapter 2. However, solubility data for Fe(III) in sulphate media is limited. In order to better comprehend Fe(OH)₃ solubility in sulphate systems solubility lines (Figure 4-6)

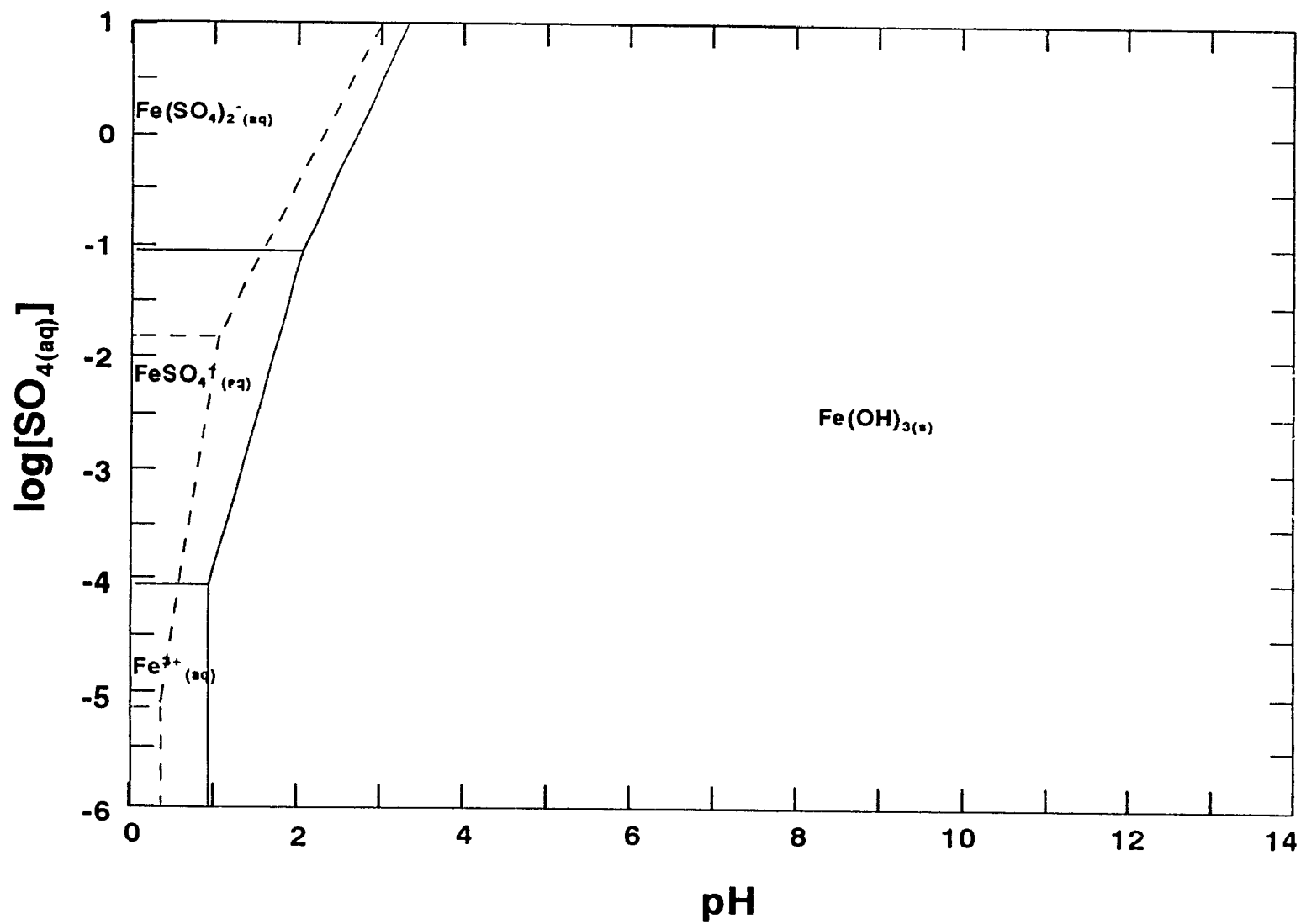


Figure 4-3a: The effect of temperature on the precipitation of ferric hydroxide, (— 298 K; - - - 353 K).

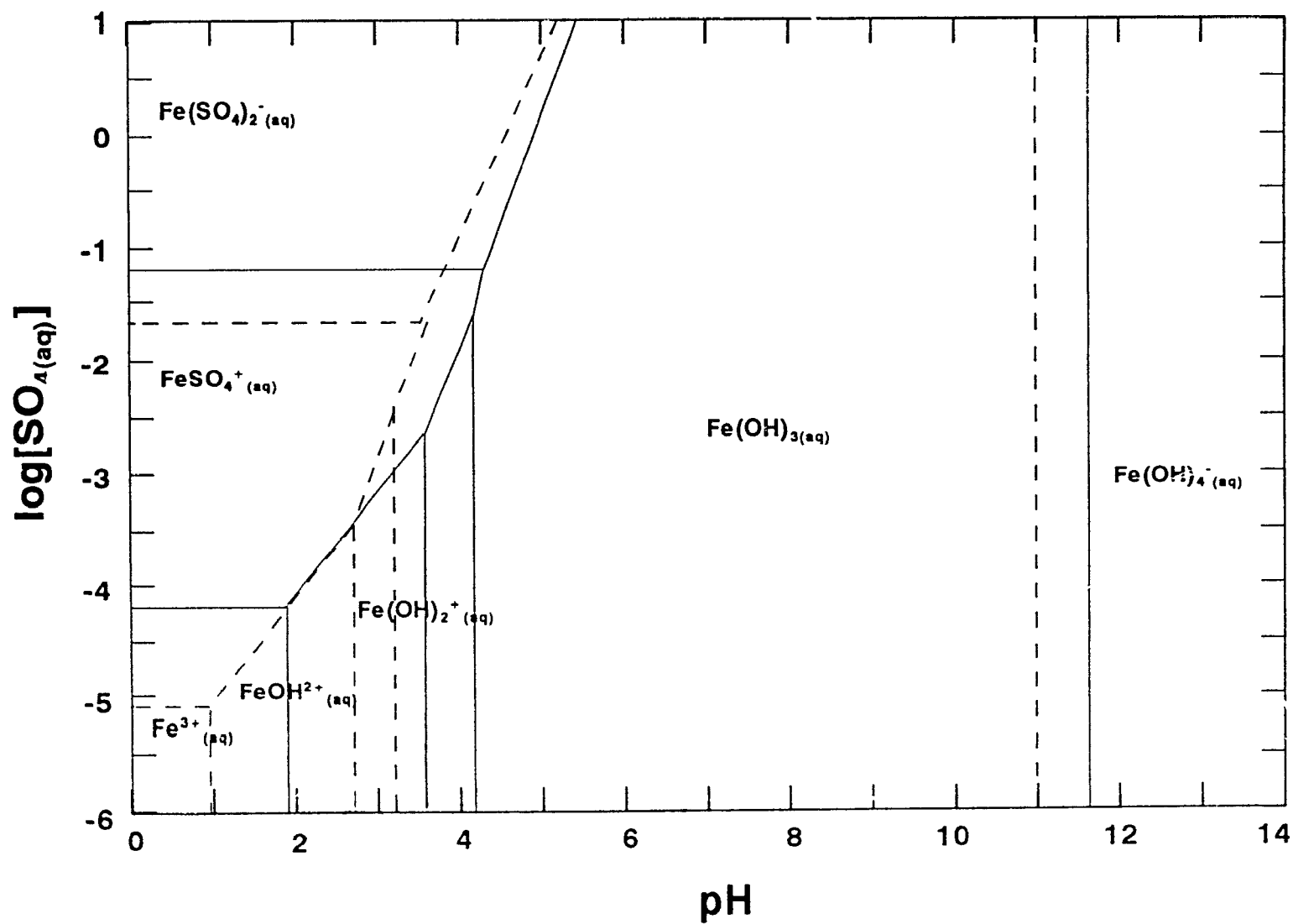


Figure 4-3b: The effect of temperature on the speciation of Fe(III), (— 298 K; - - - 353 K).

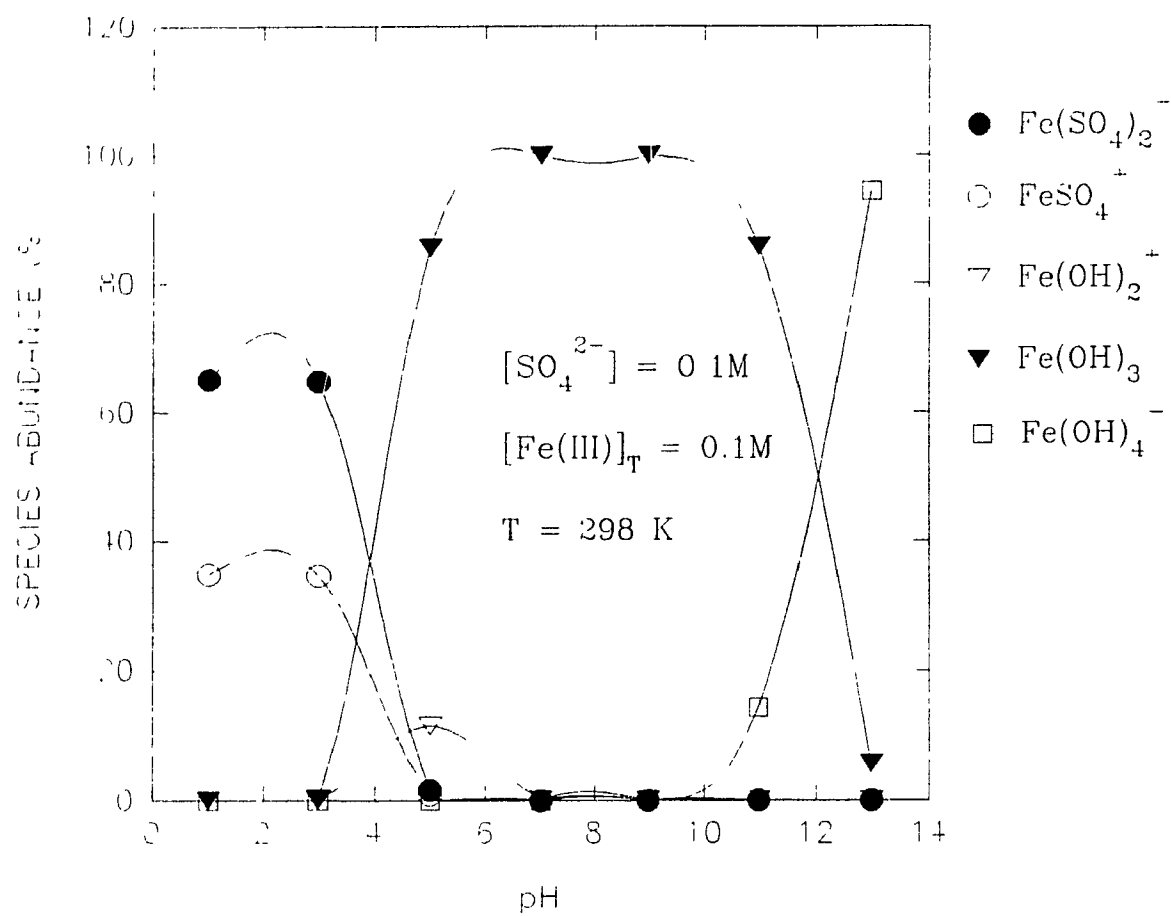


Figure 4-4: Speciation diagram for the Fe(III)-SO₄-H₂O system calculated by using F*A*C*T.

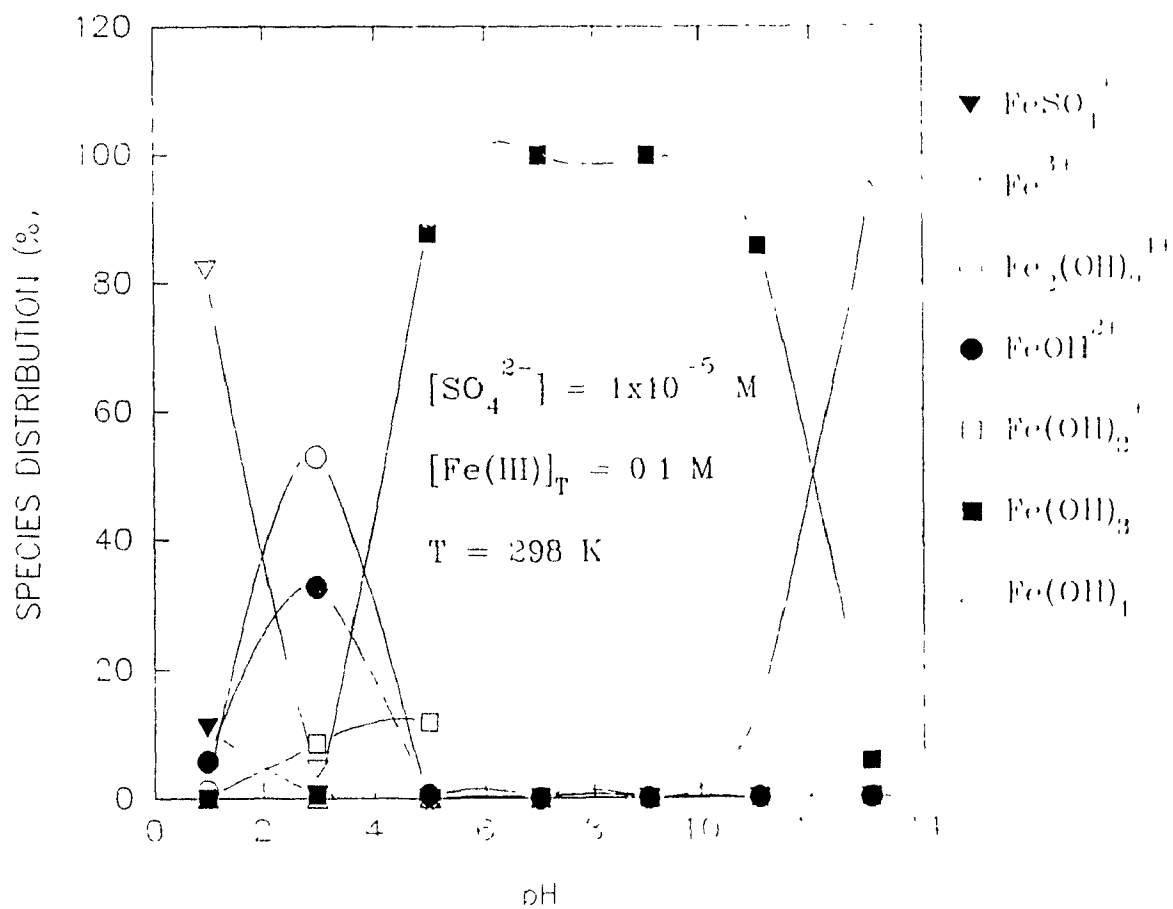


Figure 4-5a: Speciation diagram for the Fe(III)-SO₄-H₂O system calculated by using F*A*C*T for low sulphate concentrations.

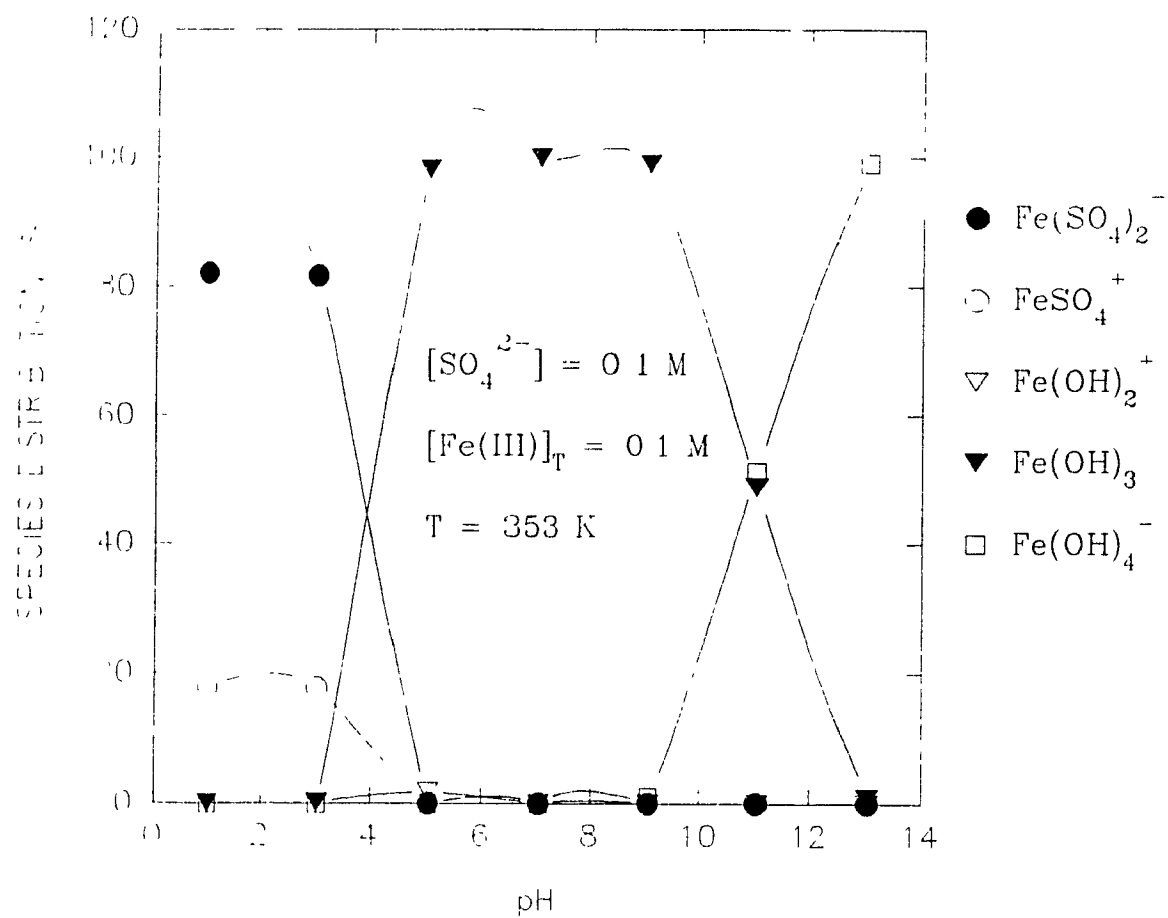


Figure 4-5b: Speciation diagram for the Fe(III)-SO₄-H₂O system calculated by using F*A*C*T for 80°C.

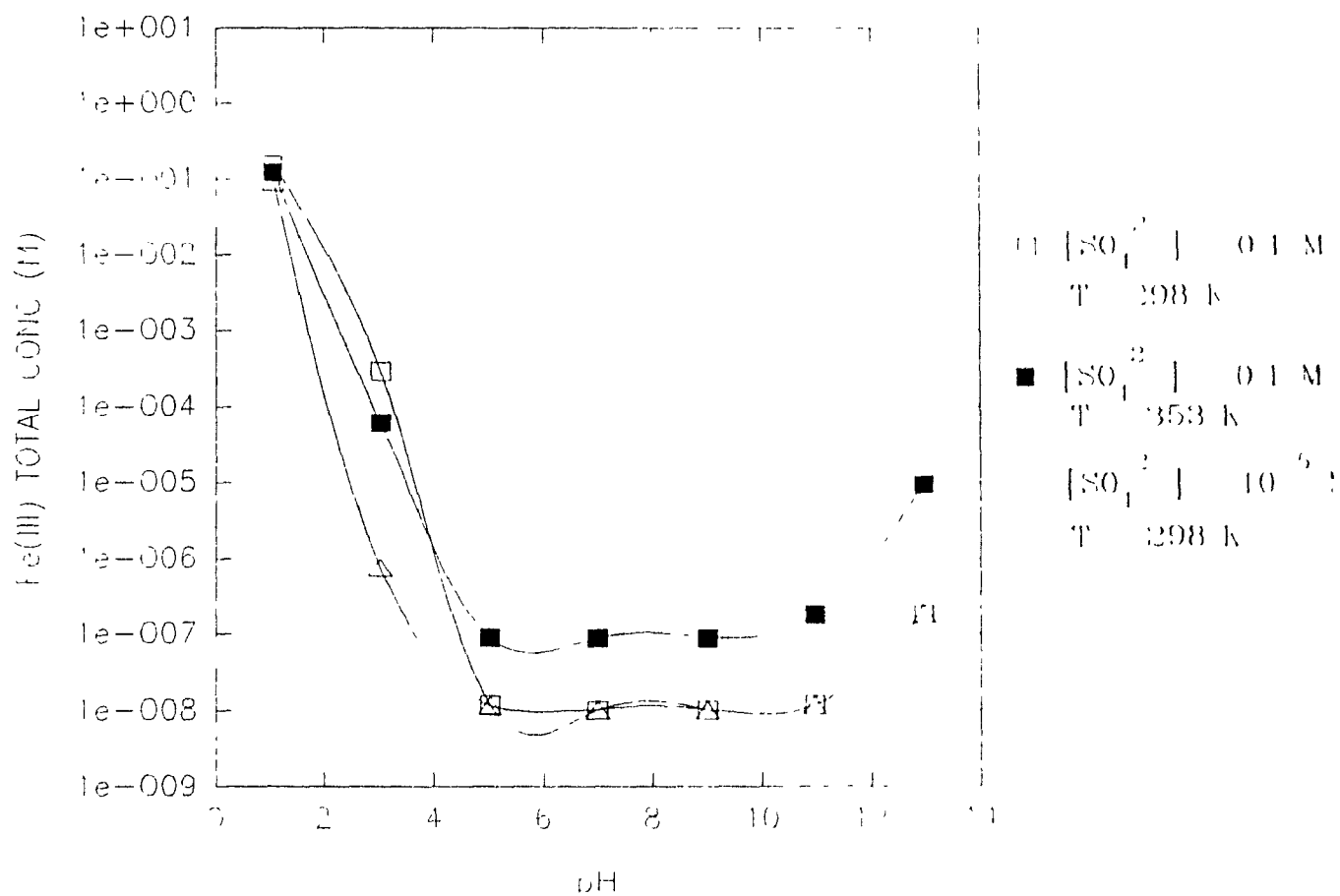


Figure 4-6: Solubility diagram for Fe(III) calculated by using F*A*C*T.

were calculated for varying sulphate concentrations at ambient and elevated (80°C) temperatures. Solubility calculations were performed using "detailed point" data supplied by F*A*C*T (Appendix A).

The solubility of the Fe(III)_f in solution is a function of both the sulphate concentration and temperature, as well as pH. Iron(III) solubility increases (i.e. the lower pH region) with sulphate concentration. This is due to the formation of sulphato complexes which dominate in the low pH region as already discussed in the preceding section. At very low sulphate concentration Fe(III) is least soluble. At pH < 5 temperature decreases the solubility of Fe(OH)_3 . This calculated trend is observed experimentally. Above this pH, the calculations indicate $\text{Fe(OH)}_{3(s)}$ to become more soluble with temperature. This is generally not observed. One reason for this discrepancy might be that at 80°C (pH 5) FeOOH would precipitate, instead of simple Fe(OH)_3 (Dutrizac, 1980), and the assumption the Fe(OH)_3 being the only precipitate formed would be invalid. This would indeed influence the reported Fe(III) solubility since the two solids have different solubility products. Furthermore the heat capacity extrapolation could also affect the calculated Fe(III) solubility.

4.5 Summary

Several important observations can be made from this study within the conditions examined:

- (1) The concentration of sulphate in solution strongly affects the degree of complexation and the solubility of Fe(III) in the low (< 5) pH region;
- (2) Fe(III)-sulphato complexes are more difficult to hydrolyze than hydroxyl complexes;
- (3) Higher temperature favours hydrolysis;
- (4) Ferric hydroxide is least soluble at ~ pH 5-8 (Figure 4-6);

This study supports and compliments much of the theory presented in the previous chapters. The most significant parameters found to affect Fe(III) hydrolysis

are pH, sulphate concentration and temperature. It is shown that neutralization must continue to a final pH (8-10) that yields the lowest possible iron(III) solubility. The speciation diagrams presented above suggest the precipitation precursors most common under specific conditions. This information is essential in the understanding of the reaction mechanisms. The findings of the present thermodynamic analysis are used to postulate possible precipitation pathways and interpret experimental observations.

CHAPTER 5: EXPERIMENTAL

This chapter describes the general experimental procedure, the reagent and the apparatus utilized in the investigation. Specific details of the experimental procedure for each test is given in Chapter 6 prior to presentation of results. This is so since no standard experimental techniques were used and the tests were of a non-routine nature.

During the course of this hydrolytic investigation several variables such as pH, rate of neutralization, rate of agitation, sulphate concentration, sludge temperature, and recycling were examined for their effect on effluent and sludge quality. Table 5-1 summarizes the series of tests undertaken in this study.

The final effluent was analyzed for iron, through atomic absorption spectrophotometry using the Varian Spectra AA-20, and sulphate, gravimetrically (Appendix B-1). The sludge/precipitate generated was evaluated by measuring settling velocity (Appendix B-2), percent solids content (Appendix B-3), volume (Appendix B-4), chemical composition (Fe, SO_4 , Na content) as well as characterization of selected samples by X-ray diffraction, scanning electron microscopy, BET^3 specific surface area, and particle size analysis⁴.

5.1 Synthetic Effluents

Experimentation was performed by using synthetically generated effluents. The iron(III) sulphate solutions were prepared by dissolving analytical grade ferric sulphate ($\text{Fe}_2(\text{SO}_4)_3 \cdot x\text{H}_2\text{O}$) reagent in distilled water. The standard ferric ion concentration used throughout most of the experiments was 0.018 M (1000 mg/L) except if otherwise stated. The solution pH was lowered (if necessary) with the drop-

³ The method is based on the work of Brunauer, Emmett, and Teller (1938). Measurements were obtained using a Micromeritics Flowsorb II 2300.

⁴ Particle size analysis was performed using a MICROTRAC Model 7991-01 Analyzer which uses light scattering to determine particle size.

wise addition of 0.9 M sulphuric acid. Additional sulphate ions were introduced in the form of analytical grade sodium sulphate (Na_2SO_4). A limited number of tests involved hydrolysis of ferric nitrate solutions prepared by the dissolution of analytical grade $\text{Fe}(\text{NO}_3)_3$.

Table 5-1: Summary of tests and relationships examined.

TEST	CONDITIONS	SECTION
Precipitation profiles	pH - 3, 6, 9	6.1
Effect of pH	pH - 4 to 9	6.2.1
Effect of neutralization rate	0.16, 0.32, 0.64, 1.275, 3.19 mM OH^-/min	6.2.2
Effect of agitation Rate	100, 200, 400, 800 rpm	6.2.3
Effect of retention time	0, 15, 30, 60, 120 min	6.2.4
Effect of temperature	25, 30, 40, 60, 80°C	6.2.5
Effect of sulphate concentration	0, 3, 6, 9, 12, g/L	6.2.6
Statistical Design Analysis	Variables - Neut. rate - pH - temperature - $[\text{SO}_4]$ Responses - sludge volume - percent solids - settling rate - $[\text{Fe(III)}]_f$	6.3
Recycling	Series A - 20 times - simple Series B - 20 times - controlled supersaturation - staged-neutralization	6.4

5.2 Apparatus

Bench scale precipitation-neutralization experiments were carried out in a 600 mL Pyrex beaker. Temperature and magnetic agitation were controlled with the aid of a Whatman 440 programmable hotplate/stirrer "datalog". The Radiometer ETS822 end point titration system was used to monitor and control the pH (± 0.01) of the test solution. The ETS822 is a modularized system composed of a pH meter (PHM82), a titrator (TTT80), and an autoburette (ABU80). The pH meter receives the electrode signal and indicates the pH value of the sample on its display. The titrator serves as the control unit for the autoburette and receives a signal proportional to the pH value. The autoburette delivers controlled increments of titrant to the titration sample. Its 4-digit LED display indicates the volume of the titrant consumed. A Radiometer combination glass pH electrode (GK240IC) and an automatic temperature compensator probe (T701) were used with the system. The pH and temperature of the system were continuously recorded with a Cole Palmer dual-channel flatbed recorder (08376-60) (Figure 5-1).

5.3 Procedure

The test volume (500 mL) of synthetic effluent was pre-heated to the desired temperature (usually 50°C) while agitation was applied at specific rate (commonly 200 rpm). Once the target temperature was reached, the neutralization agent, a solution of 1.275 M NaOH, was introduced at a preset rate. Neutralization continued at a constant rate until the target pH was reached. At this point the treatment conditions were maintained for a desired reaction period. The treated effluent and the sludge produced were evaluated.

Sample preparation for microscopic examination consisted of diluting 5 drops of sludge with approximately 50 mL of methanol. The solution was then vacuum filtered through a 5 μ m polycarbonate membrane filter (Millipore). The samples were sputter coated with gold under vacuum to render them conductive prior to examination under a Joel 820 scanning electron microscope. Some difficulty was experienced in collecting secondary electron images because the particles tended to

charge and act as capacitors. Use of a thicker gold coating was ruled out because it could have masked some of the morphological features. All of the images were collected using a low sample current to minimize the charging effect and provide good resolution. Acceleration voltages of up to 20kV were used. Detailed procedures for each series of experiments are outlined in the next chapter.

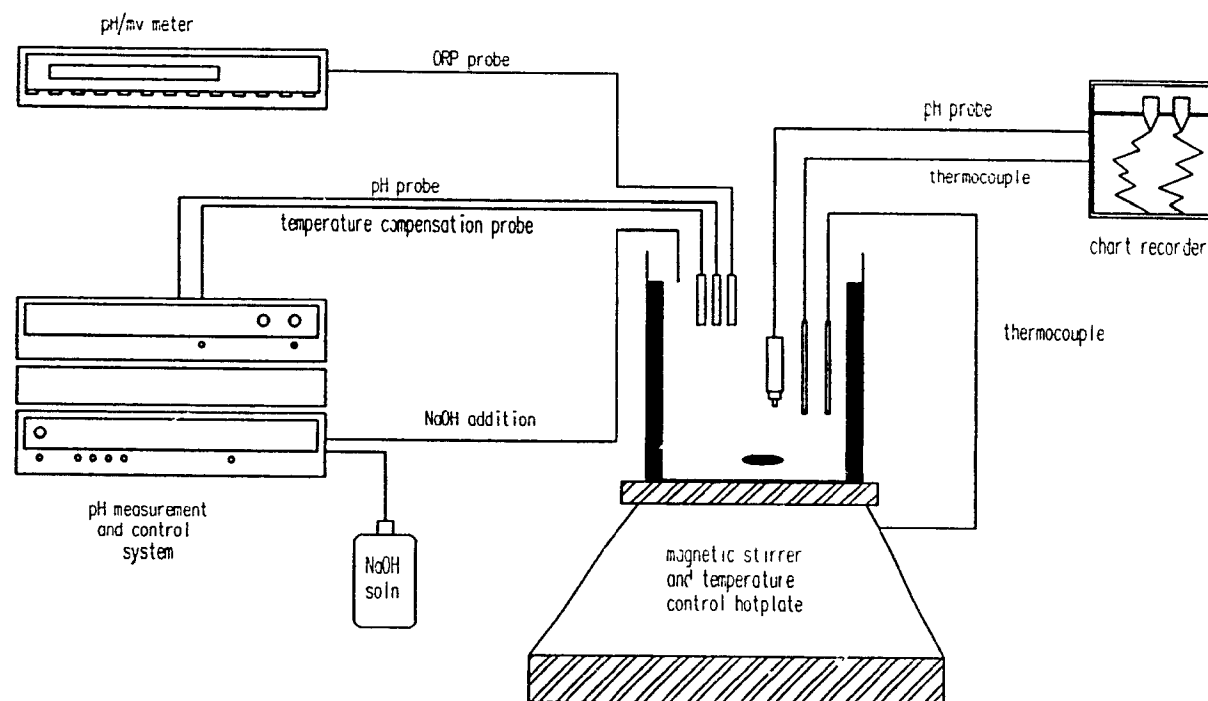


Figure 5-1: Schematic representation of hydrolysis apparatus.

CHAPTER 6: RESULTS

During the course of this work different kinds of experiments were performed. First experiments were designed aiming to analyze the precipitation system by isolating the effect of variables on the quality of the produced precipitate (Single Variable Effects, section 6.2) or by examining the interactive effect of the same variables (Statistical Design, section 6.3). Finally recycling tests were designed and performed with and without supersaturation control (Recycling, section 6.4). Before the results of each of these sections are presented, the anatomy of a typical Fe(III) hydrolytic test is examined.

6.1 Precipitation Profiles

Several authors (Dousma and de Bruyn, 1976, 1978; Flynn, 1984) have studied titration curves to analyze the Fe(III) hydrolysis system⁵. Titration curves were examined in this study for final reaction pHs 3, 6 and 9. All other conditions were kept constant at 50°C, 0.018 M Fe(III), 0.1 M SO_4^{2-} , 200 rpm.

The titration curve for the final pH 6 case is shown in Figure 6-1. Three main regions are observed. In the first region, pH increases, gradually following the constant addition of base. In this region the OH/Fe molar ratio is less than one and hydrolysis does not occur. In the second region, the pH curve flattens; the OH/Fe ratio is approximately between 1 and 2.5. In this region partial hydrolysis of Fe(III) occurs which causes the turbidity of the solution to increase. In the final region, the OH/Fe ratio exceeds 2.5, the pH curve rises steeply and precipitation begins to take place (Flynn, 1984).

An attempt was made to calculate precipitation profiles using data obtained from neutralization-precipitation tests and the corresponding titration curves. The purpose of this estimation was to check the agreement of the calculated precipitation profile and iron removal with experimental data. As well, the method was examined

⁵ Ferric sulphate dissolved in distilled water.

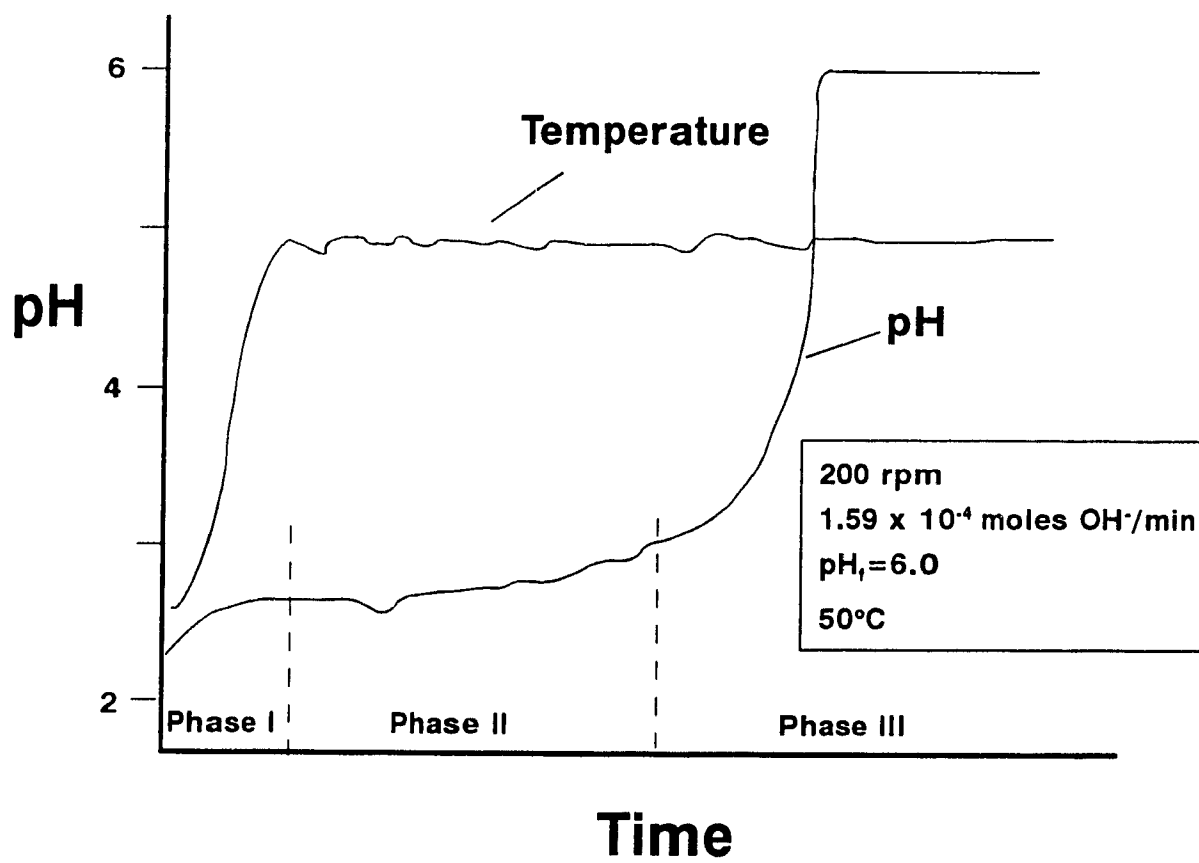


Figure 6-1: Change in pH with time during hydrolysis of Fe(III) to pH 6.

for its ability to simulate iron removal in a hydrolyzing batch system. The change in pH and hydroxyl ion demand over five minute intervals were used to estimate the concentration of iron in solution at that time.

The assumption was made that the solid precipitated was $\text{Fe}(\text{OH})_3$. Therefore, assuming one mole of Fe^{3+} precipitates for three moles of H^+ generated, the iron concentration can be estimated from the change in pH. For this exercise it was assumed that the activity of H^+ was equal to the concentration of hydrogen ions. Furthermore, the release of H^+ from the dissociation of HSO_4^- with increasing pH was ignored⁶. Table 6-1 summarizes the data and results obtained from this study.

By plotting the calculated iron removal profile against the solubility line (statistically derived from experimental data, section 6-3) for the corresponding conditions, an estimation of the saturation ratio at any time can be obtained (Figure 6-2). When the saturation ratio drops below unity spontaneous precipitation ceases. From Figure 6-2 this point corresponds to the intersection of the precipitation and solubility lines, pH 3.53. It should be emphasized here that this intersection point is expected to shift to higher pHs upon increasing the neutralization rate. In other words, rapid neutralization will raise the pH quickly while at the same time precipitation of iron (i.e. iron removal from solution) will not occur as fast. This of course relates to the slower nucleation-growth kinetics of the precipitation reaction as opposed to the fast homogeneous neutralization reaction kinetics.

Batch reactions do not occur under a steady-state level of saturation. Figure 6-3 demonstrates how supersaturation declines during the course of a batch experiment. As a result, saturation ratio must also be controlled in order to optimize

⁶ The observed discrepancy between negative values and those obtained reflect in fact the error in ignoring the dissociation of the HSO_4^- ion. Thus, if we examine for example the initial and final solutions we find this error to be 100 mg/L which is exactly the excess iron(III) concentration (-107 mg/L) estimated in Table 6.1. The calculations by which the error linked to the dissociation of HSO_4^- were estimated are described in Appendix C.

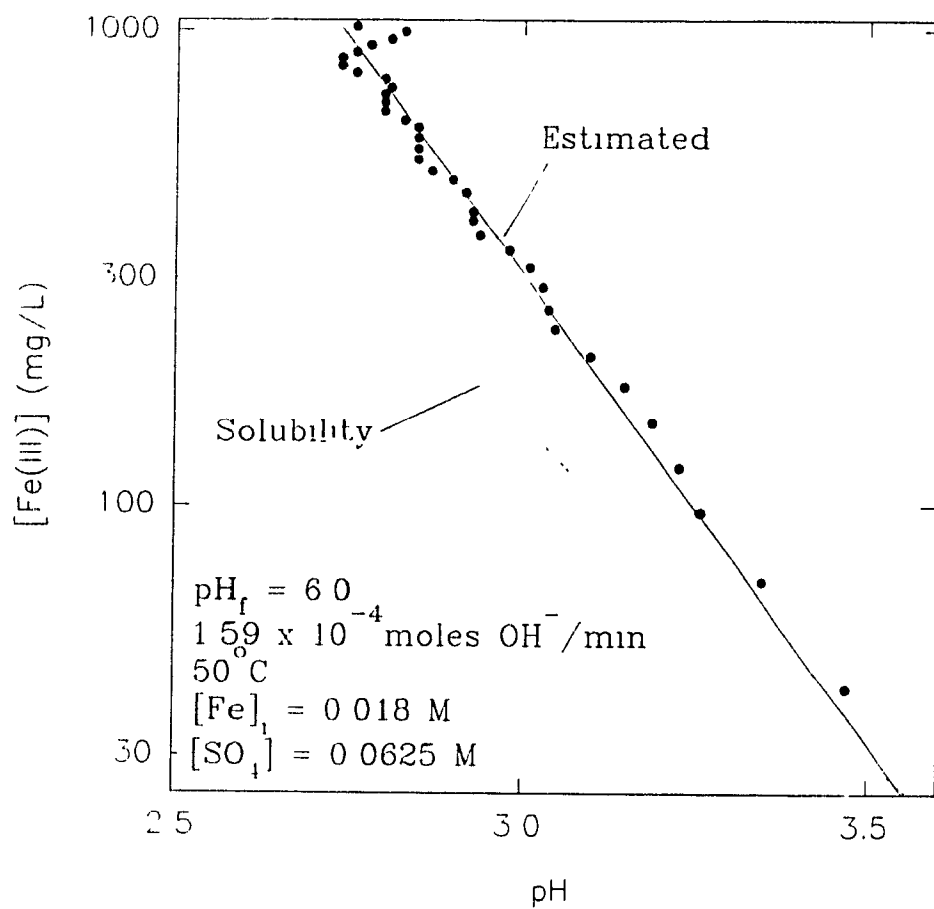


Figure 6-2: Precipitation profile of Fe(III) hydrolysis - change in Fe(III) concentration with pH.

the hydrolysis process.

Precipitation profiles were also calculated for pH 3 and 9. The results are similar to the pH 6 profile. For brevity, these profiles are not included.

Table 6-1: Precipitation profile data for Fe(III) hydrolysis to pH 6. Conditions: 50°C, 200 rpm, 1.59×10^{-4} moles OH⁻/min.

Time (min)	pH	moles H ⁺	d(moles) H ⁺	Volume NaOH (mL)	moles OH ⁻ Added	moles H ⁺ Generated	moles Fe Precipitated	[Fe] ³⁺ in Soln (mg/L)
0	2.76	8.69e-04	-	0.00	-	-	-	1017.0
5	2.83	7.40e-04	-1.29e-04	0.63	8.058e-04	6.765e-04	2.255e-04	991.8
11	2.81	7.74e-04	3.49e-05	1.36	9.231e-04	9.580e-04	3.193e-04	956.1
15	2.78	8.30e-04	5.54e-05	1.89	6.809e-04	7.362e-04	2.151e-04	928.7
20	2.76	8.69e-04	3.91e-05	2.52	8.020e-04	8.411e-04	2.804e-04	897.4
25	2.74	9.10e-04	4.10e-05	3.02	6.375e-04	6.785e-04	2.262e-04	872.2
30	2.74	9.10e-04	0.00	3.65	8.020e-04	8.020e-04	2.673e-04	842.3
35	2.76	8.69e-04	-4.10e-05	4.28	8.045e-04	7.636e-04	2.515e-04	813.9
40	2.80	7.92e-04	-7.65e-05	4.91	8.020e-04	7.255e-04	2.418e-04	786.9
45	2.81	7.74e-04	-1.80e-05	5.53	7.982e-04	7.801e-04	2.600e-04	757.8
50	2.80	7.92e-04	1.80e-05	6.03	6.350e-04	6.530e-04	2.177e-04	733.5
55	2.80	7.92e-04	0.00	6.66	8.033e-04	8.033e-04	2.678e-04	703.6
60	2.80	7.92e-04	0.00	7.29	7.994e-04	7.994e-04	2.665e-04	673.8
65	2.83	7.40e-04	-5.29e-05	7.92	8.007e-04	7.478e-04	2.193e-04	646.0
70	2.85	7.06e-04	-3.33e-05	8.42	6.362e-04	6.029e-04	2.010e-04	623.5
75	2.85	7.06e-04	0.00	9.04	7.994e-04	7.994e-04	2.665e-04	593.8
80	2.85	7.06e-04	0.00	9.67	8.033e-04	8.033e-04	2.678e-04	563.9
85	2.85	7.06e-04	0.00	10.30	7.994e-04	7.994e-04	2.665e-04	534.1
90	2.87	6.74e-04	-3.18e-05	10.93	8.033e-04	7.715e-04	2.572e-04	505.4
95	2.90	6.29e-04	-4.50e-05	11.43	6.375e-04	5.925e-04	1.975e-04	483.3
100	2.92	6.01e-04	-2.83e-05	12.06	8.033e-04	7.749e-04	2.583e-04	454.5
107	2.93	5.87e-04	-1.37e-05	12.93	1.109e-03	1.096e-03	3.652e-04	413.7
110	2.93	5.87e-04	0.00	13.31	4.845e-04	4.845e-04	1.615e-04	395.7
115	2.94	5.74e-04	-1.34e-05	13.88	7.268e-04	7.134e-04	2.378e-04	369.1
120	2.98	5.24e-04	-5.05e-05	14.44	7.140e-04	6.635e-04	2.212e-04	344.4

Table 6-1 continued.

125	3.01	4.89e-04	-3.49e-05	15.07	8.033e-04	7.683e-04	2.561e-04	315.8
130	3.03	4.67e-04	-2.20e-05	15.69	7.905e-04	7.685e-04	2.562e-04	287.2
135	3.04	4.56e-04	-1.06e-05	16.33	8.160e-04	8.054e-04	2.685e-04	257.2
140	3.05	4.46e-04	-1.04e-05	16.82	6.248e-04	6.144e-04	2.048e-04	234.3
145	3.10	3.97e-04	-4.85e-05	17.46	8.160e-04	7.675e-04	2.558e-04	205.7
150	3.15	3.54e-04	-4.32e-05	18.08	7.905e-04	7.473e-04	2.491e-04	177.9
155	3.19	3.23e-04	-3.11e-05	18.71	8.033e-04	7.721e-04	2.574e-04	149.2
160	3.23	2.94e-04	-2.84e-05	19.35	8.160e-04	7.876e-04	2.625e-04	119.8
165	3.26	2.75e-04	-1.97e-05	19.85	6.375e-04	6.178e-04	2.059e-04	96.8
170	3.35	2.23e-04	-5.14e-05	20.47	7.905e-04	7.391e-04	2.464e-04	69.3
175	3.47	1.69e-04	-5.39e-05	21.10	8.033e-04	7.493e-04	2.498e-04	41.4
180	3.61	1.23e-04	-4.67e-05	21.73	8.033e-04	7.566e-04	2.522e-04	13.3
190	4.08	4.16e-05	-8.11e-05	22.86	1.441e-03	1.360e-03	4.532e-04	-37.4
195	4.82	7.57e-06	-3.40e-05	23.49	8.033e-04	7.692e-04	2.564e-04	-66.0
200	5.76	8.69e-07	-6.70e-06	24.11	7.905e-04	7.838e-04	2.613e-04	-95.2
201	6.02	4.77e-07	-3.91e-07	24.23	1.530e-04	1.526e-04	5.087e-05	-100.9
261	6.00	2.75e-04	-7.92e-05	24.31	1.020e-04	1.812e-04	6.040e-05	-107.6

* Negative values indicate that the estimated mass of precipitated iron exceeds the initial quantity of dissolved iron.

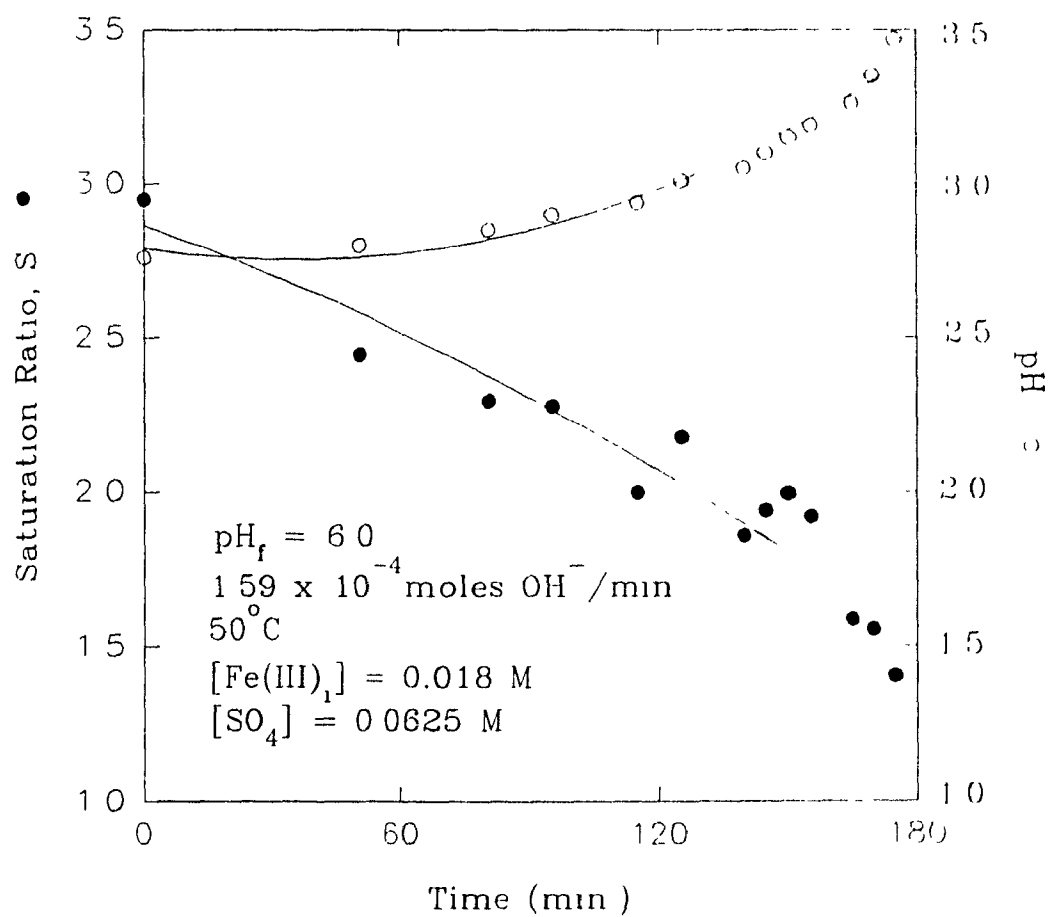


Figure 6-3: Change in saturation ratio and pH in a batch reactor with time.

6.2 Single Variable Effects

6.2.1 Effect of Final pH

Solution pH plays a predominant role in ferric hydroxide precipitation. pH control is the basis for the neutralization-precipitation approach to effluent treatment. By increasing the hydrolysis pH, up to a certain level, a lower iron concentration is produced in the final effluent. It is not clear, however, how pH affects sludge characteristics.

Treatment of a synthetic effluent containing 0.018 M (1 g/L) Fe(III) and 0.1 M SO_4^{2-} was studied. The final pH was varied from 3 to 9, with the addition of 1.275 M sodium hydroxide at a rate of 1.5 mL/min. The effluent underwent treatment at the final pH for 75 minutes at 25°C. Agitation was maintained at 200 rpm.

During neutralization a small marked increase in temperature ($\Delta T \sim 1.0^\circ\text{C}$) and an increase in solution turbidity was observed at pH 2.6-2.7 indicative of nucleation. The titration curve displayed a plateau or buffer zone in this pH region (Figure 6-4).

By neutralizing the solution to various final pH values the properties of the sludge generated were found to be significantly different. A pronounced linear ($R^2 = 0.934$) relationship was observed between pH and settling rate. As the final pH was increased the precipitate was found to settle faster (Figure 6-5).

Sludge densification was increased at low pH (3). Similarly, as the pH of the solution was raised a more voluminous sludge was generated. Aggregation was more common at high pH. The greater the extent of aggregation the more significant was the amount of water bound in the sludge. Another reason for the observed increase in sludge volume with pH might be the potential shift in coagulation mechanism from adsorption-charge neutralization at low pH to enmeshment or sweep floc coagulation with increased hydroxyl ion concentration (Knocke et al., 1987) at high pH.

The hydrolysis reaction reached equilibrium above pH 4, as observed by the diminishing demand for hydroxyl ions to maintain the solution pH (Table 6-2). At pH 3 hydrolysis continued even after one hour. The hydroxyl requirement during this

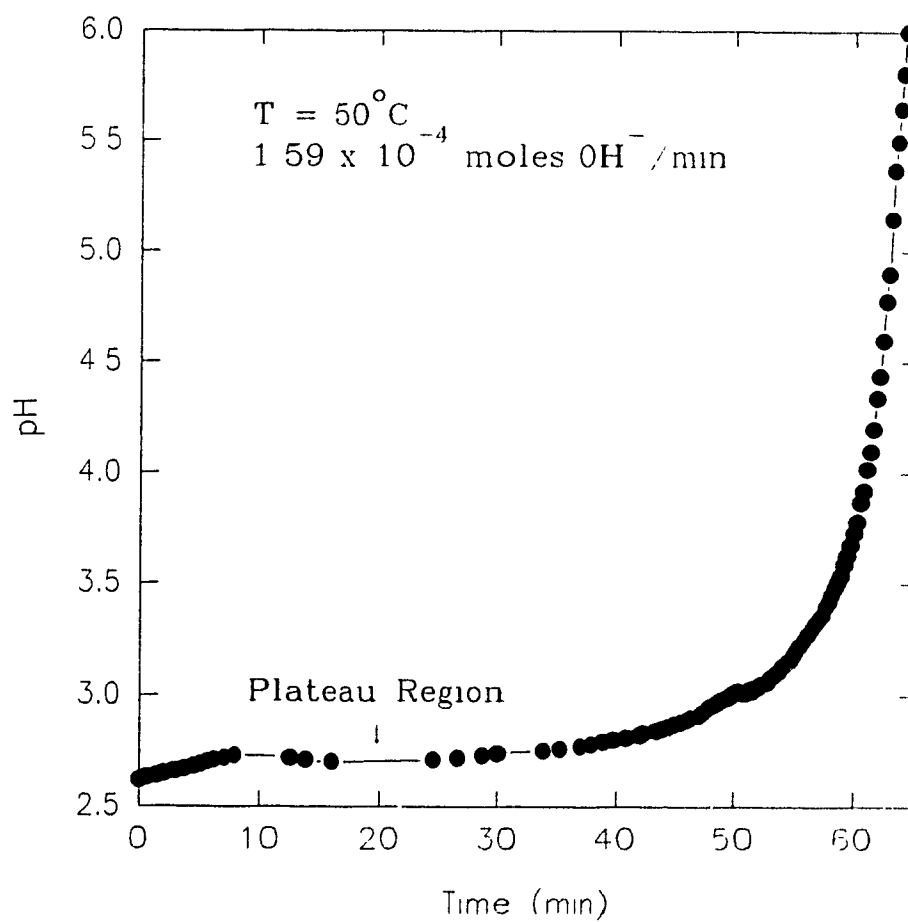


Figure 6-4: Change in pH during neutralization.

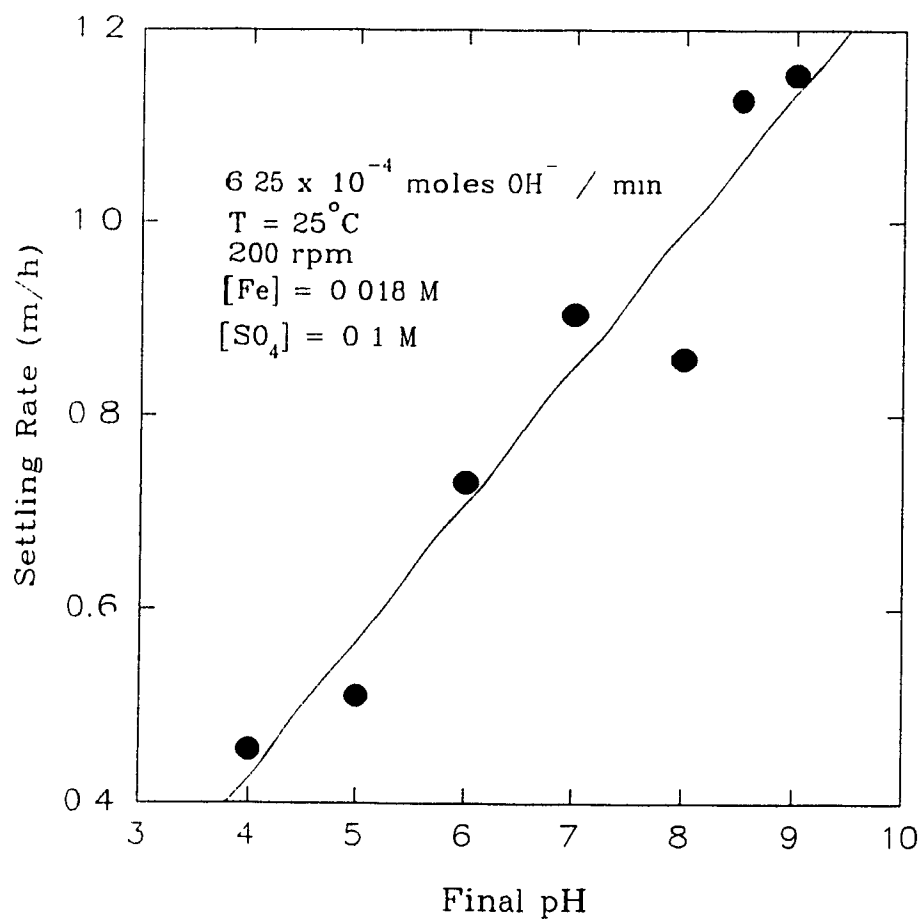


Figure 6-5: Effect of final solution pH on settling rate.

period was on average 5 times greater at pH 3 than the requirement at pH > 4. Above pH 4 little or no iron(III) (< 1 mg/L) was present in the effluent thus, the majority of the iron(III) precipitated between pH 3 and 4.

Table 6-2: Hydroxyl ions requirement to maintain final pH for 60 minutes. (Conditions: $[\text{Fe(III)}]_i = 0.018 \text{ M}$, $[\text{SO}_4]_i = 0.1 \text{ M}$, 50°C , 200 rpm, 6.4×10^{-4} moles OH^-/min).

Final pH	Moles OH^- required
3	0.125
6	0.025
9	0.028

Precipitates generated from three different levels of acidity (pH: 3, 6, 9) were characterized by x-ray diffractometry and were examined microscopically in an attempt to distinguish physical changes in the precipitates. The solids (produced at 50°C) were found to be partly crystalline goethite ($\alpha\text{-FeOOH}$) with the degree of crystallinity to progressively decrease as the pH was decreased from 9 to 6 to 3. The x-ray diffractometer patterns are shown in Figures 6-6(a-c). On the other hand precipitates produced were "sponge like" in form. The basic building units of the "sponge skeleton" were flat platelets of goethite (Plate 6-1). The solution pH appeared to determine the size of the platelets as it did with the degree of crystallinity. The platelets formed rounded clusters which were aggregated together to form a sponge-like skeleton. The size of the platelets decreased between pH 3 (Plate 6-1) and pH 9 (Plate 6-2) resulting in masses of precipitate which had a lower overall bulk density while having an increased settling rate. (The plate of the precipitate produced at pH 6 is not shown).

Finally the composition of the precipitates in terms of Fe and SO_4 content was determined from a number of solids produced under different pH conditions. The results are summarized in Figure 6-7. It can be clearly seen that the solution pH has

D00688 8/18/92 S= 0.050 T=10.000 ZINCK PH3
PDF (1) -29.713

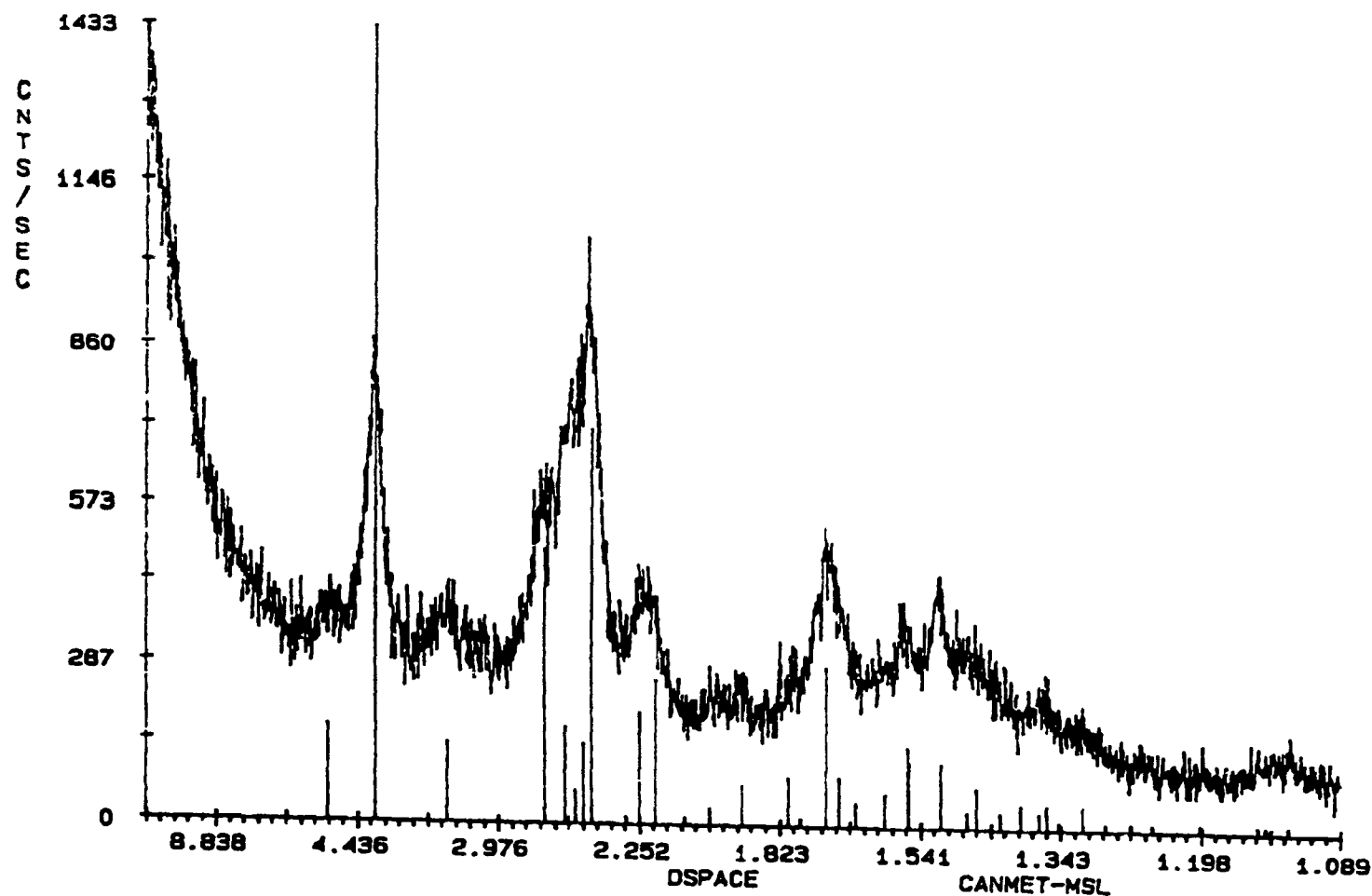


Figure 6-6a: XRD pattern of the hydrolysis precipitate generated from simple (with no seed) neutralization to pH 3. other conditions same as in 6-2). The lines correspond to the standardized XRD pattern of goethite, $\alpha\text{-FeOOH}$.

D00689 8/18/92 S= 0.050 T=10.000 ZINCK PH6
PDF (1) -34, 1266

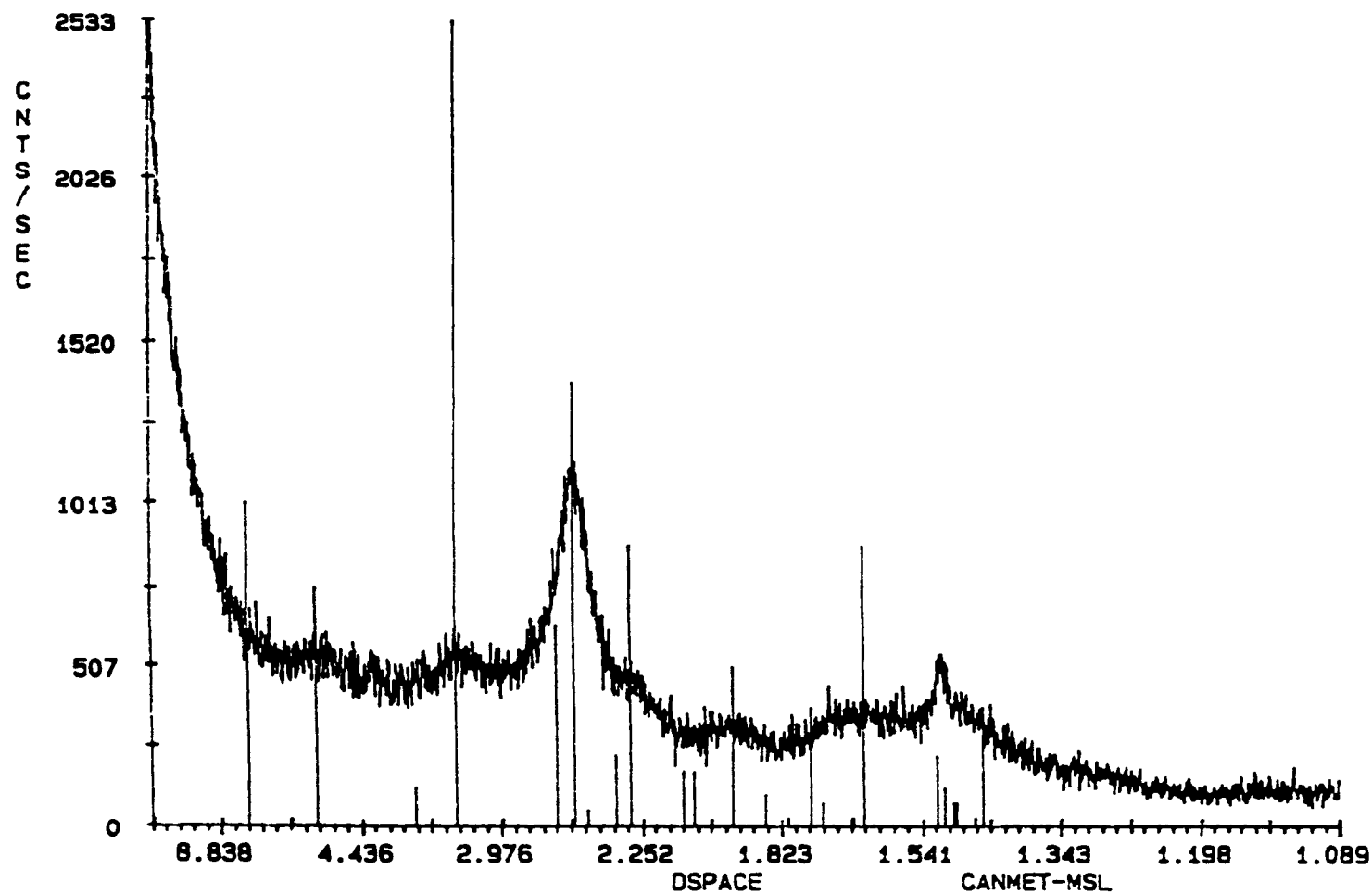


Figure 6-6b: XRD pattern of the hydrolysis precipitate generated from simple (with no seed) neutralization to pH 6. other conditions same as in 6-2). The lines correspond to the standardized XRD pattern of goethite, α -FeOOH.

000690 8/18/92 S- 0.050 T-10.000 ZINCK PH9
PDF (1) -29.713

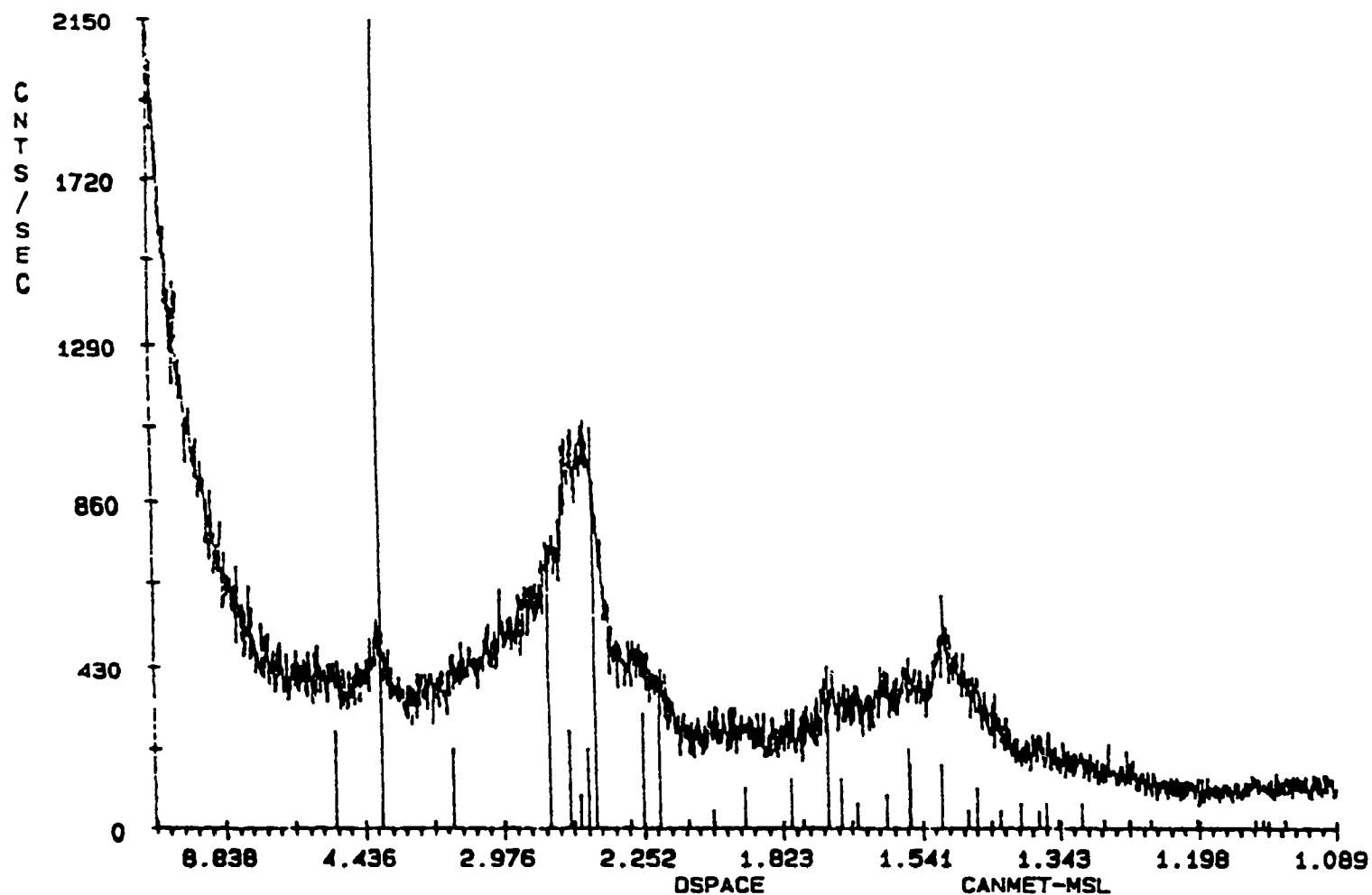


Figure 6-6c: XRD pattern of the hydrolysis precipitate generated from simple (with no seed) neutralization to pH 9. other conditions same as in 6-2). The lines correspond to the standardized XRD pattern of goethite, α -FeOOH.

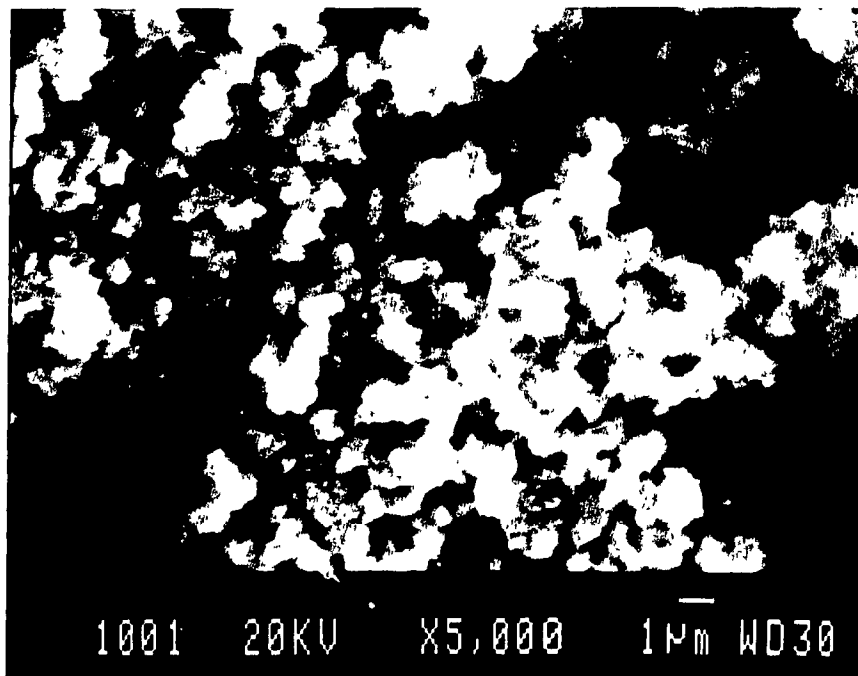


Plate 6-1: Objective of Precipitation: To study the effect of pH conditions

Production Conditions: pH 3

neutralization rate - 1.6×10^{-4} mole OH^-/min

50°C

200 rpm

No recycling

Comments: This precipitate is sponge-like. The individual flat platelets measure ~ 0.5 micrometres in diameter and the composite clusters ~ 2 micrometres in diameter. The voids in the sponge-like structure measure between 1 and 4 micrometres across.

Magnification: 5000 x

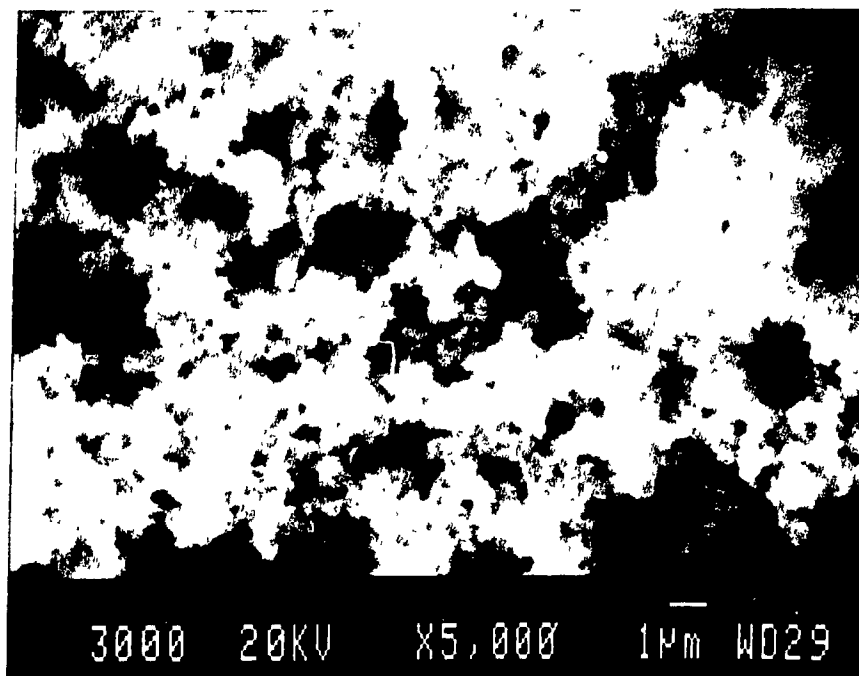


Plate 6-2: Objective of precipitation: to study the effect of pH

Production Conditions: pH 9

neutralization rate - 1.6×10^{-4} mole OH^-/min

50°C

200 rpm

No recycling

Comments : This precipitate is also sponge-like. The smallest precipitated platelets have a diameter of 0.25 microns similar to those produced at pH 6. The thinner platelets have a "wispy" appearance. The clusters are slightly larger with a diameter of >3 microns. The mode of the interstitial pores tends to be ~1 micrometre.

Magnification: 5000x

a strong influence on the sulphate content of the precipitate. The sulphate content decreases from 17% (pH 3) to 8-10% (pH 6) to 0-2% (pH 9). The sulphate content of the precipitate was found to be independent of the solution composition.

6.2.2 Effect of Rate of Neutralization

Removal of iron and other metals is a straight forward process of pH adjustment to the level of minimum metal hydroxide solubility. However, the production of a ferric hydroxide precipitate with attractive handling properties is much more difficult. If a solution of ferric sulphate is simply neutralized with excess base, iron and hydroxyl ions form chains linked with hydroxyl bridges that in turn become cross linked to large, three-dimensional networks (Dutrillac, 1980). Growth of these three-dimensional networks results in the formation of an amorphous or very poorly crystalline gel which effectively eliminates ferric ion from solution (Dutrillac, 1987). This amorphous gel however exhibits very poor handling properties such as poor filtering and settling as well as large volumes as the gel tends to incorporate significant amounts of the processing solution in its open network structure.

The rate of neutralization was studied by treating synthetic solutions containing 0.018 M Fe(III) and 0.15 M SO_4^{2-} . The tests were carried out under ambient temperature ($\sim 25^\circ\text{C}$) and 200 rpm agitation. Standard volumes (250 mL) of effluent were neutralized to pH 4 at various rates (0.125, 0.250, 0.50, 1.25, 2.50 mL/min) with 1.275 M NaOH.

The rate of neutralization was found to have a significant effect on sludge characteristics. Slowing the rate at which the neutralizing agent was added increased the settling rate and solids content as well as reducing the volume of sludge generated.

The ability of the precipitate to settle was enhanced by a slow addition of hydroxyl ions into the solution (Figure 6-8). When the pH of the solution was increased rapidly, the OH/Fe ratio escalated causing polymerization of the Fe-OH chains. Two settling rate regions were observed (Figure 6-8). Neutralization rates below 4.45×10^{-4} moles OH^-/min (0.35 mL 1.275 M NaOH/min) resulted in improved settling. Small reductions in neutralization rate significantly effected the settling rate.

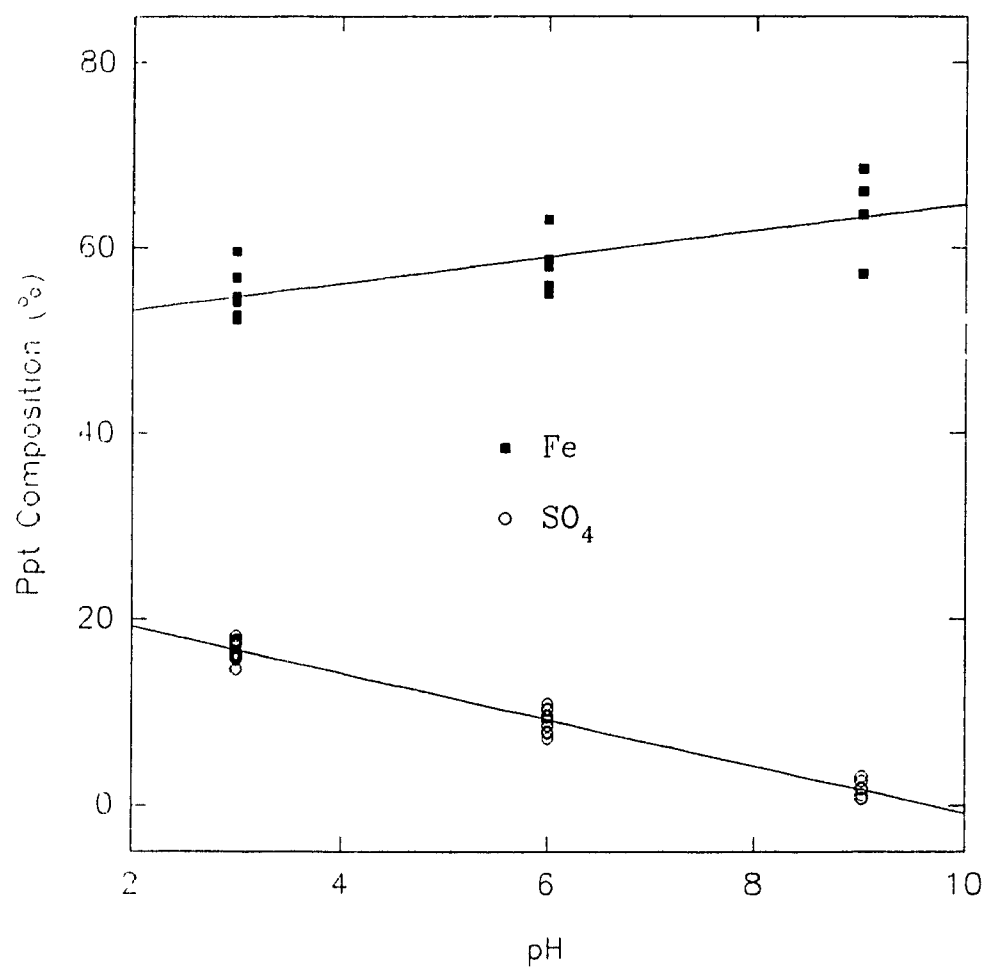


Figure 6-7: The relationship between sulphate reported in the solids and final solution pH.

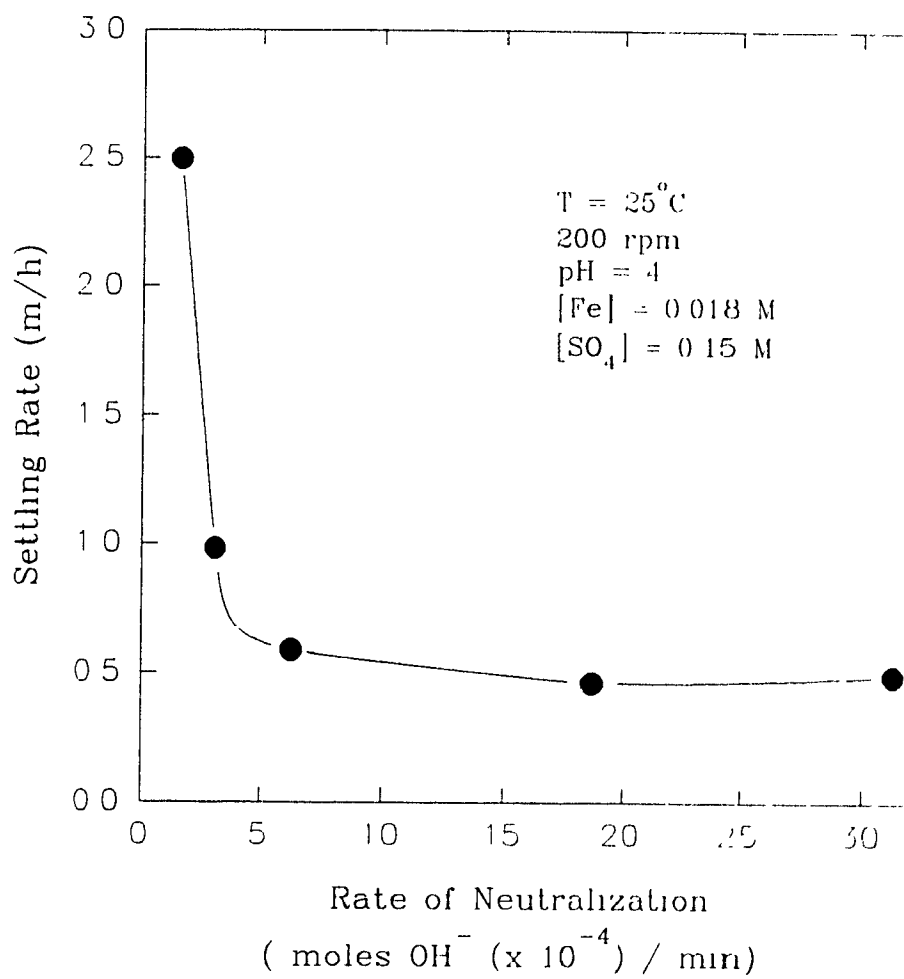


Figure 6-8: Effect of neutralization rate on settling rate.

Above 4.45×10^{-4} moles OH^-/min (0.35 mL 1.275 M NaOH/min) the system was overdosed with OH^- causing rapid polymerization and the formation of a large gel precipitate. Within this plateau region the rate of neutralization had little or no effect on the settling properties of the precipitate.

The densification of the sludge was also strongly dependent on the rate of addition of hydroxyl ions during neutralization. Precipitation of a gel-like precipitate, as a result of rapid neutralization, not only caused slow settling rates but also trapped significant amounts of process water in its open three-dimensional structure. Densification was reduced confirmed by an increase in sludge volume (Figure 6-9) and a reduction in percentage of solids in the sludge (Figure 6-10).

The relationship between neutralization rate to sludge characteristics depended on the degree to which the solution was supersaturated. When the solution was neutralized slowly, the hydroxyl ions in solution followed the demand due to hydrolysis, as shown by the dashed line in Figure 6-11. Here, the level of supersaturation was low, generally a few times greater than thermodynamic solubility and relatively better quality precipitate was produced. On the other hand, a rapid addition of hydroxyl ions into the solution resulted in a quick increase in pH. The supply of hydroxyl ions far exceeded the hydrolysis demand. The result was extremely high supersaturation level, several hundred times the solubility line. When saturation ratio was high, homogeneous nucleation was rapid and the nuclei formed were small.

6.2.3 Effect of Agitation Speed

The impact of agitation speed on the precipitation process at pH 3 and 6 was examined (Table 6-3). Solutions containing 0.018 M Fe(III) and 0.1 M SO_4^{2-} were neutralized at a rate of 6.375×10^{-4} moles OH^- per minute (0.50 mL/min. of 1.275 M NaOH) at 50°C. The reaction was allowed to continue for 60 minutes after reaching the target pH. Four agitation rates were studied; 100, 200, 400 and 800 rotations per minute (using a magnetic 3.7 cm stirring bar, d/O ratio = 2.3). Baffles were not used in the reaction vessel as sufficient mixing of the dilute slurries was accomplished

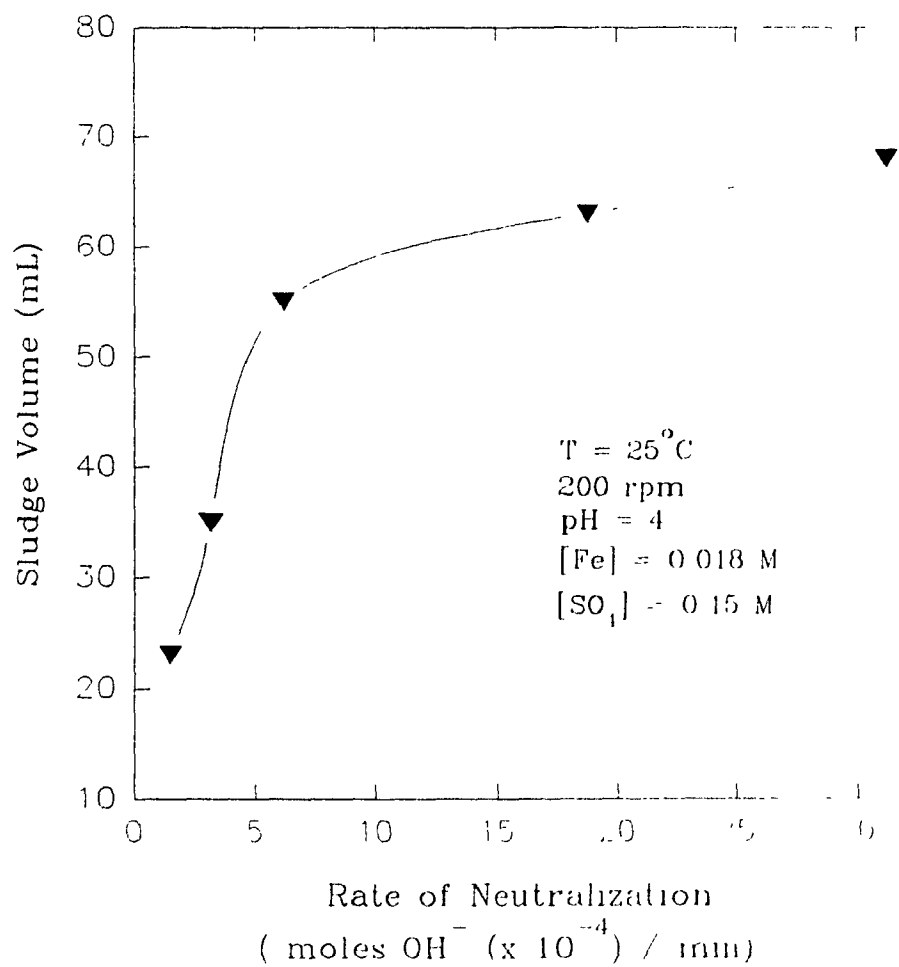


Figure 6-9: Effect of neutralization rate on sludge volume.

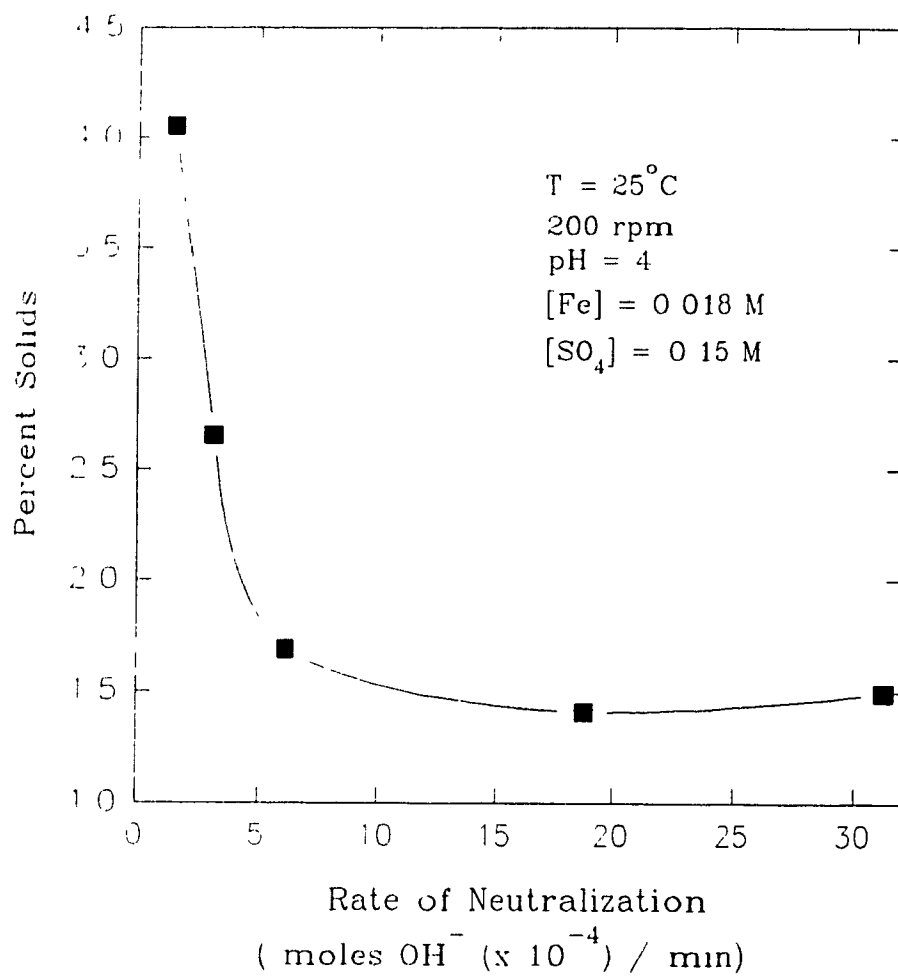


Figure 6-10: Effect of neutralization rate on the percent of solids in the treatment sludge.

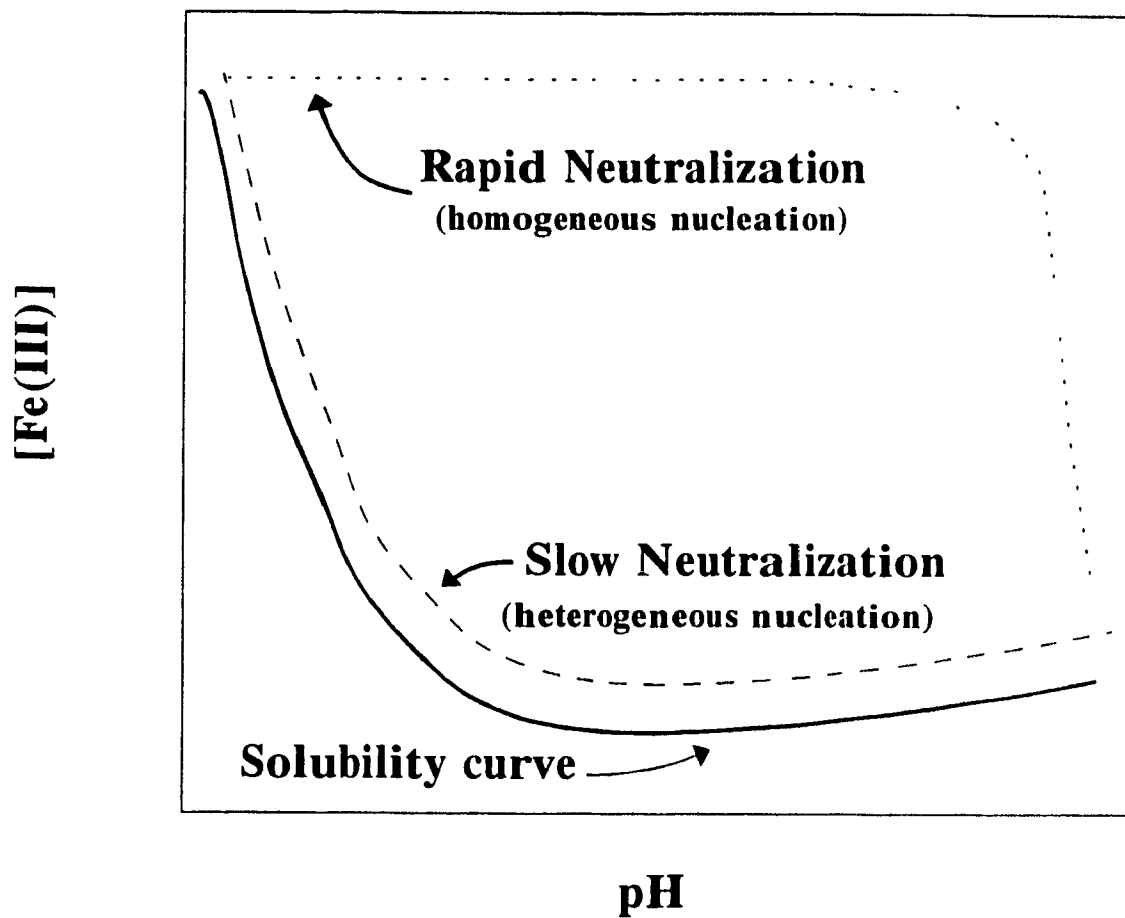


Figure 6-11: Effect of neutralization rate on the nucleation mechanisms.

with the placement of measuring devices (electrodes and probes) in the solution. However, suspension difficulties were experienced in the series of recycling tests performed (section 6.3), due to a higher concentration of solids in the slurry.

Table 6-3: The effect of agitation on sludge characteristics.

Agitation Speed (rpm)	Final pH	Settling Rate (m/h)	Sludge Volume (mL)	Percent Solids (%)	Final [Fe] (mg/L)	Ppt SO ₄ (%)
100	3.00	0.929	59	1.96	96.5	17.25
200	3.00	0.992	32	3.40	89.4	
400	3.00	0.923	20	5.35	82.5	
800	3.00	0.155	14	8.72	99.7	
100	6.00	1.68	79	1.62	0.48	9.49
200	6.00	1.95	53	2.45	0.08	
400	6.00	2.88	34	3.92	0.06	
800	6.00	3.35	23	5.61	0.08	

T = 50°C; t = 60 min.; 6.375×10^{-4} moles OH⁻/min; 0.018 g/L Fe(III); 0.1 M SO₄

The effect of agitation on the settling rate of particles precipitated at pH 3 was the inverse of those particles precipitated at pH 6 (Figure 6-12). At pH 3 the settling rate decreased with increasing agitation, the opposite of what was observed at pH 6. However, the effect of agitation on the volume of sludge (Figure 6-13) and the percent solids (Figure 6-14) was the same for both pH 3 and 6. On one hand, with high agitation large irregular and loose aggregates break down offering better packing and lower porosity. While, on the other hand, high agitation will accelerate diffusion and facilitate the transfer and deposition of fresh material to the open pores of the particle thereby producing denser precipitates.

The colour of the dry precipitate produced varied with the rate of agitation applied. A dark chocolate brown precipitate was observed with hydrolysis occurring under 100 rpm mixing. The precipitate colour lightened with increased agitation.

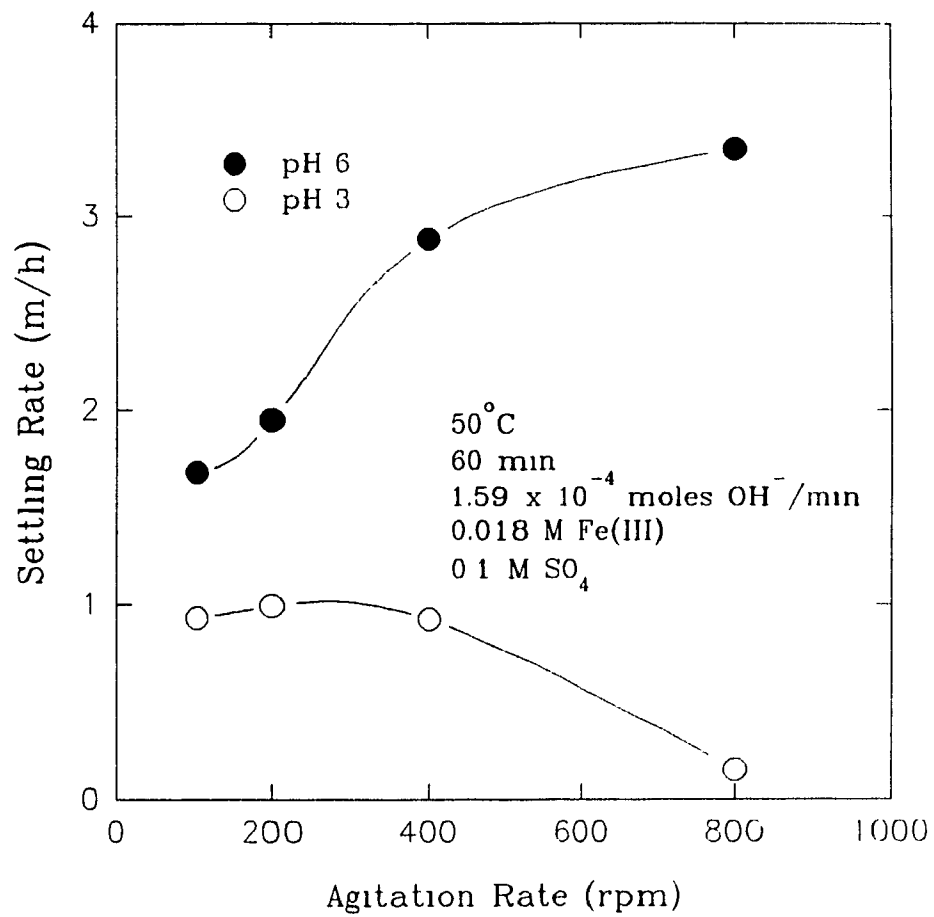


Figure 6-12: Effect of agitation rate on settling rate.

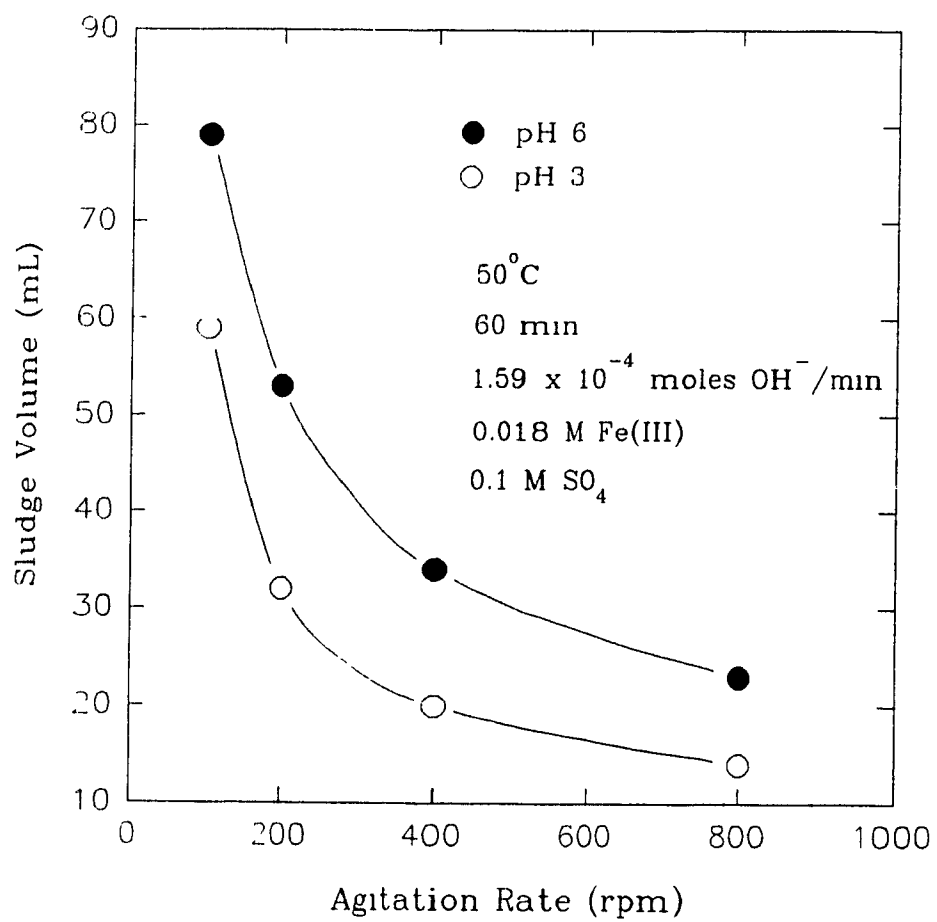


Figure 6-13: Effect of agitation rate on sludge volume.

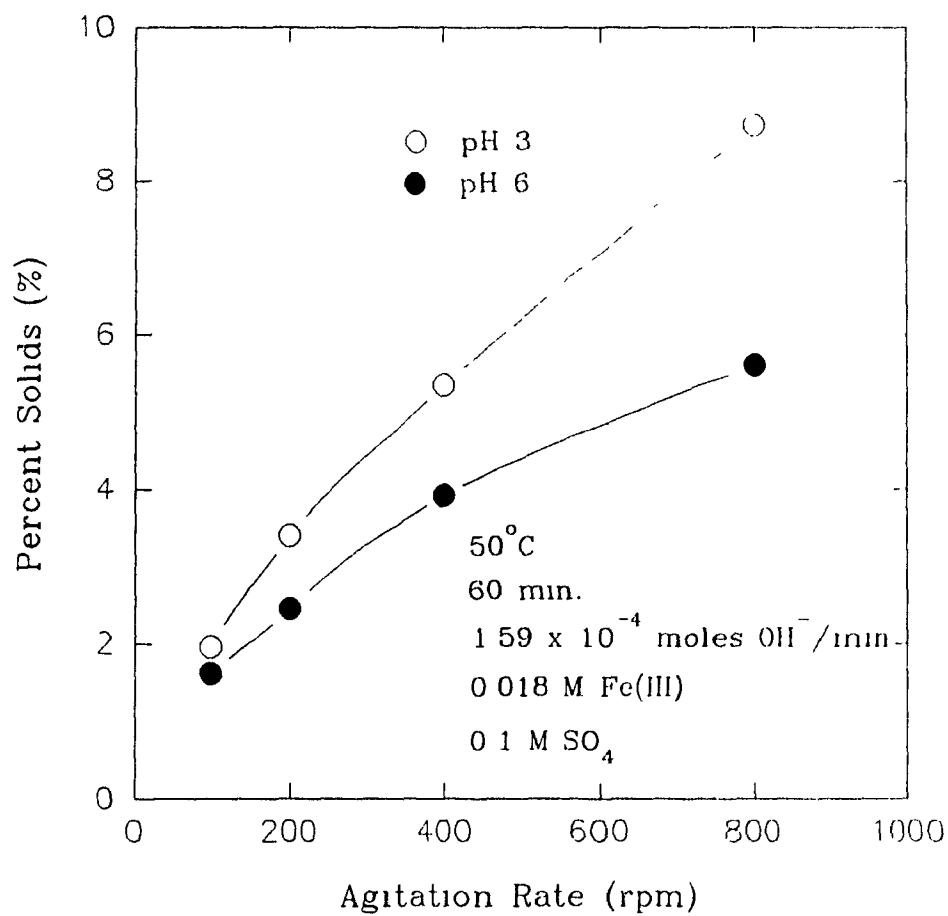


Figure 6-14: Effect of agitation rate on the percent of solids in the treatment sludge.

The precipitate generated at 800 rpm was ochre yellow in colour, suggesting that agitation rate significantly alters the morphology of the precipitate. This colour variation was observed for precipitates generated at both pH 3 and 6.

Finally, increasing agitation only mildly effected the incorporation of sulphate ion in the iron hydrolysis precipitate (Table 6-3). The percent of sulphate declined from 9.49% for 100 rpm to 7.21% for 800 rpm, while at pH 3 little or no effect was observed.

6.2.4 Effect of Retention Time

The effect of retention time on sludge and effluent quality was studied. Synthetic effluents containing 0.018 M Fe(III) and 0.1 M sulphate were neutralized at a rate of 6.375×10^{-4} moles OH^-/min . Once the final solution pH (3, 6, 9) was reached (this took approximately 33 min for pH 3, 48 min. for pH 6, and 54 min. pH 9) the treatment was either terminated ($t=0$) or the pH was maintained for a specified period of time (15, 30, 60, 120 min.). Table 6-4 summarizes the test conditions.

Table 6-4: Experimental conditions for time variable tests.

Test #	Final pH	Retention Time (min.)	Temperature (°C)	Agitation Rate (rpm)	Initial [Fe(III)] (mg/L)	[SO ₄] (M)
1	3.00	0	50	200	950	0.1
2	3.00	15	50	200	950	0.1
3	3.00	30	50	200	950	0.1
4	3.00	60	50	200	950	0.1
5	3.00	120	50	200	950	0.1
6	6.00	0	50	200	950	0.1
7	6.00	15	50	200	950	0.1
8	6.00	30	50	200	950	0.1
9	6.00	60	50	200	950	0.1
10	6.00	120	50	200	950	0.1
11	9.00	0	50	200	950	0.1

The retention time was only a significant variable effecting iron removal at low pH (3) (Table 6-5). At pH 3 a retention time of one hour was required for the hydrolysis reaction to approach equilibrium as indicated by the final iron(III) concentration. Under more basic conditions most of the iron was precipitated prior to reaching the target pH. In essence then, the effect of retention time was negligible.

The sludge characteristics were influenced by the retention time only to a marginal degree as it can be testified from the results of Table 6-5. The observed variations represent experimental scatter rather than real effects. A retention time of at least 60 minutes appears to be sufficient to obtain optimum results. The amount of sulphate reporting to the solids declined slightly with increased retention time.

Table 6-5: Effect of retention time: Summary of experimental results.

Test #	Final pH	Retention Time (min.)	[Fe] _f (mg/L)	Settling Rate (m/hr)	Sludge Volume (mL)	Solids Content (%)	Sulphate [*] Content (%)
1	3.00	0	139.0	0.8	49	2.04	18.2
2	3.00	15	119.5	0.8	40	2.11	
3	3.00	30	95.6	0.8	41	2.78	
4	3.00	60	70.1	1.0	44	2.82	
5	3.00	120	71.7	0.6	46	2.59	17.4
6	6.00	0	< 0.1	1.9	62	1.93	10.9
7	6.00	15	< 0.1	1.9	59	1.84	
8	6.00	30	< 0.1	1.9	59	1.60	
9	6.00	60	< 0.1	2.3	59	2.24	
10	6.00	120	< 0.1	1.7	53	1.95	8.50
11	9.00	0	< 0.1	3.0	55	1.78	2.6

* Percent of sulphate in the precipitate

6.2.5 Effect of Temperature

The effect of temperature on iron removal and settling rate was studied (pH~3.3, t=120 min, 100 rpm, [Fe]_i=0.0016 M, [SO₄]=0.1 M). In accordance with the thermodynamic solubility, the final iron concentration decreased with increasing temperature (Figure 6-15). The influence of temperature on iron solubility was more

pronounced at low temperatures (25-40°C) and was less pronounced above 60°C. Precipitates formed at elevated temperatures were less hydrous and settled quicker. A more detailed study on the effect of temperature on iron hydrolysis can be found in section 6.3.

6.2.6 Effect of Sulphate Concentration

The treatment of acidic mineral effluents is a site-specific process. As the concentration and composition of these effluents varies so too does the ionic strength, the Fe(III) speciation and the manner in which the effluent responds to treatment. Both the final effluent quality and sludge properties were evaluated after treatment.

Synthetic effluents containing 0.018 M Fe(III) were prepared in both nitrate and sulphate media using analytical grade $\text{Fe}(\text{NO}_3)_3$ and $\text{Fe}_2(\text{SO}_4)_3$ respectively. Additional sulphate was introduced in the form of analytical grade sodium sulphate (Na_2SO_4). The ionic strength of the solution was adjusted in the case for no sulphate using analytical grade sodium nitrate ($[\text{NO}_3^-] = 7 \times 10^{-4} \text{ M}$). The pH of the effluent was adjusted to either 3, 6, or 9 using caustic soda introduced at a rate of 6.25×10^{-4} moles OH^-/min . A summary of effluents treated is given in Table 6-6.

Table 6-6: Summary of solutions treated to evaluate the ionic strength/complexation effect.

pH	Total Sulphate Concentration (g/L)				
	0	3	6	9	12
3	-	SO_4	SO_4	-	SO_4
	$\text{NO}_3(+\text{NaNO}_3)$	NO_3	NO_3	NO_3	NO_3
6	-	SO_4	SO_4	-	SO_4
	$\text{NO}_3(+\text{NaNO}_3)$	NO_3	NO_3	NO_3	NO_3
9	-	-	-	-	SO_4
	$\text{NO}_3(+\text{NaNO}_3)$	NO_3	NO_3	NO_3	NO_3

SO_4 , NO_3 indicate initial effluent media (i.e. sulphate or nitrate respectively).

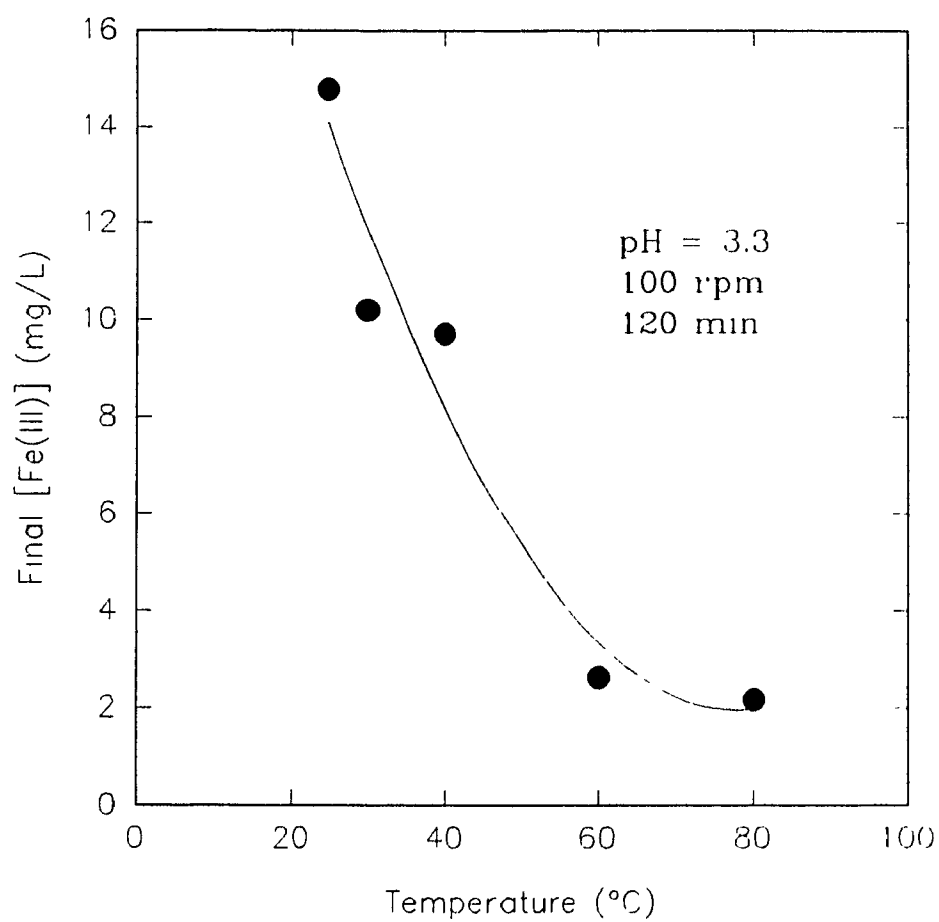


Figure 6-15: Effect of temperature on Fe(III) removal.

Results from the above tests (Table 6-7) indicate that the sulphate concentration strongly affects the sludge properties and final Fe(III) concentration. A high sulphate concentration had a detrimental effect on the sludge properties. Adding low quantities of SO_4^{2-} in a $\text{Fe}(\text{NO}_3)_3$ matrix definitely improved the properties of the precipitate up to a certain level (0.625 M (6 g/L) SO_4 , 0.018 M (1 g/L) Fe(III)), but beyond this point all properties deteriorated. With small differences this was true for either $\text{NO}_3^-/\text{SO}_4^{2-}$ or pure SO_4^{2-} solutions. The results are illustrated in Figures 6-16 to 6-18.

Table 6-7: Summary of results from nitrate and sulphate media tests.

Test #	Temp. (°C)	Time (min.)	Stir Speed (rpm)	Final pH	Neut. Rate (*)	Medium	Fe:SO ₄ Ratio (M)	Settling Rate (m/s)	Sludge Volume (mL)	Solids Content (%)	Final [Fe] (mg/L)	Final [SO ₄] (mg/L)	Fe in Ppt (%)	SO ₄ in Ppt (%)
1	50	60	200	3.00	0.125	NO ₃	1.0	NA	NA	NA	891.0	-	NA	NA
2	50	60	200	6.00	0.125	NO ₃	1.0	1.3	32.5	2.38	<0.1	-	72.4	0.0
3	50	60	200	9.00	0.125	NO ₃	1.0	1.5	27.0	2.86	<0.1	-	72.5	0.0
4	50	60	200	3.00	0.125	NO ₃	1.17	0.9	10.6	9.08	24.8	2791	59.6	14.7
5	50	60	200	6.00	0.125	NO ₃	1.17	3.5	15.0	6.24	<0.1	3245	55.9	9.6
6	50	60	200	9.00	0.125	NO ₃	1.17	3.7	15.4	5.36	<0.1	3182	68.5	0.8
7	50	60	200	3.00	0.125	NO ₃	1.34	1.1	11.0	7.71	47.5	6678	56.8	16.2
8	50	60	200	6.00	0.125	NO ₃	1.34	3.4	15.0	5.24	0.4	6130	58.7	7.7
9	50	60	200	9.00	0.125	NO ₃	1.34	3.1	13.5	5.31	<0.1	6474	57.2	1.8
10	50	60	200	3.00	0.125	NO ₃	1.52	1.0	13.5	6.19	60.5	8492	54.8	16.5
11	50	60	200	6.00	0.125	NO ₃	1.52	3.0	12.5	4.37	0.4	8955	47.5	8.6
12	50	60	200	9.00	0.125	NO ₃	1.52	3.0	15.0	4.80	<0.1	9293	66.1	1.2
13	50	60	200	3.00	0.125	NO ₃	1.69	0.5	19.0	4.44	78.0	12040	52.8	16.1
14	50	60	200	6.00	0.125	NO ₃	1.69	2.1	28.8	3.01	0.1	12467	58.0	7.9
15	50	60	200	9.00	0.125	NO ₃	1.69	3.0	22.5	3.23	<0.1	13119	63.6	3.1
16	50	60	200	3.00	0.125	SO ₄	1.17	1.5	10.7	9.99	25.8	3172	54.1	15.7
17	50	60	200	6.00	0.125	SO ₄	1.17	3.1	12.6	8.53	<0.1	3084	55.1	10.3
18	50	60	200	3.00	0.125	SO ₄	1.34	0.5	10.9	11.82	94.5	6183	52.3	15.9
19	50	60	200	6.00	0.125	SO ₄	1.34	3.8	11.9	8.61	0.2	6218	63.0	9.1
20	50	60	200	3.00	0.125	SO ₄	1.69	0.6	29.0	3.54	75.0	12058	NA	NA
21	50	60	200	6.00	0.125	SO ₄	1.69	1.2	47.0	2.28	0.1	11981	NA	NA
22	50	60	200	9.00	0.125	SO ₄	1.69	1.3	52.3	1.99	0.1	12177	NA	NA

* Neutralization rate (mL/min of 1.275 M NaOH) or 1.59×10^{-4} mole OH⁻/min

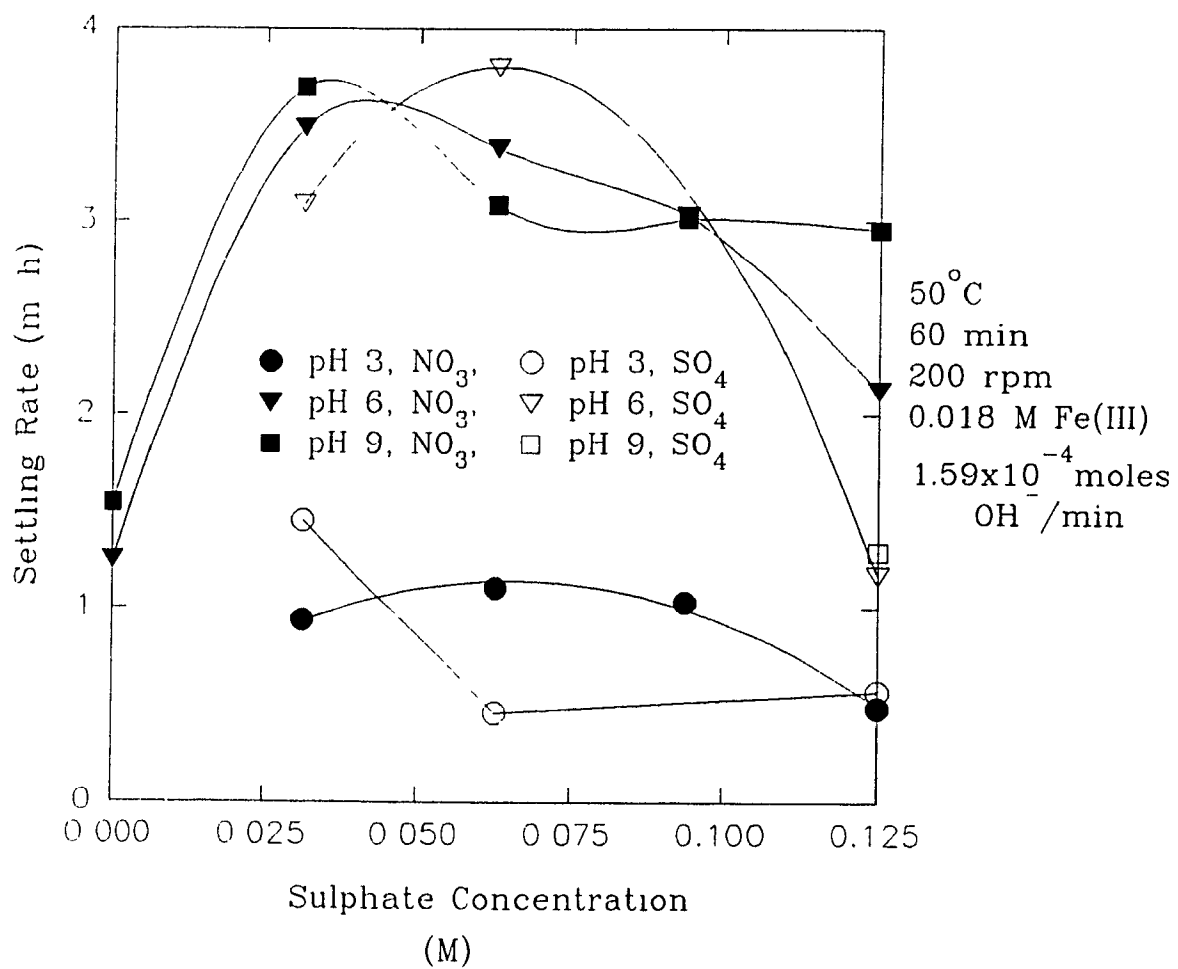


Figure 6-16: Effect of sulphate concentration on settling rate.

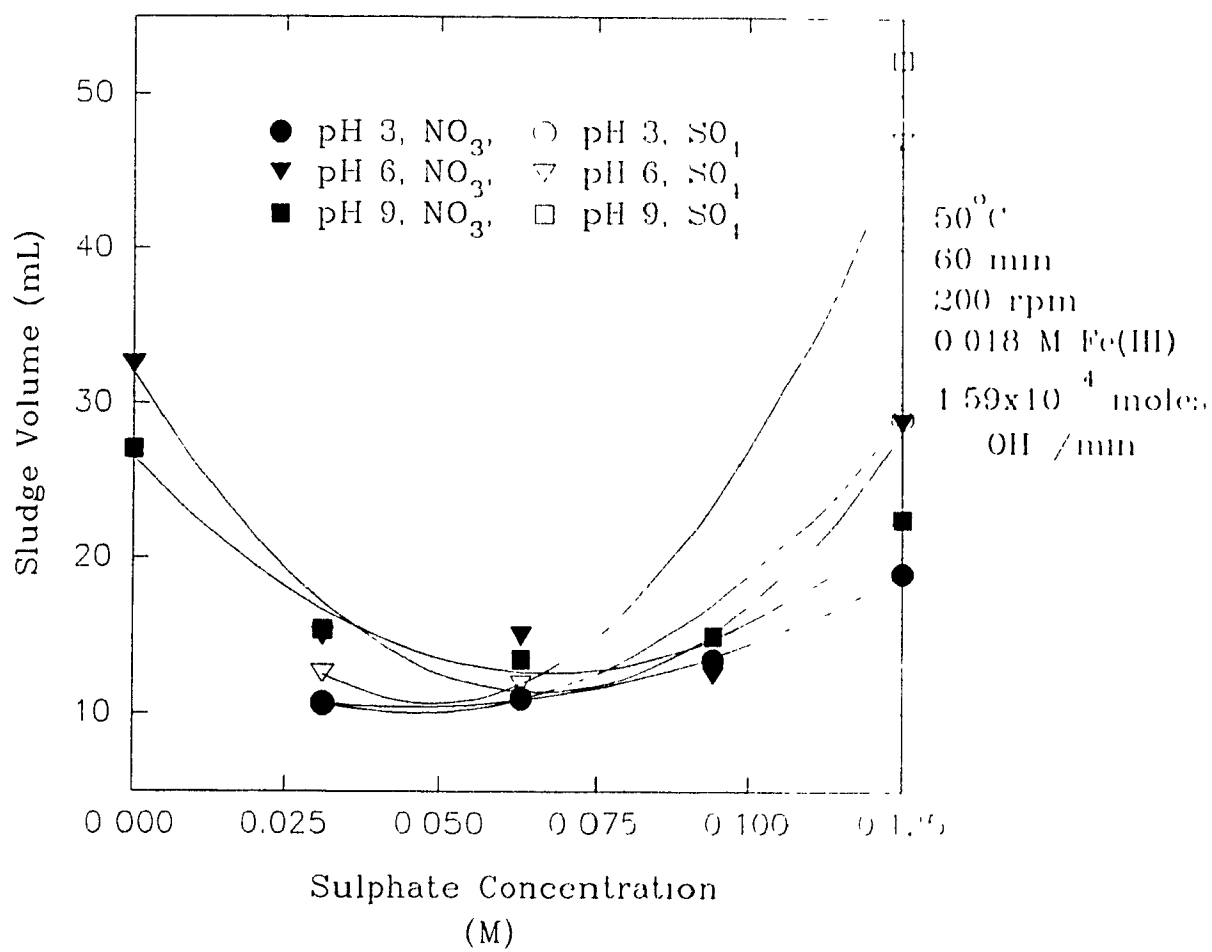


Figure 6-17: Effect of sulphate concentration on sludge volume.

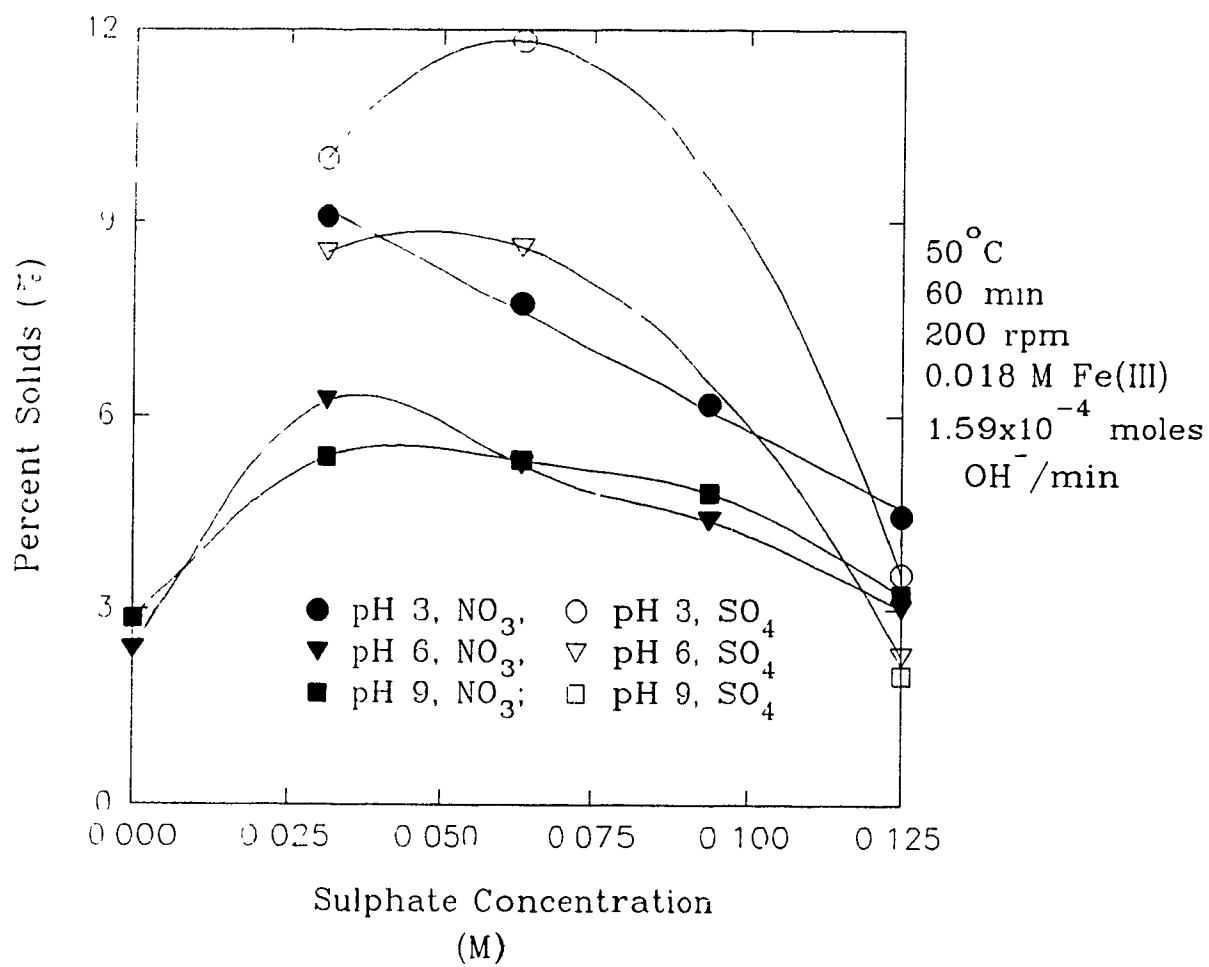


Figure 6-18: Effect of sulphate concentration on the percent of solids in the treatment sludge.

6.3 Statistical Design

Studying the effect of one variable on Fe(III) hydrolysis allows for simple interpretation. Many variables have been shown to influence hydrolytic precipitation. However, the manner in which each variable is inter-related with other parameters cannot be interpreted through single variable analysis. To investigate the relationships between several variables and the effect on the treatment results, experiments were statistically designed and performed.

In view of the number of variables and complexity of Fe(III) hydrolysis, only a select few of the process parameters could be investigated. The parameters, temperature (T), final pH (pH), rate of neutralization (using 1.275 M NaOH, NR), and the logarithm⁷ of the sulphate concentration (pS) were selected for this investigation. In Table 6-8 the range of conditions tested in this experimental program are summarized. The ranges were chosen based on preliminary results (section 6.2). In all tests 500 mL of synthetic effluent was treated for one hour at the final pH (section 6.2.4). Agitation was maintained at a rate of 200 rpm and samples were taken every 15 minutes after the final pH was reached ($t=0$).

To account for the possible interaction and curvature effects, with respect to the selected variables a second degree polynomial empirical model was selected.

$$\begin{aligned} Y = & b_0 + b_1X_1 + b_2X_2 + b_3X_3 + b_4X_4 \\ & + b_{11}X_1^2 + b_{22}X_2^2 + b_{33}X_3^2 + b_{44}X_4^2 \\ & + b_{12}X_1X_2 + b_{13}X_1X_3 + b_{14}X_1X_4 \\ & + b_{23}X_2X_3 + b_{24}X_2X_4 + b_{34}X_3X_4 + e \end{aligned} \quad (30)$$

where Y is the measured or calculated response, X_i are variables for the design, b_i , b_{ii} , b_{ij} are the first order, second order and the interaction term coefficients, respectively and "e" is the estimated error (Bacon, 1970). The ECHIP (1992) software program was used to execute the statistical calculations and to fit the data

⁷ Sulphate concentration was expressed as a logarithm in order to examine its effect on the system over different orders of magnitude.

to the second degree polynomial using regression analysis.

Table 6-8: Process variables investigated.

Process Variable	Units	Range of Conditions		
		Low	Medium	High
Temperature (T)	(°C)	25.0	50.0	75.0
Final pH (pH)	-	3.00	6.00	9.00
Neutralization Rate (NR)	mL/min* mole OH ⁻ /min	0.50 6.4 x 10 ⁻⁴	1.50 1.9 x 10 ⁻³	2.50 3.2 x 10 ⁻³
log [SO ₄] (pS) [SO ₄]	log(mg/L) mg/L	3.30 2000	3.75 5600	4.20 16 000

* 1.275 M NaOH; Other parameters: 200 rpm, time = 60 min., 1000 mg/L Fe(III)

In total, 21 randomized experiments were performed using synthetic effluent as outlined by the ECHIP program. The experimental data are given in Table 6-9.

Listed below are the empirical model equations in terms of true physicochemical units which were used to develop three-dimensional surface and two-dimensional contour response plots in order to visualize the system behaviour and determine the optimum operating conditions over the selected process design region. The solids content (%) data did not fit the second order polynomial model chosen.

Model Equations in Terms of Physicochemical Values

Settling Rate (m/hr)

$$Y_{SR} = 1.492 + 0.226T + 0.994pH - 0.468pS + 0.259T \cdot pH - 0.625T \cdot pS + 0.256pH \cdot NR - 0.306pH \cdot pS + 0.310NR \cdot pS \quad (2)$$

Table 6-9: Fe(III) hydrolysis: Response surface four-variable data.

Test #	INDEPENDENT VARIABLES				RESPONSES			
	T (°C)	pH	NR (mL/min)	pS (mg/L)	SR (m/hr)	SV (mL)	PS (%)	log[Fe _f] (mg/L)
1	25.0	3.00	0.50	4.20 (16000)	0.828	38.8	2.47	2.356
2	75.0	9.00	0.50	4.20 (16000)	1.016	60.0	0.85	-1.000
3	75.0	3.00	2.50	4.20 (16000)	0.380	68.0	1.15	2.418
4	25.0	9.00	2.50	4.20 (16000)	2.030	46.0	0.97	-1.097
5	25.0	3.00	0.50	3.30 (2000)	0.684	41.8	1.59	-1.411
6	75.0	9.00	0.50	3.30 (2000)	2.634	32.0	1.41	-1.523
7	75.0	3.00	2.50	3.30 (2000)	0.825	29.6	1.97	1.077
8	25.0	9.00	2.50	3.30 (2000)	1.668	50.0	0.85	-1.699
9	50.0	3.00	0.50	3.75 (5600)	1.020	29.6	2.00	1.832
10	25.0	6.00	0.50	3.75 (5600)	0.979	51.0	1.25	-1.222
11	25.0	3.00	1.50	3.75 (5600)	0.657	34.0	2.14	1.815
12	75.0	9.00	2.50	3.75 (5600)	2.082	36.0	1.54	-1.000
13	75.0	3.00	0.50	3.75 (5600)	0.883	16.6	3.10	1.937
14	25.0	9.00	0.50	3.75 (5600)	1.158	47.0	1.10	-1.301
15	25.0	3.00	2.50	3.75 (5600)	0.857	32.8	1.81	1.811
16	50.0	6.00	1.50	4.20 (16000)	1.264	52.0	1.10	-0.854
1	25.0	3.00	0.50	4.20 (16000)	0.700	41.1	2.71	2.176
2	75.0	9.00	0.50	4.20 (16000)	0.833	42.0	0.96	-0.959
3	75.0	3.00	2.50	4.20 (16000)	0.315	62.6	1.11	2.434
4	25.0	9.00	2.50	4.20 (16000)	1.626	40.0	1.33	-0.824
5	25.0	3.00	0.50	3.30 (2000)	0.544	40.8	1.71	1.418

Sludge Volume (mL)

$$Y_{SV} = 40.524 + 11.435pS + 8.551pS^2 + 15.828T \cdot pS \quad (3)$$

$\log [Fe_f]$ (mg/L)

$$Y_{Fe} = -1.017 - 2.899pH + 1.219pS \quad (4)$$

6.3.1 Settling Rate

Figure 6-19 shows a typical 3-dimensional representation of the estimated response surface, that is, settling rate (m/hr) as a function of the logarithm of the sulphate concentration and temperature, for constant pH (6) and rate of neutralization (1.50 mL/min, 1.275 M NaOH).

In Figure 6-19 a strong interactive effect between the sulphate concentration in the effluent and the treatment temperature can be clearly seen. Thus, while temperature had very little effect on the sludge settling rate at high sulphate concentration ($\log[SO_4] = 4.2$), a very strong effect is seen at lower sulphate concentrations. For example, the settling rate in the latter case increases from 1.01 to 1.88 m/hr by increasing the temperature from 25°C to 75°C. High sulphate concentration had a detrimental effect on the settling rate of the sludge generated, especially at elevated temperatures. The settleability of the sludge improved when the sulphate concentration was reduced and the treatment temperature was elevated.

The complex interactions of temperature, pH and sulphate concentration were further investigated by considering other 3-D plots. It was found that a higher final pH increased the settling rate. By increasing the pH from 3 to 9 (Figure 6-20) while maintaining temperature (50°C), $\log[SO_4]$ (3.75), and caustic addition rate (1.50 mL/min) constant, the settling rate increased from 0.9 to 1.9 m/hr, a two-fold increase. This trend is consistent with the findings in section 6.2.1.

From the stand point of optimum sludge settling, the best operating conditions within the ranges studied are summarized in Table 6-10.

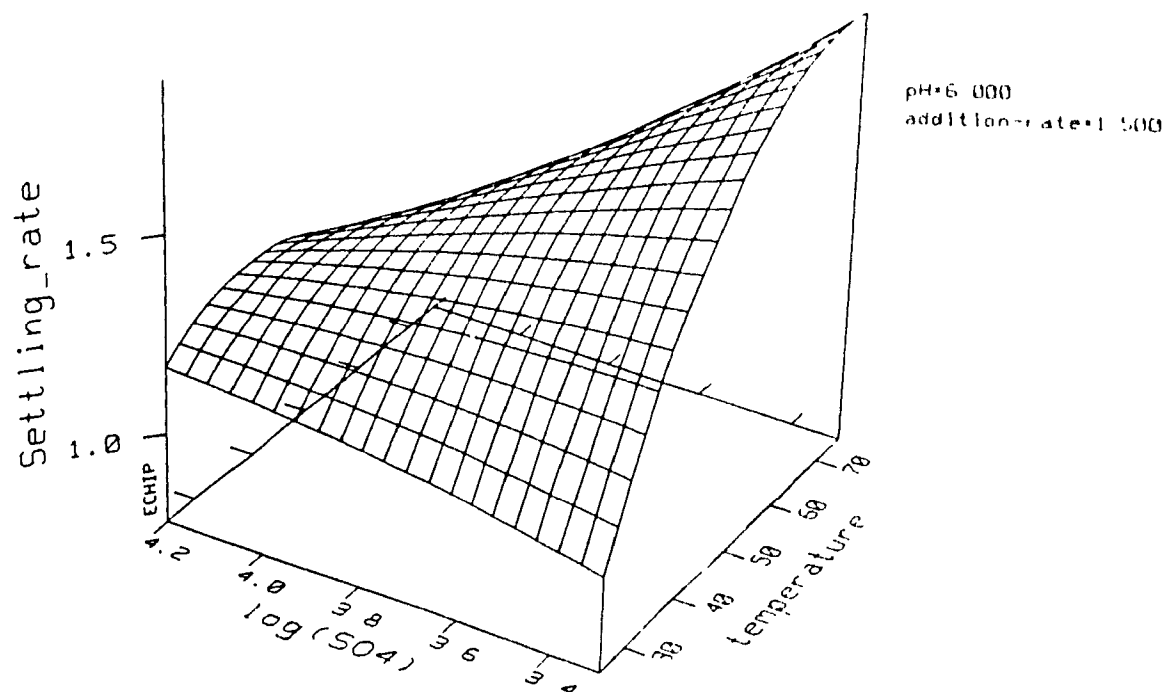


Figure 6-19: Predicted settling rate (m/hr) response surface (pH = 6.0, neutralization rate = 1.9×10^{-3} moles OH^- / min.

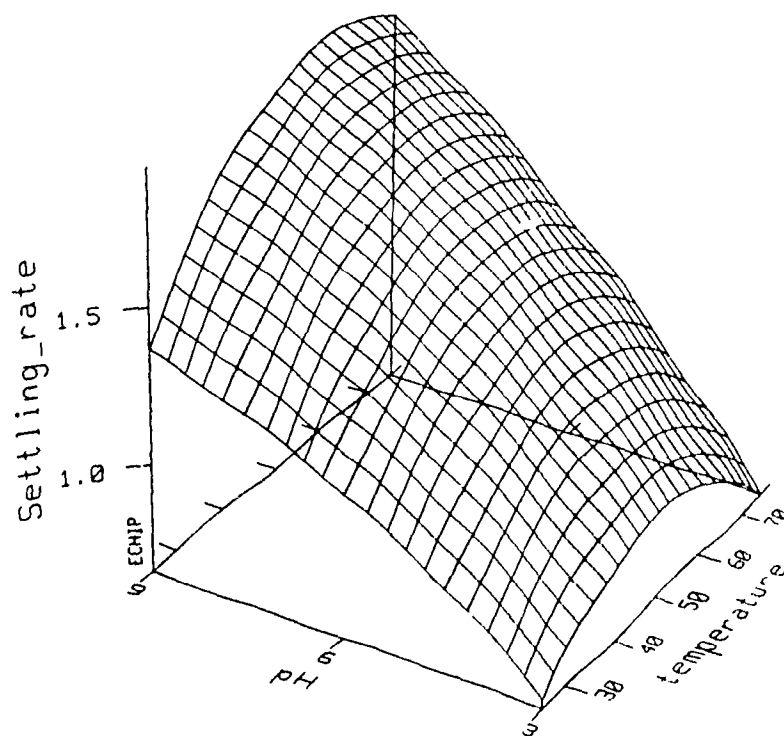
Table 6-10: Best conditions and results derived from the statistical design.

Response	Variable				Optimum Value
	T (°C)	pH	NR (moles/min)	log[SO ₄] (mg/L)	
Settling Rate (m/hr)	75.0 (High)	9.00 (High)	0.50 (Low)	3.30 (2000)	2.6
Sludge Volume (mL)	75.0 (High)	6.00 (Medium)	0.50 (Low)	3.30 (2000)	12.5
log[Fe _r] (mg/L)	25.0 (Low)	7.15 (Medium to High)	0.50 (Low)	3.30 (2000)	-2.705 (0.002)

* Identification of the variable level as low, medium or high according to Table 6-8.

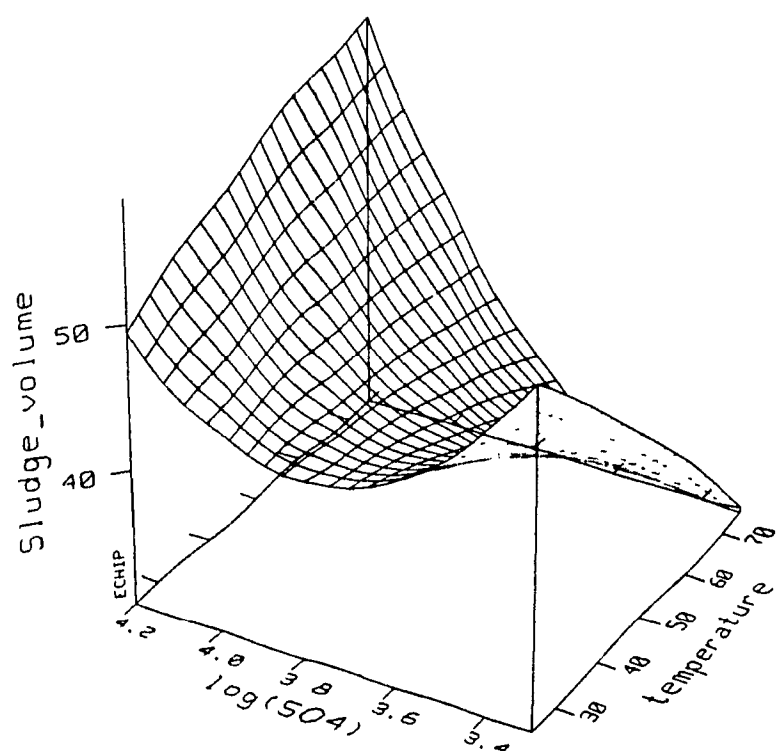
6.3.2 Sludge Volume

A 3-D representation of the sludge volume response surface generated using the ECHIP program is shown in Figure 6-21. It represents the response surface as a function of sulphate concentration (pS) and temperature (T) at fixed pH and rate of neutralization. The two latter parameters were found not to have a significant effect within the range under consideration and were thus kept constant at their intermediate levels (pH 6.00, 1.50 mL/min 1.275 M NaOH) respectively. From preliminary testing (section 6.2) it was known that these parameters did influence the volume sludge generated. In the case of neutralization rate, the effect was minimal over the range investigated (i.e. 0.5 to 2.5 mL/min) which is consistent with the results in Figure 6-8.



addition-rate=1.500
log(SO4)=3.7500

Figure 6-20: Predicted settling rate (m/hr) response surface ($[\text{SO}_4] = 5600 \text{ mg/L}$, neutralization rate = $1.9 \times 10^{-3} \text{ moles OH}^- / \text{min}$).



pH=6.000
addition-rate=1.500

Figure 6-21: Predicted sludge volume (mL) response surface (pH = 6.0, neutralization rate = 1.9×10^{-3} moles OH^- / min.

From Figure 6-21 it is clear that elevated temperatures and low sulphate concentrations (2000 mg/L) serve to decrease the volume of sludge generated. Interestingly enough, there was an intermediate region ($pS = 3.37$, $T = 50^{\circ}\text{C}$) where sludge volume was relatively small. The optimum conditions to reduce the volume of sludge generated can be determined from Figure 6-21 and are summarized in Table 6-10.

6.3.3 Final Iron Concentration

Three-dimensional graphs of final iron concentration indicate a strong interaction between final pH and sulphate concentration (Figure 6-22). Increasing the pH to a optimum value minimized the residual iron concentration in the treated effluent. The sulphate concentration in the effluent had a positive effect on the final iron concentration (i.e. solubility increased). From Figure 6-22, the solubility of iron(III) can be determined. Figure 6-22 and similar plots were utilized in this manner to construct statistical design-derived solubility diagrams.

6.3.3.1 *Solubility Diagrams*

Knowledge of Fe(III) solubility in sulphate media is necessary to successfully remove Fe(III) through hydrolytic precipitation. Literature on Fe(III) solubility under varying sulphate concentrations and temperatures is limited. Using the ECHIP program it was possible to extract iron concentration data directly from 2-D contour plots for specific pH, $\log [\text{SO}_4]$ and temperatures. The data were then assembled in the form of solubility diagrams.

The effect of sulphate concentration and temperature on the iron(III) hydrolysis solubility was examined for the pH range considered. Figure 6-23 gives the solubility of Fe(III) for varying sulphate concentrations at 50°C . Plots for 25°C and 75°C can be found in Appendix D. The amplifying effect of sulphate concentration on Fe(III) solubility was more pronounced at low pH (3). At higher pH (> 7), increasing the sulphate concentration from 6.3 g/L ($\log[\text{SO}_4]=3.8$) to 16 g/L ($\log[\text{SO}_4]=4.2$) had little effect on the solubility. From the data generated using the ECHIP program the effect of temperature on Fe(III) solubility was also examined (Figure 6-24). Elevated temperature is expected to lower Fe(III) solubility

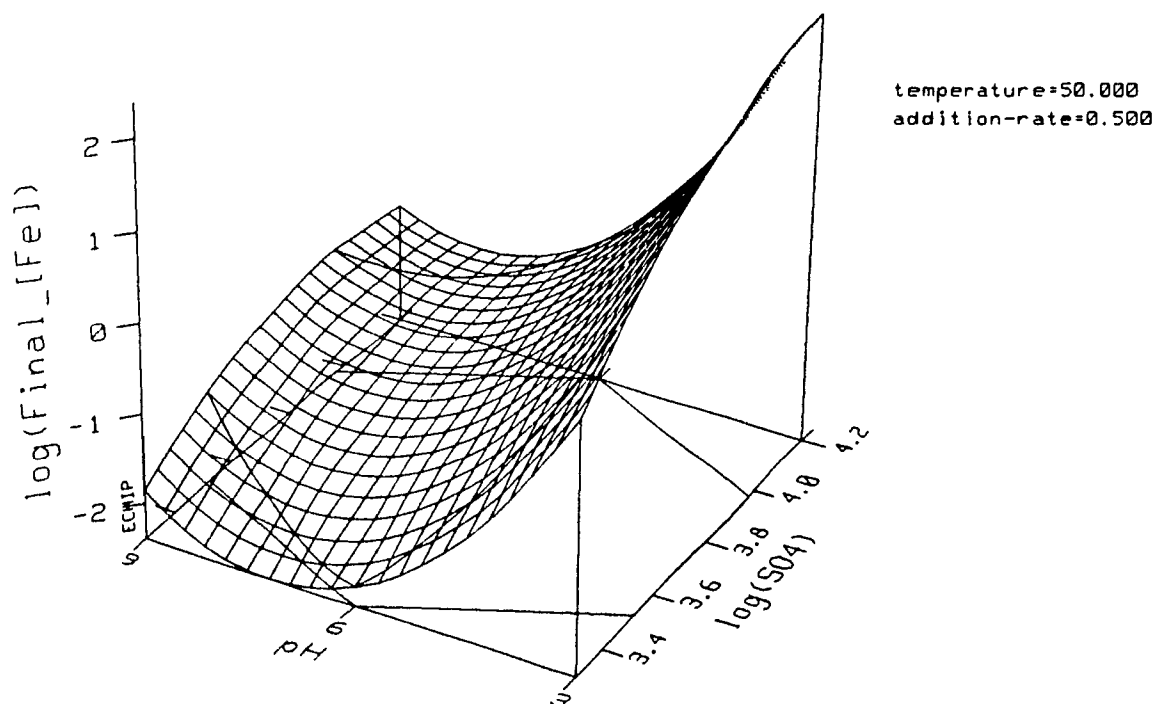


Figure 6-22: Predicted final iron concentration (mg/L) response surface (Temp = 50°C, neutralization rate = 6.4×10^{-4} moles OH^- / min.

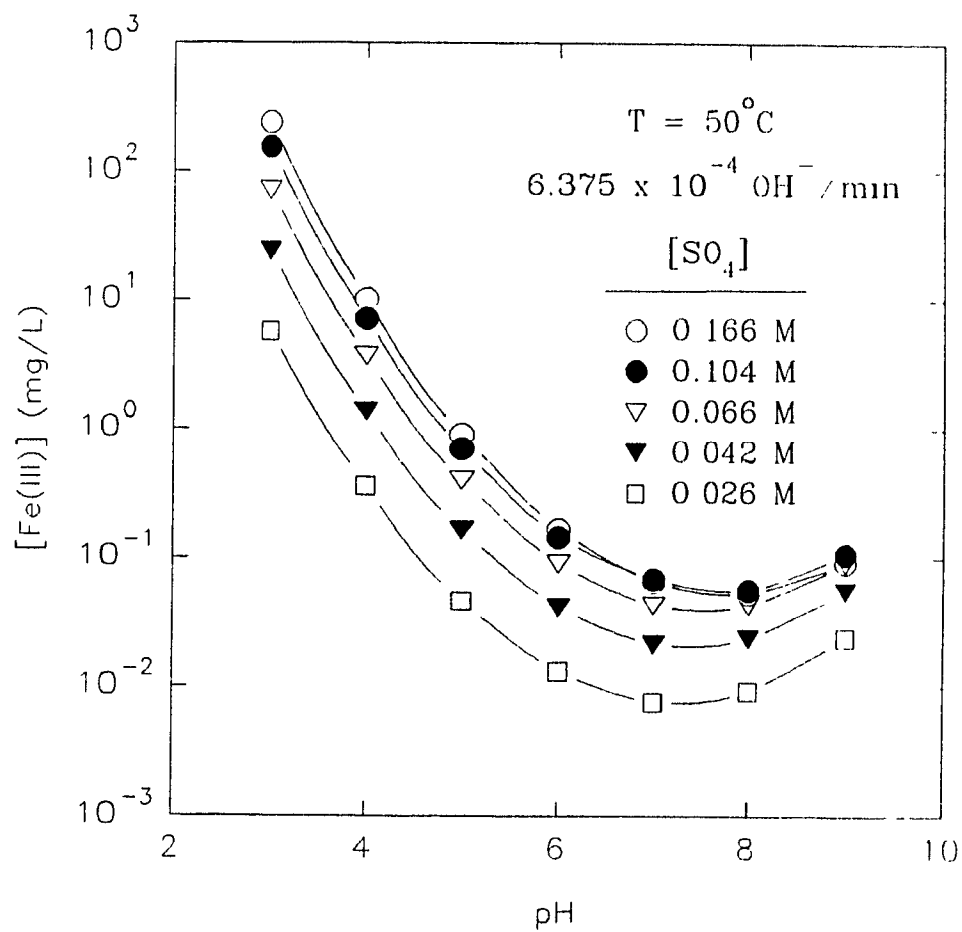


Figure 6-23: Fe(III) solubility for various sulphate concentrations at 50°C.

(Chapter 2) but the solubility lines generated from this study indicate the opposite relationship. The underlying cause for this anomaly is not clear. However, it might have to do with the fact that the real precipitates are not completely crystalline, or the precipitate may be a mixture of more than one phase as opposed to the single (and crystalline) $\text{Fe}(\text{OH})_{3(s)}$ phase, as assumed in the thermodynamic calculations (Chapter 4).

A comparison among the theoretically predicted solubility of $\text{Fe}(\text{OH})_3$ based on its solubility product and in the absence of SO_4^{2-} complexation, the solubility lines calculated in Chapter 4 using the F*A*C*T program, where sulphate complexation was taken into account, and the solubility line developed using data derived from the statistically designed experiments is shown in Figure 6-25. The theoretical line, which ignores complexation, is two orders of magnitude lower than the line constructed using F*A*C*T. The observed discrepancy between the two lines is attributed to the effect of sulphate complexation on Fe(III) solubility. The line calculated thermodynamically using F*A*C*T represents Fe(III) hydrolysis in sulphate media (0.1 M), whereas the theoretical line is calculated for an ideal, sulphate-free system.

In comparing the solubility line generated using F*A*C*T with the experimentally determined solubility line, the experimentally determined solubility is three orders of magnitude higher (in the pH region 5 to 9) although the sulphate concentrations for the two systems are equal. Several factors may give rise to this difference such as those outlined in Chapter 4. First, the assumption of zero ionic strength rule in the F*A*C*T calculations is only valid for ideal, very dilute solutions. Correcting for the true ionic strength would shift the thermodynamic (F*A*C*T) solubility line towards the experimental solubility line. Also, the theoretical solubility relationships were derived for pure $\text{Fe}(\text{OH})_{3(s)}$. However, the solubility of a compound depends on the chemical composition, the age and the degree of crystallinity of the precipitate (Section 2.2). As seen previously, different Fe(III) precipitates are formed under distinct experimental conditions. The assumption that Fe(III) removal was in the form of crystalline $\text{Fe}(\text{OH})_3$ cannot be made under all conditions. Finally, the experimental solubility line is based on spectrometrically

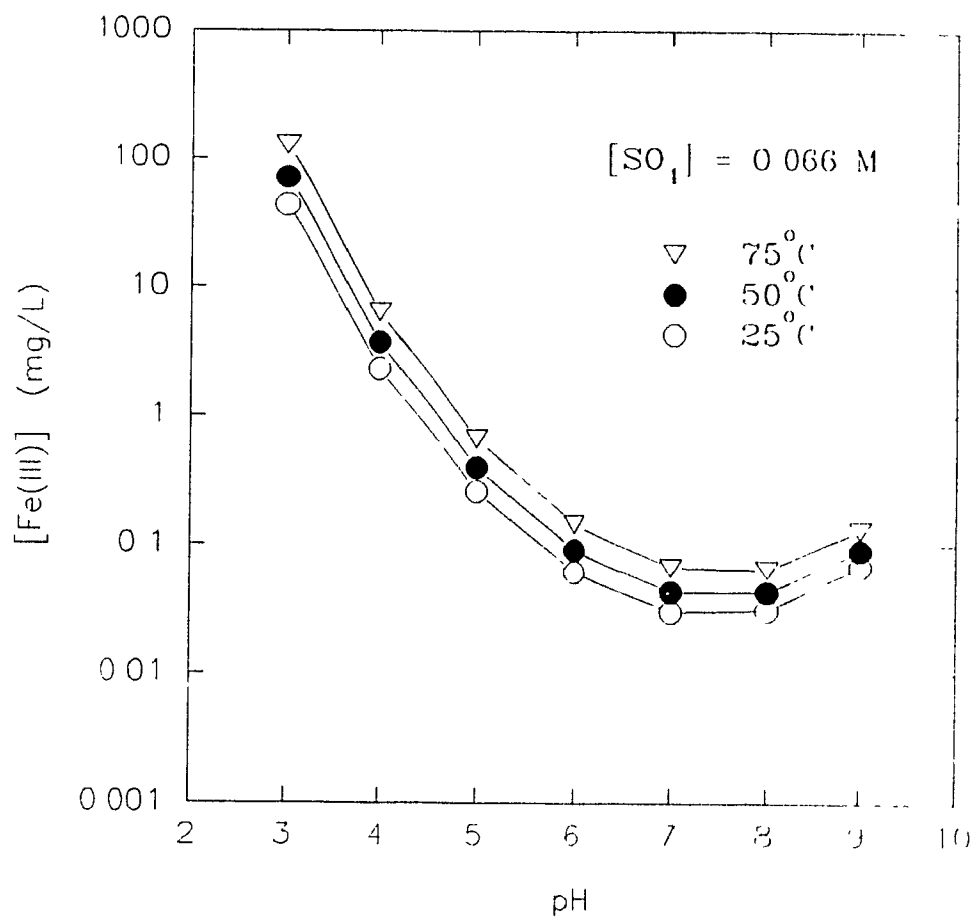


Figure 6-24: Effect of temperature on Fe(III) solubility.

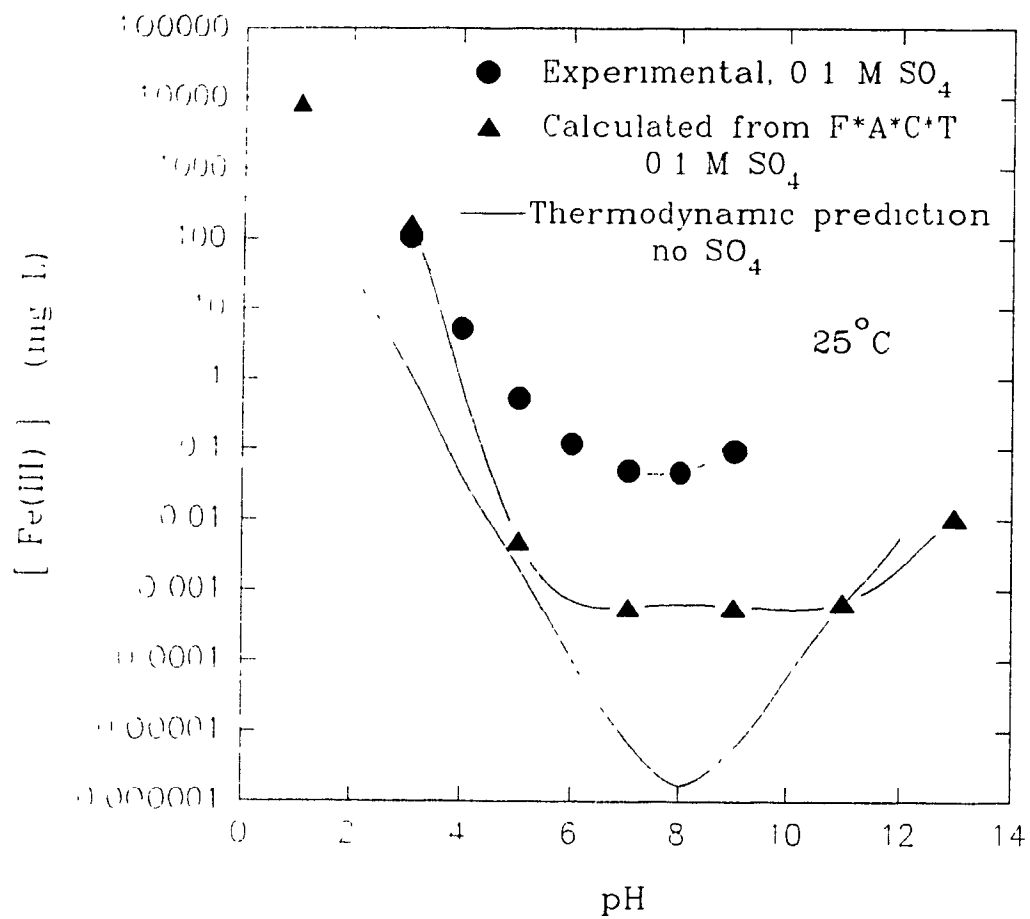


Figure 6-25: Comparison of Fe(III) solubility lines.

determined concentrations and are subject to the detection limits (0.06 mg/L) of the instrument.

Therefore, this series of solubility diagrams provide a practical reference to iron removal under different conditions (sulphate concentration, temperature). In the next section these diagrams are used to design supersaturation-controlled experiments.

6.4 Recycling

The process of recycling solids back to the reaction vessel is an established procedure in chemical precipitation. Several authors (Kuit, 1980; Vachon, 1987; Kuyucak, 1991) found recycling significantly improves the effluent treatment process in terms of sludge characteristics. The effect of precipitate recycling on Fe(III) hydrolysis however, has not been fully elucidated nor optimized.

Recycling tests were performed to determine the effect on the settling rate and solids content of the sludge. Two distinct experimental procedures were investigated. In both procedures synthetic effluent (500 mL) containing 1 g/L (0.018 M) Fe(III) and 6 g/L (~ 0.6 M) SO_4^{2-} was heated to 50°C, then the pH was adjusted at a rate of 1.6×10^{-4} moles OH^- /minute either continuously (series A) or in discrete pH steps (series B). The final pH ($t=0$) was maintained for 60 minutes. The treated effluent/sludge was cooled and stored for 16 hours. The settling rate of cooled sludge was measured prior to percent solids content determination on a representative (1 mL) sample.

6.4.1 Series A

In the first series of recycling experiments (series A), the initial precipitate was collected after sludge characterization. The effluent was heated to 50°C and the agitation rate was set at 200 rpm. Caustic soda (1.275 M) was introduced to the system at a constant rate (1.6×10^{-4} moles OH^- /minute). When the pH reached ~ 2.80 the sludge was introduced and the agitation was increased to 600 rpm. Neutralization continued until the pH reached 6 (~ 3 hours). The pH was controlled at 6 for 60 minutes. The solution/sludge was cooled and the sludge was collected

for the next recycle. All the sludge, with the exception of ~0.1 g (wet, approximately 10% of total precipitate, for percent solids determination) was recycled. The sludge was recycled twenty times. The final precipitate was examined chemically, physically and microscopically.

Recycling the precipitate significantly improved the sludge quality. The most pronounced improvement was observed with the solids content. Figure 6-26 shows the densifying effect of recycling on the percent solids in the sludge. Recycling was extremely effective up to approximately ten cycles, following this the solids content reached a plateau between 10 - 15 recycles and then began increasing once again, approaching 35% solids in the sludge after twenty recycles. Complete dewatering of the sludge was achieved in 10-20% of the time required to dewater sludge generated without recycling. This would suggest the recycled sludge consisted of discrete particles which compacted effectively compared to aggregated precipitates which were observed in systems absent of recycling. For this reason, the recycled precipitate trapped less process water in its structure.

The settleability of the recycled sludge was initially faster than the unrecycled sludge. Initial recycles produced a sludge which settled at a rate of 4 m/hr. However with continued recycling, settling rates deteriorated by about 50% of the maximum settling rate. This is attributed to an increasing abundance of fines (Figure 6-27). The fines may have come from particle attrition upon recycling or through homogeneous nucleation.

Chemical analysis on the precipitate showed that it was 60.9% Fe, 4.9% SO_4 and 0.04% Na. This chemical composition suggests the precipitate has the approximate chemical composition of goethite ($\alpha\text{-FeOOH}$, 62.9% Fe) with trace natrojarosite. Some of the sulphate reported could be attributed to either adsorption or co-precipitation. X-ray diffractometer analysis indicated a poorly crystalline goethite precipitate. Diagnostic peaks for jarosite were not observed.

Particle size measurements were performed on the precipitate. A histogram of the results exhibiting bimodal distribution is shown in Figure 6-27. The mean diameter for the entire sample was 8.87 μm .

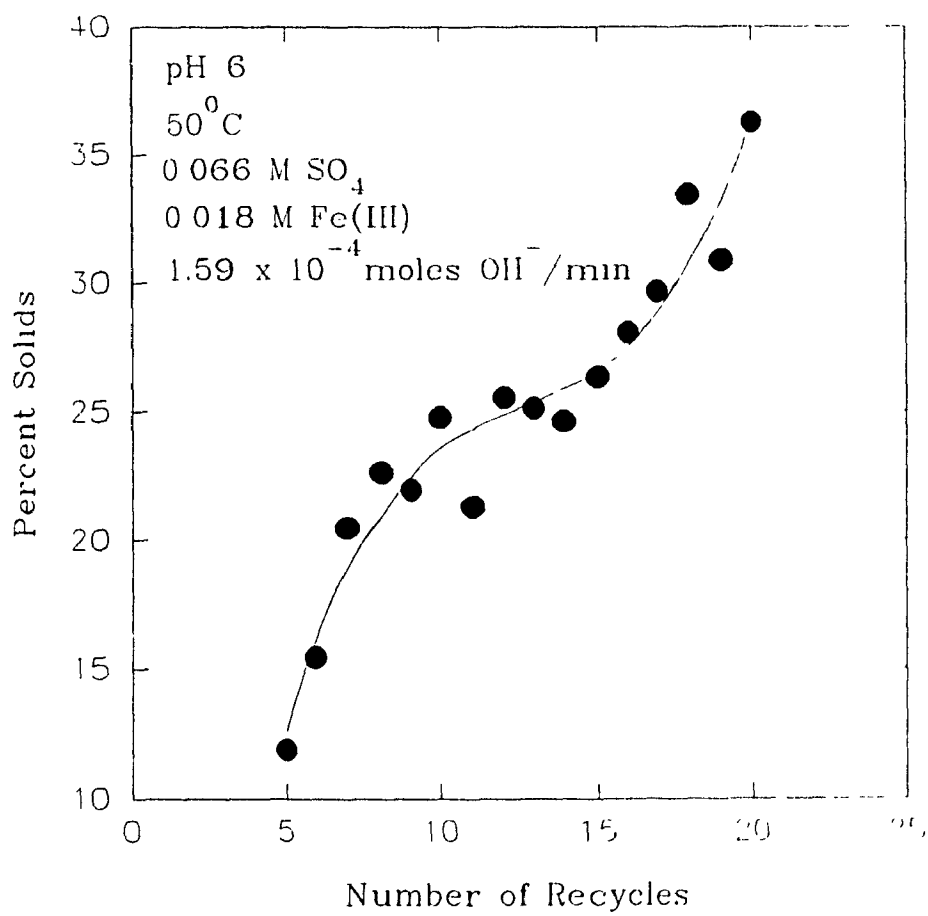


Figure 6-26: Effect of recycling on sludge densification (Series A).

BET surface measurements on the precipitate indicated the precipitate to be slightly less porous than typical amorphous Fe(III) hydrolysis products having approximately 600 m²/g (Davis and Leckie, 1978). The specific surface area was found to be 162 m²/g.

SEM photomicrographs of the recycled (20x) precipitate (A) are shown in increasing magnification order (Plates 6-3 to 6-6). The precipitates are seen to consist of relatively discrete and coarse, although porous, composite particles in contrast to the fluffy material produced without recycling (Plates 6-1 and 6-2). Recycling of precipitates apparently produced larger particles via the initial aggregation of primary fine particles and subsequently the covering of the aggregates by chemical overgrowth (heterogeneous deposition).

6.4.2 Series B

In the second series of recycling tests the level of supersaturation was controlled in order to improve precipitate density and morphology. The system was operated in the region of growth and secondary nucleation, rather than homogeneous nucleation (Figure 6-11). In series B, an attempt was made to control the saturation ratio at 3 during the recycling process by neutralizing the solution in stages. The number of neutralization stages necessary to maintain a constant level of saturation was determined from the experimental solubility line for Fe(III) at 50°C by drawing vertical and horizontal lines between the saturation line ($S=3$) and the solubility line. Construction of the diagram is illustrated in Figure 6-28. Table 6-11 outlines the stages involved in the recycling process.

The reaction time is defined as the estimated time required to reach "equilibrium" after achieving the final (increment) pH ($t=0$). Reaction time estimates are based on the observed hydroxyl ion demand after reaching the target pH. When the addition of NaOH was nil or less than approximately 0.025 millimoles OH⁻ per minute the system was assumed to be at steady state.

The sludge to be recycled was introduced at the beginning of stage 1 (pH 2.55) to provide seeds and facilitate secondary nucleation at the time of precipitation. Dissolution tests (Appendix E, Table E-1) indicated very little precipitate dissolution

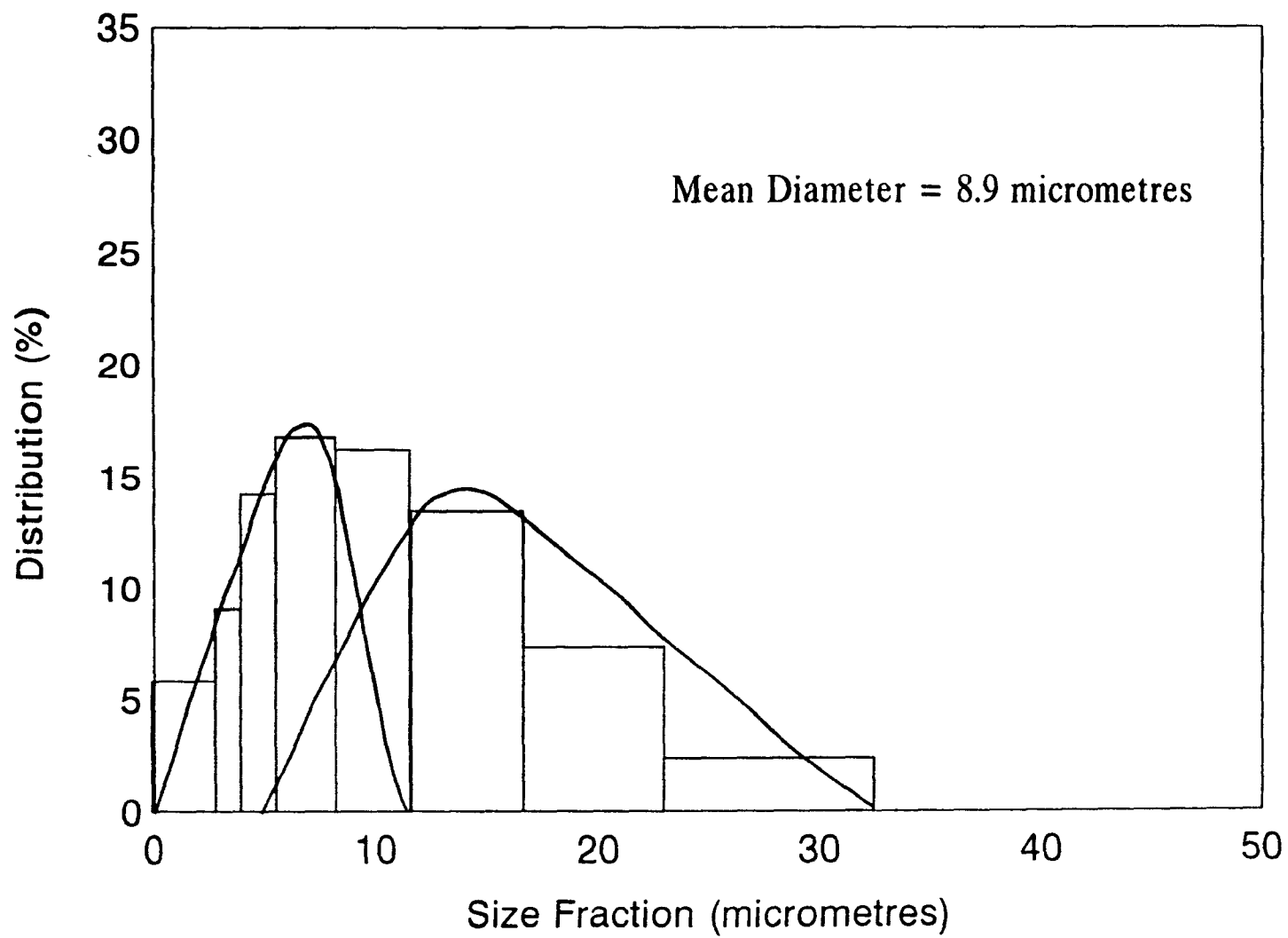


Figure 6-27: Particle size distribution for conventionally recycled (20x) solids (Series A).

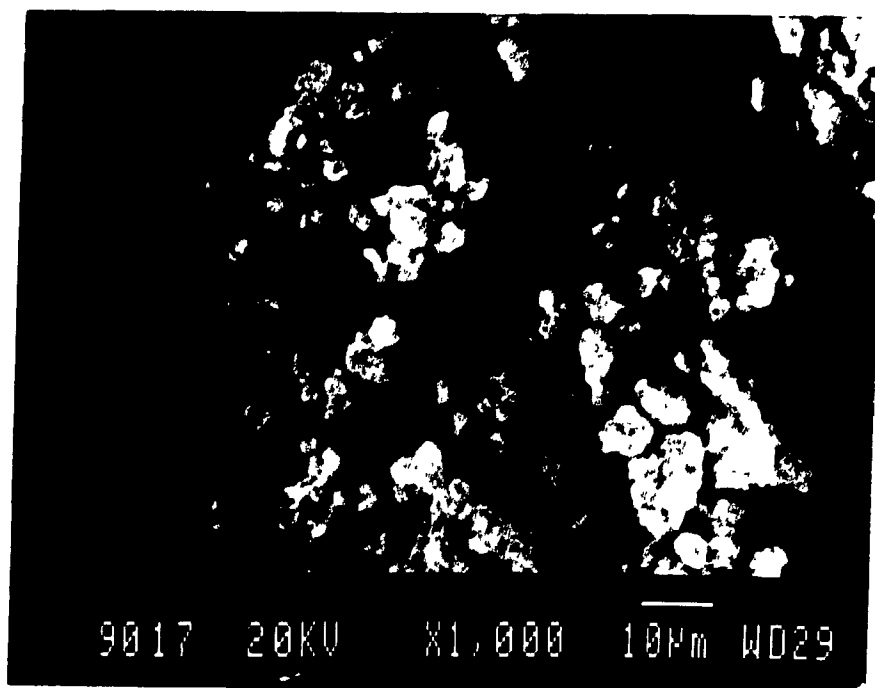


Plate 6-3: Sample: Recycle Series A (20 recycles)

Production Conditions: 50°C

1. pH 2.5 to ~2.8 @ 200 rpm
 2. seed added
 3. agitation rate increased to 600 rpm
 4. pH (final) 6, 60 min
- % Solids (max) = 35%
Number of recycles: 20
Neutralization rate: 1.6×10^{-4} mole OH^- / min.

Comments: The particles are rounded and vary in diameter from 3 to 12 micrometres, and are made up of compact spherical particles measuring 0.5 to 1.0 micrometre in diameter. These particles are highly porous and appear to have formed more by agglomeration rather than epitaxial overgrowth.

Magnification: 1000x

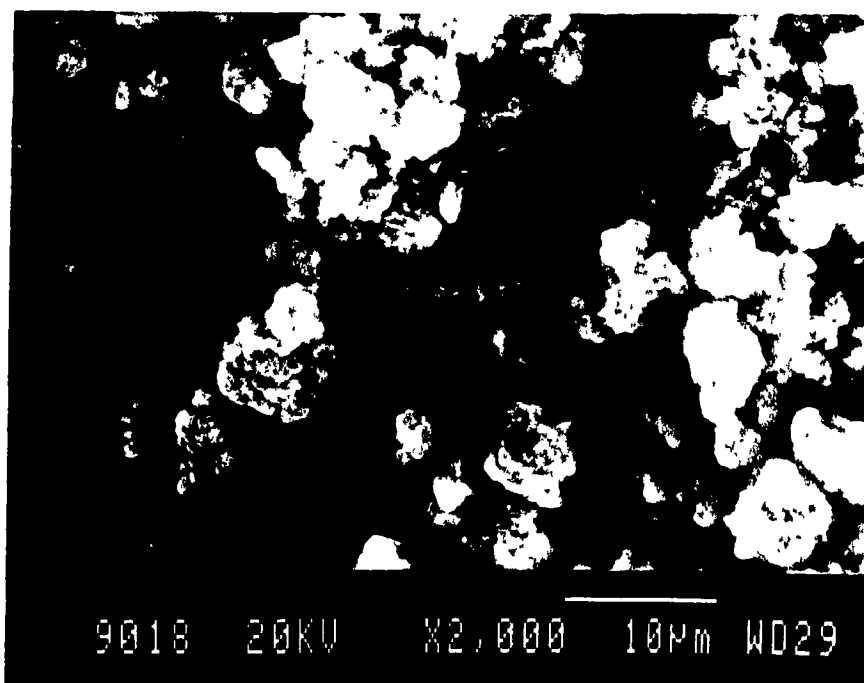


Plate 6-4: Sample: Recycle Series A (20 recycles) - continued
 Production Conditions: 50°C

1. pH 2.5 to ~2.8 @ 200 rpm
 2. seed added
 3. agitation rate increased to 600 rpm
 4. pH (final) 6, 60 min
- % Solids (max) = 35%
 Number of recycles: 20
 Neutralization rate: 1.6×10^{-4} mole OH^- / min.

Comments: The rounded nature of the particles, and the high porosity which results from the relatively loosely packed together round aggregates is illustrated by this photograph. The high porosity will result in a low bulk density and consequent low settling rate. However, the porosity of the particles formed by recycling is much lower than that of the sponge like precipitates formed when no recycling has taken place. The effect of recycling is thus to form larger, more well defined denser particles which will settle more rapidly than those which have not been subjected to recycling. The size of the particles in this photograph varies between 3 and 7 micrometres.

Magnification: 2000x

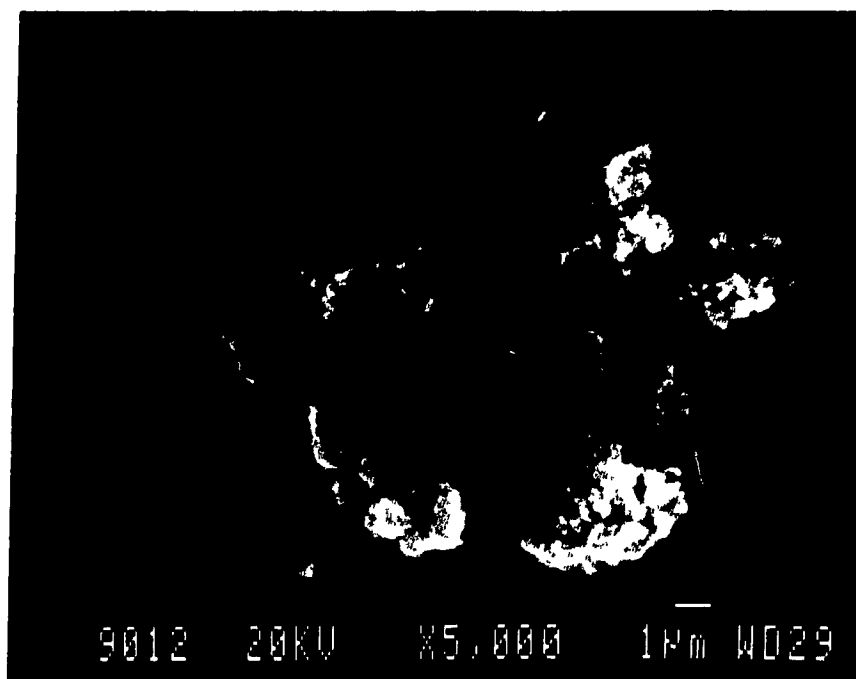


Plate 6-5

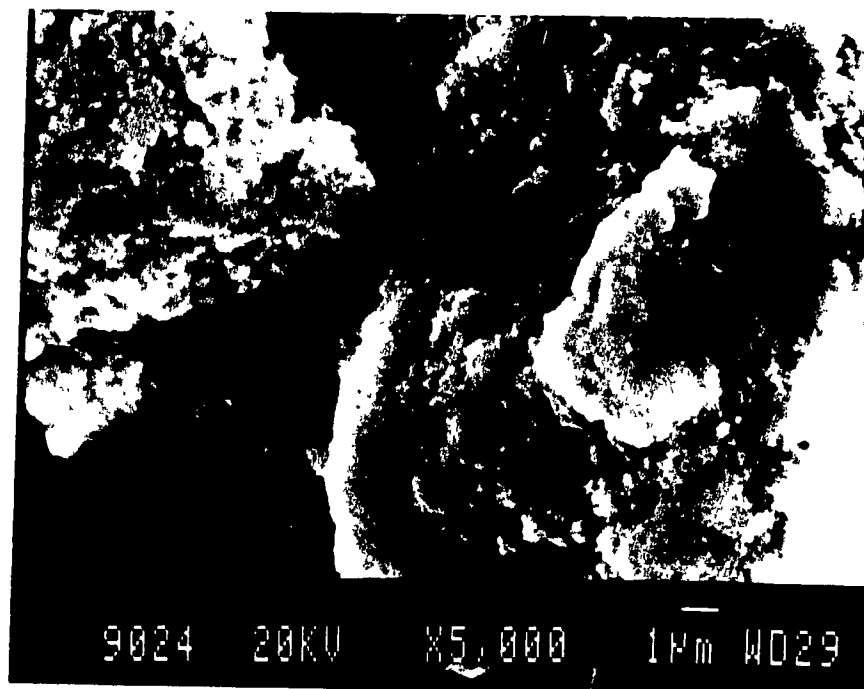


Plate 6-6

Caption on next page

Previous Page

Plate 6-5 and 6-6: Sample: Recycle Series A (20 recycles) - continued

Production Conditions: 50°C

1. pH 2.5 to ~2.8 @ 200 rpm
 2. seed added
 3. agitation rate increased to 600 rpm
 4. pH (final) 6, 60 min
- % Solids (max) = 35%
- Number of recycles: 20

Neutralization rate: 1.6×10^{-4} mole OH^- / min.

Comments: These high magnification (5000x) electron micrographs demonstrate the essential features of this precipitate which has been formed by recycling - rounded cauliflower like coarse particles consisting of relatively dense aggregates loosely packed together to leave a porous structure. The packing together of rounded particles dominates, and evidence of epitaxial overgrowth is limited.

Magnification (5000 x)

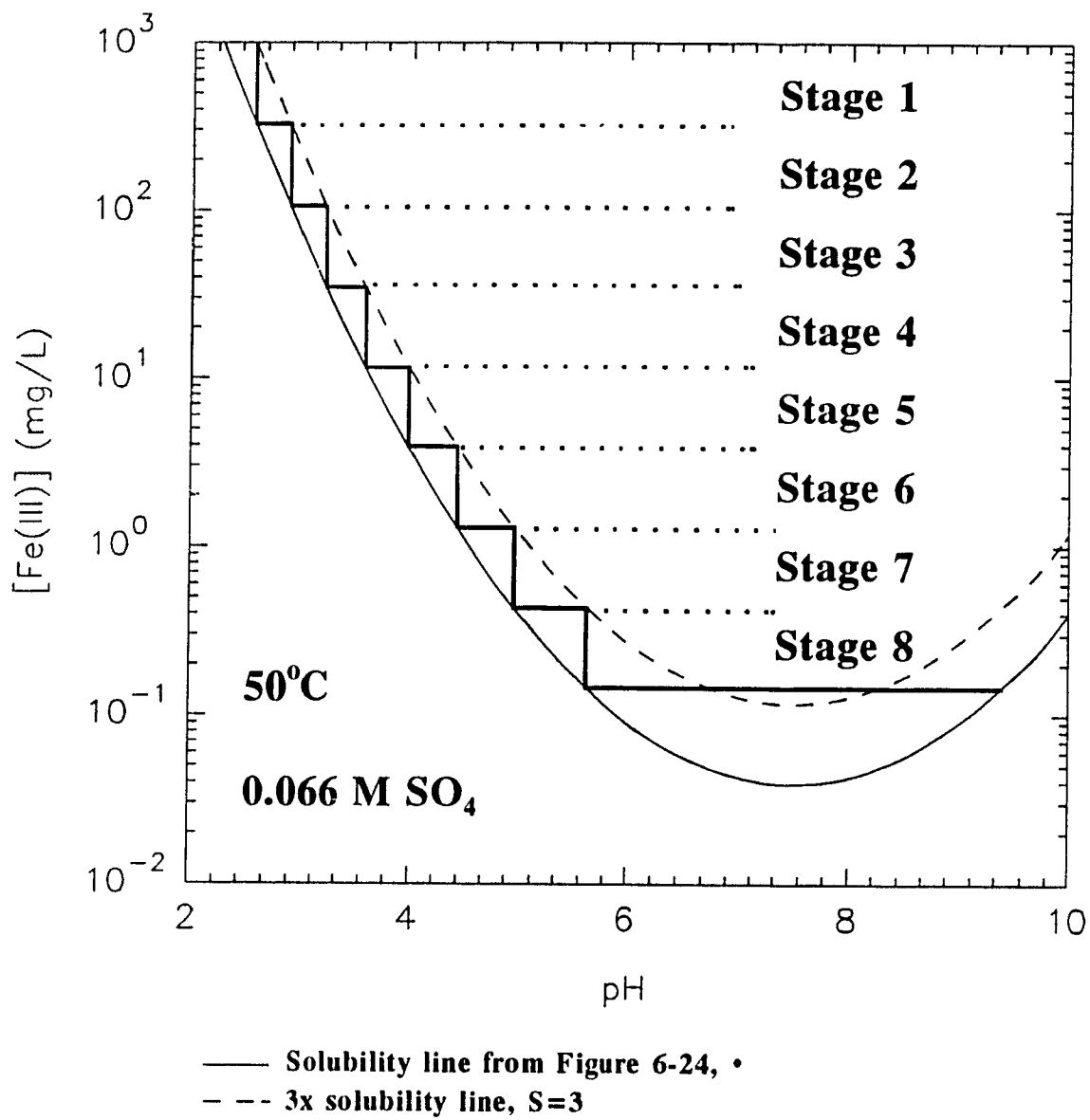


Figure 6-28: Schematic representation and derivation of the staged neutralization process.

occurred at pH 2.5. The stirring speed was set at 500 rpm for the entire length of the test (8 stages). Detailed test data is shown in Table E-2 (Appendix E).

Table 6-11: Summary of neutralization stages for Series B recycling.

Stage #	Initial pH	Final pH	Reaction Time (min.)
1	2.55	2.84	60
2	2.84	3.20	45
3	3.20	3.58	30
4	3.58	4.00	20
5	4.00	4.48	20
6	4.48	5.00	20
7	5.00	5.69	20
8	5.69	9.29	20

T = 50°C; Neutralization rate = 1.6×10^{-4} moles OH⁻ / min.

The solids were characterized similarly to Series A solids. The solids content was measured after each test by selecting a representative sludge sample (0.1-0.2 g (wet)) for percent solids determination. Staged-neutralization recycling (S=3) served to densify the sludge very effectively without exhaustive recycling. Figure 6-29 demonstrates the enhanced effect of staging on densification compared to simple recycling (Series A). The sludge generated via staged-neutralization recycling is of the order 2-3 times denser than sludge produced from simple recycling. The sludge reached its solids loading threshold (55%) after 8 recycles. The system then underwent a series of sludge dilution and compaction periods but did not adversely affect the final precipitate solids content.

In contrast to precipitate A (simple recycling), series B sludge settled rapidly and the settling rate increased with the number of recycles to a maximum of 14 m/hr (13 recycles, Figure 6-30). Continued recycling beyond thirteen times appeared to lead to some precipitate degeneration, possibly due to particle attrition giving rise to an increased concentration of suspended material after settling.

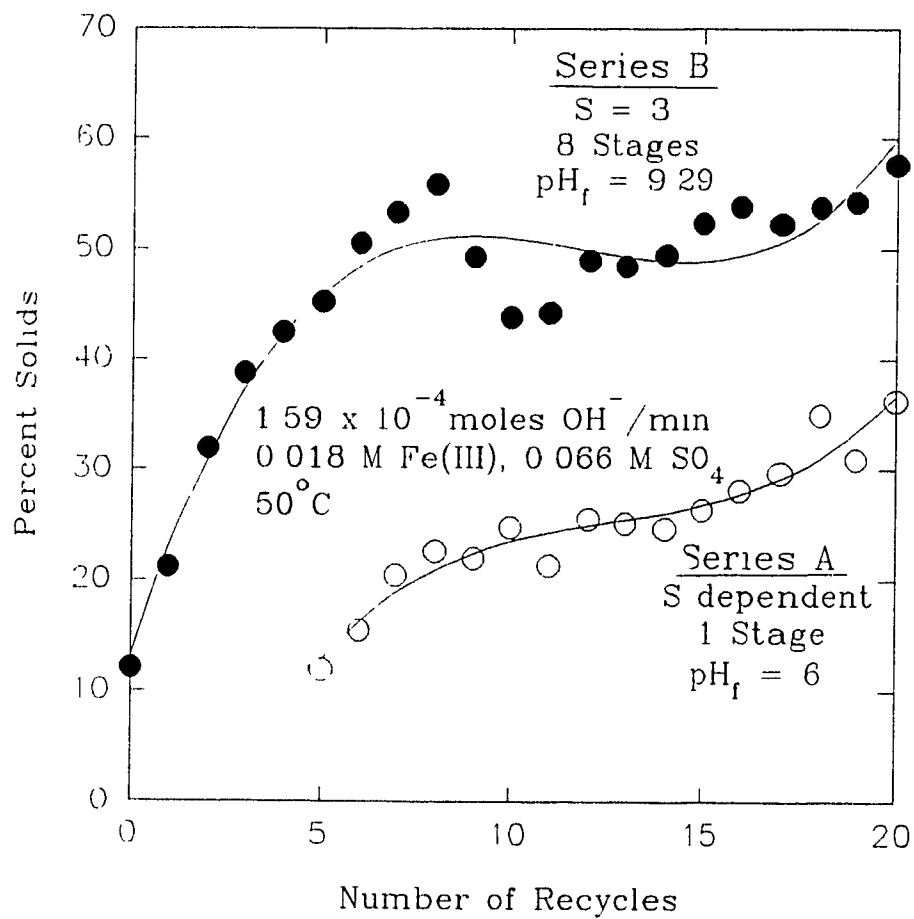


Figure 6-29: Comparison of staged-neutralization recycling with simple conventional recycling in terms of sludge densification.

Chemical analysis showed that the precipitate was 62.3% Fe, 0.65% SO₄, and 0.09% Na, again suggesting goethite, with possibly 1-2% natrojarosite. Neutralizing to a final pH of 9.29 minimized sulphate incorporation. The preweighed precipitate was heated to 200°C for 2 hours, then cooled and reweighed. The precipitate weight decreased by 10.7%, due most likely to liberation of adsorbed and hydration water.

X-ray diffraction analysis of the precipitate (Figure 6-31) concluded the precipitate was goethite (α -FeOOH). No evidence of jarosite was observed. Improvements in precipitate crystallinity compared to solids generated previously at the same final pH (9) were observed. Comparison of the XRD patterns of Figures 6-6c and 6-31 shows the staged-neutralization product to have clearly sharper peaks (in particular in the regions of 4.436 and 2.25-2.97 d-spacing) than precipitates produced by simple uncontrolled and unseeded neutralization.

The size of the particles generated from staged-neutralization recycling were twice as large as the particles from the simple recycling procedure. The mean diameter was 19.2 μ m, compared to 8.7 μ m particles from series A. Figure 6-32 displays the particle size distribution for series B. The broad, unimodal distribution is skewed to larger diameters. This implies that growth processes predominate. The BET surface area measurement was 167 m²/g for the series B precipitate.

Typical SEM photomicrographs of particles produced by staged-neutralization are shown in the following two groups of Plates. Plates 6-7 and 6-8 illustrate the physical form of the precipitate collected after ten recycles. It can be seen that recycling under low and controlled supersaturation ensured the production of dense, well grown particles as large as 30 μ m in diameter. Most of the particles were rounded and grew predominantly by epitaxial overgrowth. However, collection of fine particles ($\leq 1\mu$ m) seems to occur on the surface of larger particles, which suggests another mode of growth, one via incorporation and cementing of these tiny particles with fresh chemical overgrowth.

The second group of photomicrographs (Plates 6-9 to 6-12) basically shows the same characteristics for the precipitate collected after twenty recycles as those in Plates 6-7 and 6-8 although epitaxial overgrowth was less extensive than before.

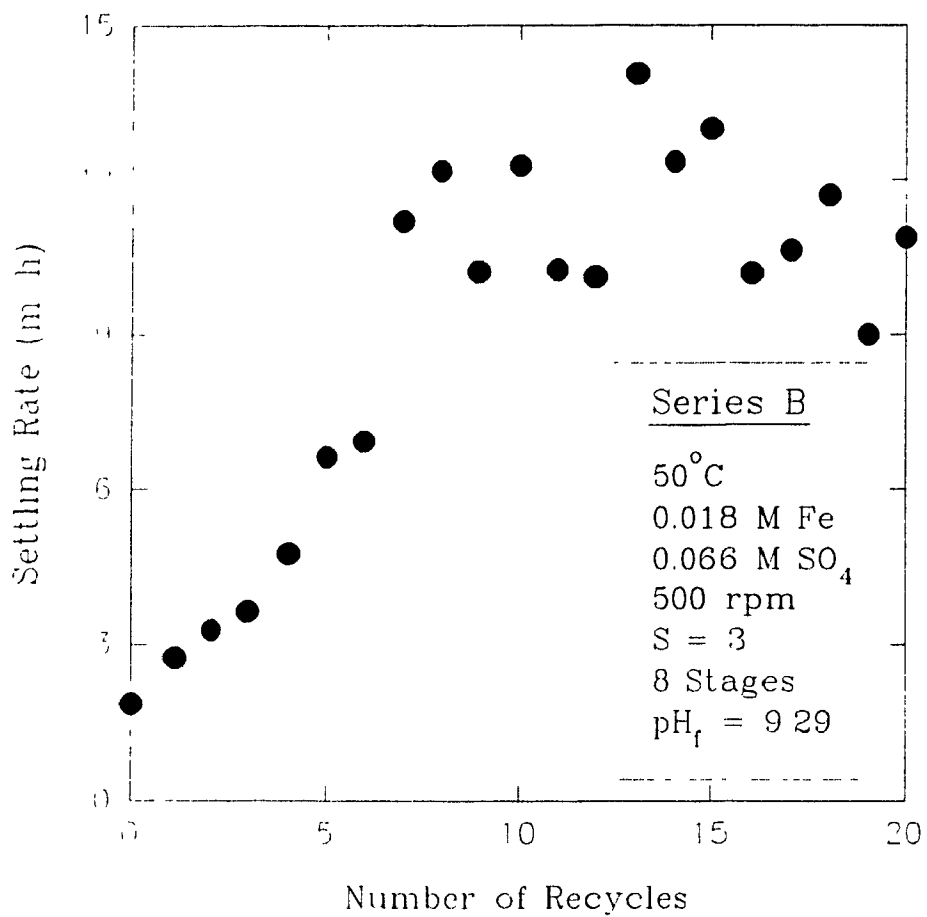


Figure 6-30: Effect of staged-neutralization recycling on sludge settleability.

D00687 8/18/92 S= 0.050 T=10.000 ZINCK R-B-20X
PDF (1) =29.713

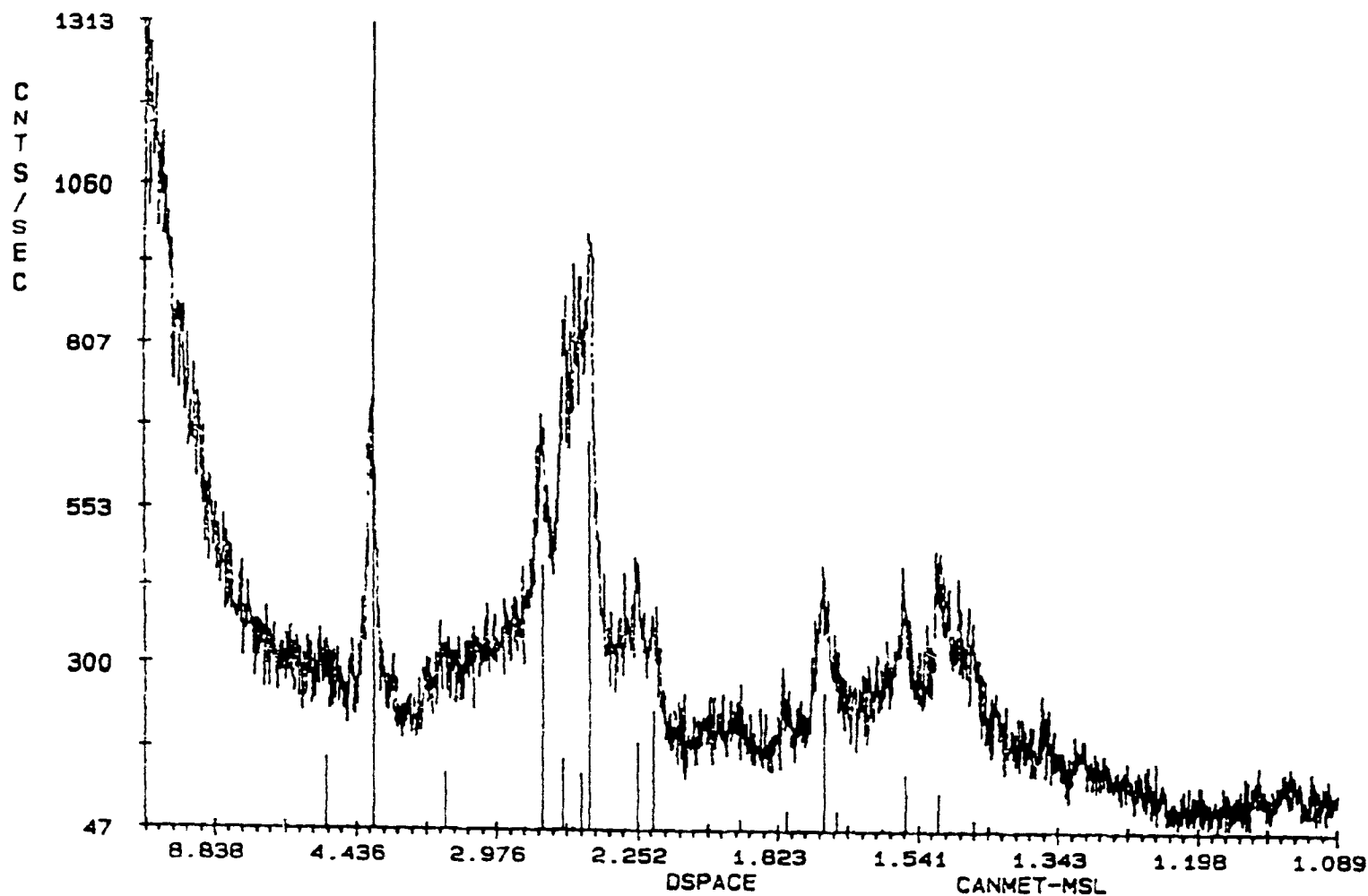


Figure 6-31: XRD pattern of the hydrolysis precipitate (goethite) generated from staged-neutralization recycling (series B - 20x). The lines correspond to the true XRD pattern of α -FeOOH.

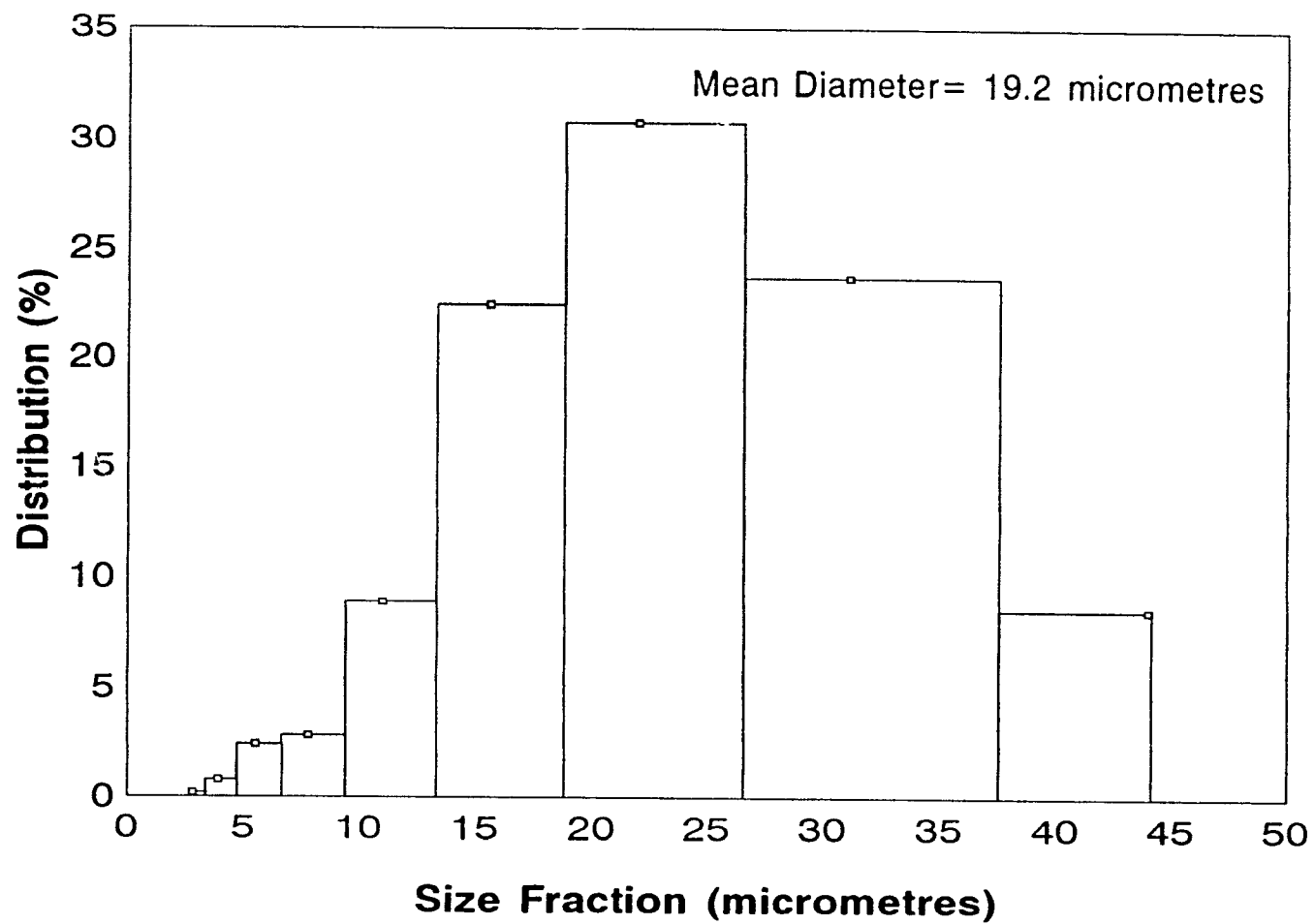


Figure 6-32: Particle size distribution for solids produced from staged-neutralization recycling (20x, Series B).

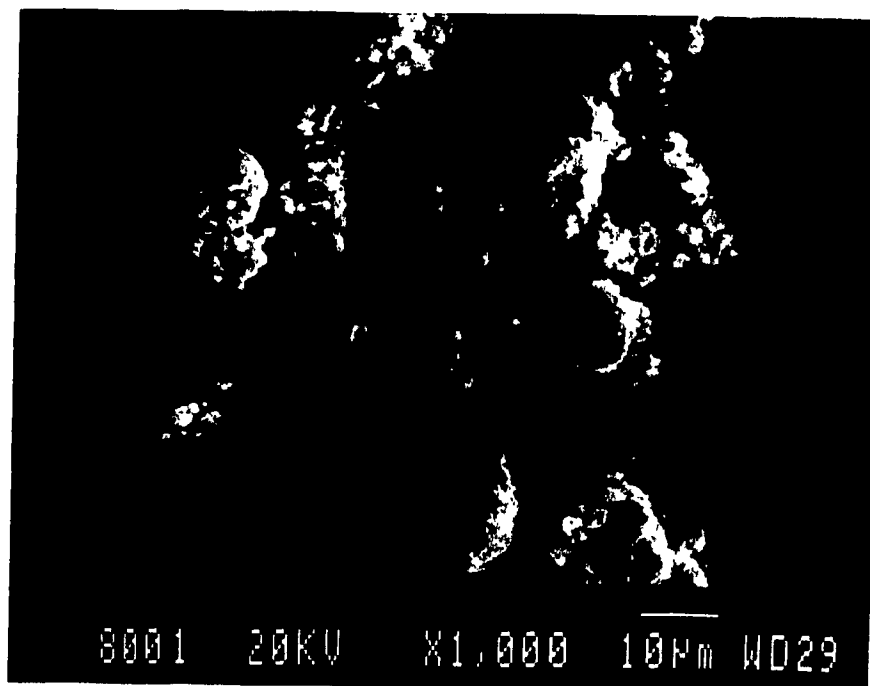


Plate 6-7: Sample: Recycle Series B (10 recycles)

Production Conditions: 50°C

1. 8 Neutralization stages

2. pH ~2.55, S=3

3. 500 rpm

4. pH 9.29

% Solids (max) = 55%

Comments: Recycling results in the formation of large particles measuring up to 30 micrometres across. These particles are rounded and have grown by accretion and epitaxial overgrowth. Recycling reduced the proportion of fines and served to classify the surviving particles to within a narrow size range.

Magnification: 1000 x

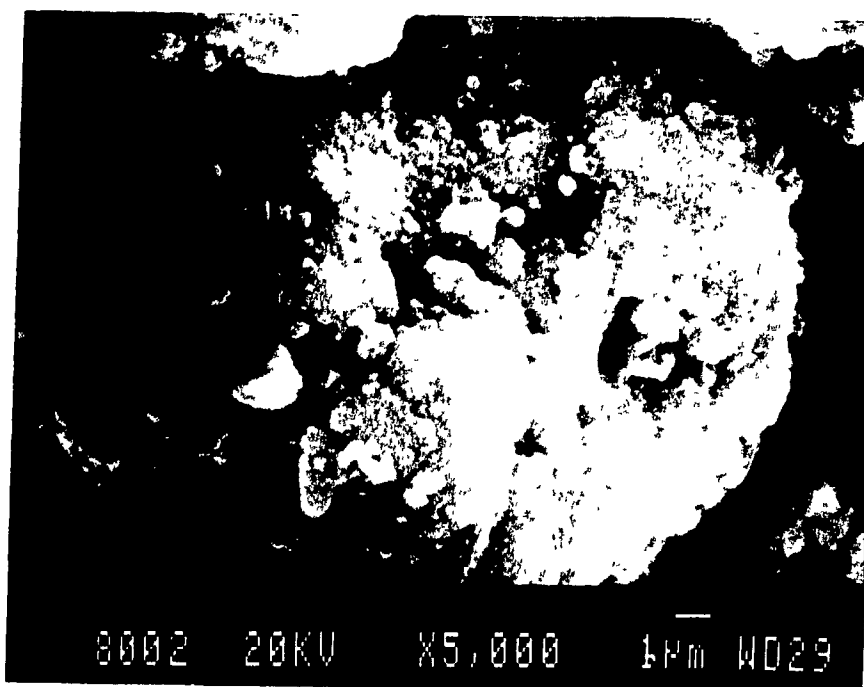


Plate 6-8: Sample: Recycle Series B (10 recycles), continued

Production Conditions: 50°C

1. 8 Neutralization stages

2. pH ~2.55, S=3

3. 500 rpm

4. pH 9.29

% Solids (max) = 55%

Comments: This higher magnification (5000x) electron micrograph illustrates the typical features of the large particles formed by recycling - rounded form, evidence of epitaxial overgrowth and growth by accretion, and a low porosity. In this series of recycled materials growth by chemical overgrowth was pronounced.

Magnification: 5000x

Eventually, more irregular cemented aggregates of varying sizes appeared to form upon prolonged recycling. This might reflect the lack of a uniform and sufficient hydrodynamic mixing environment to ensure good solids suspension and avoidance of poorly agitated pockets in the reactor. It should be noted (Chapter 5), that no baffles, or intensive mechanical agitation was applied but only magnetic agitation. This apparently was not adequate to deal with the increasing load of solids. Plates 6-11 and 6-12 show particles with predominant epitaxial growth morphology. In conclusion, recycling (after 8 cycles) under low and controlled supersaturation ensures the production of structurally stable and well grown dense particles orders of magnitude better than the typical precipitates produced in conventional effluent treatment operations.

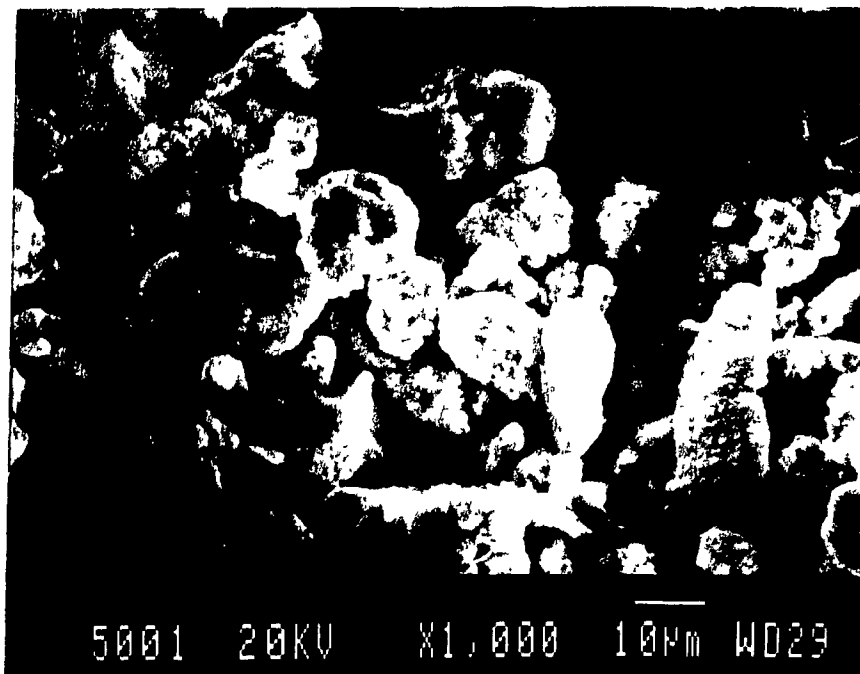


Plate 6-9: Sample: Recycle Series B (20 recycles)

Production Conditions: 50°C

1. 8 Neutralization stages
2. pH ~2.55, S=3
3. 500 rpm
4. pH 9.29

% Solids (max) = 55%

Comments: All of the particle are rounded, have a smooth surface, and vary in size from 5 to 25 micrometres. Chemical overgrowth, the dominant feature of all of the particles, is responsible for the smooth outer surfaces for internally reducing the porosity of the particles. It is postulated that the mechanism involved first the formation of smaller compound particles by accretion, and with further recycling these compound particles are welded together by internal and external epitaxial overgrowth.

Magnification: 1000x

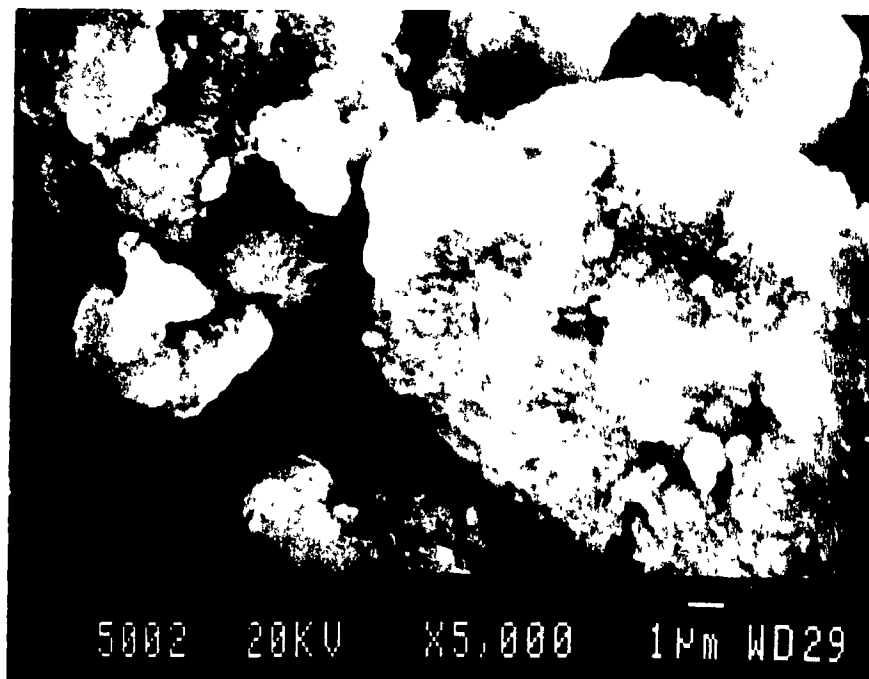


Plate 6-10: Sample: Recycle Series B (20 recycles), continued
 Production Conditions: 50°C

1. 8 Neutralization stages
 2. pH ~2.55, S=3
 3. 500 rpm
 4. pH 9.29
- % Solids (max) = 55%

Comments: The mechanism of accretion is more pronounced in the case of the smaller particles while the larger particles are held together by chemical overgrowth. Smaller accretions are welded to the smooth surface of the larger particles suggesting that the growth mechanism involves collection of particles on the outer surface of stable larger particles in which chemical overgrowth has formed a smooth substrate, followed by chemical overgrowth. The upper size limit to which particles will grow is determined by the hydrodynamics of the system as is the shape of the particles.

Magnification: 5000x

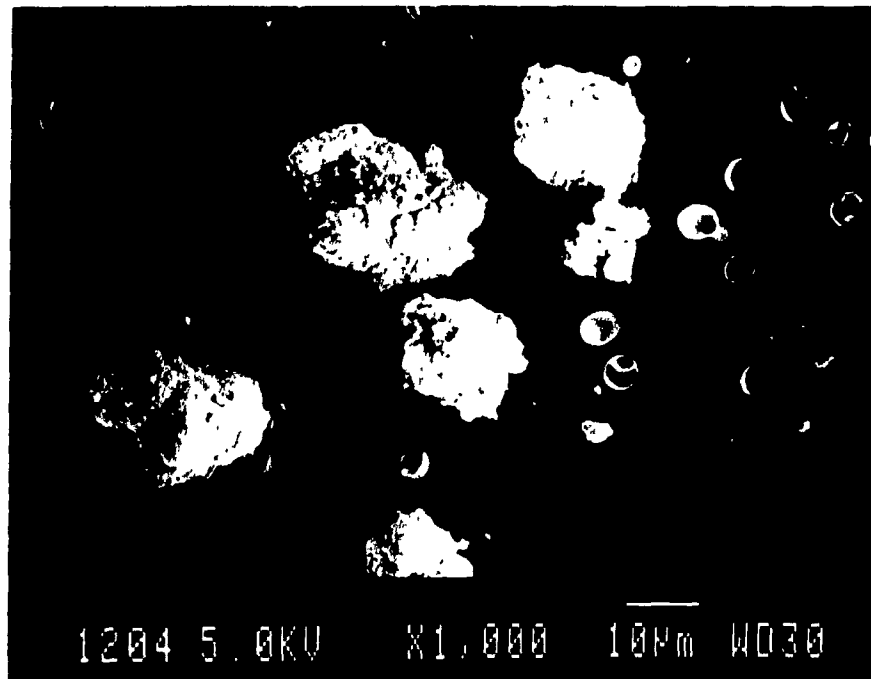


Plate 6-11

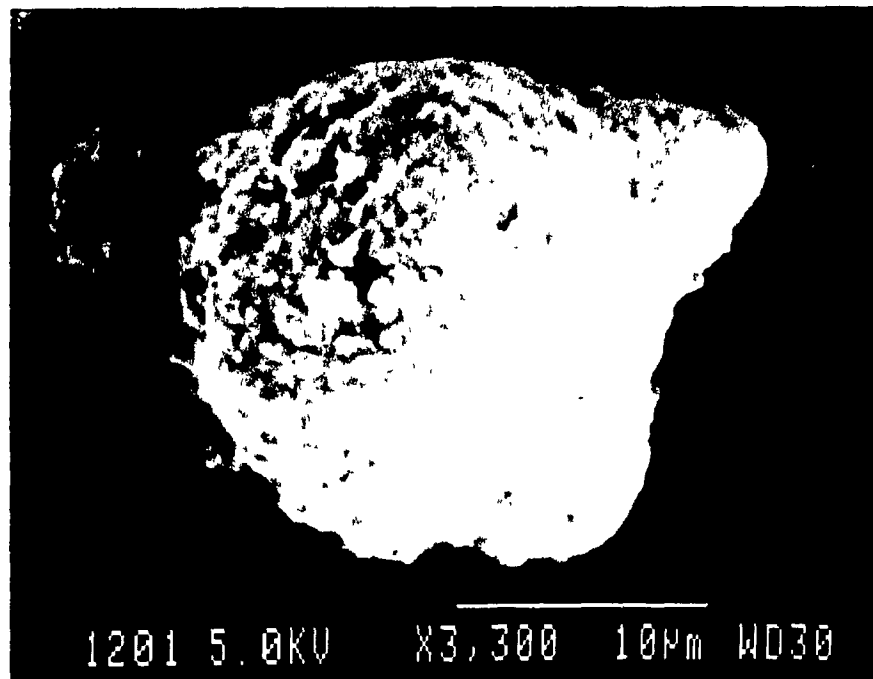


Plate 6-12

Caption on next page

Previous Page

Plate 6-11 and 6-12: Sample: Recycle Series B (20 recycles), continued

Production Conditions: 50°C

1. 8 Neutralization stages

2. pH ~2.55, S=3

3. 500 rpm

4. pH 9.29

% Solids (max) = 55%

Comments: The surface of the particles consists of a smoother base on top of which are smaller round accretions frequently less than a micrometre in diameter. Note the enhanced particle uniformity resulting from controlled supersaturation.

Magnification: 1000x and 3300x, respectively

CHAPTER 7: DISCUSSION

7.1 Solids Composition

The hydrolysis product generated from neutralization of the Fe(III)-SO₄ system depends on several factors such as solution pH, temperature, aging, and ion co-existence as discussed in Section 2.2.

By considering the results in Figure 6-7 the effect of pH on precipitate composition is clearly evident. At low pH (3), the sulphate content in the precipitate is significant (~17%). As the final pH of the hydrolyzing solution was raised, the sulphate concentration in the precipitate declined linearly. At pH 9, little or no sulphate was present. This trend suggests that the amount of sulphate in the precipitate is dependent only on the solution pH, not on other factors such as excess⁸ sulphate concentration in the solution.

The solid precipitated is believed to be strongly dependent on the precipitation precursor. The predominant precursor, as discussed in Chapter 4, will depend on solution conditions, the most significant of which are pH and anion concentration. Thermodynamic estimates predicted the predominant precursor at pH 3, 6, and 9 should be FeSO₄⁺ or Fe(SO₄)₂⁻ (depending on pS) for pH 3, Fe(OH)_{3(aq)} for pH 6 and similarly, Fe(OH)_{3(aq)} for pH 9 (Chapter 4). It might be possible then in principle, at least for the precipitate formed at pH 3, that part of the sulphate content of the precursor complex to be incorporated in the resultant solid. In other words, the exchange of SO₄²⁻ ligands with OH⁻ may not be complete when the polynuclear precursor of the solids compound forms. This view is presently advocated by colloid chemists (Blesa and Matijević, 1989), who postulate that upon oxolation the SO₄²⁻ bridging ligands of the polymer become incorporated in the precipitate. Previous investigations report that Fe₄SO₄(OH)₁₀ (Matijević et al., 1975)

⁸ There appears a specific amount of sulphate present in the precipitate and this amount is dependent on the pH. The amount of sulphate in the solution above this limiting amount (~ 3 g/L) will not effect the sulphate reporting to the solids.

or $\text{Fe}_4\text{SO}_4(\text{OH})_{10}\text{H}_2\text{O}$ (I) (Flynn, 1990) form in ferric sulphate solutions at $\text{pH} < 3$. The empirical formula for the precipitate produced in the present work at $\text{pH} 3$ was calculated to be $\text{Fe}_6\text{SO}_4(\text{OH})_{10}$, not $\text{Fe}_4\text{SO}_4(\text{OH})_{10}$. The excess iron might correspond to another phase, such as FeOOH , mixed with $\text{Fe}_4\text{SO}_4(\text{OH})_{10}$. Although formula calculations neither confirm nor disprove this theory. In other words we might have a mixture of two phases, i.e. a sulphate-bearing phase and an oxyhydroxide phase. As pH increases the yield of the minor sulphate bearing phase (I) decreases (empirical formula calculation at $\text{pH} 6$: $\text{Fe}_{10}\text{SO}_4(\text{OH})_{20}$ and $\text{pH} 9$: FeOOH) as would be expected from the iron(III) speciation diagrams (Chapter 4).

As well, the precipitate composition for the most part is independent of the amount of sulphate in solution. The speciation, on the other hand, depends both on pH and sulphate concentration. It is interesting to note that if the sulphate content of the precipitate is excluded (from empirical formula calculation) then the remaining composition of the solid (independent of pH) corresponds to FeOOH . X-ray diffractometer measurements (Figures 6-6 and 6-31) have indeed suggested almost all the solids precipitated, with the exception rapidly neutralized solids, to be partly crystalline goethite ($\alpha\text{-FeOOH}$)⁹. On the other hand, the composition of the precipitate produced from nitrate only tests (72% Fe) corresponds to empirical formula Fe_2O_3 , i.e. an amorphous ferric oxide-like phase.

Recall that by the time pH has been raised to 3 (following the controlled neutralization procedure adopted in this work, Chapter 5), some 80% of Fe(III) has been already precipitated out of the solution (Table 6-1). This suggests that if indeed a sulphate-bearing phase (like I) forms, the phase (being inherently unstable) undergoes transformation to a single oxyhydroxide phase with the concomitant release of sulphate ions. Flynn (1990) does indeed report phase I to be unstable at temperatures in excess of 50°C as do Robins and Huang (1987), who claim that upon

⁹ The term goethite has been used throughout this thesis to denote the oxyhydroxide precipitated formed. However, from a rigorous point of view goethite is the name of a distinct crystalline phase ($\alpha\text{-FeOOH}$).

aging of the amorphous precipitate, sulphate is released and α - and β -FeOOH form. The presence of sulphate in the precipitate can be due on the other hand to sulphate adsorption on the iron oxyhydroxide surface or a combination of coprecipitation and adsorption. The direct relationship between pH and sulphate incorporation suggests that the sulphate presence may be due to a pH dependent adsorption mechanism.

The surface (outer Helmholtz plane) of the goethite particle has a positive surface charge below the zero point charge. Hydrogen ions act as potential determining ions in acidic environments giving the particle a positive surface charge. It is thought that as the zero point charge is exceeded the surface potential of the particle is reversed and either hydroxyl ion adsorption or deprotonation determines the potential. It seems likely that the positive edge double layer is responsible for the adsorption of sulphate ions acting as counter-ions. Then, the simultaneous observed small ($\sim 1\%$) Na^+ exchange capacity may be attributed to a slight negative double layer on the surface which results either from isomorphous substitution or adsorption (van Olphen, 1977). Increasing the solution pH serves to reduce the positive surface potential on the FeOOH particles, which explains the decrease in sulphate adsorption with increased pH. Above the zero point charge, anion adsorption ceases. In addition to sulphate (or bisulphate) ions being adsorbed as ion pairs (i.e. counter-ions to the H^+ ions of the double layer) it is possible also to have direct chemisorption on the oxyhydroxide surface itself. It is thought in other words, that the same way sulphate forms complexes with Fe^{3+} in solution, sulphate can form complexes as well with the surface Fe(III) ions. These surface complexes become weaker upon pH increase, the same way the soluble complexes are converted to the respective hydroxyl complexes. In conclusion, the presence of sulphate in the low pH precipitates can be either due to coprecipitation or adsorption. Which of the two mechanisms dominates cannot be determined at this point.

7.2 Reaction Pathways

The study of the precipitation of ferric oxyhydroxide from $\text{Fe(III)-SO}_4\text{-H}_2\text{O}$ solution is full of experimental and conceptual difficulties related to multiple reaction

pathways that occur simultaneously and are impossible or difficult to separate (Blesa and Matijević, 1989). The evolution from aqueous precursor to ferric oxyhydroxide involves replacement of sulphate ions with hydroxyl ions, olation, and oxolation processes. First, the Fe(III)-sulphate complexes undergo complete or partial replacement of the sulphate ions with hydroxyl ions (Figure 7-1). This mechanism can explain the absence of sulphate in the chemical structure of the precipitate if we assume complete ligand exchange. On the other hand, in the case of partial replacement, new pathways leading to formation of sulphate-bearing species like the following $(\text{H}_2\text{O})_n(\text{OH})_m\text{Fe-O-SO}_2\text{-O-Fe}(\text{OH})_m(\text{H}_2\text{O})_n$ can be postulated (Blesa and Matijević, 1989). The resulting hydroxy complexes would then undergo polymerization through hydroxyl-bridging (olation) (Figure 7-1). The process of olation seems to be predominant in the first stages of polymerization. The final stage polymerization involved in the formation of goethite is oxolation. The lower portion of Figure 7-1 suggests a possible oxolation mechanism in the formation of goethite. Oxolation involves the formation of oxobridges from two hydroxide ligands through dehydration. Oxolation transforms the ferric hydroxide polymer into the more stable precipitate, goethite.

In contrast with some early theories, oxolation is accepted to occur even under rapidly neutralized environments (Blesa and Matijević, 1989). However, the degree of oxolation might be different. The gel formation experienced with iron(III) hydrolysis seems not only to be a result of incomplete oxolation but of also rapid homogeneous nucleation, causing colloid formation.

7.3 Crystallization Mechanism

7.3.1 Absence of seed

The mechanism of "crystallization" in the absence of recycling resembled homogeneous nucleation of ultra-fine sub-micron size particles and aggregation. The ultra small platelets ($< 0.1 \mu\text{m}$; Plates 6-1 and 6-2) originally formed minimized the surface area and free energy by forming larger aggregates.

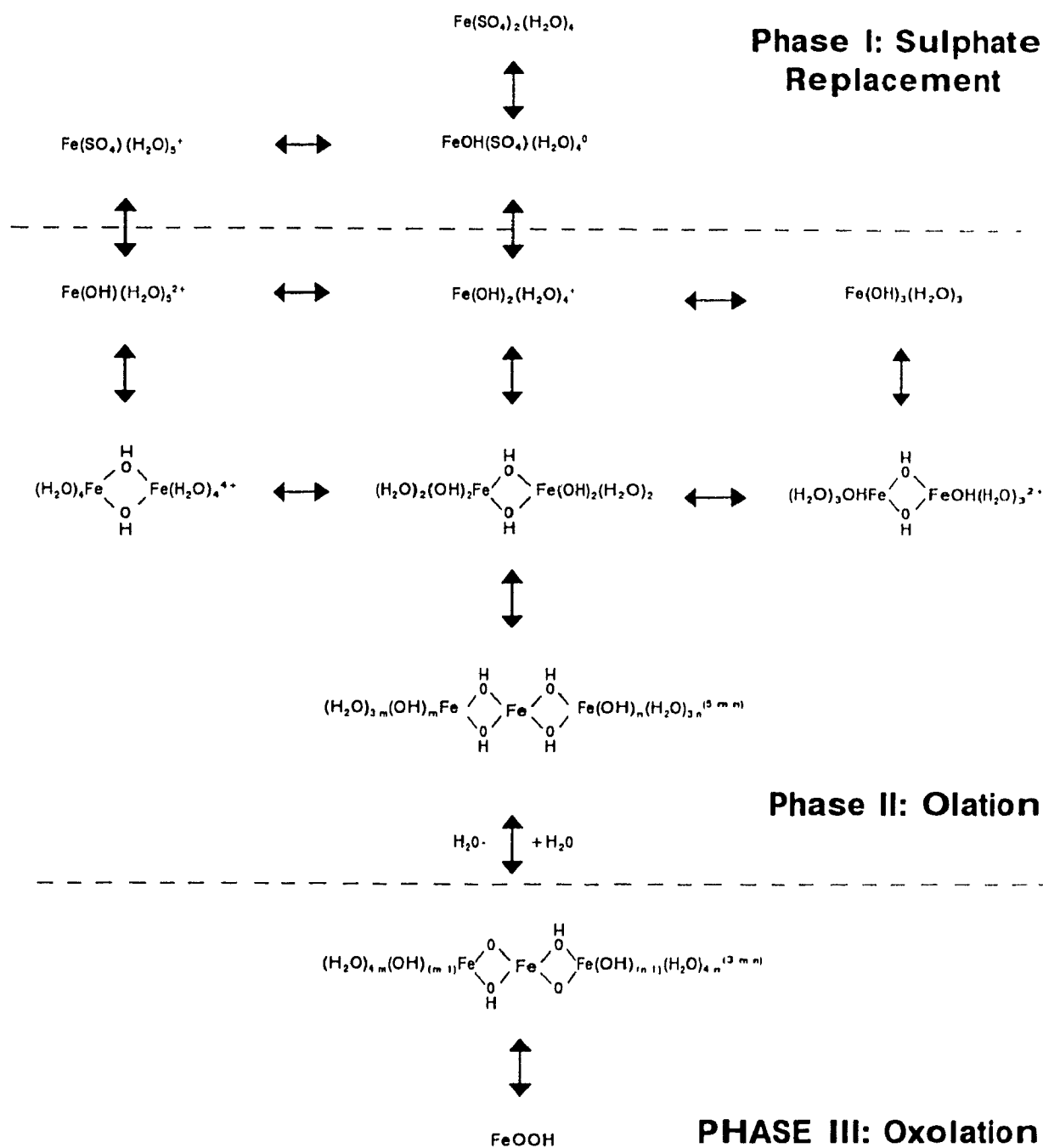


Figure 7-1: Possible precipitation pathways for Fe(III) hydrolysis from sulphate-bearing solutions (adapted from Blesa and Matijević, 1989).

The fact that the growth occurred through aggregation suggests that the platelets were attracted to one another, or that the surface charge was not significant enough to cause repulsion between the platelets. The role of increasing pH in enhancing the compactness of the precipitate can be attributed to the lowering of the surface charge as the ZPC was approached.

7.3.2 Recycling

Recycling improved precipitate (goethite) crystallinity and enhanced sludge densification and settleability. The method of recycling has a profound effect on the properties of sludge generated. Conventional (simple) recycling produces less dense particles which as a result settle slower (settling rate 4 m/hr) than precipitates recycled under a controlled level of supersaturation (settling rate 12 m/hr).

Morphological variations, as indicated by SEM photomicrographs, confirm increased particle porosity in conventionally recycled precipitates. Morphological comparison of the precipitates from each recycling series suggested that different nucleation/growth mechanisms occurred in Series A and B type recycle processes.

The results suggest that conventionally recycled precipitates aggregate by cluster-particle collisions rather than cluster by cluster which is more common to simple solid formation procedures (no recycling). A cluster is an aggregate of particles and in cluster-particle collisions individual particles penetrate into and fill the porous structure. The extent to which this mechanism plays a role in the final precipitate morphology and size distribution is determined by the colloid stability of the particles in solution and the particle population density in solution. Upon recycling, the latter (population density) increases and the extent of aggregation is enhanced. However, when recycling is performed under controlled supersaturation, surface nucleation and growth of the particles (epitaxy) is promoted. This is supported by morphological features including a relatively smooth particle surface and low particle porosity. Growth via aggregation occurs to some extent, however it is thought to be a result of particle abrasion. Over time, recycling at high impeller speeds and increased particle population density caused the surface of the particle to abrade producing fines. Particle abrasion is thought to be responsible for the

decrease in settling rate observed with continued recycling (Figure 6-30). Alternately, it might be thought that poor mixing conditions in the single precipitation reactor used, contributed to local pockets of high supersaturation (especially with the high solids content tests), leading to homogeneous nucleation and the production of colloidal particles (fines). Similarly, the sigmoidal shape of the sludge density curve (Figure 6-29) is very likely due to particle abrasion and aggregation. The particle population density threshold coincided with 55% solids in the sludge. As the threshold was approached, particle abrasion occurred resulting in fines. These fines then aggregated. The aggregates may serve as a net trapping many fines. As the solids density rose the probability of particle abrasion increased. This cycle would continue until the system reached equilibrium. The constant level of saturation served to control and limit the homogeneous nucleation event, while the rough aggregate surface accelerates the growth process.

Another striking feature of the precipitate generated by recycling under controlled saturation was the increased uniformity in particle size and shape observed by comparing Plate 6-3 with Plates 6-9 to 6-12. The uniform shape and the degree of roundness may be a result of abrasion, although it seems that size and shape characteristics are overall dictated by chemical factors rather than mechanical ones. The physical appearance of the particles after 10 recycles (Plate 6-8) was similar to particles after 20 recycles (Plate 6-10). Equally important, the size of Series B particles was greater than twice the recycle A (conventional) particles.

The physical properties of the precipitate produced in series B indicate that nucleation mostly occurred on the surface of the recycled material. Contact nucleation on the walls of the vessel was not observed in Series B (controlled S) however, it was observed in Series A (conventional) recycling. The mechanism of growth is unclear, although it is thought to be two dimensional growth of surface nuclei by mononuclear growth as indicated by the smoothness of the particle surface. Mononuclear growth implies the time between two nucleation events on a given surface area is longer than the time necessary to grow a two dimensional layer over the whole surface. The seed particles first introduced into the reactor ($R=0$) had a

sponge like structure. This rough surface allowed for faster growth than would a smooth surface.

The rate of agitation has consistently been shown to be a very important factor in hydrolytic precipitation. Increased solution velocity served to increase particle/sludge density and settling rate. The role agitation played in hydrolytic precipitation was three-fold. First, increasing the agitation rate accelerated the diffusion the ferric ions to the particle surface. Similarly, agitation retarded high local level of supersaturation. Local pockets in which the saturation ratio was high encouraged homogeneous nucleation. Increased agitation rates then tended to reduce locally high supersaturation levels by maintaining a constant saturation ratio in the reactor and facilitated accelerated diffusion of Fe^{3+} ions to the precipitate surface. Finally, agitation played a role in particle aggregation as discussed in the next section (7.4.4). The crystallization phenomena believed to govern the hydrolytic precipitation of ferric oxyhydroxide in the present work are summarized in Figure 7-2.

7.4 Colloid Stability

Colloid instability is essential in producing sludges with favourable handling properties. Unlike in powder technology, in wastewater treatment the aim is to aggregate/coagulate the sludges into a dense mass. The degree of stability experienced by a system appears to be dependent on several factors such as solution composition and treatment parameters.

The rate of sedimentation of suspended particles increased markedly upon aggregation due to the increased aggregate size. However, sludges of aggregated precipitates are usually much more voluminous than those of stable suspension of the same concentration. At first, it seems somewhat paradoxical that the repelling particles of a stable suspension should obtain a higher degree of compaction in the sludge than the attracting particles of an aggregated suspension. Individual particles form a closely packed dense sludge, although mutual repulsion between the particles may keep them from coming into actual contact as illustrated in Figure 7-3(a). In

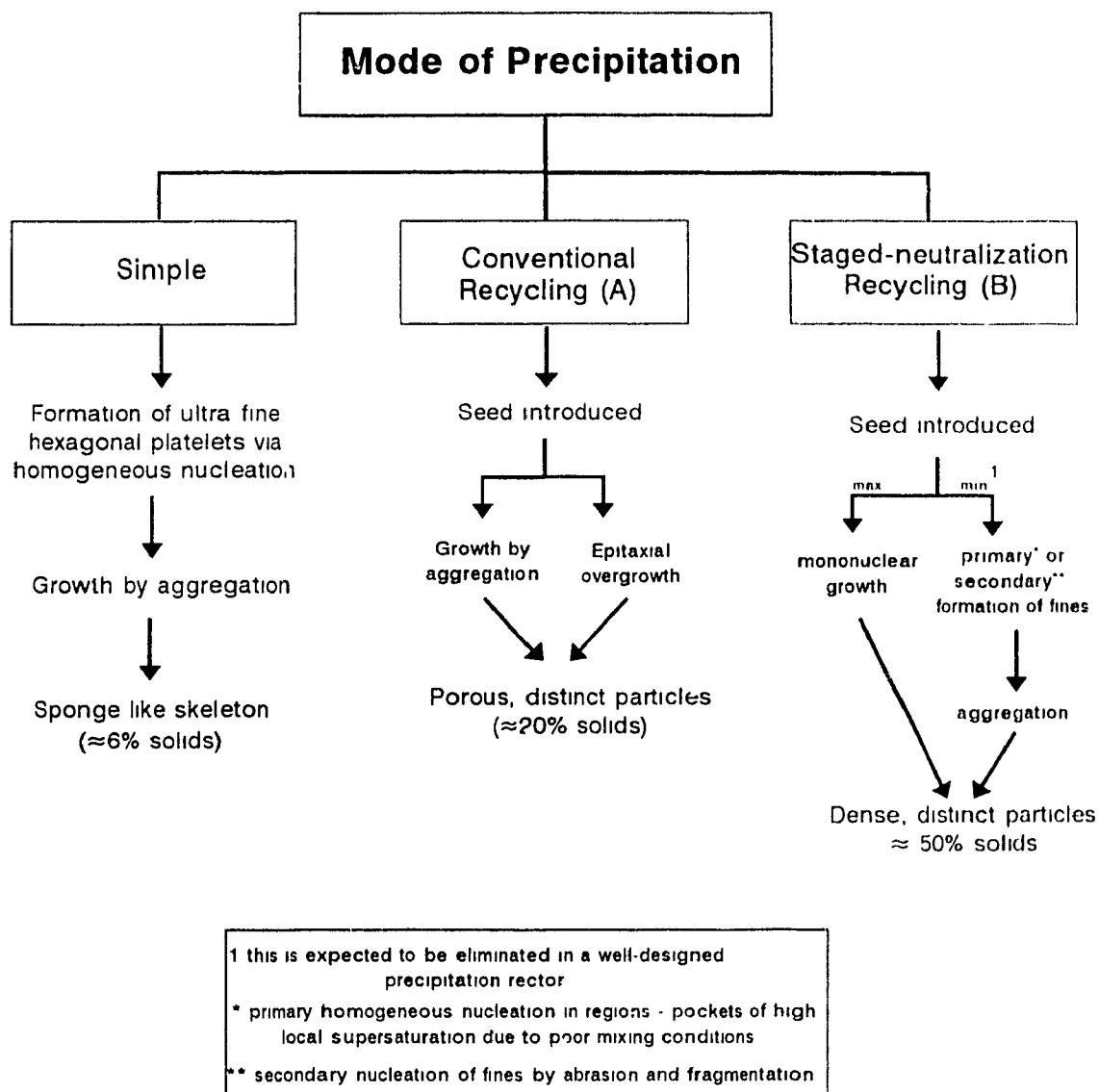


Figure 7-2: Summary of proposed crystallization mechanisms.

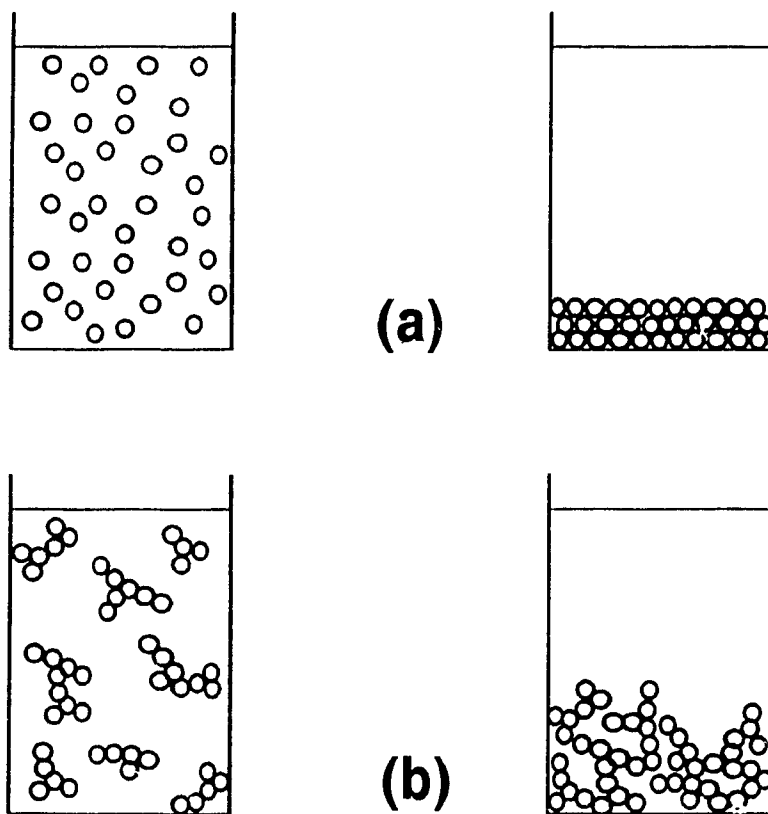


Figure 7-3: Sedimentation in a stabilized and in an aggregated suspension (a) stabilized suspension; dense close-packed sludge (b) aggregated suspension; loose, voluminous sediment (van Olphen, 1977).

the destabilized suspension, on the other hand, the haphazardly formed voluminous flocs settle as such and form a voluminous sludge with large void spaces in and between the agglomerates (Figure 7-3(b)).

The final solution pH influences degree of aggregation experienced by the sludge. Experimental results show that increasing the solution pH accelerates sedimentation while producing a voluminous sludge. Conversely, at low pH (3) the sludge settles much more slowly, but yields a closely packed, dense precipitate. As the solution pH is raised, the surface charge on the particles is reduced as the point of zero charge is approached. The common practice is to neutralize and hydrolyze the solution to a pH between 9 - 11. This results in faster settling rates but as well voluminous precipitates are produced.

The rate of agitation also affects the degree of aggregation. Rapid mixing causes gentle flocs to break apart. This break-up results in sludge densification as void spaces are reduced. The effect of increased dispersion energy on aggregation in terms of settling properties is unclear; however, it appears to be inter-related with solution pH. One would expect that floc-break-up would result in a decrease in settling rate. This was the case for pH 3 but at pH 6 the settling rate increased with faster agitation rate (Figure 6-12).

7.5 Implications of Current Research on the Existing Practise of Neutralization

It is probably the most important finding of this work that performing neutralization in stages under a low and controlled supersaturation environment yields precipitates with superior properties. In the present work, as explained in section 1.3, it was essential to work with a neutralizing agent (such as NaOH) that would allow to understand the crystallization of ferric oxyhydroxide without the implications of the formation of another solid phase (i.e. gypsum). Now that the outcome of this fundamental crystallization approach proved successful, extension of this work to a lime neutralization system should be undertaken to verify its effectiveness under simulated industrial conditions. This approach has already been started to be investigated (Zinck, 1993) and early results of a series of staged-

neutralization tests with lime yielded precipitates in excess of 57% solids. The sludge generated from treating a synthetic effluent ($[\text{Fe(III)}] = 0.018 \text{ M}$, $[\text{SO}_4^{2-}] = 0.06 \text{ M}$) contained 66.5% gypsum and 33.5 % FeOOH . Unlike in most treatment processes the hydrolysis product (FeOOH) and gypsum were two distinct solid phases, which is another manifestation of the power of the supersaturation-controlled precipitation technique devised in this work. Additional tests are being completed to evaluate the effectiveness of the staged-neutralization approach for real mixed metal effluent solutions and at ambient temperature.

Conversion of existing or design of new neutralization circuits on the basis of this new staged-neutralization approach should not impose serious engineering difficulties provided that pilot plant studies confirm the effectiveness of the process. The conversion of the staged-neutralization approach to a continuous industrial process is envisaged as a replacement of each step of neutralization path (refer to Figure 6-28) with a continuous stirred tank of cascade of reactors. Each reactor is to operate (steady-state) at the corresponding "final" pH of each step. Since saturation ratio 3 required 8 stages a compromise will be to operate the cascade of reactors under $S=5$ for which case only 4 tanks-in-series will be required (Figure 7-4). Since the solids densification data (Figure 6-29) suggested 8 recycles to be sufficient for maximum solids content the cascade will have to be designed to operate with such recycle ratio as well. Appropriate reactor design, i.e. selection of agitators, installation of baffles, pH control etc. will be part of the next phase of process development work required to test and demonstrate the new staged-neutralization technique.

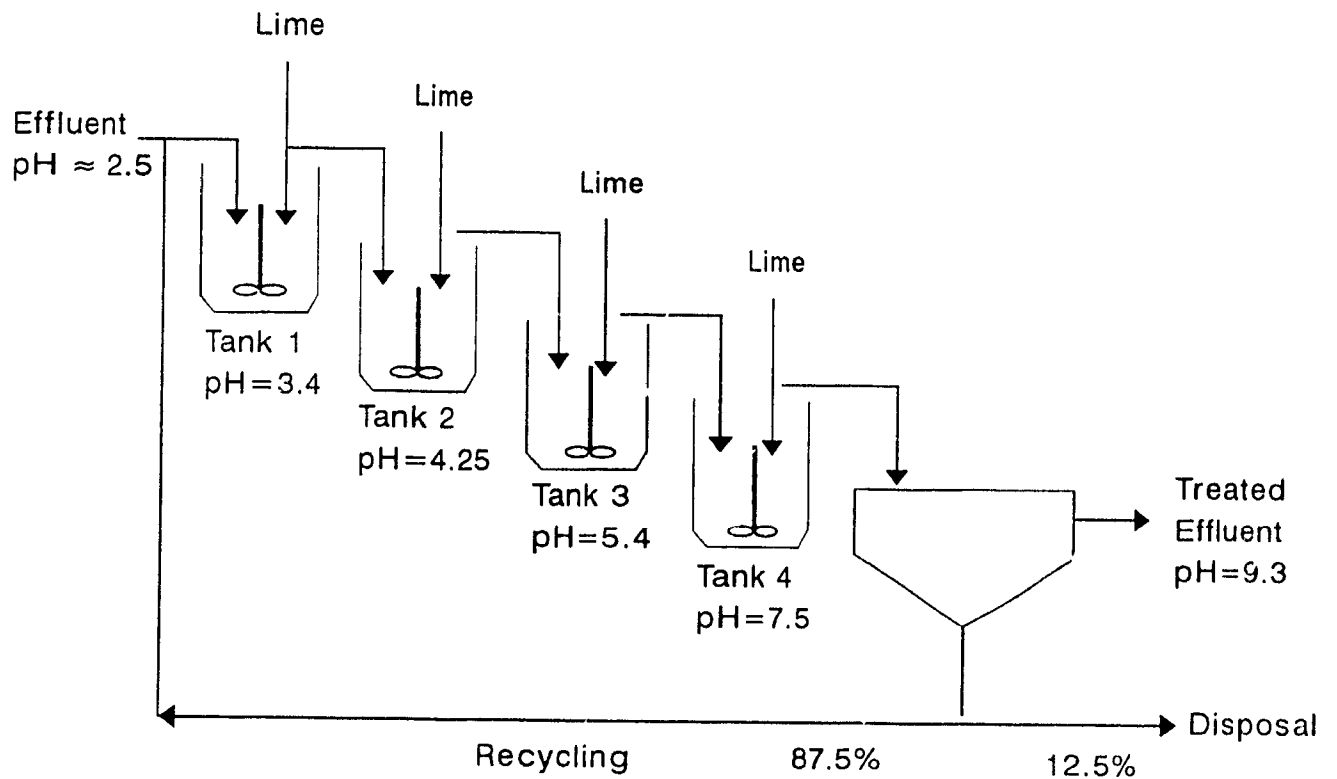


Figure 7-4: Set-up for continuous staged-neutralization recycling process for $S=5$.

CHAPTER 8: CONCLUSIONS AND FUTURE WORK

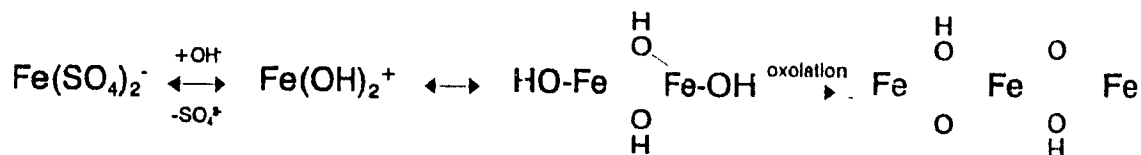
8.1 Conclusions

Iron hydrolysis is an effective method for the removal of iron(III) from a sulphate effluent stream. The final iron(III) concentration can be reduced to less than 0.05 mg/L by neutralization/hydrolysis. The sludge generated commonly is gelatinous in nature and possesses very poor handling properties. However, the physical properties of the sludge can be greatly improved by changing previous neutralization/hydrolysis procedures. Through a systematic investigation of the effect of process parameters on the properties of the precipitated solids, it was determined that pH, temperature, rate of neutralization and agitation were critical. The final solution pH was found to influence settleability, densification and volume generation of the sludge. As well the final pH determined the degree of sulphate incorporation in the precipitate: 17% at pH 3, 7% at pH 6 and 1% at pH 9. It is quite likely that sulphate had associated with the precipitated solids through an adsorption rather than coprecipitation mechanism, especially for the high pH regions. The solids produced at 50°C were identified to be "partly crystalline" ferric oxyhydroxide, most likely goethite (α -FeOOH). The composition of the solids at pH 3 had the following apparent chemical formula: $\text{Fe}_a(\text{SO}_4)_b(\text{OH})_c$. This composition reflects either the presence of a co-precipitated sulphate-containing phase or adsorbed SO_4^{2-} ion. The solids possessed very high specific surface area and their morphology was that of a highly aggregated mass of ultra fine platelets.

Slow neutralization was essential for sludge densification. Rapid neutralization led to the formation of minute particles that settled very slowly leading to a dilute gel-like sludge. Sludge densification and settling rate were both vastly improved by neutralizing slowly and precipitating from a high hydrodynamic shear environment. Rapid agitation tended to rework fragile porous precipitates into dense, compact aggregations with improved settling rates.

The mechanism of goethite (α -FeOOH) precipitation, through controlled iron(III) hydrolysis from sulphate-bearing effluents was deemed to proceed through

complete (or partial-depending on the experimental conditions) exchange of the sulphate ligands of the precursor sulphato complexes with hydroxyl ions prior to the olated polymerization. The olated polymer dehydrated over time through oxolation to a goethite-like structure. The simplified process is represented below.



Solubility lines for iron precipitation for varying sulphate concentrations and temperatures were derived from statistically generated experimental data and were compared to solubility lines calculated using F*A*C*T. These solubility diagrams were used to design recycling tests under controlled supersaturation.

Recycling the precipitate densified the sludge and produced faster settling rates. However, the conditions of recycling influenced the physical properties of the sludge more so than the act of recycling. A controlled level of supersaturation ($S=3$) during neutralization/hydrolysis more than doubled the sludge density and tripled the settling rate. The control of the saturation ratio allowed for surface nucleation and epitaxial growth to occur. In conventional recycling, growth resulted mostly from aggregation. The hierarchy of precipitation was then: (1) gel formation (rapid neutralization, 1-2 % solids), (2) "sponge" precipitate structure formed from hexagonal platelets (slow neutralization, ~6% solids), (3) growth by aggregation (conventional recycling, 22% solids), (4) epitaxial growth (staged-neutralization recycling, 55% solids). Based on the findings of this work a new approach to neutralization of iron(III) rich, sulphate-bearing effluents involving a multi-stage cascade of precipitation reactors operating each at fixed pH levels is proposed for further investigation.

8.2 Future Work

The process developed shows very promising results, however further tests are required in several areas, these include: (1) continuous operation (as opposed to a batch process), (2) ambient temperature (compared to 50°C), and (3) neutralization using lime (instead of caustic soda). Much of this work has been completed in an auxiliary study (Zinck, 1993), as described in section 7.5. Additional research to support this study and improve the understanding of the fundamental mechanisms of iron(III) hydrolysis and neutralization are advocated. Some topics suggested for further research are as follows:

- electrophoresis studies to determine the role of surface charge and media conditions on precipitation, adsorption and aggregation;
- investigate and quantify surface adsorption using Fourier Transform Infrared Spectroscopy;
- study reaction mechanics on the basis of particle size distributions. For example, estimate the degree of aggregation and abrasion through detailed particle size analysis at specific stages throughout the process;
- estimate the optimum solids loading capacity by measuring particle abrasion indirectly from turbidity measurements;
- study the effect of various additives on the crystallization and aggregation of hydrolysis products;
- investigate the kinetics of lime dissolution;
- apply the principles developed in this study to other metal precipitation systems such as;
 - sulphide precipitation, and
 - gypsum precipitation.

REFERENCES

- American Water Works Association (AWWA) Committee Report, State of the art of coagulation., JAWWA, **63**(2):99-108, 1971.
- Arden, T.V., The hydrolysis of ferric iron in sulphate solution., J. Chemical Society, pp.350-363, 1951.
- Ardizzone, S. and L. Formaro, Hydrothermal preparation of goethite crystals., Surface Tech., **26**:269-274.
- Atkinson, R.J., A.M. Posner, and J.P. Quirk, Adsorption of potential-determining ions at the ferric oxide-aqueous electrolyte interface., J. Physical Chemistry, **71**:550-558, 1967.
- Bacon, D.W., Making the most of a "One-Shot" experiment., Ind. Eng. Chem., **67**(7):27-34, 1970.
- Baes, C.F., Jr. and R.E. Mesmer, The Hydrolysis of Cations, Wiley-Interscience, NY, pp. 226-237, 1976.
- Bale, C.W., A.D. Pelton and W.T. Thompson, Facility for the Analysis of Chemical Thermodynamics (F*A*C*T), McGill University, Montreal, Quebec, 1991.
- Barin, I., O. Knacke and O. Kubaschewski, Thermochemical Properties of Inorganic Substances, Springer-Verlag, Berlin, 1977.
- Barners, H.E. and R.V. Scheurman, Handbook of Thermochemical Data for Compounds and Aqueous Species, Wiley-Interscience, NY, 1978.
- Bell, A. V., Some recent experience in the treatment of acidic, metal bearing acid mine drainage., CIM Bulletin, **68**:9-46, December, 1975.
- Benefield, L.D., J.F. Judkins, Jr., and B.L. Weand, Process Chemistry for Water and Wastewater Treatment, Prentice-Hall, New Jersey, pp. 191-238, 1982.
- Benjamin, M.M. and J.O. Leckie, Multiple-site adsorption of Cd, Cu, Zn, and Pb on amorphous iron oxyhydroxide., J. Colloid and Interface Science, **79**(1):209-222, 1981.
- Bennett, R.C., H. Fiedelman and A.D. Randolph, Crystallizer influenced nucleation., Chemical Engineering Progress, **69**(7):86-93, 1973.

- Biedermann, G. and P. Schindler, On the solubility of product of precipitated iron(III) hydroxide., *Acta Chemica Scandinavica*, **11**:731-740, 1957.
- Birkner, F.B. and J.K. Edzwald, Nonionic polymer flocculation of dilute clay suspensions., *JAWWA*, **61**(12):645-651, 1969.
- Birkner, F.B. and J.J. Morgan, Polymer flocculation kinetics of dilute colloidal suspensions., *JAWWA*, **60**(2):175-191, 1968.
- Black, A.P., F.B. Birkner and J.J. Morgan, Destabilization of dilute clay suspensions with labelled polymers., *JAWWA*, **57**(12):1547-1600, 1965.
- Blesa, M.A. and E. Matijević, Phase transformations of iron oxides, oxohydroxides, and hydrous oxides in aqueous media., *Advances in Colloid and Interface Science*, **29**:173-221, 1989.
- Bosman, D.J., The improved densification of sludge from neutralized acid mine drainage., *Journal of the South African Institute of Mining and Metallurgy*, **74**(9):340-348, April, 1974.
- Botsaris, G.D., Secondary nucleation - A review., in Industrial Crystallization., J.W. Mullin, (ed.), Plenum Press, N.Y., pp. 3-22, 1976.
- Brady, G.W., C.W. Kurkjian, E.F.X. Lyden, M.B. Robin, P. Saltman, T. Spiro, and A. Terzis, The structure of an iron core analog of Ferritin., *Biochemistry*, **7**(6):2185-2192, 1968.
- Brunauer, J., P.H. Emmett and E. Teller, Adsorption of gases in multimolecular layers., *J. American Chemical Society*, **60**:309, 1938.
- Breeuwsma A., and J. Lyklema, Interfacial electrochemistry of haematite (α -Fe₂O₃). *Discussions Faraday Society*, **52**:324-333, 1971
- Bryson, A.W. and W.A.M. Te Riele, Factors that effect the kinetics of nucleation and growth and the purity of goethite precipitates produced from sulphate solutions., in Iron Control in Hydrometallurgy., J.E. Dutrizac and A.J. Monhemius (eds.), Ellis Horwood Limited, Chichester, Ch. 18, pp. 377-390, 1986.
- Burkhart, L. and J. Voigt, Aqueous precipitation in hydrometallurgy., in Hydrometallurgical Reactor Design and Kinetics., R.G. Bautista, R.J. Wesely and G.W. Warren (eds.), TMS-AIME, p. 441-456, 1986.
- Burkin, A.R., The Chemistry of Hydrometallurgical Processes., E. & F.N. Spon Ltd., p.59, 1966.

Burrill, K.A., A model for crystal growth rates under surface diffusion control in impure solution., *Journal of Crystal Growth*, **12**:239-244, 1972.

Chen, T.T. and L.J. Cabri, Mineralogical overview of iron control in hydrometallurgical processing., *in Iron Control in Hydrometallurgy*, J.E. Dutrizac and A.J. Monhemius (eds.), Ellis Horwood Limited, Chichester, Ch. 1, pp. 19-55, 1986.

Christensen, A.N., M.S. Lehmann, and A. Wright, Kinetics of rust formation: A small angle neutron scattering investigation on iron(III) hydroxide., *Acta Chemica Scandinavica*, **A 37(1)**:63-69, 1983.

Christensen, H.H. and O.K. Borggaard, The protolytic properties of iron(III)-EDTA complexes in weakly alkaline solution and the solubility product of iron(III) hydroxide., *Acta Chemica Scandinavica*, **A31(9)**:793-798, 1977.

Concha, F. and E.R. Almendra, Settling velocities of particulate systems. 2. Settling velocities of suspensions of spherical particles., *International Journal of Mineral Processing*, **6**:31-41, 1979.

Cornell, R.M., Comparison and classification of the effects of simple ions and molecules on the transformation of ferrihydrite into more crystalline products., *Z. Pflanzenernähr. Düng. Bodenkd.*, **150**:304-307, 1987.

Cornell, R.M., The influence of some divalent cations on the transformation of ferrihydrite to more crystalline products., *Clay Miner.*, **23**:329-332, 1988.

Cornell, R.M. and R. Giovanoli, The influence of copper on the transformation of ferrihydrite into goethite and jacobite in alkaline media., *Polyhedron*, **7**:385-391, 1988.

Cornell, R.M. and W. Schneider, Formation of goethite from ferrihydrite at physiological pH under the influence of cysteine, *Polyhedron*, **8**:149-155, 1989.

Davey, P.T. and T.R. Scott, Removal of iron from leach liquors by the "goethite" process., *Hydrometallurgy*, **2**:25-33, 1976.

Davis, J.A., R.O. James and J.O. Leckie, Surface ionization and complexation at the oxide/water interface I. computation of electrical double layer properties in simple electrolytes., *J. Colloid and Interface Science*, **63(3)**:480-499, 1978.

Davis, J.A. and J.O. Leckie, Surface ionization and complexation at the oxide/water interface II. Surface properties of amorphous iron oxyhydroxide and adsorption of metal ions., *J. Colloid and Interface Science*, **67(1)**:90-107, 1978.

Dénès, G., Preparation, characterization, magnetic and Mössbauer spectroscopic studies of microcrystalline and amorphous iron trihydroxide. *in Production and Processing of Fine Particles.*, A.J. Plumptre (ed.), Pergamon Press, New York, pp. 615-626, 1988.

Derjaguin, B.V. and L. Landau, *Acta Physicochim, U.R.S.S.*, 14:633, 1941.

Dinardo, O., P.D. Kondos, D.J. MacKinnon, R.G.L. McCready, P.A. Riveros, and M. Skaff, Study on metals recovery/recycling from acid mine drainage., MEND Project Report, 3.21.1(a), 1991.

Dirksen, J.A. and T.A. Ring, Fundamentals of crystallization: Kinetic effects on particle size distributions and morphology., *Chemical Engineering Science*, 46(10):2389-2427, 1991.

Dousma, J. and P.L. de Bruyn, Hydrolysis-precipitation studies of iron solutions I. Model for hydrolysis and precipitation from Fe(III) nitrate solutions., *J. Colloid and Interface Science*, 56(3):527-539, 1976.

Dousma, J. and P.L. de Bruyn, Hydrolysis-precipitation studies of iron solutions II. Aging studies and the model for precipitation from Fe(III) nitrate solutions., *J. Colloid and Interface Science*, 64(1):154-170, 1978.

Dousma, J. and P.L. de Bruyn, Hydrolysis-precipitation studies of iron solutions III. Application of growth models to the formation of colloidal α -FeOOH from acid solutions., *J. Colloid and Interface Science*, 72(2):314-320, 1979.

Dousma, J., D. den Ottelander and P.L. de Bruyn, The influence of sulphate ions on the formation of iron(III) oxides., *J. Inorganic and Nuclear Chemistry*, 41:1565-1568, 1979.

Dove, P.M. and J.D. Rimstidt, Solubility of scorodite, $\text{FeAsO}_4 \cdot 2\text{H}_2\text{O}$: Reply., *American Mineralogist*, 72:845-848, 1987.

Dunning, W.J., Ripening and ageing processes in precipitates., *in Particle Growth in Suspensions.*, A.L. Smith (ed.), Ch. 1, Academic Press, London, 1973.

Dutrizac, J.E., The physical chemistry of iron precipitation in the zinc industry., *in Lead-Zinc-Tin '80.*, J.M. Cigan, T.S. Mackey and T.J. O'Keefe (eds.), TMS-AIME, Warrendale, pp. 532-564, 1980.

Dutrizac, J.E., An overview of iron precipitation in hydrometallurgy., *in Crystallization and Precipitation*, G.L. Stathdee, M.O. Klein and L.A. Melis (eds.), Pergamon Press, pp. 259-283, 1987.

Dutrizac, J.E., and S. Kaiman, Synthesis and properties of jarosite-type compounds., *Canadian Mineralogist*, **14**:151-158, 1976.

ECHIP, Inc., Software and Course Text, Bob Wheeler, 1989.

Elwell, D. and H.J. Scheel, Crystal Growth from High-Temperature Solutions., Academic Press, London, pp. 138-201, 1975.

Environment Canada, Mine and Mill Wastewater Treatment, Environment Canada Report, EPS 2/MM/#, December, 1987.

Environmental Protection Agency (EPA), Studies on limestone treatment of acid mine drainage, Water Pollution Control Series, Report No. 14010 EIZ, 1970.

Erikson, L., E. Matijević and S. Friberg, Desorption of hydrolyzed metal ions from hydrophobic interfaces. I. Latex-aluminum nitrate systems., *J. Colloid and Interface Science*, **43**(3):519-598, 1973.

Estrin, J., Secondary Nucleation., *in Preparation and Properties of Solid State Materials.*, W.R. Wilcox, (ed.), Volume 2, Marcel Dekker, N.Y., pp. 1-42, 1976.

Feitknecht, W. and W. Michaelis, Über die hydrolyse von eisen(III) perchloratlösungen, *Helv. Chim. Acta.*, **45**:212, 1962.

Feitknecht, W. and P. Schindler, Solubility constants of metal oxides, metal hydroxides and metal hydroxide salts in aqueous solution. *Pure and Applied Chemistry*, **6**:130-198, 1963.

Filon, M.P., K. Ferguson, and L.L Sirois, Acidic drainage research in Canada., *in Proc. 23rd CMP Conf.*, Ottawa, Ontario, Paper 10, p. 21, January 22-24, 1991.

Firth, B.A. and R.J. Hunter, Flow properties of coagulated colloidal suspensions., *J. Colloid and Interface Science*, **57**(2):248-256, 1976.

Filippou, D., V.G. Papangelakis and G.P. Demopoulos, A new method for the estimation of acid activities through speciation, and its application to process solutions of $\text{ZnSO}_4\text{-FeSO}_4\text{-Fe}_2(\text{SO}_4)_3\text{-H}_2\text{SO}_4$., *in Hydrometallurgy: Fundamentals, Technology and Innovation*, J.B. Hiskey and G.W. Warrent (editors), TMS-SME, Littleton, Colorado, Chapter 14, pp. 223-240, 1993.

Flynn, C.M., Jr., Hydrolysis of inorganic iron(III) salts., *Chemical Reviews*, **84**(1):31-41, 1984.

Flynn, C.M., Jr., Dense hydrolysis products from iron(III) nitrate and sulphate solutions., *Hydrometallurgy*, **25**:257-270, 1990.

Fox, L.E., The solubility of colloidal ferric hydroxide and its relevance to iron concentrations in river water., *Geochimica et Cosmochimica Acta*, **52**(3):771-777, 1988.

Fuerstenau, D.W., in The Chemistry of Biosurfaces., M.L. Hair (ed.), Marcel Dekker, New York, Vol. I, p. 143, 1971.

Garside, J. Industrial crystallization from solution., *Chemical Engineering Science*, **40**(1):3-26, 1985.

Garside, J. and R.J. Davey, Secondary contact nucleation: Kinetics, growth and scale-up., *Chemical Engineering Communications*., **4**:393-424, 1980.

Garside, J. and R.I. Ristic, Growth rate dispersion among ADP crystals formed by primary nucleation., *J. Crystal Growth*, **61**:215-220, 1983.

Garside, J. and N.S. Tavaré, Non-isothermal effectiveness factors for crystal growth., *Chemical Engineering Science*, **36**:863-866, 1981.

Gayer, K.H. and L. Woontner, The solubility of ferrous hydroxide and ferric hydroxide in acidic and basic media at 25°C., *Physical Chemistry J.*, **60**:1569-1571, 1956.

Gionet, Mellor, Liebhaf Associates Ltd., Generation and stability of Canadian mine/smelter effluent treatment sludges., Report for CANMET, DSS Contract No. 23440-5-9161/15-SQ, July, 1987.

Graczyk, T. and Hornof, V., Flocculation of metal-bearing waste water using cellulose and its graft copolymers., *J. Applied Polymer Science*., **29**:1903-1910, 1984.

Gregory, J., Effect of polymers on colloid stability., in The Scientific Basis of Flocculation., K.J. Ives (ed.), pp. 101-130, 1978.

Hague, D.N., Fast Reactions., Wiley, New York, pp.80, 1971.

Hem, J.D., Reactions of metal ions at surfaces of hydrous iron oxide., *Geochim. Cosmochim. Acta*, **41**:527-538, 1977.

Hohl, H. and W. Stumm, Interaction of Pb^{2+} with hydrous $\gamma-Al_2O_3$., *J. Colloid and Interface Science*, **55**(2):281-288, 1976.

Hsu, P.H. and S.E. Ragone, Aging of hydrolysed iron (III) solutions., J. Soil Science, 22(1):17-31, 1972.

Huck, P.M. and B.P. LeClair, Polymer selection and dosage determination methodology for acid mine drainage and tailings pond overflows., Flocculation and Dispersion Symposium, Toronto, Ontario, November 4-5, 1974, Chemical Institute of Canada, 1974.

Huck, P.M., B.P. LeClair, and P.W. Shilbey, Operational experience with a base metal mine drainage pilot plant., 29th Annual Purdue Industrial Waste Conference, Purdue University, 1974.

Huck, P.M. and B.P. LeClair, Treatment of base metal mine drainage, 30th Industrial Waste Conference, Purdue University, Lafayette, Indiana, May 6-8, 1975, Engineering Bulletin of Purdue University, Engineering Extension Series, No. 149, 1976.

Huck, P.M., K.L. Murphy, and B.P. LeClair, Scavenging and flocculation of metal-bearing wastewaters using polyelectrolytes., Environmental Protection Service Report No. EPS 4-WO-77-7, November, 1977.

Hunter, R.J., Zeta Potential in Colloid Science. Applications and Principles., Academic Press, London, pp. 386, 1981.

Iler, R.K., in Surface and Colloid Science., E. Matijević (ed.), Vol. 6, Wiley - Interscience, N.Y., 1973.

Inouye, K., Ozawa, Y., Kaneko, K. and Ozeki, S., Changes in precipitates from aqueous mixed solution of ferric chloride (III) and ferric sulphate (III) by hydrolysis., Nihon Kagaku Kaishi, 10:1281-1286, 1986.

Jagannathan, R. and J.S. Wey, Diffusion-controlled growth in a crowded environment., J. Crystal Growth, 51:601:606, 1981.

Jenke, D. R., and F. E. Diebold, Recovery of valuable metals from acid mine drainage by selective titration., Water Res., 17(11):1585-1590, 1983.

Keight, D.V., Comments on: An investigation into nucleation kinetics of urea crystallization in water by means of crystal-size distribution analysis., Ind. Eng. Chem. Process Des. Dev., 17(4):576, 1978.

Kenney, J.T., W.P. Townsend and J.A. Emerson, Tin and iron oxide deposits on polyethylene teflon, on paraffin., J. Colloid and Interface Science, 42(3):589-596, 1973.

Kern, R., Metastable synthesis of bulk and surface phases., in Reactivity of Solids., P. Barret and L.-C. Dufour (eds.), Mineral Science Monographs, **28A**, Elsevier, Amsterdam, pp. 23-24, 1985.

Kiyama, M., T. Akita, S. Shimizu, Y. Okuda and T. Takada, Conditions favourable for the formation of γ -FeOOH by aerial oxidation in an acidic suspension of iron metal powder., Bulletin of the Chemical Society of Japan, **45**(11):3422-3426, 1972.

Kiyama, M. and T. Takada, Iron compounds formed by aerial oxidation of ferrous salt solutions., Bulletin of the Chemical Society of Japan, **45**(6):1923-1924, 1972.

Kiyama, M. and T. Takada, The hydrolysis of ferric complexes. Magnetic and spectrophotometric studies of aqueous solutions of ferric salts., Bulletin of the Chemical Society of Japan, **46**(6):1680-1686, 1973.

Knight, R.J. and R.N. Sylva, Precipitation of hydrolysed iron(III) solutions., J. Inorganic and Nuclear Chemistry, **36**:591-597, 1974.

Kuit, W. J., Mine and tailings effluent treatment at Kimberley, B.C. operations of Cominco Ltd., CIM Bulletin, **73**:105-112, December, 1980.

Kuyucak N., T.W. Sheremata and K.G. Wheeland, Evaluation of improved lime neutralization processes. Part I: Lime sludge generation and stability., 2nd Int. Conf. on the Abatement of Acidic Drainage, Montreal, Quebec, September 16-18, 1991.

Lamb, A.B. and A.G. Jacques, The slow hydrolysis of ferric chloride in dilute solutions. II. The change in hydrogen ion concentration., J. American Chemical Society, **60**:1215-1225, 1938.

La Mer, V.K. and R.H. Smellie, Jr., Flocculation, subsidence and filtration of phosphate slimes, Part II., J. Col. Science, **11**(6):710-719, 1956.

Langmuir, D., The gibbs free energy of substances in the system Fe-O₂-H₂O-CO₂ at 25°C. U.S. Geological Survey Professional Paper 630-C, C224-C235, 1969.

Langmuir, D. and D.O. Whittemore, Variations in the stability of precipitated ferric oxyhydroxides., in Nonequilibrium Systems in Natural Water Chemistry., American Chemical Society, Advances in chemistry series 106, pp.209-234, 1971.

Lewis, D.G. and V.C. Farmer, Infrared absorption of surface hydroxyl groups and lattice vibrations in lepidocrocite (γ -FeOOH) and boehmite (γ -AlOOH), Clay Minerals, **21**:93-100, 1986.

Lewis, D.G. and U. Schwertmann, The influence of Al on iron oxides. Part III. Preparation of Al goethites in KOH., *Clay Minerals*, 14:115-126, 1979.

Loganathan, P. and R.G. Burau, Sorption of heavy metal ions by a hydrous manganese oxide., *Geochimica et Cosmochimica Acta*, 37:1277-1293, 1973.

Lyklema, J., Surface chemistry of colloids in connection with stability., *in The Scientific Basis of Flocculation.*, K.I. Ives (ed.), Sijthoff & Noordhoff, p. 3-36, 1978.

MacDonald, R.J.C., P.D. Kondos, S. Crevier, P. Rubinsky and M. Wasserlauf, Generation of, and disposal options for Canadian Mineral Industry effluent treatment sludges., *Tailings and Effluent Management Symposium*, Halifax, Nova Scotia, August 20-24, 1989.

Margulis, E.V., Getskin, L.S., Zapuskalova and L.I. Beisekeeva, Hydrolytic precipitation of iron in the $\text{Fe}_2(\text{SO}_4)_3\text{-NaOH-H}_2\text{O}$ System., *Russian Journal of Inorganic Chemistry*, 22(4):558-561, 1977.

Mates, T.E. and T.A. Ring, Steric stability of alkoxy-precipitated TiO_2 in alcohol solutions., *Colloids and Surfaces*, 24:299-313, 1987.

Matijević, E., Colloid stability and complex chemistry., *J. Colloid and Interface Sci.*, 43(2):239, 1973.

Matijević, E., Monodispersed metal (hydrous) oxides - A fascinating field of colloid science., *Acc. Chem. Res.*, 14:22-29, 1981.

Matijević, E., R.S. Sapienszko, J.B. Melville, Ferric Hydrous Oxide Sols I. Monodispersed basic iron(III) sulphate particles., *J. Colloid and Interface Science*, 50(3):567-581, 1975.

Matijević, E. and P. Scheiner, Ferric Hydrous Oxide Sols III. Preparation of uniform particles by hydrolysis of Fe(III)-chloride, -nitrate, and -perchlorate solutions., *J. Colloid and Interface Science*, 63(3):509-524, 1978.

McAndrew, R.T., S.S. Wang and W.R. Brown. Precipitation of iron compounds from sulphuric acid leach solutions., *CIM bulletin*, 68(753):101-110, 1975.

Monhemius, A.J., Precipitation diagrams for metal hydroxides, sulphides, arsenates and phosphates., *Trans. IMM*, 86:C202-C206, 1977.

Montgomery, James M., Consulting Engineers, Inc., Water Treatment Principles and Design., John Wiley & Sons, Inc., New York, pp. 116-134, 1985.

Mullin, J.W., M. Chakraborty and K. Mehta, Nucleation and growth of ammonium sulphate crystals from aqueous solution., *J. Applied Chemistry*, **20**:367-371, 1970.

Murphy, P.J., A.M. Posner and J.P. Quirk, Gel filtration chromatography of partially neutralized ferric solutions., *J. Colloid and Interface Science*, **52**(2):229-238, 1975.

Murphy, P.J., A.M. Posner and J.P. Quirk, Characterization of hydrolyzed ferric ion solutions. A comparison of the effects of various anions on the solutions., *J. Colloid and Interface Science*, **56**(2):312-319, 1976.

Murray, J.W., Iron Oxides., in Marine Minerals., Mineralogical Society of America Short Course Notes, 6:47-98, 1979.

Nielsen, A.E., Kinetics of Precipitation, Pergamon Press, New York, pp.11-29, 1964.

Nielsen, A.E., in Crystal Growth., H.S. Peiser, (ed.), Pergamon Press, N.Y., p.419, 1967.

Nielsen, A.E. and O. Söhnel, Interfacial tensions electrolyte crystal-aqueous solutions, from nucleation data., *J. Crystal Growth*, **11**:233-242, 1971.

Nienow, A.W. and R. Conti, Particle abrasion at high solids concentration in stirred vessels., *Chemical Engineering Science*, **33**:1077-1086, 1978.

Okó, U. M., and W.L.W. Taylor, Treatment of acid mine wastewater at Falconbridge's Hardy Crown Pittar project., *CIM Bulletin*, **67**:43-49, April, 1974.

O'Melia, C.R., A review of the coagulation process., *Public Works*, **100**:87-98, 1969.

Ozaki, M. and E. Matijević, Preparation and magnetic properties of monodispersed spindle-type γ -Fe₂O₃ particles., *J. Colloid and Interface Science*, **107**(1):199-203, 1985.

Packham, R.F., Some studies of the coagulation of dispersed clays with hydrolyzing salts., *J. Colloid Science*, **20**:81-92, 1965.

Papangelakis, V.G. and G.P. Demopoulos., Acid pressure oxidation of arsenopyrite: Part 1. reaction chemistry., *Can. Metal. Quat.*, **29**(1):1-12, 1990.

Parks, G.A., The isoelectric points of solid oxides, solid hydroxides, and aqueous hydroxo complex systems., *Chemical Reviews*, **65**:177-198, 1965.

Paspopov, Y.G., D.G. Kleschov, N.G. Krasnobai, R.N. Pletnev, and A.I. Scheinkman, On the mechanism of crystal formation in the FeSO₄-H⁺/OH⁻-H₂O-O₂ system. *Minerals Chemistry and Physics*, **30**:35-31, 1991.

Patrizi, A., G. Persia, and A. Pescetelli, The new electrolyte zinc plant at Porto Vesme, Italy., in Zinc '85, K. Tozawa (ed.), Mining and Metallurgy Institute of Japan, Tokyo, pp. 413-434, 1985.

Powers, H.E.C., Nucleation and early crystal growth., *Industrial Chemist*, 39:351-355, 1963.

Ritcey, G. M., Tailings Management, Problems and Solutions in the Mining Industry, Elsevier, Amsterdam, pp.411-517, 1989.

Robins, R.G. and J.C.Y. Huang, The adsorption of arsenate ion by ferric hydroxide., in Arsenic Metallurgy Fundamentals and Applications., R.G. Reddy, J.L. Hendrix, and P.B. Queneau, (eds.), TMS, pp. 99-112, 1987.

Rousseau, R.W., K.K. Li and W.L. McCabe, The influence of seed crystal size on nucleation rates., in Analysis and Design of Crystallization Processes., R.W. Rousseau and M.A. Larson, (eds.), AIChE Symposium Series, 72(153):48-52, 1976

Ruehrwein, R.A. and D.W. Ward, Mechanism of clay aggregation by polyelectrolytes., *Soil Science*, 73(6):485-492, 1952.

Sapieszko, R.S., R.C. Patel and E. Matijevic, Ferric hydrous oxide sols. I. Thermodynamics of aqueous hydroxo and sulphato ferric complexes., *J. Phys. Chem.*, 81(11):1061-1068, 1977.

Schindler, Von, P., W. Michaelis and W. Feitknecht, Löslichkeitsprodukte von metalloxiden und -hydroxiden. 8. Die löslichkeit gealterter eisen(III)-hydroxid-fällungen., *Helv. Chim. Acta*, 46:444-449, 1963.

Schneider, W. and B. Schwyn, The hydrolysis of iron in synthetic, biological, and aqueous aquatic media., in Aquatic Surface Chemistry., W. Stumm (ed.), John Wiley & Sons, Ch. 7, pp. 167-196, 1987.

Schwoyer, W.L. and L.B. Luttinger, Dewatering of metal hydroxides., 27th Industrial Waste Conference, Purdue University Lafayette, Indiana, May 2-4, 1972, *Engineering Bulletin of Purdue University, Engineering Extension Series*, No. 141, 1973.

Scott, J.S., Water pollution controls in the Canadian metal mining industry., Mine Environment Consulting, report prepared for CANMET, November, 1992.

Shaw, D.J., Introduction to Colloid and Surface Chemistry., 2nd ed., Butterworths, London, pp. 167-186, 1970.

Shea, T.G., Use of polymers as a primary coagulant., Proceedings AWW Seminar, June 4, 1972.

Sillén, L.G. and A.E. Martell, Stability Constants of Metal-ion Complexes., The Chemical Society of London, special Publication No. 17, 1964.

Skelley and Loy, Engineers-Consultants, Processes, procedures and methods to control pollution from mining activities., U. S. Environmental Protection Agency, Washington, D.C., EPA-430/9-73-011, October, 1973.

Spiro, T.G., S.E. Allerton, J. Renner, A. Terzis, R. Bils and P. Saltman, The hydrolytic polymerization of Iron(III)", J. American Chemical Society, **88**(12):2721-2726, 1966.

Stipp, S.L., Speciation in the Fe(II)-Fe(III)-SO₄-H₂O system at 25°C and low pH: Sensitivity of an equilibrium model to uncertainties., Environ. Sci. Technol., **24**:699-706, 1990.

Stumm, W. and C.R. O'Melia, Stoichiometry of coagulation., JAWWA, **60**(5):514-539, 1968.

Sugimoto T. and E. Matijević, Formation of uniform magnetite particles by crystallization from ferrous hydroxide gels., J. Colloid and Interface Science, **74**(1):227-243, 1980.

Sung, C.Y., J. Estrin and G.R. Youngquist, Secondary nucleation of magnesium sulphate by fluid shear., AIChE Journal, **19**(5):957-962, 1973.

Sylva, R.N., Hydrolysis of Iron(III)., Reviews of Pure and Applied Chemistry., **22**:115-132, 1972.

Tamamushi, B. and K. Tamaki, The action of long-chain cations on negative silver iodide sol., Koll-Z, **163**:122-126, 1959.

Tavare, N.S. and M.R. Chivate, Analysis of batch evaporative crystallizers., Chemical Engineering J., **14**:175-180, 1977.

Temmel, F.M., Treatment of acid and metal bearing wastewaters by the high density sludge process., Regional Technical Meeting AISI, pp. 343-362, 1972.

Tewari, P.H. and A.B. Campbell, Colloidal forces in deposition of suspended particles onto surfaces., in Recent Developments in Separation Science., Vol. IV, N.N. Li (ed.), pp. 83-92, 1978.

- Towe, K.M. and W.F. Bradley, Mineralogical constitution of colloidal "hydrous ferric oxides", *J. Colloid and Interface Science*, **24**:384-392, 1967.
- Toyokura, K., Crystallization Concepts., *in Encyclopedia of Chemical Processing and Design*, Vol. 13, J. McKetta and W.A. Cunningham (eds.), Marcel Dekker, N.Y., p. 407-420, 1981.
- Toyokura, K., J. Mogi and I. Hirasawa, Secondary nucleation of K-Alum by minimum size seeds in a stirred vessel., *J. Chemical Engineering of Japan*, **10**(1):35-39, 1977.
- Umetsu, Y., K. Tozawa and K. Sasaki, The hydrolysis of ferric sulphate solutions at elevated temperatures., *Metallurgical Society of CIM Annual Volume*, **16**(1-4):111-117, 1977.
- Vachon, D., R.S. Siwik, J. Schmidt, and K. Wheeland, Treatment of acid mine water and the disposal of lime neutralization sludge., *Proceedings of Acid Mine Drainage Seminar/Workshop*, Halifax, Nova Scotia, March 23-26, 1987, Environment Canada, pp. 537-564, 1987.
- Van der Woude, J.H.A. and P.L. de Bruyn, Formation of colloidal dispersions from supersaturated iron(III) nitrate solutions. I. Precipitation of amorphous iron hydroxide., *Colloids and Surfaces*, **8**(1):55-78, 1983.
- Van der Woude, J.H.A., P. Verhees and P.L. de Bruyn, Formation of colloidal dispersions from supersaturated iron(III) nitrate solutions. II. Kinetics of growth at elevated temperatures., *Colloids and Surfaces*, **8**(1):79-92, 1983.
- Van der Woude, J.H.A. and P.L. de Bruyn, Formation of colloidal dispersions from supersaturated iron(III) nitrate solutions. III. Development of goethite at room temperature., *Colloids and Surfaces*, **9**(2):173-188, 1984.
- Van der Woude, J.H.A., P. Verhees and P.L. de Bruyn, Formation of colloidal dispersions from supersaturated iron(III) nitrate solutions. IV. Analysis of slow flocculation of goethite., *Colloids and Surfaces*, **9**(3/4):391-400, 1984.
- van Olphen, H., An Introduction to Clay-Colloid Chemistry., Wiley-Interscience, New York, pp. 16-42, 92-120, 1977.
- Verwey, E.J.W. and J.Th.G. Overbeek, Theory of the Stability of Lyophobic Colloids., Elsevier Scientific Publishing Company, Amsterdam, pp. 164-185, 1948.
- Viola, M.S. and G.D. Botsaris, simulation of nucleation kinetics - An application to secondary nucleation, *Chemical Engineering Science*, **34**:993-999, 1979.

Vlek, P.L.G., Th.J.M. Blom, J. Beek and W.L. Lindsay, Determination of the solubility product of various iron hydroxides and jarosites by the chelation method., Soil science of America, Proceedings, **38**(3)429-433, 1974.

Vogel, A.I., A Textbook of Quantitative Inorganic Analysis, Including Elementary Instrumental Analysis., Wiley, New York, pp. 462-465, 1962.

Wakeman, R.J., S.T. Thuraisingham and E.S. Tarleton, Colloid science in solid liquid separation. Is it important?, Filtration and Separation, **26**(4):277,279-283, 1989.

Walton, A.G., The Formation and Properties of Precipitation., Chemical Analysis, Vol. 23, P.J. Elving and I.M. Kolthoff (eds.), John Wiley and Sons, N.Y., pp. 1-42, 1967.

Wang, M.-L., H.-T. Huang and J. Estrin, Secondary nucleation of citric acid due to fluid forces in a Couette flow crystallizer., AIChE Journal, **27**(2):312-315, 1981.

Wagman, D.D., W.H. Evans, V.B. Parker, I. Halow, S.M. Baily and R.H. Schumm., Selected Values of Thermodynamic Properties, National Bureau of Standards 270, US Dept. of Commerce, Wash., (1968, 1971).

Wendt, H., Die kinetik der bildung des binuklearen eisen(III)-hydroxo-komplexes $\text{Fe}_2(\text{OH})_2^{4+}$., Elektrochem., **66**:235, 1962.

Yakovlev, Y.B., F.Y. Kul'ba, A.G. Pus'ko and M.N. Gerchikova, Hydrolysis of iron(III) sulphate in zinc sulphate solutions 25, 50 and 80°C., Russian Journal of Inorganic Chemistry, **22**(1):27-29, 1977.

Yakovlev, Y.B., F.Y. Kul'ba, A.G. Pus'ko and N.A. Titova, Hydrolysis of iron(III) sulphate in mixtures of zinc, ammonium, and copper sulphates at 25°C., Russian Journal of Inorganic Chemistry, **23**(2):229-232, 1978.

Yates, D.E., Ph.D. Thesis., University of Melbourne, 1975.

Yates, D.E. and T.W. Healy, Proceeding International Conference Colloid Surface Science, **1**:7, 1975

Zinck, J.M., work in progress, CANMET, 1993.

APPENDIX A: THERMODYNAMIC CALCULATIONS

APPENDIX A: Thermodynamic Calculations

A-1 Predominance Area Diagrams

Four specific conditions were applied in the calculation of predominance area diagrams using the F*A*C*T system.

Condition 1: - 298 K

-Concentration of all aqueous species included in the calculation were varied from 0.1 to 0.00001 M.

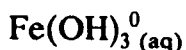
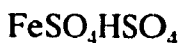
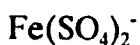
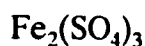
-Fe(OH)₃ was included in the calculation. All other solids were suppressed since at low temperature thermodynamic equilibrium is not reached and from laboratory tests performed its known Fe(OH)₃ is the dominant hydrolytic precipitate.

Condition 2: -Same as condition 1 except ferric hydroxide precipitation was suppressed to observe the Fe(III) speciation.

Condition 3: -Same as condition 1 except the calculations were performed for 353 K. Heat capacity data was extrapolated when required.

Condition 4: -Same as condition 3 except Fe(OH)₃ precipitation was suppressed.

The following is a list of all the Fe(III) species included in the calculations.



The optional compound considered was $\text{Fe}(\text{OH})_3(\text{s})$ (condition 1 & 3). The formation of all other species and compounds was suppressed. Oxyanions were not included in the calculations as they do not occur in the system defined.

The program PREDOM generates a predominance area diagram at a specified temperature showing which of all possible stoichiometric phases is most stable over the ranges of chemical potential entered by the user in terms of partial pressures or activities.

The compound with the most negative Gibb's energy of formation for the activity of SO_4^{2-} and pH associated with a particular co-ordinate on the diagram is the one that is most stable. Repeated calculation of which species has the most negative Gibb's energy, thereby establishing domains of predominance for particular Fe(III) containing phases, is the essence of PREDOM.

A-2 Speciation Diagrams

Speciation diagrams were calculated from data produced using the "Detailed Point Calculation" feature in F*A*C*T for the case where the precipitation of $\text{Fe}(\text{OH})_3$ was suppressed. By selecting coordinates on the predominance area diagram F*A*C*T calculates the concentration (or activity) of each species in solution at that point. By summing the concentrations of all the Fe (III) species a total Fe(III) is found. Three speciation diagrams were calculated (Figures 4-4 and 4-5).

A-3 Solubility Diagrams

Solubility diagrams were calculated using data generated by the "Detailed Point Calculation" feature in the PREDOM program for the Condition 1 parameters. In a similar manner in which speciation diagrams were calculated the total Fe(III) concentration remaining after precipitation was plotted against the solution pH.

APPENDIX B: EXPERIMENTAL PROCEDURES

APPENDIX B: Experimental Procedures

B-1: Sulphate Determination by Barium Sulphate Precipitation

(modified from Vogel, 1962)

Purpose:	To determine the concentration of sulphate in a liquid or solid sample.
Apparatus and: Reagents	400 mL beaker burette or pipette hot plate/stirrer magnetic stir bar or glass stirring rod Millipore filter apparatus and filter paper convection oven preheated at 60°C analytical balance concentrated HCl 5% barium chloride solution
Procedure:	Place 10 mL of a liquid sample or 0.3 g of a solid sample into the beaker. Add 0.3-0.6 mL conc. HCl. Allow the precipitate to dissolve completely. Dilute to ~ 225 mL with distilled water. Heat solution to boiling. Add drop-wise from burette or pipette 10-12 mL of warm 5% barium chloride. Stirring constantly during addition. Let the precipitate settle for a minute or two. Test the supernatant for complete precipitation by adding a few drops of barium chloride solution. If no precipitate forms allow solution to stand for 24 hours. Meanwhile, oven dry filter paper, cool in desiccator and weigh to four significant digits. After 24 hours check solution for complete precipitation. If no additional precipitate is formed the barium sulphate is ready for filtration. Collect the precipitate and re-check filtrate for complete precipitation. Dry precipitate at 60°C for 2-4 hours. Cool in a desiccator. Weigh filter paper and precipitate to four significant digits.
Calculation:	Multiply weight of precipitate by 0.4116 (% SO ₄ in BaSO ₄) to obtain the weight of SO ₄ . Divide weight of SO ₄ by sample volume or weight to get concentration or weight percentage.

B-2: Settling Rate Determination Procedure

Purpose: To determine the free settling rate of a precipitate.

Apparatus: 1 L graduated cylinder fitted with a rubber stopper (I.D. = 5.96 cm)
45 cm long ruler

Procedure:

- a) Calibrate the volume (mL) fractions on the graduated cylinder into distance (cm) markings by using the ruler.
- b) Fill the cylinder with the liquor.
- c) Shake gently the cylinder until the liquor is thoroughly mixed.
- d) Record the height of the solid-liquid interface at one minute intervals for ten minutes, every two minutes for the next ten minutes, every five minutes until 45 minutes has passed, then at 60 minutes and finally at 24 hours.

Calculation: Construct an arithmetic plot of the solid-liquid interface height in centimetres versus time in minutes. Draw a line of best fit through the linear portion of the graph. Determine the free settling rate as the slope of the line. Settling rate is expressed in cm/min or m/hr.

B-3: Percent Solids Determination Procedure

Purpose: To determine solids concentration in a sludge.

Apparatus: Pump, with an operating range of 1-20 mL/min.
Millipore filter apparatus
Convection oven preheated at 60°C
Analytical balance

Procedure: Allow the sludge to settle completely (until there is not change in sludge volume over a 24 hour period). Carefully separate the settled sludge from the mother liquor by using a pump. Weigh the sludge to four significant digits. Filter the sludge to remove excess water. Dry the filter cake in a conventional oven at 60°C for 16 to 24 hours. Reweigh the dry precipitate until a consistent weight is achieved.

Calculation: Percent solids is calculated by dividing the dry weight by the wet weight and multiplying by 100%.

B-4: Sludge Volume Determination Procedure

Purpose: To determine the volume of the sludge.

Apparatus: Imhoff settling cone

Procedure: a) Fill the cone with the mixed liquor
b) Allow the sludge to settle for 24 hours.

Calculation: Record the volume of the precipitate in millilitres.

**APPENDIX C: THE INPUT OF HSO_4^- DISSOCIATION IN Fe(III)
PRECIPITATION CALCULATIONS**

APPENDIX C: The Input of HSO_4^- Dissociation in Fe(III) Precipitation Calculations

Initial Conditions: pH = 2.76, $[\text{Fe(III)}] = 0.018 \text{ M}$, $[\text{SO}_4^{2-}]_T = 0.0025 \text{ M}$

But according to the speciation diagram of Figure 4-4 at pH 2.76 iron(III) is present as 66% $\text{Fe}_3(\text{SO}_4)_2$ (i.e. 0.012 M) and 34% FeSO_4^+ (i.e. 0.006 M). The sulphate ion concentration taken up by the two Fe(III) complexes is then $2 \times 0.012 \text{ M} + 0.006 \text{ M} = 0.03 \text{ M}$. The remaining sulphate content of the solution (i.e. $0.0625 - 0.03 = 0.0325$) is present as a mixture of $\text{HSO}_4^-/\text{SO}_4^{2-}$.

The bisulphate ion dissociation reaction:



has an equilibrium constant of 10^{-2} . After solving the problem for $[\text{HSO}_4^-] + [\text{SO}_4^{2-}] = 0.0325$ and pH 2.76 it is determined $[\text{SO}_4^{2-}] = 0.0273 \text{ M}$ and $[\text{HSO}_4^-] = 0.052 \text{ M}$. At the end of the hydrolysis reaction all HSO_4^- will have been dissociated to H^+ and SO_4^{2-} releasing 0.0052 M H^+ which corresponds to the amount of H^+ generated by $0.00174 \text{ M Fe}^{3+}$ undergoing complete hydrolysis. This amount of Fe^{3+} is $\sim 100 \text{ mg/L}$, i.e. the same amount by which the precipitated iron(III) was underestimated (see Table 6-1).

APPENDIX D: STATISTICAL DESIGN DERIVED SOLUBILITY DATA

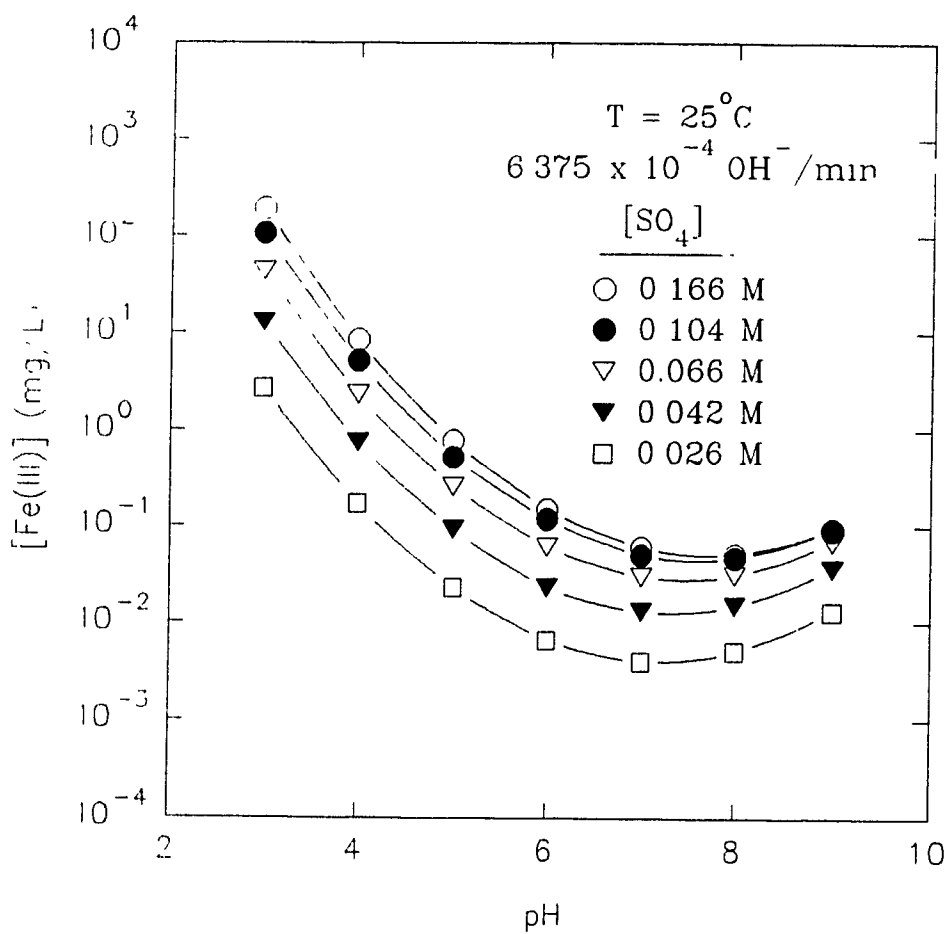


Figure D-1: Fe(III) solubility for various sulphate concentrations at 25°C.

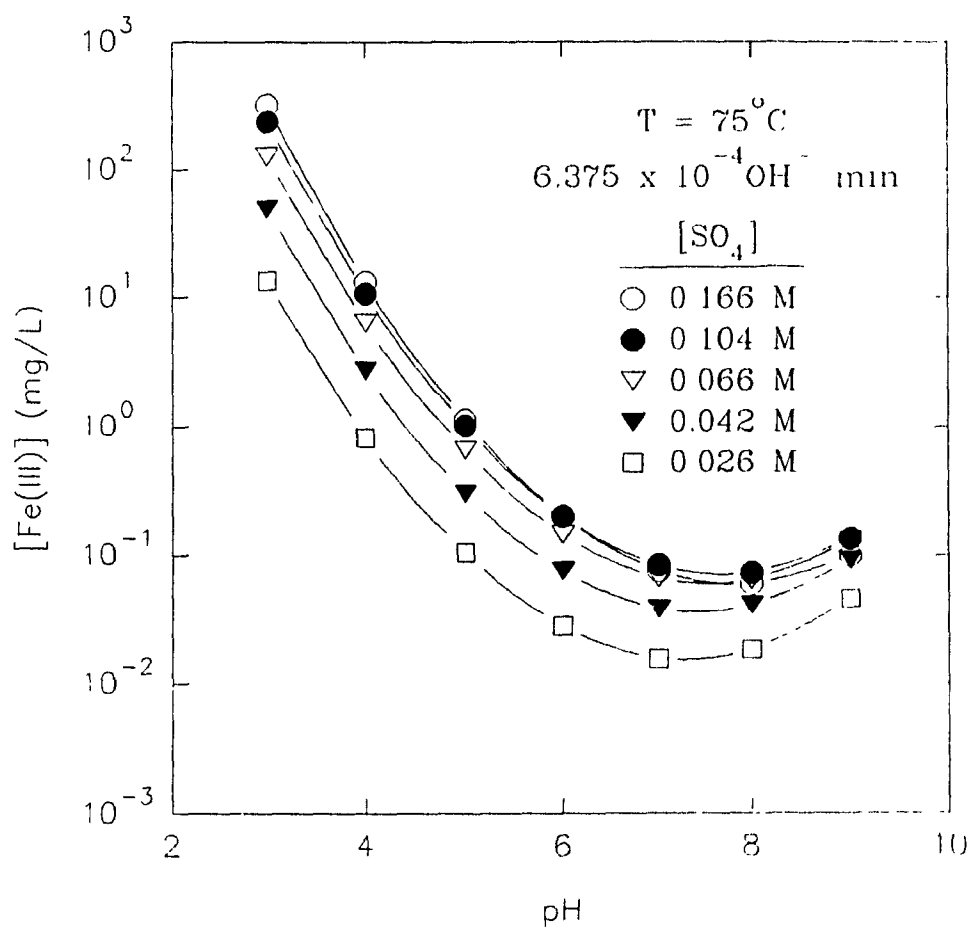


Figure D-2: Fe(III) solubility for various sulphate concentrations at 75°C.

APPENDIX E: RECYCLING

E-1: Dissolution Tests

To evaluate the possible redissolution of the precipitate upon recycling dissolution tests were performed. In these tests water was acidified to six different pH values using sulphuric acid. ~ 1 gram precipitate produced in series A was introduced to a 500 mL Pyrex beaker containing 300 mL acidified water. The mixture was agitated at 500 rpm for 2 hours. The solution was filtered and the filtrate analyzed for Fe using atomic absorption.

Table E-1: Dissolution test results.

pH	[Fe] _f (mg/L)
2.5	0.47
3.0	0.07
3.5	0.03
4.0	0.04
5.0	0.04
6.0	0.04

Table E-2: Detailed data from a series B stage-neutralization recycling test.

pH _i	pH _f	Time to reach pH _f (min.)	NaOH [*] Volume to reach pH _f (mL)	Equilibrium time (min)	Vol. to maintain pH _f (mL)	Total time (min)	Total volume NaOH [*] (mL)	Cum Time (min)
2.55	2.84	100	12.45	60	1.07	160	13.63	160
2.84	3.20	31	3.863	45	0.138	76	4.001	236
3.20	3.58	11	1.368	30	0.104	41	1.472	277
3.58	4.00	6	0.690	20	0.083	26	0.773	303
4.00	4.48	4.5	0.445	20	0.090	24.5	0.535	327
4.48	5.00	3.5	0.354	20	0.120	23.5	0.474	350
5.00	5.69	5	0.463	20	0.134	25	0.597	375
5.69	9.29	24	3.027	20	0.211	44	3.238	419

* 1.275 M NaOH

7 hours